International Journal of Fusion Energy

Vol. 3, No. 1 January 1985

International Journal of Fusion Energy

Vol. 3, No. 1, January 1985

International Journal of Fusion Energy (ISSN: 0146-4981) is published quarterly by the Fusion Energy Foundation, 304 West 58 Street, Fifth Floor, New York, N.Y. 10019, Tel. (212) 247-8439.

Subscription price: $80 per volume (four issues) domestic; $100 per volume foreign. Payment must be in U.S. dollars.

Address all correspondence to IJFE, Fusion Energy Foundation, Box 1438, Radio City Station, New York, N.Y. 10101.

Postmaster: Send address changes to IJFE, Fusion Energy Foundation, Box 1438, Radio City Station, New York, N.Y. 10101.

Editorial Policy

The International Journal of Fusion Energy (IJFE) is an independent scientific journal published quarterly by the Fusion Energy Foundation. The IJFE is dedicated to the promotion of fundamental advance in science, with special emphasis on the following areas:

1. The physics of plasmas at high energy densities, and research bearing on the scientific and technological mastery of nuclear fusion processes.
2. Coherent, directed forms of electromagnetic action, including laser and particle beams and superconductivity.
3. The physics of living processes, with applications to fundamental problems of biology and medicine.

In addition to research articles and state-of-the-art reviews, the IJFE welcomes short, informal communications addressing questions of interest to researchers and others in the cited areas. Contributions in other fields will be accepted on the basis of extraordinary scientific interest or manifest relevance to the three specific fields covered by the journal.

IJFE will also run abstracts of relevant, recent published and unpublished work as a regular service to the reader. The editors will be grateful for references to significant new work, not previously covered in the abstracts and other departments of the journal.

International Journal of Fusion Energy

Vol. 3, No. 1 January 1985

4
Editorial

7
Editor's Note

Articles

9
The Morphology of the Electron
Winston H. Bostick

53
Missing Energies at the Pair Production by Gamma Quanta
Erich R. Bagge

57
The Relation Between Angular Momentum and Star Formation in Spiral Galaxies
L. Carrasco and A. Serrano

63
New Frontiers in Biophysics
James Frazer, PhD

Reports

68 Recent Experimental Results of the Plasma Focus Group At Darmstadt, West Germany: A Review and Critique

74 The Polarized Fusion Program at LLNL

75 Muon Approach to 'Cold' Fusion Makes Progress

76 Radiative Collapse to Super Densities: A Review of the Work of B.E. Meierovich

78 Overview on Aging of Tissue

82 Environmental Effects on Flax Genetics Updated

83 Growth of Neurons in Adult Brains of Birds Demonstrated

84 Coherent Effects of DNA Explored

87 Basic Electrodynamics Riemann and His Italian School Vs. Maxwell

89 On Electrodynamics (English translation of E. Betti's 1869 paper)

91 A Contribution to Electrodynamics (English translation of B. Riemann's 1858 paper)

94 A Modern Approach to Astronomy from the Point of View of Kepler

Abstracts

97 Fusion

102 Astrophysics

103 Information for Contributors

Editorial

The Expanded IJFE

Among persons engaged in fundamental scientific research today, there should be little resistance to the opinion that the frontiers of fundamental progress are dominated increasingly by expanding possibilities in three areas: (1) highly organized plasmas of increasing energy-flux density (or, the equivalent); (2) advances in matters of coherent, directed radiation of energy, some of which fairly deserve the epithet "revolutionary"; and, (3) the expansions of new directions in biological science, of which the most important, for the longer term, is at present reflected in the specialization termed "nonlinear spectroscopy." All three areas of work are closely interrelated: the first two areas obviously so; the connections of the first two to nonlinear spectroscopy may be less apparent to most at first glance, but the connections are nonetheless significant and even profound.

The study of negentropic processes in plasma physics and biology has been at the center of the Fusion Energy Foundation's attention since the activities of 1973-1975 that led into the formation of the FEF 10 years ago. The devotion to this continuing point of reference, over the intervening years, implies that the time has come to expand as much as possible the role which the the IJFE assumes in aid of progress in the three, interrelated areas.

Some Relevant Points From the Background

Over the past 10 years, we have devoted a relatively large ration of our effort to the subject of nuclear fission energy-production. In retrospect, the Foundation should be satisfied that its support for fission energy is both practically and scientifically coherent with our primary, longer-range commitment to development of "commercial" forms of fusion energy applications. Scientifically, and in matters of design and construction of energy-producing systems, fission energy and the "first generation" (at least) of "commercial" fusion-based energy production overlap most substantially. Practically, the wider application of fission energy systems is economically indispensable to provide the ration of energy-flux-density per capita needed for the transition to a fusion-based economy. The Foundation should, and will continue to treat fission energy matters with those leading points in mind. However, fusion energy was and remains our first and abiding love.

There is another leading aspect of the work of the FEF during these past 10 years, typified by the Foundation's participation in elaborating the LaRouche-Riemann method of economic analysis and forecasting.

The germ of a qualitative advance in economic science began to be developed from 1952 onwards, in the discovery made then by Lyndon H. LaRouche, Jr., that Riemann's program in mathematical physics provided implicitly a solution to the problem of correlating changes of rates in technological progress with changes in rates of real economic growth. By "economic science," as opposed to what is taught in universities as "economics," today, we signify the development of the science of "physical economy" begun by Gottfried Leibniz during his work of the period 1672-1716, a branch of physical science centered upon the coherence of Leibniz's Principle of Least Action and his discovery of the concept named "technology."

Whereas Leibniz's thermodynamical definition of "technology" was a continuation of the directions in synthetic geometry's applications to physics set into motion by Nicholas of Cusa, Luca Pacioli, and Leonardo da Vinci, beginning with the work of Karl Gauss on self-similar conic-spiral functions and the fusion of the work of the contributions of the 1794-1814 Ecole Polytechnique with German science, beginning 1815-1827, a new, and more profound development emerged within physical synthetic geometry, the (synthetic-geometrical) notions of functions of a complex variable.This represented the most fundamental advance in the underlying assumptions of mathematics in more than 2,000 years, an accomplishment associated most prominently with the work of Gauss, Lejeune Dirichlet, Bernhard Riemann, and their collaborators.

For reason of various and readily located causes, the bearing of these advances in mathematical physics on Leibniz's earlier definitions for physical economy was overlooked, until LaRouche stumbled upon this, beginning in 1952. True, the Russian, one-time associate of the Pasteur Institute, Professor Vladimir I. Vernadsky, is notable among those who emphasized, beginning in the early 1920s, the relevance of Riemannian physics to both fission energy production and matters of geobiochemistry, which implies the connection to physical economy,* but the originality of LaRouche's discovery of the connection of Riemannian physics to economic science stands, nonetheless.

As Leibniz's elaboration of physical economy implies, the placement of technology and thermodynamics in the underlying formulation of mathematical functions of economic science, places those subject matters properly at the center of economic policy-shaping. As a corollary, it also obliges scientists treating those subject matters to emulate the characteristic feature of that "crash program" known as the Carnot-Monge Ecole Polytechnique, to take the physical economy's priorities into account in setting general and broad priorities for laboratory and related work.

During December 1978, in the course of two FEF seminars held in New York City on the subject of Riemann's 1859 paper, "Propagation of Plane Air Waves of Finite Magnitude," the newsweekly *Executive Intelligence Review* and FEF organized a joint task force to develop a computer-based economic forecasting package incorporating Riemann's principle. That principle is of crucial significance for reflecting the "step-functions," upwards or downwards, which correlate, respectively, with increases or decreases in the effective level of technology employed by the economy. The *Executive Intelligence Review* was concerned primarily with the economic forecasting as such, and the FEF chiefly with the relevance of this to policy-shaping in matters of technology and energy.

Earlier, the same approach had been crucial in the formation of the FEF. A March 1973 paper on the subject of integration of economic and biosphere processes, under the guidance of Riemann's program, had led to defining the part energy policy must play in informing both national economic policy and policies bearing on the technologies of energy-production to be developed and employed.

Ten years later, we look back at such work of 1973-1975 as the accomplishment of insightful and useful amateurs, compared with the refinements in knowledge accumulated since. Despite the rudimentary skills embodied in those earlier efforts, the principles adopted then are valid today.The physical principles underlying the "negentropic" distinction between living and nonliving organic processes are the same, universal principles, properly recognized to underlie the universe in which life occurs.

*Vernadsky, "father of the Soviet A-bomb project," has had his ups and downs as alternately celebrity and "nonperson" in the Soviet literature over the decades. Like Plato's version of dialectical method, totally refuting the parody of this by G.W.F. Hegel and Karl Marx, Riemann's and Vernadsky's Platonic method are not welcome where Soviet "diamat" holds ideological sway in science.

In those respects, what is ever more widely known today as the LaRouche-Riemann method has often influenced, quite properly, the directions of choices of and approach to subject matter, from the Foundation's prebeginnings to the present time.

The Coherence

The most obvious of the common denominators among the three areas indicated at the outset of this editorial, is that a successful result is a "negentropic" result. The "negentropy" accomplished appears in the forms, either of a useful increase in the measurable energy-flux density of the process transformed, or some change in organization of the process which is functionally equivalent to an increase of the effective energy-flux density. Mathematically, from the standpoint of the geometrical physics of a Gauss, Dirichlet, Riemann, et al., this qualitative transformation is associated with the addition of a singularity to the process, as the case of Riemann's cited 1859 paper merely, if most efficiently, illustrates this.

Professor Winston Bostick's contribution included in this issue illustrates the point for plasma physics generally. The implications for coherent directed-energy applications are too obvious to require elaboration in this editorial. In nonlinear spectroscopy, the same principle appears as central to the physics of living processes qua living processes. This point seems already firmly established as a matter of principle in the youthful and promising DNA experiments; it also seems clear enough, implicitly, for important work to be done with chlorophyll.

It were advantageous that relevant aspects of the work in these three areas be viewed from the standpoint of efforts to establish a common language, through which knowledge adduced in one or two areas might be more quickly, and more fruitfully, applied in the other.

The expansion of the IJFE begun with this present issue is intended to provide research workers and others in these areas with a concentration and scope of communication of ongoing thought and experiment in a degree not provided at present by other professional publications.

Our historical model of reference, chosen to guide us in this work of expansion, is the noble *Crelle's Journal*. That journal contributed a noble and leading part in the fostering of the advancement of science in 19th-century Germany, and, consequently, in the world at large. With a clear general objective in view, but providing a free-wheeling forum for papers and correspondence focused upon the issues, we hope to contribute to acceleration of progress in the three areas, as *Crelle's* contributed centrally to the accomplishments envisioned and steered by Alexander von Humboldt and his collaborators. Even to fall far short of as much as *Crelle's Journal* contributed is a most worthy undertaking.

To aid this catalytic process, our editorial policy includes attention to relevant aspects of the internal history of past science. We must scrutinize the assumptions which habits have embedded in prevailing scientific opinion. Where such an assumption represents an obstacle to fruitful designs of experiment today, it is urgent that we examine the way in which that assumption was adopted earlier; we must find our way back to the point where a wrong choice of axioms was made during the past. We shall be aided to advance with lighter, faster steps, as we discard the shackles of deeply embedded, but wrong-headed and profoundly respected assumptions bequeathed from the past.

In summation, we the publishers, referees, and editors each have our points of view; but, within the area of the subject matters indicated, to those of you working in these areas or fields bearing upon them, we say to you, as *Crelle's Journal* said to the scientific community of its time: "This is your journal, for your use and your advantage. May you be aided to accelerate science's indispensable contribution to the general advancement of the human condition."

Editor's Note

The worldwide scientific community advances as its members share ideas with one another and new ideas are born that dictate new theoretical and experimental work to be done. It is well to listen to all ideas, for the seed of a most fruitful concept may arise from a seemingly insignificant member of the scientific community. The value of a scientist as he or she strives toward a better understanding of the physical and biological universe as created is determined solely through his or her ability to think, observe, interpret, and integrate concepts and ideas and formulate new theories and perform new experiments. Value is not determined by rank, salary, possessions, sex, race, religion, or place of birth, or pride. A good scientist wishes to serve mankind, stimulate creativity, help make life more abundant and full of joy, lift the physical burden and aid in the creation of a better understanding of the physical and biological worlds.

As new discoveries are made that create profound changes and outlook among the peoples of the world, it becomes all too clear that the scientists must engage in an intellectual, spiritual, and moral revolution. In order to accomplish this, scientists may work in their own nation-state or in other nation-states and the fruits of their investigations may be communicated by means of scientific publications or personally in order to share ideas and work together on theory and experiment for the purpose of achieving a greater and more accurate scientific knowledge of the biological and physical worlds.

On the biological side, science has brought about such things as the proper control of many diseases, increased longevity, the correction of some physiological malfunctions, improved nutrition, more accurate and rapid diagnosis and treatment of many diseases, the eradication of nearly all incipient epidemics, and many life-sustaining methods and devices, to name a few. On the physical side, science has led to the development of the new, abundant nuclear energy sources such as fission and fusion; of rapid transportation, communications, and computations; and of the transmission to the Earth of radio signals from a 6-watt nuclear-powered transmitter on a satellite 7 billion miles from the Earth (approximately 75 times the distance of the Earth from the Sun), just to name a few examples.

Such applications of science give man unprecedented power over nature and space. This gift will be a great joy to mankind if society is intellectually, spiritually, and morally deserving of it—otherwise, mankind will have set the stage for the creation of a hell here on Earth and in space. So how much of a hell will come to be before man changes—each and everyone—and makes such plans as are acceptable to God?

New Concepts

In this issue of IJFE are concepts, some new, that it is hoped will spur on the required revolution in scientific thinking.

The classical electron was once a massless, rigid sphere with a massless charge on its surface; the mass of this electron resided in the electric field produced by the charge from the surface of the sphere to infinity. The classical view is still useful, but it fails to completely describe the nature of the electron. Herein, Winston Bostick presents an electron in the form of a continuous right-handed spiral intertwined with a left-handed spiral so as to form a continuous closed circuit through which the electronic charge flows at the velocity of light. This electron has all the properties demanded of an electron, including its longitudinal polarization, as discovered by several investigators in 1957.

This model may at first seem complicated, but as Bostick shows, it is a more complete description of the electron as it is known today.

In contrast, consider the model of the neutrino accepted today by the scientific establishment. The neutrino was born massless by Pauli in 1927 and now in its old age has a mass less than 46 electron volts and takes on the form of a left-handed spiral from its spin of ½ lined up along its direction of motion. At the same time, researchers postulate that from the antiworld the antineutrino forms a right-handed spiral. Thus the neutrino has longitudinal polarization. And yet free neutrinos have not been isolated per se to date. Indeed, how could they be? It would require 10^{18} meters of lead to stop one-half of the neutrinos traveling through it.

The paper in this issue by Erich Bagge, based on his experimental work, indicates that the neutrino concept may be purely a figment of the imagination of high-energy physicists. Do particles in the antiworld have mass or energy that may be drawn upon by the real world at will, or is the real world in a sea of antiparticles of the antiworld, from which energy may be drawn by the real world under very limited conditions such as β emission with energy balance between the two worlds maintained by some other event elsewhere between the two worlds? Experiments indicate that antimatter and matter do not mutually repel each other, but mutually attract. And yet, be this as it may, the antiworld and the real world do not seem ready to instantly destroy each other and create a sea of radiation. It should also be noted

that continued research in high-energy physics requires the development of unlimited sources of energy such as fission and fusion, which logically should have preceded it.

A Geometrical Framework of Physics

Physics has made great strides in the understanding of the physical world by means of relating physical phenomena to a geometrical framework of symmetry, and this is a very important aspect. Early theories and equations of physics reflected the harmony of the world as shown by Kepler's laws, for example. And in the 19th century, E. Galois developed an abstract theory of groups, which was expanded by several others. Leonhard Euler (1752) had recognized the usefulness of the group in physics from a topological viewpoint. Euler proved a simple relation between the number of vertices, V, edges, E, and faces, F, of a convex, three-dimensional polyhedron. This relation is given by the equation $V - E + F = 2$. In the study of crystal structure, A. Bravais showed in the 19th century that there are 14 types of space lattices. This was followed by the work of E.V. Federov (1885) and Schönflies (1891) that showed that the 14 types of lattices combined with 32 point groups with lattice translations and rotations yields 230 possible invariant groups of crystal lattices. All 230 space groups predicted have now been found in various crystal forms—and no more. Contrast this to high-energy physics, where the modifications of invariants—charm, color, beauty, strangeness, up, and down—in describing particles leads away from science and into the realm of epicycles.

Group theory enters physics in a most fundamental way; that is, the *relativity group*, G^{rel}, that shows space-time is a homogeneous manifold upon which G^{rel} acts. G^{rel} is not determined uniquely by the principle of relativity. Three more postulates are needed; that is, (1) a two-coordinate system, where the coordinate system of the observed physical phenomena and that of the observer are at rest, yields the Euclidean group $\mathcal{E}(3)$; (2) the two coordinate systems are allowed to be in relative uniform motion and time remains absolute (this is then the Galilei group, $\mathcal{G}$; and (3) velocity of light has the same speed for all inertial observers (not compatable with absolute time) then this inhomogeneous group, the Lorentz group, also called the Poincaré group, $\mathcal{P}$, is obtained.

These space-time symmetries lead to invariance (symmetries) and the conservation law of particle physics, which deals with time parity, T, reflection (or inversion) parity of space parity, P, reflection of charge (charge conjugation), C, isotopic spin, I, and isotopic parity, G.

Thus, under G^{rel} are the three groups $\mathcal{E}(3)$, $\mathcal{G}$, $\mathcal{P}$ from which to choose the one appropriate to the problem at hand, and the group chosen will be expressed in tensors [or vectors as is the case with $\mathcal{E}(3)$, which consists of all rotations and translations in ordinary Vector Calculus], $\mathcal{E}(3)$, $\mathcal{G}$, and $\mathcal{P}$ each will have a defining matrix representation that is a classification of irreducible tensors that amount to the decomposition of the matrix into its irreducible constitutents. At this state a study might have begun on the representation of G^{rel} but it must be extended to the permutations that act on the indices of the tensors. Perhaps some practical restrictions may be used in addition.

It should be noted further that the three groups above do depend continuously on some parameter and are known as *Lie Groups* after a Norwegian mathematician Sophus Lie. The Lie Group is based upon infinitesimal transformation, linearized multiplication in terms of their coefficients called *infinitesimal generators*, which form a vector space known as *Lie Algebra* and conversely the group can be reconstructed from its algebra. This is important to physics for it contains the essential information that can be extracted from the symmetry of a system; that is to say, the conservation laws it verifies. This connection was formulated by the German mathematicians David Hilbert (1916) and Emmy Noether (1918) as a theorem as follows: "If a LaGrangian theory is invariant under an N-parameter Lie Group of transformation (in the sense of the action integral, I, of the LaGrange function L, i.e., $I = \int L\, dt$ is invariant) then the theory possesses N-conserved quantities." This theorem is a cornerstone of classical physics, and by means of the correspondence principle, of quantum mechanics as well.

The group $\mathcal{E}$ is a six-parameter Lie Group. Its invariant LaGrangian system possesses three invariant components of total momentum and three of angular momentum. Groups $\mathcal{G}$ and $\mathcal{P}$ both have ten parameters and contain $\mathcal{E}$ as a subgroup. The four additional constants of motion are the total energy (Hamiltonian) and the three components of the motion of the center of mass that guarantees that the center of mass moves as a *free particle*.

Since some papers in this issue and in future issues of the IJFE will be concerned about the geometrical framework to which symmetry elements are related through group theory and topology and from which conservation or invariant parameters are determined, then it seems apropos to include these few brief notes on group theory and its development over the past 100 years. These tools have yielded a most fruitful insight into description of the great order and coherence of the nature of the physical and biological world, from the very smallest particle to the Universe itself—as created by God, not as events of chance. The rapidity with which knowledge and its applications have increased yields an ever increasing power to man over nature and the need for a commensurate development of man's intellectual, spiritual, and moral talents. The purpose of this journal is to enhance this process.

—Dr. Robert J. Moon, Editor-in-chief

The Morphology of the Electron

by Winston H. Bostick

Stevens Institute of Technology
Hoboken, NJ 07030
and
University of New Mexico
Air Force Weapons Laboratory
Albuquerque, NM 87106

Abstract—The author's experimental work in plasma physics for the last 36 years has shown that under many different circumstances plasmas containing nonrelativistic or relativistic electrons can spontaneously organize themselves into force-free, minimum-free-energy vortex filaments of a Beltrami morphology. So abundant are these manifestations of nature's ability to create macroscopic filamentary structures that the author has been inspired to try a filamentary model for the electron in order to explain the existence of the de Broglie waves, electron spin (via the Poynting vector), electron mass via electric and magnetic vectors, electron self-equilibrium and stability—ultimately equilibrated by the self-gravity of its own intense electric and magnetic fields. The result is a concept of the electron, photon, and all other elementary onta (never say "particles") that philosophically brings the quantum theory, the prodigal son of physics, back into the family of classical physics.

No vexing self-energy infinities occur. Newtonian lump point mass and lump point charge are banished. Since the electron's charge circulates as a continuous filament it will not radiate as it lies in a stationary atomic state. The concepts of onta of finite rest mass and zero rest mass are geometrically clarified as never before. The correct dispersion relationship for the de Broglie waves of a free electron are geometrically exhibited by the filamentary model with incandescent clarity. Since the model shows how all mass and momentum must be electromagnetic in character, it becomes obvious that all forces—the strong, the electroweak, the gravitational—must be electromagnetic in character. The mysterious strong short-range nuclear force will go the way of the epicycles of Ptolemaic astronomy. It is demonstrated that the de Broglie waves have an analogue in the inertial waves of fluid mechanics.

Introduction

The calculation procedures according to the prescriptions of quantum mechanics or wave mechanics, most of which apply to the behavior of electrons, are highly successful and yield accurate numbers. This author bows before the strain of genius in the human race that has brought about these achievements. The early introduction of simplistic concepts of the point-mass, point-charge electron and the strictly probabilistic wave function was an expediency that enabled the mathematical structure of quantum mechanics to develop to its present useful state.

But the author wishes to enter his philosophical dissent

against the continuation of the unqualified and unquestioningly accepted "portrait" of this mathematical-point electron that is presented in texts and treatises on quantum mechanics. This catechism about the intrinsic nature of the electron has already been perpetuated for more than two generations, the only serious challenge being mounted by Albert Einstein in his friendly arguments with Niels Bohr. It is the author's belief that this catechism on the basic nature of the electron and other *onta* (from the Greek ονται, "existing things, reality, truth"—our improvement on the term *particle*), useful though it has proved to be, represents the weakest philosophical link in that portion of our cosmology that attempts to reconcile quantum physics with classical physics.

The author takes issue with the narrowness and nonphysical nature of Max Born's (Born 1971) interpretation of the quantum-mechanical wave function as merely a "probability wave" $\Psi(z,t)$, where the probability of finding the electron of infinitesimal size between z_1 and z_2 at the time t is given by $\int_{z_1}^{z_2}\Psi\Psi^* dz$, with Ψ^* the complex conjugate of Ψ. Niels Bohr's strong and effective advocacy of this interpretation earned it the name of "the Copenhagen School." Perhaps this school was mesmerized by the Greek name *electron*, whose Greek mystique conjures up something like a smooth sphere of unblemished white marble, like the Ptolemaic "heavenly body," albeit of infinitesimally small radius.

The electron of the Copenhagen School has a lump, leadlike Newtonian mass m that generates a lump momentum mv when the mass has a velocity v. The electron carries an electric charge e that is generally assumed to be uniformly painted on the surface of the sphere, which would cause the electron to have infinitely large self-electrical energy and hence an infinite mass m if its radius r goes to 0. Quantum mechanics (wave mechanics) is built upon the wavelike nature of the electron [discovered theoretically by de Broglie and Einstein (Born 1971, Pais 1983) and confirmed experimentally by Davison, Germer, and Thomson]. In the Compton effect, the electron acts more like a "particle" than a wave as it is bounced away when an X-ray photon collides with it. The electron is thus said to have a Dr. Jekyll–Mr. Hyde type of duality, sometimes behaving like a spherical particle, sometimes masquerading as a wave.

By some mysterious, unknown, unexplained mechanism, this spherical particle is then said to be coupled to an unphysical probabilistic wave that is described by the wave function Ψ (or Ψ^*), which satisfies Schrödinger's wave equation (or Heisenberg's wave mechanics). By some unexplained hokus pokus, completely outside the processes of classical mechanics, this lump mass m is supposed to produce a spin angular momentum equal to $h/4\pi = \hbar/2$, and the spinning charge e somehow produces a magnetic moment $\mu \cong e\hbar/2mc$. The electric and magnetic energies somehow are not very closely related to the mass m.

However, the wavelike properties of the electron as delineated by the Schrödinger equation or Heisenberg's wave mechanics and Dirac's equation are all important in explaining the construction and properties of all atoms and molecules with numbers that agree well with experimentally determined quantities. Because of these spectacular numerical triumphs, all of the philosophical sins of the conception of the electron as a point charge and a point mass are forgiven and forgotten in current acceptance and practice.

This catechism is completely at a loss to give a physical reason for the necessity that all onta have a wave function, why most onta should possess a spin, why most of them should be charged. The catechism has no straightforward, clearly visualizable explanation for the fact that some onta have zero rest mass and others have finite rest mass. The catechism hides behind the "quantum curtain" through which no one is allowed to see. The "quantum curtain" is automatically lowered on the stage of inquiries by the invocation of the Heisenberg uncertainty principle, $\Delta p_x \Delta x \geq \hbar/2\pi$, which is interpreted as saying that an investigator cannot legally entertain fantasies (no matter how attractive) about hidden variables whose dimensions or momenta might be smaller than the limit of Δp_x or Δx set by the Heisenberg principle.

The catechism does not seem at all embarrassed over the fact that it makes no attempt to show that the electron's momentum mv and spin might be associated with its Poynting vector $\mathbf{E} \times \mathbf{H}c/4\pi$, and that its energy (or mass) might be electromagnetic in character, although for the photon, it is conceded that the momentum, spin, and energy must be electromagnetic in character. How can the catechism have the audacity and inconsistency to preach that the Almighty in constructing the elementary onta indulged in the use of two different kinds of mass and momentum, lump and electromagnetic? This inconsistency in itself is sufficiently gross to validate the necessity of making philosophical corrections in the manner in which quantum mechanics is now taught.

Since 1948, the author has been an experimental worker in the field of plasma physics, and beginning in 1954 this work has led to the observation of the spontaneous formation of interesting structures out of ionized gas and magnetic fields, structures that are now called plasmoids. Some of these structures have the shape of barred-spiral and ring-spiral galaxies. Some of these structures have the morphology of the pairs of flux tubes seen in Type II superconductors, and others have some of the char-

An expansion of this work will appear later in book form that shows that similar conceptions work equally well for other elementary onta—the proton, neutron, meson, and so on.

References are given alphabetically following Chapter 3 of the paper and appear in the text in parentheses in name-date style.

acteristic diamagnetic effects of Type I superconductors. Some of these structures can be observed to bounce off one another like billiard balls. Other of these structures are observed to "eat each other up" and accelerate electrons and positive ions to MeV energies (the solar flare effect).

This experimental work, which began at Tufts University and Lawrence Livermore National Laboratory and has since been carried out largely in the Physics Department at Stevens Institute of Technology with the author's colleagues Vittorio Nardi, William Prior, and a number of graduate students, has been amply reported in standard scientific journals and proceedings of conferences of the International Atomic Energy Agency and elsewhere. We recognize that these spontaneously arising structures are force-free, minimum-free-energy structures that have a certain amount of equilibrium and stability, or nature would not have produced them.

It is the author's belief that the emergence of spontaneously arising macroscopic structures in the laboratory that replicate cosmic phenomena, such as barred-spiral galaxies, as well as quantum phenomena, such as superconductivity, represent a stage of unification in our understanding of nature at least as important as the currently much-sought-after "Holy Grail"—the "unification" of the strong forces, weak forces, electromagnetic forces, and gravity.

In 1955, the author began to think along these lines: In plasma physics we can observe nature making spontaneously out of plasma (that is, electrons, positive ions, and magnetic fields) macroscopic structures (plasmoids) that are relatively force-free and minimum-free-energy, that have integrity so that they can bounce off one another, that have sharp boundaries, that have spin and magnetic moment, that can react with one another and give off energy. Why cannot these plasma structures be macroscopic models that suggest the manner in which submicroscopic elementary onta (usually called particles) like the electron might be molded force-free and minimum-free-energy, equilibrated and stable in all frames of reference, out of the electric and magnetic fields?

Our objective is to produce a model of a structure having a physical wave, a wave function Ψ, that preserves the probabilistic properties so dear to quantum mechanics, its complex conjugate Ψ^*, its mass being entirely electromagnetic (as is the photon's), its spin $\hbar/2$ being carried by the Poynting vector (that is, by the electric and magnetic fields), a magnetic moment that can be computed by classical means. Furthermore, we can try to construct a model of the electron that has such a shape and such dimensions that it can be held together by the cohesive forces of the self-gravitational effects of its own concentrated electric and magnetic fields.

This article presents in detail the electromagnetic filamentary model of the electron that the author has developed beginning in 1955. It contains a number of significant improvements and additions beyond the more sketchy treatment published earlier (Bostick 1978).

In Chapter 1 we present the basic construction that yields a "high-fidelity" model of the electron accounting for the rest energy, spin, anomalous gyromagnetic ratio, and dispersion relationships. A heuristic model of the photon is also presented. The elementary hydrodynamics analogue of the electron model is described, and implications for the relationships between c, e, m_e, h, and $\alpha = 1/137$ are discussed. The de Broglie waves are interpreted as transverse "acoustical" waves on the electron filament.

In Chapter 2 we consider the morphology and dynamics of the filamentary electron in a potential well (for example, in an atom). Novel insights are derived into the underlying geometry of the various "energy levels," helping, among other things, to demystify the "Pauli exclusion principle."

In Chapter 3 we describe in detail the spectacular array of spontaneously formed plasma structures observed in the plasma focus and related devices. The creation of these structures in energy-densification processes suggests an invariant, geometrical action-principle reflected in the similar morphology of macroscopic systems (for example, galaxies) and microscopic systems ("elementary particles").

The idea of a spatially extended, dynamic electron has been suggested by a number of authors, including Conant (1978) and Yadava (1976).

The structure of the electron as developed by the author, in contradistinction to the electron of the Copenhagen School, could actually exist. We could call it the *existential* electon. But better than the French *existential* or Greek for the verb "to be," we should use a dynamic, robust, life-possessing Hebrew word. The Hebrew word "to live" in this robust sense is *hayah*, which comes from the same root as the Hebrew toast *l'chaim*—to life! The corresponding Hebrew word for living is *chaiyah* (kī ēē' yah). Let us thus call our living electron the *chaiyah* electron to give it some of the robustness that the Hebrew Jesus must have conveyed to his congregation when he declared in Aramaic, "I am come that ye might have *life* and have it more abundantly!"

We must also choose a suitable name for the general process whereby Nature in spontaneously producing organized structures seems to fly in the face of the famous Boltzmann declaration that "Entropy Strebt nach Maximum" (entropy, or the measure of disorganization in nature, tends to increase to the maximum: water runs downhill, heat flows from high temperature to low temperature, and so on). The term "negentropy" has been coined for this process, but the author feels that "negentropy" is far too inelegant a name for such an elegant and lively process. The author suggests the Hebrew toast, *"L' chaim,"* for this process that brings nature to life and life through nature.

Chapter 1

The *Chaiyah* Electron

In this chapter we shall construct a filamentary model for a *chaiyah* electron in which all momentum, mass, spin, and energy are electromagnetic in origin. The striking similarity between the harmonic characteristics (dispersion relationships) of an electron, on the one hand, and an electromagnetic wave (photon) in a waveguide, on the other, suggests that the electron arises as a singular form of electromagnetic "energy storage." Whereas the photon in the waveguide has been confined by *external* constraints, we must seek a means whereby the electromagnetic energy associated with the electron might be self-confined in a filamentary configuration.

One energy confinement and densification process is well known in plasma physics and electron-beam physics as the "pinch effect": a beam or filament of rapidly flowing charge generates a magnetic field that opposes the explosive Coulomb force between like charges. In the relativistic limit, when the velocity of the charge flow approaches that of light, the "pinch" force exactly cancels out the electric force, and the current channel becomes locally stable and self-confined. One might indeed be tempted to think of an electron as a circular filament in which an evenly distributed negative charge e flows at the speed of light. However, this model fails, among other things, to provide insight into the anomalous relationship observed between electron spin and magnetic moment—the fact that the observed moment is *twice* that which would be expected for a rotating charge having the observed electron spin.

This and other considerations dictate that our electron model must have a richer inner structure, must possess additional degrees of freedom. A clarification is provided by the example of energy storage in a rapidly spinning elastic ring. Here the additional degree of freedom is represented by the elasticity. In this case, when the tangential velocity goes to the speed of light, we find that *only one half* of the stored energy expresses itself in terms

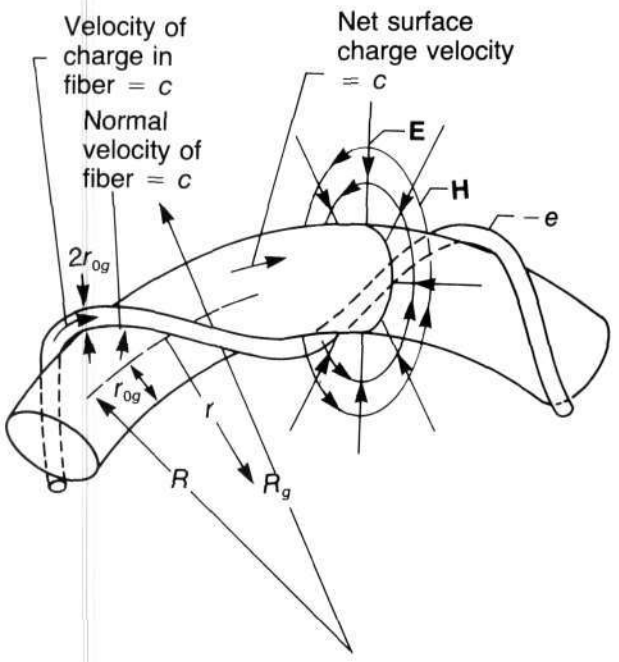

Figure 1. Detail showing the way in which the gravitationally equilibrized, charged fiber produces the surface charge and current for the torus core radius r_0. Note that the surface charge is negative.

of angular momentum; the other half of the energy is stored in the potential energy of elastic deformation of the ring.

Returning to the problem of the electron model, we find that the required "elasticity" for a current filament can be supplied by the self-gravitation associated with the electromagnetic mass of the current configuration, if the filament is configured in the form of a closed helix wound around an imaginary torus (Figure 1). Appropriate choice of parameters makes it possible to match very closely the observed characteristics of the electron. In addition, the famous de Broglie waves now appear as simple transverse deformation waves propagating along the elastic filament.

How Is an Electron Like A Photon and How Not?

Albert Einstein, who invented the photon, wrote in his latter days a letter to O. Klein in which he declared that there were many oafs who thought they understood the photon, but they were deluding themselves. Einstein also stated that before he tried to understand the meson he would like to understand the electron. In an attempt to further our understanding of both the electron and photon let us contemplate their similarities and differences.

Even though the photon is traditionally considered to be an "uncharged particle of zero rest mass" and the electron a "charged particle of finite rest mass," the formal similarities in their dispersion relationships suggest that there is a strong similarity between these "particles" (onta), when the photon is confined to a waveguide, as in Figure 2.

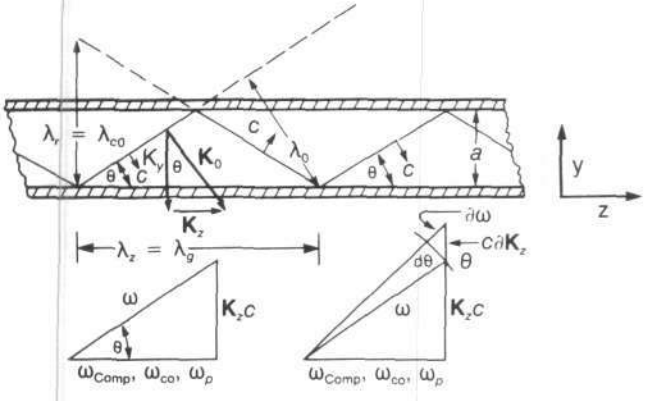

Figure 2. Electromagnetic wave (made up of photons) with free-space wavelength λ_0 propagating in the TE_{01} mode between two parallel plates (a waveguide) at $y = 0$ and $y = a$: $\lambda_z = \lambda_g = \lambda_0/(\sin\theta)$; $v_p = c/(\sin\theta)$; and $c = \lambda_0\nu$. The cutoff wavelength $\lambda_{c0} = 2a$. Wave fronts are shown propagating at a normal velocity c.

For such a waveguide photon we have

$$\omega^2 = \omega_{co}^2 + k_z^2c^2, \tag{1}$$

where ω_{co}^2 is the cutoff frequency $2\pi c/2a$, and $k_z = 2\pi/\lambda_g$, where $\lambda_g = \lambda_z$ is the guide wavelength. The observed energy of the photon (in or out of the waveguide) is $\hbar\omega = h\nu$, where $\nu = \omega/2\pi$ is the observed frequency of the photon as it passes by in the waveguide and also as it flies by in free space. A similar relationship obtains for an electromagnetic wave (photon) propagating in an ionized gas of electron density n_e and plasma frequency $\omega_p = (4\pi n_e^2/m_e)^{1/2}$; in this case

$$\omega^2 = \omega_p^2 + k_z^2c^2, \tag{2}$$

where k_z is the wave number of the wave in the direction of propagation. The dispersion relationships for a photon show that there is a kind of "rest mass energy" for the photon given by $\hbar\omega_{co}$ for the waveguide mode (and $\hbar\omega_p$ for the plasma mode) of propagation. Indeed, for the waveguide case, if we make $\omega = \omega_{co}$, $\lambda_g \to \infty$, $v_g = 0$, the photon (or electromagnetic wave) will be boxed up inside the cavity with *no net* momentum in any direction. The photon's energy in this mode is all "rest mass energy" and can be determined by weighing the cavity before and after the photon is placed inside the resonant cavity. One is weighing the energy of the photon or the electromagnetic wave, and it is perfectly straightforward to assume that all of this energy is contained in the **E** and **H** vectors. Thus, there is no necessity to invoke the assumption of Newtonian lump mass or lump momentum for the photon.

For the electron, in comparison, we have

$$\omega^2 = \omega_{Comp}^2 + k_z^2c^2, \tag{3}$$

where $\omega_{Comp} = m_ec^2/\hbar$ is the Compton frequency and $k_z = 2\pi/\lambda$ (with $\lambda = h/mv = h/p$ the de Broglie–Einstein wavelength). The total energy of the electron is $mc^2 = \hbar\omega = h\nu$, where $\nu = \omega/2\pi$ is the observed frequency of the electron as it passes by with a velocity v. The electron dispersion relationship corresponds exactly to Einstein's formula for the relativistic electron mass:

$$m = m_{0e}/\sqrt{1 - (v/c)^2} \tag{4}$$

or

$$(mc^2)^2 = (m_ec^2)^2 + (mvc)^2, \tag{5}$$

where $mc^2 = \hbar\omega$ is the total energy and $m_ec^2 = \hbar\omega_{Comp}$ is the rest energy of the electron.

Now, if an entity like a photon or an electromagnetic wave, when boxed up in a waveguide or resonant cavity, can have a "rest energy," as does the electron, can one create a model of a *chaiyah* electron that exhibits some of the characteristics of a boxed-up photon or an electromagnetic wave in a guide? One must recognize that such a model must embody an electric charge, a spin ½, a

magnetic moment, and an anomalous gyromagnetic ratio.

In attempting to construct such a model we shall search for some broad philosophical, global, guiding principles such as those employed by Einstein in his formulation of special relativity: Since we observe the electron to live as a stable entity in a variety of frames of reference, we shall, as much as possible, search for a model of the electron that is in equilibrium and is stable in all frames of reference. This *chaiyah* criterion will be the first of our guiding principles, and we might add that such a principle has been largely ignored heretofore in all models of elementary onta in which the onta are assumed to be mathematical points.

Our second guiding principle will be that all energy, mass, and momentum must be electromagnetic in character as it is in an electromagnetic wave and also in a photon. There should be no Newtonian "lump" mass or "lump" momentum. Our third guiding principle will be that the de Broglie–Einstein waves and the wave functions Ψ and Ψ^* of quantum mechanics should have more than the Born probabilistic interpretation: The wave functions should have a physical reality, like transverse waves on a tensioned string, for example. Indeed, the author is obliged to concede that the only way he can accomplish these aforestated *chaiyah* objectives is through a filamentary model of the electron.

The construction of a filamentary electron model stems from a rationale to which the founding fathers of quantum mechanics (Bohr, Born, Schrödinger, Heisenberg, de Broglie, Einstein, and others) were not privy. This rationale is based on fairly recent experimental results (Bostick 1956, 1957, 1958, 1977; Bostick, Nardi, and Prior 1972a, 1972b, 1980; Bostick et al. 1966; Laurence 1956; Wells 1976) concerning plasmoids—minimum-free-energy, equilibrium structures with a certain degree of stability. These structures spontaneously spring into existence in high-energy-density, magnetized plasmas. This rationale is a compelling reason for constructing an electron model out of a filament (rather than conceptualizing it as a point or a sphere, for example): the observed macroscopic, spontaneously arising structures for carrying current in a plasma are *thin vortex filaments*. In a plasma where the electrons are relativistic, these filaments have been observed to have diameters as small as 0.2 μm. The condensation of energy density and plasma density into these current-carrying filaments is essentially a phase-transition phenomenon, as is superconductivity in metals. The formation of a *chaiyah* electron or a *chaiyah* photon out of electric and magnetic fields would be an analogous type of phase transition.

The Elastic Flywheel Model

In considering a model for the energy storage in onta like the electron, let us contemplate first the storage of both kinetic energy $\frac{1}{2}m_0v^2$ and elastic potential energy $\frac{1}{2}k(2\pi R)^2$ in the rim of a perfectly elastic flywheel (Figure 3), where m_r is the mass of the rim and k is the elastic spring constant of the rim. It can be shown easily that for an equilibrium radius, $\frac{1}{2}m_0v^2 = \frac{1}{2}k(2\pi R)^2$; that is, the virial theorem holds.

The elastic rim on the elastic flywheel could be visualized as a toroidal, massless elastic sausage casing with a spring constant k, in which the sausage meat of mass m_0 circulates without friction with a velocity v. We shall assume that the initial radius $R_0 = 0$.

An interesting example evolves in the relativistic gedanken experiment where the velocity of the sausage meat v approaches the speed of light c. Then the kinetic energy $mc^2 - m_0c^2$ approaches mc^2, where $m = \gamma m_0$; $1/\gamma = \sqrt{(1 - \beta^2)}$, $\beta = v/c$, $\gamma \gg 1$, and $\frac{1}{2}k(2\pi R)^2$, the elastic potential energy, still equals the kinetic energy. The total energy then approaches $2mc^2$. If a student picks up the torus and weighs it on the scale, he will record a weight of $2m$. If his physics teacher asks him to compute the angular momentum of such an effective relativistic mass $2m$ traveling at the speed $v \to c$ at a radius R, he will say that the angular momentum (or spin) s is equal to $2mcR$. However, we know that he is wrong because the elastic potential energy that contributes to the total energy does not contribute to the spin. We know, there-

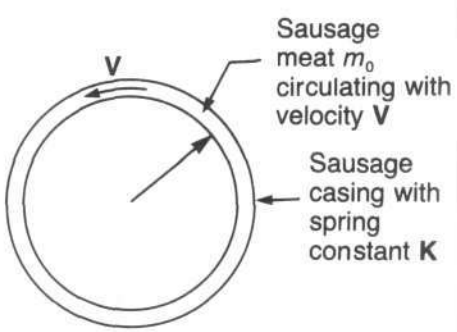

Figure 3. The perfectly elastic flywheel.

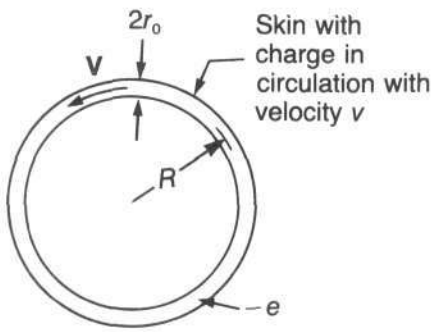

Figure 4. The transformation of Figure 3 into an electromagnetic flywheel. The diameter of the thin toroidal shell is $2r_0$, and the radius of the toroid measured from the center is R.

fore, that the spin is only mcR, not $2mcR$, and we could say, therefore, that the spin is ½; that is, just one half of what one naively would expect. The elastic containing force enables equilibrium to be attained (that is, it holds the torus together) and in doing so causes the spin to be half.

Let us now construct the electromagnetic counterpart of the mechanical meat-sausage-casing flywheel of Figure 3.

Suppose the toroidal sausage casing consists of a massless superconductor (thin toroidal shell) that has a linear spring constant k. We charge the casing uniformly with a massless charge $-e$ that circulates with a velocity $v = c$ in the toroidal direction. The concept of the charge and its circulation are invoked merely to generate the electric field $\mathbf{E}$ and magnetic field $\mathbf{H}$ in the region $r_0 < r \lesssim R$ in Figures 4 and 5. The energy and angular momentum are stored in these vectors and (largely) in this space.

The total electromagnetic energy E for $r_0 \ll R$ is given approximately by

$$E \cong 2\pi R \int_{r_0}^{R} \frac{(|\mathbf{E}|^2 + |\mathbf{H}|^2)}{8\pi} \cdot 2\pi r\, dr \qquad (6)$$

$$= \frac{e^2}{\pi R} \ln\left(\frac{R}{r_0}\right) = mc^2,$$

where $|\mathbf{E}| = |\mathbf{H}| = e/\pi r R$ cgs. The current is $ec/2\pi Rc = e/2\pi R$.

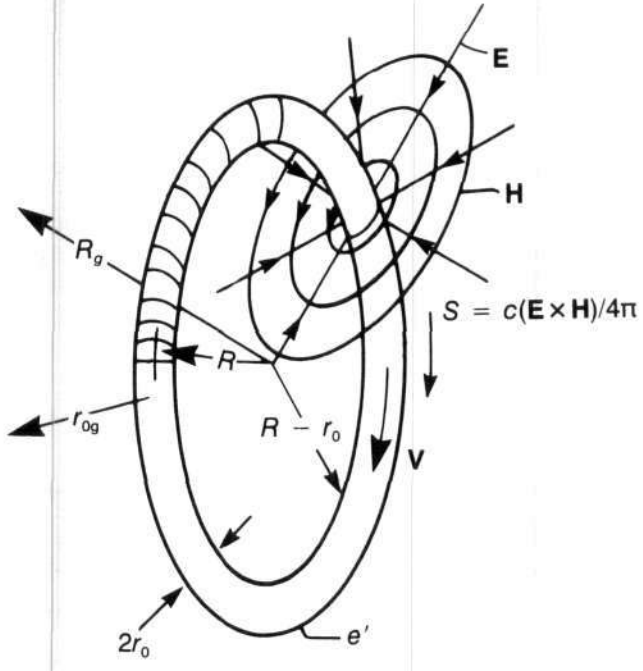

Figure 5. The electromagnetic flywheel with **E** and **H** vectors.

It is crucial that the charge e circulate at $v = c$ so that $\mathbf{E}$, which tends to explode the channel by increasing r_0, is perfectly balanced by $\mathbf{H}$, which tends to compress the channel about r_0. It is crucial that the charge be distributed in a *continuous filament* so that it does not radiate (by synchrotron radiation) as it is centripetally accelerated.

The Poynting vector $\mathbf{S} = c(\mathbf{E}\times\mathbf{H})/4\pi$ carries the angular momentum or spin, and this spin is given by

$$2\pi R \cdot R \int_{r_0}^{R} \frac{(|\mathbf{E}| \times |\mathbf{H}|)}{4\pi c} (2\pi r\, dr) \cong \frac{e^2}{\pi c} \ln\left(\frac{R}{r_0}\right)$$

$$= mRc.$$

The elastic potential energy $\frac{1}{2}k(2\pi R)^2$ stored in the elastic casing is equal to the electromagnetic energy E, so that the total energy stored in the ring is $2mc^2 = m_T c^2$, and the mass of the ring, if weighed on a scale, is $m_T = 2m = 2E/c^2$. However, the angular momentum or spin is mRc and not $2mRc$ ($= m_T Rc$), and hence the spin can be said to be ½.

The Filamentary Electron

The ultimate examples in high-density electromagnetic energy storage are the elementary onta, for example, the electron. We shall now show that the model of Figures 4 and 5, when given the appropriate microscopic dimensions for the electron, accounts for the electron's rest energy, the spin $\hbar/2$, the "double" magnetism, and the anomalous gyromagnetic ratio, approximately equal to $e/2m_e c \cdot 2(1 + \alpha/2\pi)$, where $\alpha = e^2/\hbar c = 1/137$.

If we set the spin of the torus of Figure 5 equal to the spin of the electron, $\hbar/2$, where $\hbar = h/2\pi$, and h is Planck's constant,

$$\hbar/2 = (e^2/\pi c)\,[\ln(R/r_0)] = \text{spin}. \qquad (8)$$

Here $e^2/\hbar c = (\pi/2)/\ln(R/r_0) = 1/137 = \alpha$, the fine-structure constant. The charge $-e$ is now the electron's charge.

If the monopole electric energy ΔE in the spherical region (see Figure 5) of radius $R_g \geqslant 2\pi R$ is added to $2E$ to obtain the new total energy $E_1 \equiv 2(E + \Delta E)$, the new total mass $m_1 = 2(E + \Delta E)/c^2$, where $\Delta E \cong e^2/4\pi R$, and thus

$$m_1 \cong \frac{2e^2}{\pi R c^2} \ln\left(\frac{R}{r_0}\right)\left(1 + \frac{1}{4\ln(R/r_0)}\right) \qquad (9)$$

$$= 2m\left(1 + \frac{\alpha}{2\pi}\right).$$

Since the magnetic field falls off as a dipole field in the region $R_g \geqslant 2\pi R$, this ΔE makes essentially no contribution to the spin, although it does contribute to the total

energy and hence to the total mass m_1; that is, in the region $R_g \geq 2\pi R$, the Poynting vector vanishes.

The current in the torus is $e/2\pi R$ and the magnetic moment of the torus is $\mu = \pi R^2 i = eR/2$ (cgs). The magnetic moment for the electron can be written as $\mu_e = e\hbar k'/2m_e c$, where k' is a constant approximately equal to 1, now to be evaluated in terms of the torus. If we put μ for the torus equal to μ_e and $m_1 = m_e$, the electron mass,

$$\frac{e\hbar k'}{2m_1 c} \cong \frac{e\hbar k'}{2 \cdot 2m(1 + \alpha/2\pi)} = \frac{eR}{2}, \tag{10}$$

$$R = \frac{\hbar k'}{2m\left(1 + \frac{\alpha}{2\pi}\right)c}, \tag{11}$$

and

$$\frac{\hbar}{2} = mRc = \frac{m\hbar k' c}{2m(1 + \alpha/2\pi)c}, \tag{12}$$

with

$$k' \cong 1 + \frac{\alpha}{2\pi}. \tag{13}$$

Thus the gyromagnetic ratio for the torus is given by

$$g = \frac{\mu}{s} = \frac{e\hbar k'/2m_1 c}{\hbar/2} \cong \frac{2e}{2m_1 c}\left(1 + \frac{\alpha}{2\pi}\right), \tag{14}$$

which is of the same form as that for the second-order correction for the electron. In determining $\Delta E = e^2/4\pi R$, the region $R_g \geq 2\pi R$ (see Figure 5) was obviously very roughly estimated. For the torus $\alpha = (\pi/2)/\ln(R/r_0)$ and

$$R \cong \frac{\hbar}{m_1 c} = \frac{\lambda_c}{2\pi},$$

where λ_c is the Compton wavelength of the electron.

The electron model of Figure 5 also exhibits quantization of magnetic flux θ. For the torus of core radius r_0 and large radius R

$$\theta \cong 2\pi R \int_{r_0}^{R} |\mathbf{H}|\, dr = 2\pi R_0 \int_{r_0}^{R} \frac{e\, dr}{\pi r R} \tag{15}$$

$$= 2e \ln\left(\frac{R}{r_0}\right) = \frac{\pi\hbar c}{e} = \pi \text{ fluxons}$$

since $e^2/\hbar c = (\pi/2)/\ln(R/r_0)$ and one fluxon equals $\hbar c/e$.

Thus the energy storage in the model of Figure 5 becomes a high-fidelity analogue of the electron itself.

This electron at rest thus has no net momentum in any direction. It behaves like an electromagnetic wave that is "guided" by the circulating toroidal charge into a circle and therefore is trapped, like a photon in a resonant cavity. And the frequency corresponding to this electron's rest mass is

$$\nu_0 = \frac{c}{2\pi R} = \frac{c}{\lambda_{\text{Comp}}} = \frac{c(m_{0e}c)}{h}$$

$$= \frac{m_{0e}c^2}{h} \qquad \text{and } h\nu_0 = m_{0e}c^2.$$

We now address ourselves to the construction of a "sausage casing" that can have a tensile strength in the toroidal direction (Bostick 1978; there are some mistakes in reasoning in this reference that the author hopes he has corrected here). Consider a charged toroidal thread of the same general form as Figure 5, where the large radius is R_g, the small radius r_{0g}, and the charge $-e$ is circulating with $v = c$. The values of r_{0g} considered here are much smaller than r_0.

$$|\mathbf{E}| = |\mathbf{H}| = e/\pi r_g R_g \qquad \text{for } r_{0g} < r_g < R_g. \tag{16}$$

The electromagnetic field energy of this torus is

$$E_f \cong \frac{e^2}{\pi R_g} \ln\left(\frac{R_g}{r_{0g}}\right); \ln\left(\frac{R_g}{r_{0g}}\right) \gg 1. \tag{17}$$

The energy density ${}_dE_f$ of this electromagnetic field is

$${}_dE_f = \frac{1}{8\pi}(|\mathbf{E}|^2 + |\mathbf{H}|^2) = \frac{1}{4\pi}\frac{e^2}{\pi^2 R_g^2 r_g^2}. \tag{18}$$

The mass density ρ associated with this electromagnetic field is

$$\rho(r_g) = \frac{1}{4\pi c^2} \cdot \frac{e^2}{\pi^2 R_g^2 r_g^2}. \tag{19}$$

By Gauss's theorem the gravitational field f_g associated with this spatial distribution of e can be calculated thus:

$$2\pi r_g f_g = 4\pi G \int_{r_{0g}}^{r_g} 2\pi r_g \rho\, dr_g$$

or

$$f_g = \frac{e^2 G}{\pi^2 c^2 R_g^2 r_g} \ln\left(\frac{r_g}{r_{0g}}\right). \tag{20}$$

The gravitational constant, G, is equal to

$$6.67 \times 10^{-8} \text{ dyne cm}^2 \text{ gm}^{-2}.$$

The energy density ${}_dE_g$ associated with this gravitational field is

$$ {}_dE_g = \frac{-f_g{}^2}{8\pi G} = \frac{-G}{8\pi}\left(\frac{e^4}{\pi^4 c^4 R_g{}^4 r_g{}^2}\right) \ln^2\left(\frac{r_g}{r_{0g}}\right). \quad (21) $$

The total energy E_g in this spatial distribution of ${}_dE_g$ is

$$ \begin{aligned} E_g &\approx -2\pi R_g \int_{r_{0g}}^{R_g} {}_dE_g 2\pi r_g dr_g \\ &\approx -2\pi R_g \int_{r_{0g}}^{R_g} \frac{2\pi G e^4 \ln^2 (r_g/r_{0g}) dr_g}{8\pi \cdot \pi^4 c^4 R_g{}^4 r_g} \quad (22) \\ E_g &\approx -\frac{Ge^4}{6\pi^3 c^4 R_g{}^3} \ln^3\left(\frac{R_g}{r_{0g}}\right). \end{aligned} $$

Overall equilibrium between the expanding forces in the filamentary direction due to E_f and the contracting forces in the filamentary direction due to E_g occurs when $|E_g| = |E_f|$, or

$$ \frac{e^2}{\pi R_g} \ln\left(\frac{R_g}{r_{0g}}\right) = \frac{Ge^4}{6\pi^3 c^4 R_g{}^3} \ln^3\left(\frac{R_g}{r_{0g}}\right) \quad (23) $$

which gives

$$ \ln\left(\frac{R_g}{r_{0g}}\right) = \frac{6^{1/2}\pi c^2 R_g}{eG^{1/2}}. \quad (24) $$

On the other hand, local equilibrium in force density will occur at the value of r_g where ${}_dE_f = |{}_dE_g|$ or

$$ \frac{e^2}{4\pi^3 R_g{}^2 r_g{}^2} = \frac{Ge^4}{8\pi^5 c^4 R_g{}^4 r_g{}^2} \ln^2\left(\frac{r_g}{r_{0g}}\right) $$

or where

$$ \ln\left(\frac{r_g}{r_{0g}}\right) = \frac{2^{1/2}\pi c^2 R_g}{eG^{1/2}}. \quad (25) $$

If we take R_g, for example, to equal $R = \hbar/m_0 c$, the Compton wavelength divided by 2π, then

$$ \ln\frac{R_g}{r_{0g}} = 1.2 \times 10^{17}, $$

$$ \frac{R_g}{r_{0g}} = e^{1.2 \times 10^{17}} = 10^{5.2 \times 10^{16}}. $$

The particular value ($\equiv {}_e r_g$) of r_g at which local force density equilibrium occurs is given by

$$ \frac{\ln (R_g/r_{0g})}{\ln ({}_e r_g/r_{0g})} = 3^{1/2} = 1.73 $$

or

$$ \begin{aligned} \frac{{}_e r_g}{r_{0g}} = \left(\frac{R_g}{r_{0g}}\right)^{1/1.73} &= (e^{1.2 \times 10^{17}/1.73}) \\ &= e^{0.69 \times 10^{17}} = 10^{3 \times 10^{16}} \end{aligned} $$

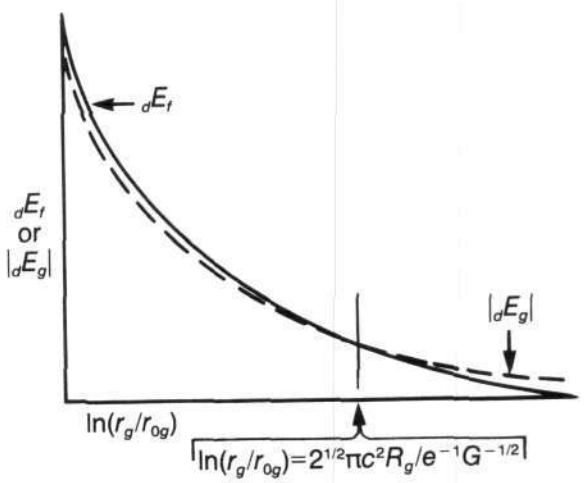

Figure 6. Plot of $|{}_dE_f|$ and $|{}_dE_g|$ as a function of $\ln(r_g/r_{0g})$ (not to scale).

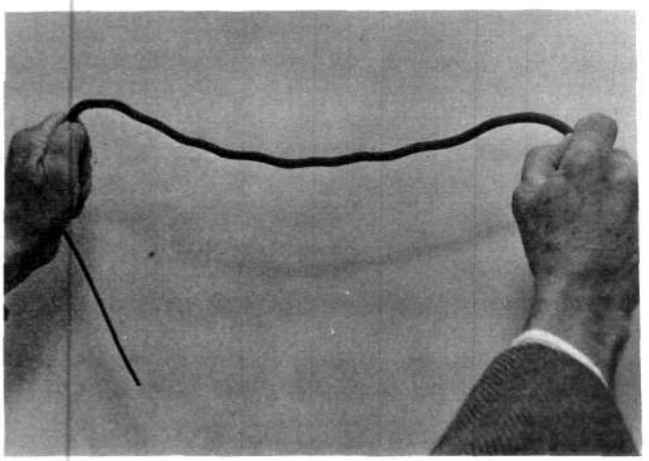

Figure 7. The helical equilibrium configuration formed by a rubber rod under lengthwise compression inside a rubber hose under lengthwise tension.

and

$$\frac{R_g}{{}_e r_g} = 10^{2.2 \times 10^{16}}. \tag{26}$$

A plot of ${}_dE_f$ and $|{}_dE_g|$ as a function of $\ln(r_g/r_{0g})$ would look something like Figure 6 (not to scale), where it can be seen that

$${}_dE_f > |{}_dE_g| \quad \text{for } \ln\left(\frac{r_g}{r_{0g}}\right) < \frac{2^{1/2}\pi c^2 R_g}{eG^{1/2}} \tag{27}$$

and

$${}_dE_f < |{}_dE_g| \quad \text{for } \ln\left(\frac{r_g}{r_{0g}}\right) > \frac{2^{1/2}\pi c^2 R_g}{eG^{1/2}}. \tag{28}$$

The overall gravitationally equilibrized filament, therefore, will behave like a rubber rod inserted through the hole in a rubber hose; the rod is under compression and the hose is under tension. If the rod is free to twist inside the hose, the ensemble will assume a helical configuration as shown in the photograph in Figure 7. Thus, we can expect this massless ($E_g = -E_f$), gravitationally equilibrized fiber to assume a helical configuration as shown in Figures 1, 8, and 9. The locus of this fiber becomes the torus of small radius r_0, and the net velocity c of the charge $-e$ in the toroidal direction (for the torus of Figures 1, 5, 8, and 9) is the result of the circulation velocity of c along the helical, gravitationally equilibrized fiber and the local normal velocity of this helical fiber on the surface torus of small radius r_0. The helical fiber thus becomes the massless helical spring ("sausage casing") with the spring constant k to give equilibrium to the torus of Figure 5 against expansions of R, to make the total mass $m_T \cong 2m$, and give spin ½. Now

$$E_f = |E_g| = \frac{e^2}{\pi R_g} \ln\left(\frac{R_g}{r_{0g}}\right)$$

$$= \frac{e^2}{\pi R_g} \cdot \frac{6^{1/2}\pi c^2 R_g}{eG^{1/2}} = \frac{6^{1/2} e c^2}{G^{1/2}} \tag{29}$$

$$E_f = |E_g| = 2.7 \times 10^{15} \text{ erg}$$

$$= 1.7 \times 10^{27} \text{ eV} \cong 3 \times 10^{21} \text{ electron masses},$$

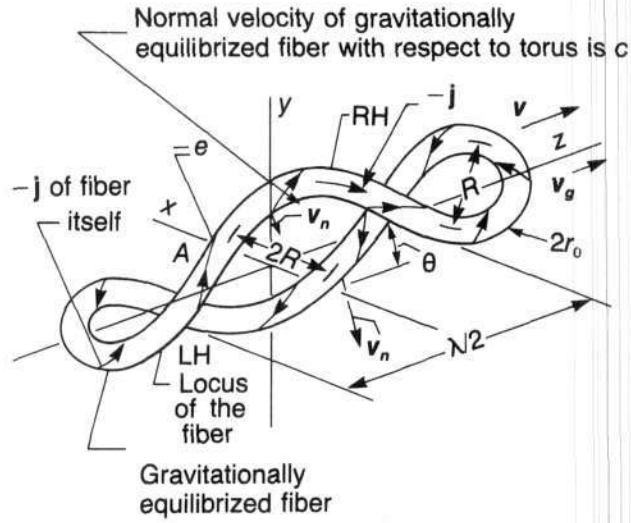

Figure 8. The helical configurations assumed by the torus of core radius r_0 when it is projected at a velocity v_g with respect to an observer. Note that $v_n = c$ and $v = c$.

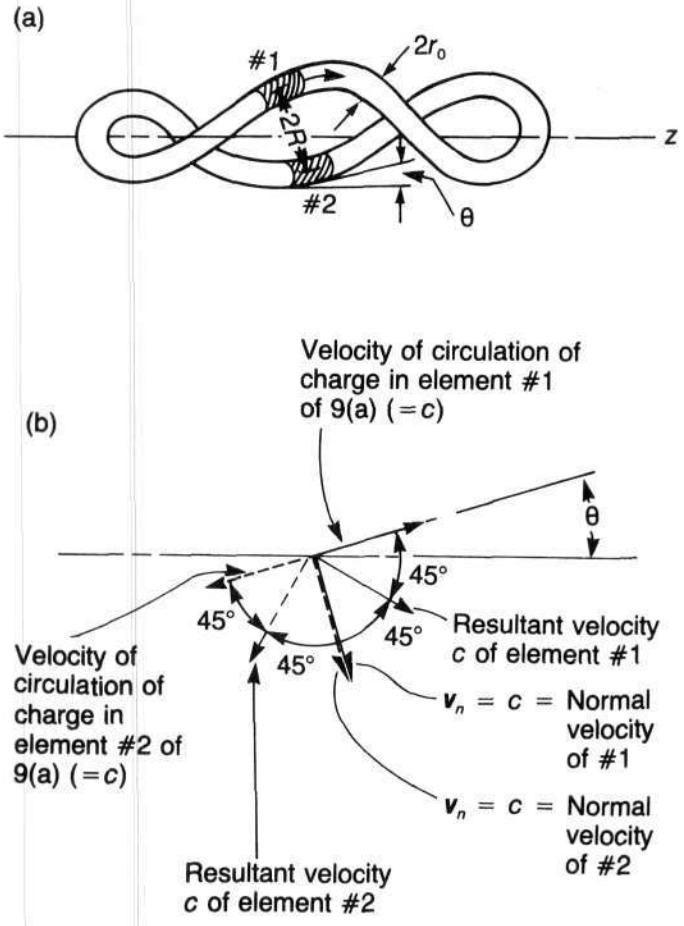

Figure 9. Illustration showing how the two segments 1 and 2 in the configuration of Figure 8 have no net Lorentz force on one another because their resultant currents are mutually perpendicular. In the vortex analogue these two segments will keep their spacing $2R_v$ only if they both have their normal velocities equal to $v_1 r_1/2R_v$.

which is large but not infinite, and $E_f + E_g = 0$, so that these two giants are exactly in balance. The value of

$$\ln (R_g/r_{0g}) = 1.2 \times 10^{17} \tag{30}$$

and if we take R_g to be equal to R, the Compton wavelength divided by 2π, r_{0g} is much smaller than r_0 and can provide essentially a skinlike charge on the torus of small radius r_0. The torus of Figure 5 is in neutral equilibrium for perturbations in r_0 because $|\mathbf{E}| = |\mathbf{H}|$. It should, therefore, not be subject to the sausage and kink instabilities of pinch-effect fame.

The stress (in dynes per centimeter squared or tons per centimeter squared) of this gravitationally equilibrized fiber is fantastically large. For the gravitationally equilibrized fiber of radius r_{0g} whose locus makes the torus of small radius r_0 and whose configuration supplies the spring constant k for the electron, we can calculate the gravitational tension in the fiber necessary to equilibrize the gravitational attractive force (tensile force along the fiber) with explosive electromagnetic force that tends to tear the fiber.

The value of

$$|E_g| = E_f = ec^2/\sqrt{G} = 2.7 \times 10^{15} \text{ erg.} \tag{31}$$

The tension can be roughly computed to be $E_f/2\pi R = 1.2 \times 10^{24}$ dynes $= 1.2 \times 10^{16}$ metric tons.

The importance of this type of model for elementary onta is being recognized by the elementary particle physicists who are using models based on the "theory of light strings" to describe hadrons when they speak of tensions of 13 tons in the strings (Schwarz 1975).

De Broglie–Einstein Waves as Transverse Waves on the Electron Filament

The propagation speed of a transverse wave that could be propagated on the toroidal tensioned filament of Figures 1, 4, and 5 is given by [tension/(mass per unit length)$^{1/2}$] $= (m_0c^2/2\pi R)^{1/2}/(m_0/2\pi R)^{1/2} = c$. When such a "rest energy" torus as that of Figures 1, 4, and 5 is projected with a velocity v_g with respect to the observer it is quite conceivable that there will be excited transverse waves that are the observed de Broglie–Einstein waves. As a heuristic or intuitive guide concerning the shape the torus with a group velocity v_g would assume, let us contemplate a fluid-mechanical analogue of the torus of Figure 5, namely, a toroidal vortex where the vortex lines are under tension. As we shall show later in this chapter, the magnus forces on such a toroidal vortex projected through the background fluid medium in a direction lying in the plane of the torus will distort the toroidal vortex into a shape similar to that shown in Figures 8, 9, 10, and 11 in order for the configuration to be an equilibrium configuration.

This fluid-mechanical analogue heuristically suggests that the simple *chaiyah* electron model of Figure 5, when projected with a velocity v_g in the plane of the torus, is obliged to assume the dynamic configuration of Figures 8, 9, 10, and 11 if it is to be an equilibrium configuration. In the waves that occur on the filament of Figures 8 through 11 the most appropriate choice for the normal velocity v_n of the filament is $v_n = c$. As we shall show, this choice gives the desired dispersion relationship of Eqs. (1) and (3). It is required that $v_n = c$ if the group velocity v_g is to be $c(\sin\theta)$ and $v_p = c/(\sin\theta)$ as they are for a photon or electromagnetic wave in a waveguide and for a de Broglie–Einstein wave.

The configuration of Figures 8, 9, 10, and 11 is very complex, and it is far beyond the mental resources of this old experimentalist to produce an analytic proof of its equilibrium and stability. The tensile force that arises from the helical, springlike, gravitationally equilibrized fiber is still there in the filament. It is possible at least to make the following simple statement about the two shaded filament segments shown in Figure 9(a). Figure 9(a) shows two shaded filament segments (of the configuration of Figure 8) that remain separated at the same distance $2R$ from one another. Figure 9(b) shows the resultant velocity of each of these elements of length. Each resultant is the sum of the velocity c of circulation of the charge within the filament and the normal velocity $v_n = c$ of the filament, which gives rise to the de Broglie–Einstein waves. The two resultant velocities of the charges on the two shaded elements of length are perpendicular (one to the other) and therefore cannot exert any Lorentz force on one another.

It is the normal velocity $v_n = c$ everywhere in the two helical configurations of Figure 8 that gives rise to the phase velocity $v_p = c/(\sin\theta)$ and the group velocity $v_g = c(\sin\theta)$ and to the two wave functions

$$\Psi \cong R \exp[i(\omega t - kz)]$$

and

$$\Psi^* \cong R \exp[-i(\omega t - kz)]$$

which are solutions to the Schrödinger wave equation (see Chapter 2) for a free electron (one that is not constrained by any potential well). We choose to let the wave function Ψ represent the left-handed helix of Figures 8 and 9(a) in the following manner: a snapshot of Ψ at a time t is shown in Figure 10(a), where the axis of the left-handed helix is the z axis and the two axes perpendicular to the z axis are x and iy. Figure 10(b) is the wave function Ψ^*, which is the right-handed helix.

At a given value of z the wave functions Ψ and Ψ^* represent the displacements of the tip of the vectors $x \pm iy$ rotating as shown in Figure 10(c) in time with the frequencies ω and $-\omega$. This rotation of these vectors $x \pm iy$ is the result of a *simultaneous translation* of the

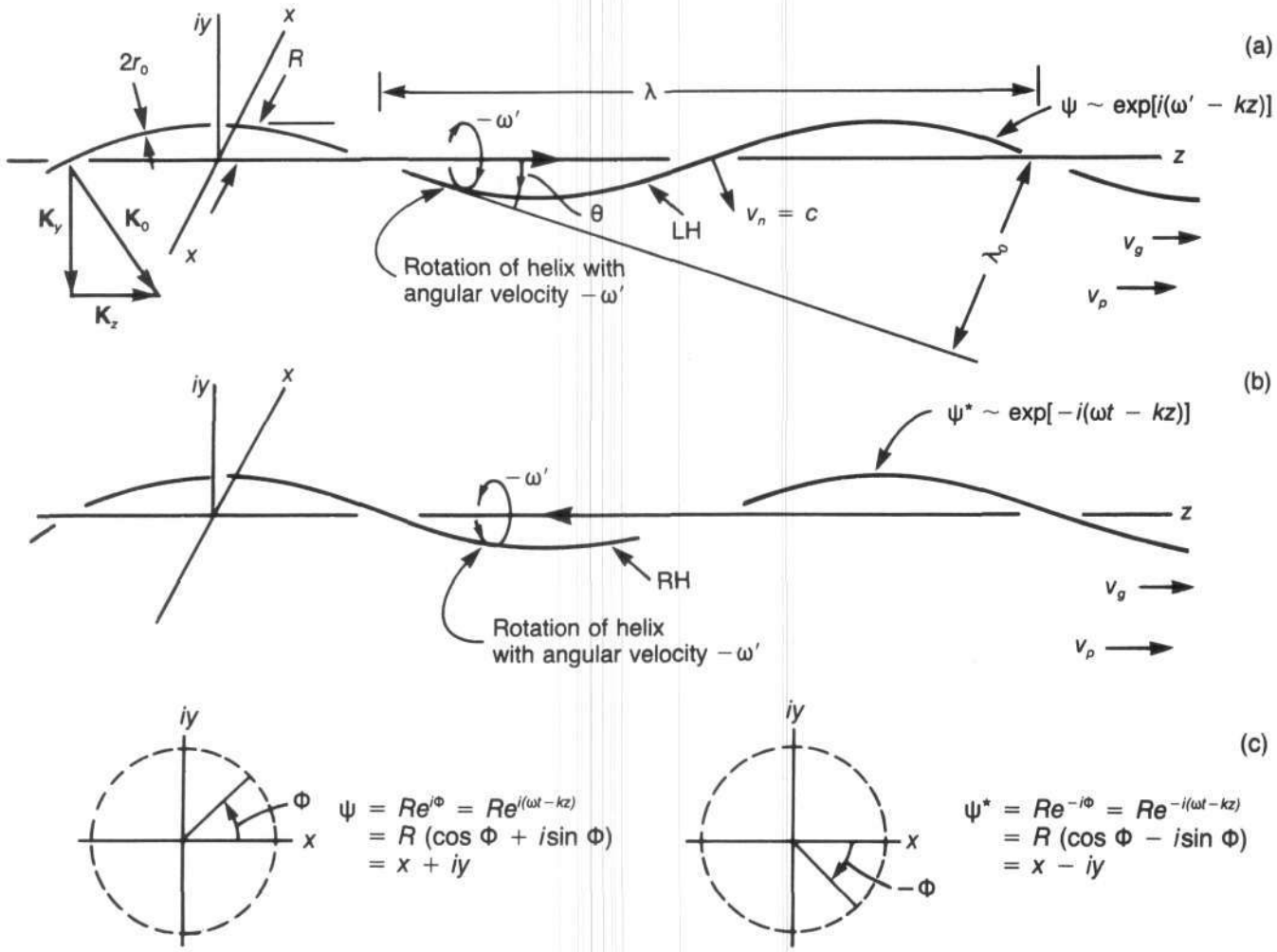

Figure 10. Illustration of how the wave functions Ψ and Ψ^* are the animated configurations of Figures 8 and 9(a).

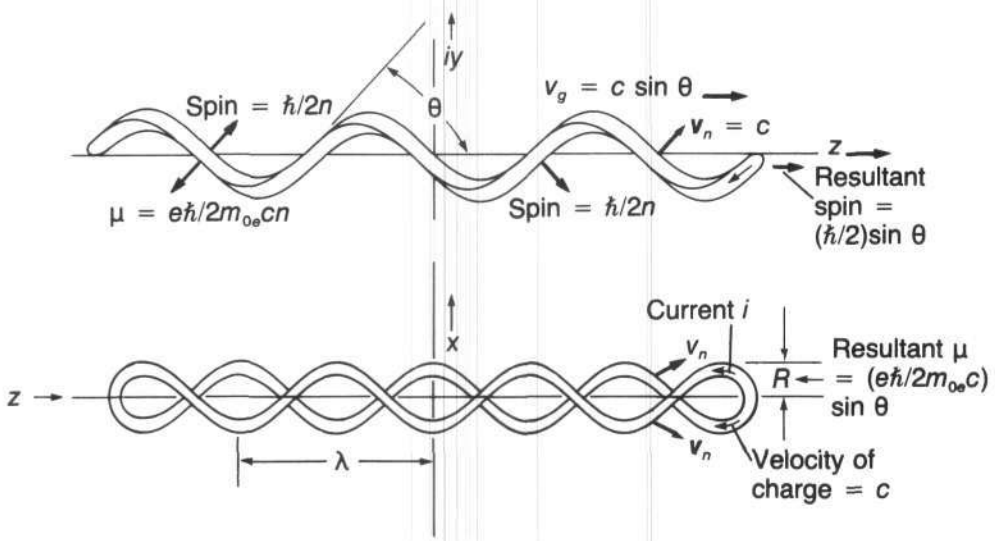

Figure 11. Elaboration of Figure 10 showing distributed nature of spin and gyromagnetic ratio μ, where n is the number of half wavelengths.

helices of Figures 10(a) and 10(b) in the z direction and a *rotation* of the helices at angular frequencies of ω' and $-\omega'$ (not to be confused with ω). At a fixed value of time the vectors $x \pm iy$ again rotate as shown in Figure 10(c) with variations in z, where $k = 2\pi/\lambda$. The simultaneous translation and rotation of the helices is required to produce the normal velocities $v_n = c$ that are required by the form of Ψ and Ψ^* for de Broglie–Einstein waves. The resultant wave functions Ψ and Ψ^* based on the motion of these helices then have $v_g = c/(\sin\theta)$, $v = c/(\sin\theta)$, $v_g v_p = c^2$, and $\omega = v_p k$, and the required dispersion relationship of Eq. (4). It is to be emphasized that the frequency of the wave functions Ψ and Ψ^* observed in the laboratory is ω and that this ω is not to be confused with ω'.

It can be noted from Figures 8, 10, and 11 that

$$\lambda = \int d\lambda = \frac{R}{\tan\theta}\int_0^{2\pi} d\phi = 2\pi\,\frac{R}{\tan\theta}. \tag{32}$$

Now since $v_g = c\sin\theta$ and since $R = \hbar/m_{0e}c$, where m_{0e} is the rest mass of the electron,

$$\lambda = \frac{2\pi R}{\tan\theta} = 2\pi R\,\frac{\cos\theta}{\sin\theta} = \frac{2\pi R\sqrt{1-\sin^2\theta}}{\sin\theta}$$

$$= \frac{h}{m_{0e}c}\,\frac{\sqrt{1-(v_g/c)^2}}{v_g/c} \tag{33}$$

$$= \frac{h}{m_{0e}v_g/\sqrt{1-(v_g/c)^2}} = \frac{h}{m_e v_g} = \frac{h}{\gamma m_{0e} v_g}$$

where

$$m_e = m_{0e}/\sqrt{1-\beta^2} = \gamma m_{0e}$$

$$\beta = v_g/c, \qquad \text{and} \qquad \gamma = (1-\beta^2)^{-1/2}.$$

Thus also

$$\nu\lambda = v_p = c^2/v_g = c^2 m_e\lambda/h$$

or

$$h\nu = m_e c^2. \tag{34}$$

Note that

$$\gamma = 1/\cos\theta = \sec\theta. \tag{35}$$

This model of the electron thus comes forward with a derivation of the most famous of all energy-storage relationships; that is, that the total energy $m_e c^2$ is equal to $h\nu$, where ν is the observed frequency and h is Planck's constant. The model displays the dispersion relationship of Eqs. (1), (2), and (3), which are so similar to those of the photon in a waveguide. And indeed the normal velocity $v_n = c$ in Figures 8, 9, 10, and 11 is the analogue of the wave front whose velocity is c in Figure 2 in the photon in a waveguide. And in Figures 1, 8, 9, 10, and 11 the charged filament of the electron is constrained in the x and y directions but is moving with a group velocity v_g in the z direction, as is the photon in Figure 2. In Figures 1, 8, 9, 10, and 11 the total energy of the electron is electromagnetic, as it is for the photon in Figure 2.

The analogue between the electromagnetic wave (photons) in a waveguide in Figure 2 and the double-helix electron model of Figures 8, 10, and 11 is complete if we draw the extension of the angle θ in Figure 10(a) so that the wavelength λ_0 can be drawn. This wavelength λ_0 is the spacing between "wave fronts" of the helix (whose normal velocity is c), and the λ_0 of Figure 2 is the free-space wavelength of the wave fronts of the electromagnetic waves that are proceeding at a normal velocity c at an angle θ with respect to the waveguide walls. It is obvious that in Figure 10(a) the de Broglie wavelength $\lambda = \lambda_z = 2\pi/k_z = \lambda_0/\sin\theta = \lambda_{\text{de Broglie}}$, just as in Figure 2 the guide wavelength $\lambda_g = \lambda_0/(\sin\theta)$. The vector diagram in Figure 10(a) of the propagation vector $\mathbf{k}_0$ resolved into its two components $\mathbf{k}_z$ and $\mathbf{k}_y$ is the selfsame diagram we find in Figure 2. In the electron model in Figure 10(a),

$$\lambda_0 = \frac{c}{v} = \frac{2\pi c}{\omega} \quad \text{and} \quad \frac{1}{\lambda_0^2} = \frac{1}{\lambda^2_{\text{Comp}}} + \frac{1}{\lambda^2},$$

$$\lambda = 2\pi R/\tan\theta, \quad R = \frac{\lambda_{\text{Comp}}}{2\pi}.$$

The full wave function is

$$\psi = A(z,t)e^{i(\omega t - kz)}, \tag{36}$$

where $A(z,t)$ is an amplitude function that propagates the wave packet with the group velocity v_g. Then the accepted quantum-mechanical probability distribution $\Psi\Psi^*$ is $A^2(z,t)$, and the "probability" of finding the "particle," at a time t, between z_1 and z_2 is

$$\int_{z_1}^{z_2} \psi\psi^*\, dz, \tag{37}$$

which is the fraction of the configuration of Figure 8 contained between z_1 and z_2.

With the portrait of Figures 8, 10, and 11, the "uncertainty" of location of the "particle" in the z direction, $\Delta z \cong n\lambda$, where n is the number of wavelengths in the train of the wave packet. The uncertainty of momentum in the z direction, $\Delta p_z \geq (h\nu/c)\tfrac{1}{2}\pi n$. Thus $\Delta z \Delta p_z \geq (\lambda/2\pi)\,(h\nu/c)\tfrac{1}{2}\pi n = \hbar$, and Heisenberg's celebrated uncertainty principle is "obeyed," as certainly it must be

because the uncertainty principle is essentially a restatement of the fundamental relation between time and frequency as mediated by the Fourier transform.

The relationships for the electromagnetic energy of a torus (6), the spin of the torus (7), and the magnetic moment of the torus (10) were developed for the simple torus of Figure 5. Let us now consider what these relationships become when applied to the free *chaiyah* electron of Figures 8, 10, and 11, where the de Broglie wavelength λ, Ψ, Ψ^*, the angle θ, $v_g = c \sin \theta$, and $v_p = c/(\sin \theta)$ are displayed in all their glory. If there are n half-wavelengths ($\lambda/2$) in the wave packet, the total length of the filament is $2\pi Rn/(\sin \theta)$. The charge per unit length of the filament is $\sigma = (e \sin \theta)/c2\pi Rn$. The current is $(ec \sin \theta)/c2\pi Rn = (e \sin \theta)/2\pi Rn$. The electric and magnetic fields at a distance r from the center of the filament are

$$|\mathbf{E}| = |\mathbf{H}| = \frac{2\sigma}{r} = \frac{e \sin \theta}{\pi Rrn} \tag{38}$$

as compared with $e/\pi Rr$ for Figure 5.

Now in a calculation for the electromagnetic energy E_f contained in the region $r_0 < r < R$ similar to that of Eq. (6):

$$\begin{aligned} E_f &= \frac{2\pi Rn}{\sin \theta} \int_{r_0}^{R} \frac{|\mathbf{E}|^2 + |\mathbf{H}|^2}{8\pi} 2\pi r \, dr \\ &= \frac{2\pi Rn}{\sin \theta} \int_{r_0}^{R} \frac{e^2 \sin^2 \theta}{4\pi(\pi Rrn)^2} 2\pi r \, dr \\ &= \frac{e^2 \sin \theta}{\pi Rn} \ln \frac{R}{r_0} = mc^2, \end{aligned} \tag{39}$$

where the rest mass of the electron $m_{0e} = 2m(1 + \alpha/2\pi + \cdots) \approx 2m$. In a calculation for the spin, similar to that of Eq. (7),

$$\begin{aligned} \text{spin} &= \frac{2\pi RnR}{\sin \theta} \int_{r_0}^{R} \frac{\mathbf{E} \times \mathbf{H}}{4\pi} 2\pi r \, dr \\ &= \frac{2\pi R^2 n}{\sin \theta} \int_{r_0}^{R} \frac{e^2 \sin^2 \theta \, 2\pi r \, dr}{4\pi(\pi Rrn)^2} = \frac{e^2 \sin \theta}{\pi nc} \ln \frac{R}{r_0} \\ &= mRc = \frac{\hbar}{2} \end{aligned} \tag{40}$$

equals the totality of all spins summed up algebraically, *not* vectorially (see Figure 11).

The sum of the components in the z direction of the spins of each loop ($\lambda/2$) is

$$\frac{e^2 \sin^2 \theta}{\pi nc} \ln \frac{R}{r_0} = mRc \sin \theta = \frac{\hbar}{2} \sin \theta, \tag{41}$$

if we remember that $R = \hbar/m_{0e}c$ and $m_{0e} \cong 2m(1 + \alpha/2\pi + \cdots) \cong 2m$. Since $\sin \theta = v_g/c$, the component of the spin in the $+z$ direction increases from 0 to $\hbar/2$ as v_g increases from 0 to c, and electrons in relativistic beta decay should have a spin of $\hbar/2$ lined up with the z axis as $\sin \theta \to 1$, which is indeed experimentally the case in beta-ray decay (Segré 1959).

The magnetic moment μ/n of each loop is

$$\frac{\mu}{n} = i \times \text{Area} = \frac{e \sin \theta}{\pi Rn} (\pi R) \left(\frac{R}{\sin \theta} \right) = \frac{eR}{2n}.$$

The algebraic sum of the magnetic moments of n loops is $eR/2 \cong e\hbar/2m_{0e}c$. The vector sum of all the magnetic moments of the individual loops is

$$-\frac{eR}{2} \sin \theta, \tag{42}$$

and this resultant in the $+z$ direction is equal to $e\hbar/2m_{0e}c$ only when $\sin \theta \to 1$, that is, when the electron becomes relativistic, and indeed this is experimentally the case in beta-ray decay.

Discussion

The model of Figure 5 was a rough, heuristic step to introduce the method of calculating the electromagnetic energy E [Eq. (6)], the spin [Eq. (7)], the magnetic moment $\mu = eR/2$ [Eq. (10)], the total rest mass $\cong 2m(1 + \alpha/2\pi + \cdots) = 2m$ [Eq. (9)], and the gyromagnetic ratio $g = \mu/s \cong (2e/2m_1c)(1 + \alpha/2\pi + \cdots)$ [Eq. (14)]. The shape that the *chaiyah* electron assumes in order to exhibit the proper dispersion relationship consistent with $\lambda = h/m_e v$, $m_e = m_{e0}(1 - \beta^2)^{-1/2}$, the Heisenberg uncertainty relation, the Ψ and Ψ^*, the probability distribution, $\Psi\Psi^*$, is illustrated in Figures 8 through 11.

Any other models of onta that assume that the mass, spin, and magnetic moment are generated by a charged Newtonian lump mass concentrated at a mathematical point are invalid because they will explode; they cannot generate the spin and μ, and the wave functions Ψ and Ψ^* have no physical ingredients and no physical coupling with the mass, charge, and current. They will radiate their energy away by synchrotron radiation. These models can exist only in the minds of individuals who gladly and completely embrace the point mass of the Copenhagen School and the purely probabilistic interpretation of Ψ because of the beautiful mathematical edifice of quantum mechanics that has been constructed therewith. Such onta are not in any sense *chaiyah* onta. They are mathematical artifices rather than philosophical realities, whether they be models of the electron, photon, meson, kaon, quarks, and so on. Indeed, the *chaiyah* electron model is basic to the fundamental character and morphology of mass, charge, and current.

The *chaiyah* electron of Figures 8 through 11 illuminates the Einstein relationship $m_r = m_{e0}(1 - \beta^2)^{-1/2}$ and the de Broglie relationship $\lambda = h/m_r v$ as never before. The *chaiyah* electron provides Einstein (albeit belatedly) with the wave functions Ψ and Ψ^* that have the physical content he was always searching for in his discussions with Max Born. I believe that Max Born would not begrudge Einstein that physical content of Ψ now that it has been demonstrated by the *chaiyah* electron. Max Born and Erwin Schrödinger would be the first to rejoice in the triumph of Einstein's faith in a "non-dice-playing God." The *chaiyah* electron snatches total victory from the trophy case of the Copenhagen Schoolhouse and places some modest *bon points* in the lap of the philosophical, steadfast, intuitive Einstein. At the same time, the *chaiyah* electron basically preserves the probabilistic nature of the wave function and therefore does not invalidate the effective mathematical structure of quantum mechanics as it has developed.

At the risk of giving offense to the great and many contributors who have created the present magnificent mathematical structures of quantum mechanics and quantum electrodynamics, this author suggests that the present accepted state of this field is analogous to the chapter in elementary textbooks on electricity and magnetism where lumped-constant LRC circuits are introduced. The lumped-constant circuit is a very useful and mathematically convenient fiction for many of the lower-frequency applications, but for the higher frequencies (for example, microwave radar) distributed quantities must be reckoned with. The *chaiyah* electron is this author's attempt to introduce distributed charge, mass, momentum, current, spin, magnetic moment, and thereby show that the de Broglie–Einstein wave and the wave functions Ψ and Ψ^* are not ad hoc, but are a necessity in order for all these distributed quantities to produce an equilibrized and stable structure as observed from all frames of reference. The Copenhagen point-mass and point-charge electron cannot be in equilibrium, stable, or observable in *any* frame of reference!

The Fluid Mechanical Analogue Of the *Chaiyah* Electron

In the energy stored in vortices in fluid mechanics it is possible to make a complete macroscopic analogue of the flywheel model of the electron of Figures 5, 8, 9, 10, and 11. This analogue should throw light upon many aspects of our constructions up to now.

Consider a vortex produced between the two solid plates, as shown in the idealized velocity profile in Figure 12, where the undisturbed hydrostatic pressure in the liquid is p_0. Most of the kinetic energy is contained in the irrotational region where $r_1 < r < \infty$ and

$$v = \frac{v_1 r_1}{r} = \frac{\Gamma}{2\pi r} \tag{43}$$

The vortex circulation is $\Gamma = 2\pi v_1 r_1$. The kinetic energy KE per unit length of the vortex is

$$\mathrm{KE} \cong \int_{r_1}^{r_2} 2\pi r \rho v^2 \, dr = \rho 2\pi \frac{\Gamma^2}{4\pi^2} \int_{r_1}^{r_2} \frac{dr}{r} = \frac{\rho \Gamma^2}{2\pi} \ln\left(\frac{r_2}{r_1}\right). \tag{44}$$

The vessel must be terminated at a radius $r_2 < \infty$ if the kinetic energy is to remain finite. The pressure is given by (for $r_1 < r < \infty$)

$$dp = \frac{-\rho v^2}{r} dr = -\rho v_1^2 r_1^2 \frac{dr}{r^3}.$$

Then,

$$\begin{aligned} p &= p_0 - \int_r^\infty \rho v_1^2 r_2^2 \frac{dr}{r^3} \\ &= p_0 - \frac{\rho v_1^2 r_1^2}{2\pi r^2} = p_0 - \frac{\rho v^2}{2} \end{aligned} \tag{45}$$

which gives the pressure profile shown in Figure 12. There is a pressure differential $p_0 - p = (\rho v^2/2)$ (where ρ is the density of the fluid) across each metal plate, which one can consider to be produced by elastic bands attached to the inner surfaces of the plates. The elastic potential energy in these stretched bands per unit volume is $\rho v^2/2$, which is locally equal to the kinetic energy density.

If we take the rectilinear vortex segment of Figure 12 and permit it to be a torus of rest mass m_{0v}, defined as E_{0v}/c_s^2, where E_{0v} is the kinetic energy of rotating fluid in

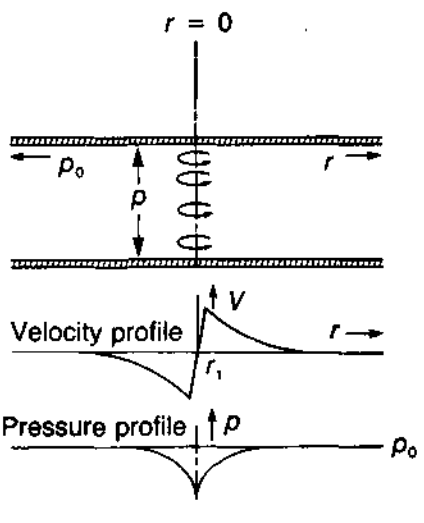

Figure 12. Profiles of a rectilinear fluid-mechanical vortex formed in the fluid betwen two parallel plates.

the vortex and c_s is the sound speed, we can construct a macroscopic vortex analogue of the electron model of Figures 5 and 8 through 11 complete with de Broglie (inertial) waves, $E = h_v\nu$, and $m = m_0(1 - \beta^2)^{-1/2}$. We illustrate his construction: We can calculate this kinetic energy E_{0v} to be

$$E_{0v} \cong 2\pi^2\rho {v_1}^2 {r_1}^2 R_v \ln\left(\frac{R_v}{r_1}\right) = \frac{\rho\Gamma^2}{2} R_v \ln\left(\frac{R_v}{r_1}\right), \quad (46)$$

where R_v is the large radius of the toroidal vortex and Γ is the vortex circulation. If we now translate the toroidal vortex through the background fluid medium, with a group velocity v_g (with respect to this medium) parallel to the plane of the vortex, the magnus forces will deform the vortex into the shape of Figures 10 and 11 and the wave functions ψ and ψ^* generated by the two counter-rotating translating helical vortex filaments (which are inertial waves) "swim" upstream through the background medium. The wave function (see Figure 10) $\psi(z,t) = R_v \exp[i(\omega t - kz)]A(z,t)$ is the helical centerline of the left-handed helix rotating in the right-handed sense and $\psi^* = R_v \exp[-i(\omega t - kz)]A(z,t)$ is the centerline of the right-handed helix rotating in the left-handed sense. Both helices are also being translated in the z direction. $A(z,t)$ is the amplitude or the envelope function of the wave packet. These rotating translating helices of Figures 10 and 11 should be recognized as inertial waves. $k = 2\pi/\lambda$. The normal velocities v_n shown in Figures 8, 10, and 11 are then $v_n = v_1 r_1/2R_v$, the phase velocity $v_p = \omega/k = v_n/(\sin\theta)$; the limiting value for v_n is c_s, the speed of sound in the fluid. If v_n were greater than c_s, shock waves would form and dissipate energy. Thus, $v_g v_p \leq {c_s}^2$.

If we recognize from Figures 8, 10, and 11 that (for a vortex and the electron model) $\lambda = 2\pi R_v/(\tan\theta)$, we can write

$$v_g = v_n \sin\theta = \frac{v_1 r_1}{2R_v}\sin\theta$$

$$= \frac{\pi v_1 r_1}{\lambda}\frac{\sin\theta}{\tan\theta} \quad (47)$$

or

$$\lambda = v_1 r_1 \pi \cos\theta / v_g.$$

In a gedanken experiment we now make a very special vortex that can execute the waves indicated in Figures 8, 10, and 11 in which $v_n \to c_s$, and which possesses no more than the minimum values of v_1, r_1, and R_v to accomplish this. The rest mass of this special vortex we shall now call $m_{0v} = E_{0v}/{c_s}^2$. Also now $v_g v_p = {c_s}^2$.

We further define a macroscopic quantum of action h_v as $h_v = m_{0v} v_1 r_1 \pi = m_{0v} R_v c_s 2\pi$.

Then we can write

$$\lambda = \frac{m_{0v} v_1 r_1 \pi \cos\theta}{m_{0v} v_g} = \frac{h_v \cos\theta}{m_{0v} v_g}$$

$$= \frac{h_v}{m_{0v} v_g/\sqrt{1 - \sin^2\theta}} \quad (48)$$

$$= \frac{h_v}{m_{0v} v_g/\sqrt{1 - {\beta_v}^2}} = \frac{h_v}{m_v v_g},$$

where

$$m_v = m_{0v}(1 - {\beta_v}^2)^{-1/2} = \gamma m_{0v};\ \beta_v = v_g/c_s.$$

The frequency $\nu = \omega/2\pi$ measured by an observer at rest in the background fluid is given by

$$\nu\lambda = v_p = {c_s}^2/v_g = {c_s}^2 m_v \lambda/h_v. \quad (49)$$

or

$$h_v \nu = m_v {c_s}^2, \quad (50)$$

the total energy stored in this vortex (of the shape of Figures 8, 10, and 11) as it moves with a group velocity v_g with respect to an observer in the frame of the background fluid medium.

Thus, with the definition of $m_{0v} = E_{0v}/{c_s}^2$ and the knowledge that the vortex will change into the configuration of Figures 8, 10, and 11 with the rotating and translating helical wave functions ψ and ψ^*, we have derived again the most famous of all energy-storage formulas; namely, the Planck quantum hypothesis that the energy is proportional to the frequency.

It has been shown by Hasimoto (1972) that an ideal vortex filament can be expected to support helical waves that act like de Broglie waves because the appropriate equation is a nonlinear Schrödinger-type equation. Hasimoto's discovery adds strength to our prediction that the vortex will "swim upstream" with the de Broglie-type waves as indicated in the general configuration of Figures 8, 10, and 11.

Perhaps even the worthy Knights of the Round Table in hot pursuit of the Holy Grail of Grand Unification can pause momentarily to notice that the parallel between the de Broglie–Einstein waves and the helical "inertial waves" on a vortex filament in fluid mechanics (as discussed in this chapter) is also a form of unification within our science and philosophy, modest perhaps by their standards, but certainly not trivial.

How About the Quantities c, e, m_e, h, and α?

Now that the model of Figures 1, 8, 10, and 11 has shown itself to be a high-fidelity replica of the electron itself, we ask ourselves the question, "What light can this model shed upon the values of the constants such as c, e, m_e, h, and α?"

The value of c is that charge-circulating velocity that permits equilibrium in the radius r_0 of the torus of Figures 1, 5, 8, and 11; that is, the value that equates the electric field **E**, that tends to burst r_0 to **H**, that tends to contract r_0.

The value of h should be such that the two elements of length diametrically across the torus in Figure 5, a distance of $2R$ apart, can communicate with one another with their fields that are established at the speed of light, in a time approximately $R/c = 1/\omega_c$, where ω_c is the Compton frequency,

$$\omega_c = m_{0e}\hbar = 2\pi c/\lambda. \tag{50A}$$

That is,

$$c/\omega_c \cong R = \hbar/m_{0e}c \tag{51}$$

and this is true and consistent with the Planck relation that $\hbar\omega_c = m_{0e}c^2$.

This is tantamount to saying that the two shaded elements of Figure 9 (in the configuration of Figures 8 through 11) must be able to communicate with one another across the spacing $2R$ in a time approximately equal to $2/\omega$, where ω is the frequency observed by the Earth frame as the electron (Figures 8–11) proceeds with a group velocity v_g with respect to the Earth frame. As we have seen, the transformation from Earth frame to electron frame involves the dispersion relation $\omega^2 = \omega_c^2 + k^2c^2$ that comes from the Einstein relation $m_e = m_{e0}(1 - \beta^2)^{-1/2}$, which we have derived with the help of the geometrical relation $\lambda = 2\pi R/(\tan\theta)$ from Eq. (32) and Figure 10.

For another onta, the proton for example, m_0 and ω_c are larger, R is smaller, and the value of h is consistent with the values of R, m_0, and ω_c for the proton.

Remarks similar to those made for the electron can be made about the macroscopic quantum of action $h_v = m_{0v}v_1r_1\pi$ for the vortex analogue of the electron: The spacing $2R_v$ of two diametrically opposite vortex segments (corresponding to the spacing $2R$ for the electron in Figures 8, 9, and 10) must be such that the segments can communicate with one another in a time $\approx 2/\omega_c$ through their velocity fields whose maximum velocity is the speed of sound c_s. That is, $c_s/\omega_c \cong R_v$, where $\omega_c = m_{0v}c_s^2/h$, and this is true and consistent with the Planck relation that $h_v\omega_c = m_{0v}c_s^2$ since $v_n = c_s = v_1r_1/2R_v$.

When the vortex moves in the z direction with a velocity v_g with respect to the Earth's frame, its shape becomes that of Figures 8, 10, and 11, and the dispersion relationships are completely analogous to those for the electron.

We have seen that the value of

$$\alpha = \frac{e^2}{\hbar c} = \frac{1}{137}$$

is related to the structure of the model by

$$\frac{e^2}{\hbar c} = \frac{\pi/2}{\ln(R/r_0)}$$

and this is consistent with the spin

$$\frac{\hbar}{2} = \frac{e^2}{\pi c}\ln\left(\frac{R}{r_0}\right),$$

the rest mass

$$m_{0e} \cong \frac{2e^2}{\pi Rc^2}\ln\left(\frac{R}{r_o}\right)\left(1 + \frac{\alpha}{2\pi}\right),$$

and the gyromagnetic ratio

$$g \cong \frac{e}{2m_{0e}c}\left(1 + \frac{\alpha}{2\pi}\right)2.$$

The value of r_0 (and hence $\ln R/r_0$ and $\alpha = e^2/\hbar c$) very likely depends in some way upon the properties of the gravitationally equilibrized fiber shown in Figures 1 and 8, which acts like a helical spring to produce the spring constant k and the effective surface charge on the torus of Figures 1, 8, and 9. D. Conant (1978) shows great insight in arriving at the value of α via general and fundamental arguments and indeed relates it to the gravitational constant G.

The *Chaiyah* Photon

Now since the similarity of the dispersion relationships for the electron [Eqs. (1)-(3)] and an electromagnetic wave (photons) in a waveguide, and of Figures 2, 8, 10, and 11 have helped us develop a completely electromagnetic model of the electron, perhaps this model of the electron can heuristically help us to construct a model of the photon.

For this purpose, we note that an electromagnetic wave involves electricity and magnetism on an equal footing. Therefore, we shall assume that the photon contains "magnetically charged" filaments as well as electrically charged filaments. The author prefers to think of these electric and magnetic charges in the photon as "induced" or "virtual" charges that behave like filamentary charges because of the fields that surround them.

The model of the photon is developed as follows: the "toroidal" filament of Figures 5 and 8 through 11 of core

radius r_0 and charge $-e$ is severed and straightened out into an arrow of core radius r_{0p} and projected along with three other filaments as shown in Figure 13. The three other filaments are one with a charge of $+e$, and the other two with magnetic charges of north and south poles as shown. The separation of opposite filaments is $2R_p$. The configuration rotates with an angular frequency ω so that the peripheral velocity of each filament is c, as shown in Figure 13, to make the right-hand circularly polarized photon, where $\omega = 2\pi\nu$, $\omega R_p = c$, $\lambda\nu = c$, $\lambda = 2\pi R_p$, and $\nu = c/2\pi R_p$.

If the length of the configuration (wave packet) is $n\lambda$, the electric field $|\mathbf{E}|$ at a distance r_p from each of the filaments is $|\mathbf{E}| = e/\pi r_p R_p n$ and the magnetic field $|\mathbf{H}|$ is $|\mathbf{H}| = |\mathbf{E}|$. Then, since there are four filaments, the photon electromagnetic energy is

$$
\begin{aligned}
E_p &\cong \frac{4\cdot 2\pi\, Rpn}{8\pi}\int_{r_{0p}}^{R_p}\frac{2e^2}{\pi^2 r^2 R_p^2 n^2}\cdot 2\pi r\, dr \\
&= \frac{4e^2}{\pi n R_p}\ln\left(\frac{R_p}{r_{0p}}\right) = \frac{8e^2}{n\lambda}\ln\left(\frac{\lambda}{2\pi r_{0p}}\right) \\
&= \frac{8e^2\nu}{nc}\ln\left(\frac{R_p}{r_{0p}}\right) = \frac{8\hbar\nu\alpha}{n}\ln\left(\frac{R_p}{r_{0p}}\right) \\
&= \frac{4h\nu\alpha}{\pi n}\ln\left(\frac{R_p}{r_{0p}}\right) = \frac{4h\nu}{\pi n 137}\ln\left(\frac{R_p}{r_{0p}}\right).
\end{aligned}
\tag{52}
$$

The electron model of Figures 5 and 8 through 11 has come forward, as we have already seen with the famous Planck energy-storage relationship that $E = h\nu$. Now we see that this model of the photon *also* comes forward with the relationship that $E_p \sim h\nu$. To make this relationship an equality, so that $E_p = h\nu$, it is necessary that $1/\pi \ln R_p/r_{0p} = 137n/4$.

Thus, if the number n of the wavelengths in the wave packet is altered, the value of $\ln R_p/r_{0p}$ must adjust itself accordingly. The value of R_p remains constant, given by $\lambda = 2\pi R_p$. Thus, it must be r_{0p} that makes the adjustment to preserve $E_p = \hbar\omega = h\nu$.

The spin of this photon model is given by $(h\nu/c^2)R_p c = \hbar$, which is what it should be; that is, the model portrays a spin-1 photon. A left-handed circularly polarized photon is produced by rotating the filamentary configuration of Figure 2 in the opposite sense. The momentum $h\nu/c$ of the photon is obtained by integrating the Poynting vector.

Stability of the Filamentary Photon

The attractive force supplying the centripetal acceleration on the negatively charged electrical filament, for example, is supplied by its Coulomb attraction for the positive filament. The magnetic forces due to the oppositely directed currents in these filaments are just balanced out by the magnetic forces due to rotation. The zero resultant of these magnetic forces can be understood in another way by recognizing that an element of length of the positive filament moves resultantly perpendicular to the velocity of the corresponding element of length of the negative filament. The effective pitch angle θ of the photon model is always 45°.

We have emphasized that the flywheel configuration of Figure 2 can exist as a dynamical equilibrium configuration only because of the elastic force constant that gives rise to a potential energy $\frac{1}{2}k(2\pi R^2)$. We also strongly suggest that the fluid-mechanical vortex moving with velocity v_g (parallel to its plane) with respect to an observer in the background medium can be an equilibrium configuration only if it swims flagellatingly upstream as shown by the shapes in Figures 8 through 11 with the appropriate normal velocities $v_n = c_s = (v_1 v_2/2)R_v$. By heuristic analogy with the fluid-mechanical vortex, we have suggested that the filamentary electron will assume the similar configurations of Figures 8 through 11.

Indeed, the formation of macroscopic helical configurations by current-carrying plasma filaments has been observed, for example, by the Stevens plasma-focus group in a contact print of a plasmoid on CR-39 etchable track detector (Bostick et al. 1983) and in the fountain pinch experiments by Komelkov (1960). The formation of helical configurations by current-carrying plasma filaments has also been predicted by Shavronov (1966). Only the

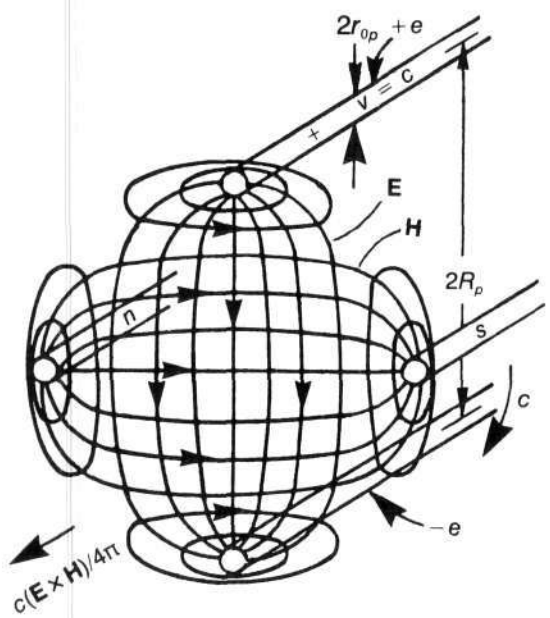

Figure 13. Model of a right-handed circularly polarized photon made up of two + and − charged filaments and two north and south "charged" filaments projected in the z direction with a velocity c, while at the same time the configuration rotates with a peripheral velocity c.

configurations of Figures 8 through 11 can generate the wave functions Ψ and Ψ^* that have the proper dispersion relationship [Eq. (3)] for an electron's observed de Broglie–Einstein waves. And since only equilibrium and stable structures can live and be observed, Nature herself has given us the proof that the *chaiyah* electron of Figures 8 through 11 is an equilibrium, stable structure, a proof that the author freely admits is far beyond his meager mathematical talents.

Conclusion

The basic similarities and differences between the *chaiyah* electron and photon now enable us to make an important and highly instructive unifying cosmological and morphological statement: Onta of finite rest mass have their filamentary charges and Poynting vectors circulating at the speed of light in closed, toruslike structures (Figures 5, 8, and 11). Onta of zero rest mass have their filamentary charges projected rectilinearly like arrows at the speed of light, but also, like arrows, the configuration of filaments (for example, the photon in Figure 13) rotates as it flies. Photons being reflected between two surfaces (in a waveguide) can acquire rest mass. Electrons accelerated to $\beta \rightarrow 1$ and $\gamma \gg 1$ essentially lose their rest mass for all practical purposes, that is, $m_{0e} \ll m_e$.

Einstein (1953) speaks of an averaged "inward pressure" that is equal to one-half the average mass density of the universe and that binds the electromagnetic energy of the onta of finite rest mass into those onta. This averaged inward pressure we would identify with the elastic hoop stress force (sausage casing with spring constant k) formed by the gravitational fiber in the configuration shown in Figures 1, 5, 8, and 11 that is responsible for spin-½.

The author penitently confesses and concedes that he has not begun to tackle such important problems as the scattering of the *chaiyah* electron by other onta. He has approached only the problem of a free electron moving at a group velocity v_g with respect to the observer in this chapter and the electron in various potential wells in Chapter 2. But scattering depends upon the wave nature of the onta. Now that we realize that our filamentary onta have real physical waves, not just "probabilistic waves," the exploration of the scattering process should become a more exciting adventure.

If the self-assigned search for the Holy Grail of Grand Unification of "all forces" is to succeed, all of us participating investigators must eventually recognize that the concept of Newtonian lump mass is a leaden millstone tied 'round our necks; we are drowning in our own formalism and, no matter how many Nobel prizes are parceled out, we will never get it right until we remove that millstone. It is our misfortune that our elementary textbooks for centuries have been so thickly plastered over with "Newton's Three Laws" and Mickey Mouse exercises involving Newtonian mass points. Newton's contemporary Leibniz, instead of treating the planets as *fait accompli* mass points, attempted to derive their revolutions, rotations, and coalescence out of a continuum primordial fluid, like a plasma; but Leibniz is scarcely ever mentioned in our elementary textbooks. What we have said thus far in this chapter should be sufficient to convince an intuitive reader that since all mass and momentum are electromagnetic in origin, all forces must be basically electromagnetic in character.

Chapter 2

The *Chaiyah* Electron In Potential Wells

In Chapter 1 we developed a *chaiyah* filamentary, electrodynamic electron, which has the appropriate dispersion relationships for a de Broglie–Einstein wave in the mode of a "free" onta with no interfering potentials. In this chapter we demonstrate how the *chaiyah* electron can reproduce the harmonic characteristics prescribed by the Schrödinger equation for an onta resonating in various potential wells.

Standing-Wave Solution of The *Chaiyah* Electron

In Chapter 1 the form and substance of the wave function Ψ and its complex conjugate Ψ^* have been discussed for the free electron. Now this same wave function will be discussed in the context of "a particle in a one-dimensional box"; that is, an electron in a potential well with infinitely high barriers at each end. The electron is assumed to form a resonance by being reflected at such barriers placed at $z = L/2$ and $z = -L/2$, and the wave functions Ψ and Ψ^* traveling in the $+z$ and $-z$ directions have all of the properties of the free electron discussed in Chapter 1. The conventional solutions of the Schrödinger equation in quantum mechanics for this simple case are similar to those for a standing wave on a violin string clamped at both ends.

The reader may promptly raise the question as to why the author should repeat this elementary exercise that is so well known. The reply is that since the helical electron model of Chapter 1 has within it a mass that is completely electromagnetic, a spin that is carried by the Poynting vector, and a magnetic moment, we wish to inquire about shapes that these helical waves might assume when they are placed in a box. Furthermore, since the wave functions Ψ and Ψ^* of Chapter 1 are invested with *more* physical significance than the "probability amplitude" of the accepted current interpretation of quantum mechanics, we wish to relate these *real* waves with the "probability amplitude" for the electron in a box.

A *chaiyah* electron such as that shown in Figure 11 with a normal velocity in the $-z$ direction approaching an infinite potential barrier at $z = 0$ will undergo a reflection in which the reflected nose of the wave train will be telescoped back through the oncoming tail of the incident wave. To draw a detailed perspective picture of this event is a rather difficult and involved procedure. Suffice it to state that the incident wave functions similar to those in Figures 10 and 11 are $\Psi = R \exp[-i(\omega t + kz)]$ (left handed) and $\Psi^* = R \exp[i(\omega t + kz)]$ (right handed), and the reflected waves are $\Psi = R \exp[i(\omega t - kz)]$ (left handed) and $\Psi^* = R \exp[-i(\omega t - kz)$ (right handed).

During the time interval that the wave train is being reflected, the telescoping configuration exists. If the incidence is other than perfectly normal, the reflected wave need not telescope through the incident wave; the angle of reflection will be equal to the angle of incidence. If there are two barriers and a resonance is set up, with normal incidence, then it is the situation of an electron in a one-dimensional box, and the fundamental or first harmonic mode will be created when the length L of the box is equal to $\lambda/2$ of the electron.

Einstein stated, "Subtle is the Lord, but malicious He

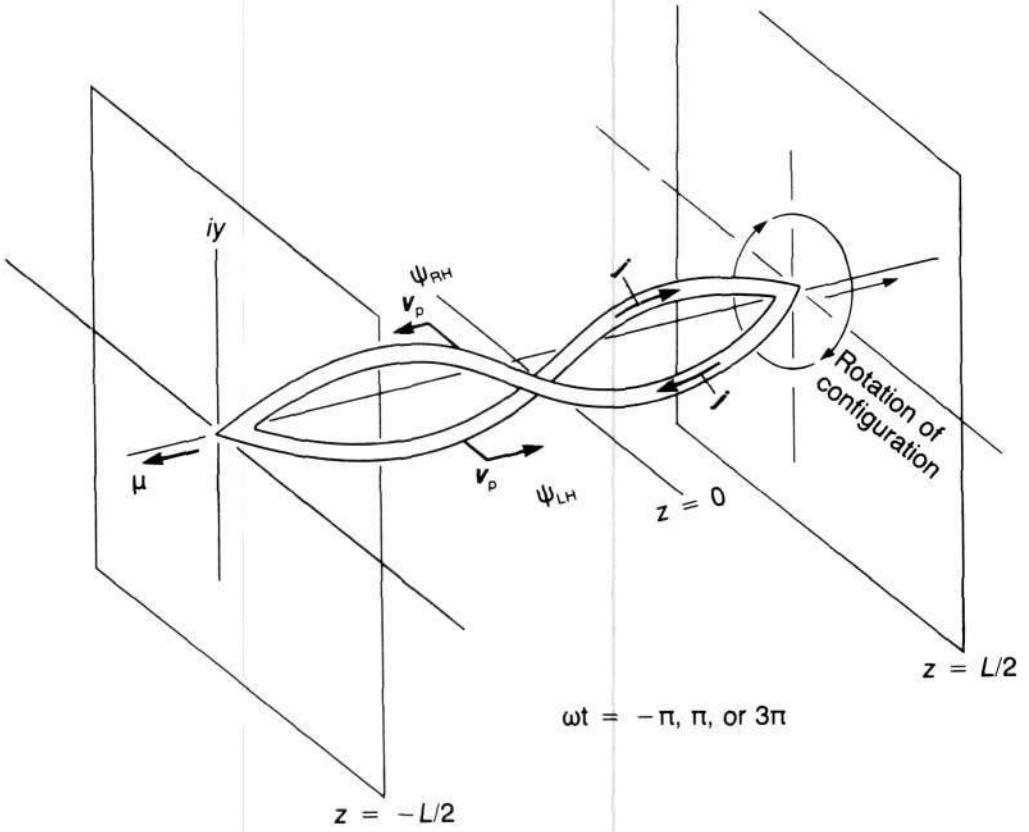

Figure 14. First-harmonic eigenfunction (resonating standing wave) for electron between two infinite potential barriers.

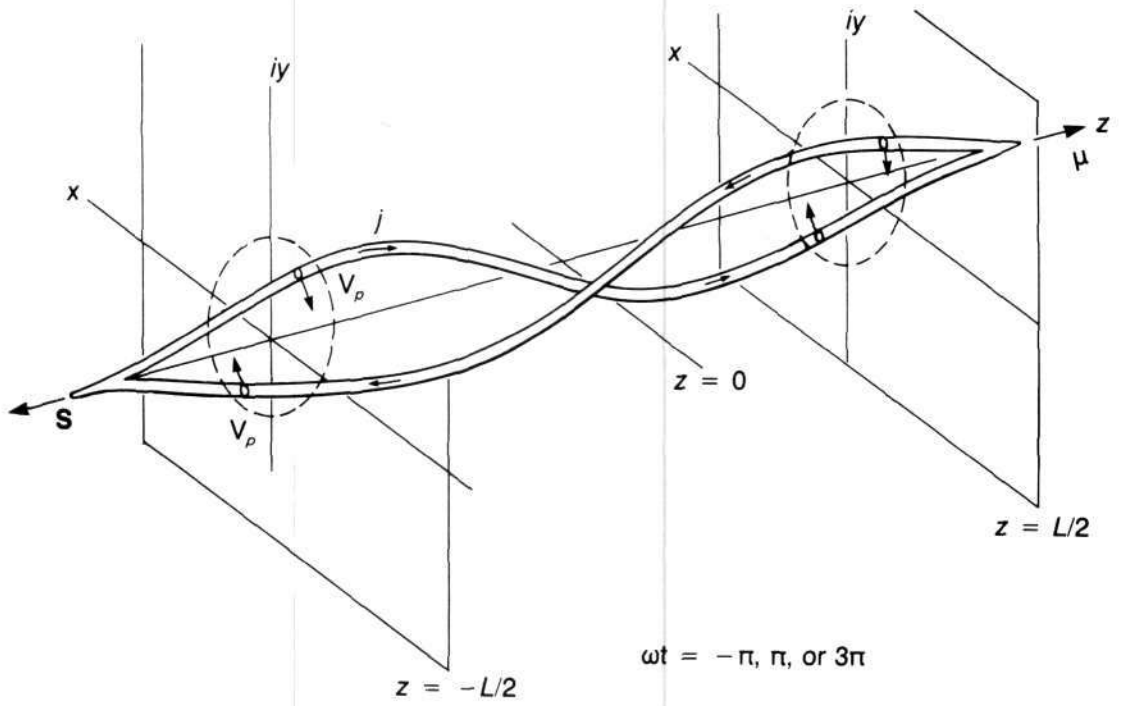

Figure 15. First-harmonic eigenfunction for the electron between two finite potential barriers.

is not." Emboldened by this encouraging proclamation, we shall attempt to divine the way in which Nature sets up this resonance with the *chaiyah* electron. Let us now place the barriers at $z = -L/2$ and $z = L/2$. We seek a solution where a standing-wave pattern is produced by waves proceeding in opposite directions, where the filament is a continuous loop producing spin and magnetic moment, and where the amplitude of the wave functions vanishes at $z < -L/2$ and $z > L/2$.

A suitable resonance is diagrammed in Figure 14. Such a solution would be formed of $\Psi_{RH} = R \exp[i(kz + \omega t)](\cos kz)$ and $\Psi_{LH} = R \exp[-i(kz - \omega t)](\cos kz)$ for $-L/2 < z < L/2$ and $\Psi_{LH} = \Psi_{RH} = 0$ for $z < -L/2$ and $z > L/2$, where a resonant wavelength $\lambda/2 = L$, or $k = 2\pi/\lambda = \pi/L$ is selected. Then for each one of these wave functions the probability distribution function $\Psi_{RH}\Psi^*_{RH}$ or $\Psi_{LH}\Psi^*_{LH}$ is $\cos^2 kz = \cos^2(\pi/L)z$.

As the two waves proceed in opposite directions, the entire configuration appears to rotate (like someone swinging a basket or a jump rope) in the $\omega t = \phi$ direction. The above configuration is that for the first harmonic for $n\lambda/2 = L$, where $n = 1$. For successive harmonics $n = 2, 3, 4, \ldots$

But in drawing the picture of Figure 14 (as well as Figures 15 through 21) we have left out half of the picture. We must realize that the electron of Figure 11 is traveling to the right and is composed of both Ψ and Ψ^*. When it is reflecting from a barrier the reflection "wave" is *also* composed of both Ψ *and* Ψ^*. A standing wave is composed of two waves traveling in opposite directions. Therefore, the true and complete picture for Figure 14 should be composed of two more filaments that make a "basket" that will be swinging in the opposite sense. This complete picture is confusing to draw. It should be understood, therefore, in all the standing-wave situations pictured and discussed for Figures 14 through 21 that only half the picture is presented. In all cases the filament is a continuous completed "series circuit" and the current flows through this circuit in series.

Note that the right-hand and left-hand filaments rotate in the *same* direction and have phase velocities v_p that are in *opposite* directions—just the reverse of the situation for the free electron described in Chapter 1.

If we should have chosen to produce the standing-wave function

$$
\begin{aligned}
{}_1\Psi_{SW} &= \Psi_{LH,v_p=+} + \Psi_{RH,v_p=-} \\
&= R \exp[i(kz - \omega t)] + R \exp[-i(kz + \omega t)]
\end{aligned}
\tag{53}
$$

or

$$
\begin{aligned}
{}_1\Psi_{SW} &= R \exp(-i\omega t)[\exp(ikz) + \exp(-ikz)] \\
&= R \exp(-i\omega t)(2 \cos kz),
\end{aligned}
$$

the standing-wave function ${}_1\Psi_{SW}$ would be similar to that for the "fundamental" on a violin string or for the accepted quantum-mechanical solution of a "particle in a box" with the quantum number equal to 1: Wave function ${}_1\Psi_{SW}$ is a complete complex number, whereas the violin-string wave function is usually only the real part of the complex number, that is, the projection of ${}_1\Psi_{SW}$ on the x–z plane.

The corresponding probability distribution function, which is ${}_1\Psi_{SW}\,{}_1\Psi^*_{SW} = 4 \cos^2 kz$, can be normalized to $2 \cos^2 kz$, so that

$$
\int_{-L/2}^{L/2} {}_1\Psi_{SW}\,{}_1\Psi^*_{SW}\, dz = 1. \tag{54}
$$

With a violin string there is only *one* string with two traveling waves in opposite directions adding up to a standing wave on that *one* string. With the electron model of Chapter 1 inserted into the one-dimensional box of Figure 14, there remain *two* helical filaments (as we have already stated, there are actually four). The configuration of the two filaments corresponding to $\Psi_{LH,v_p=+}$ and $\Psi_{RH,v_p=-}$ is, as a combined entity, swung around in the $\omega t = \phi$ direction, somewhat like a basket being held by a child at each end; as we have already stated, the standing wave on a jumping rope is the result of two two-oppositely traveling helical waves on a *single* jumping rope. If we add the two functions $\Psi_{LH,v_p=+}$ and $\Psi_{RH,v_p=-}$ *algebraically* we obtain ${}_1\Psi_{SW}$, the mathematical function of the standing wave on the jumping rope. But the configuration of the *two* swung filaments $\Psi_{LH,v_p=+}$ and $\Psi_{RH,v_p=-}$ is shown in Figure 14 (and remember, there is actually another "basket" being swung in the opposite sense).

With the barriers at $z = -L/2$ and $z = +L/2$ representing an infinite potential, the wave functions (and the filament displacement) must be $(x^2 + y^2)^{1/2} = 0$ at these values of z. If the potential barriers at $z = L/2$ and $-L/2$ were finite, the wave function would approach the z axis exponentially and would be extended somewhat into the regions $z < -L/2$, $z > L/2$. This exponential solution would be joined onto the solution for the "particle" in the box with continuity in value and slope in the customary manner. The actual shape of the helical filaments and the wave functions is diagrammed in Figure 15. The standard textbook quantum-mechanical solution for this case is obtained by adding these two wave functions and then taking only the real part that is the projection on the x–z plane.

It must be kept in mind that the x,y versus z scale of the diagrams in Figures 8, 9, 10, 11, 14, and 15 is highly distorted. For example, if the length $L/2$ in Figures 14 and 15 is comparable to the Bohr orbit of the hydrogen atom, the value of R of the wave function is only about 1/137th as large as $L/2$.

The solutions to the Schrödinger equation with the boundary conditions of this simple, infinite potential well give the complex number as a function of z and t. The interpretation of the wave function in terms of the electron model of Chapter 1 gives a coherent system of **E**

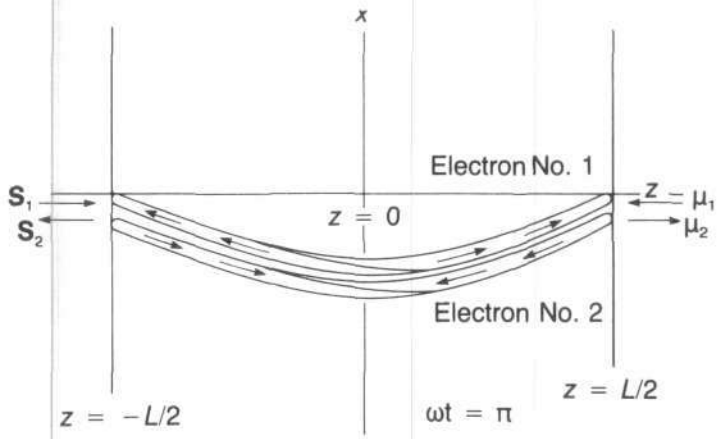

Figure 16. Nesting of two paired electrons with opposite spins in the first-harmonic eigenstate in a one-dimensional box. No more can be added in this box in this state—the Pauli exclusion principle.

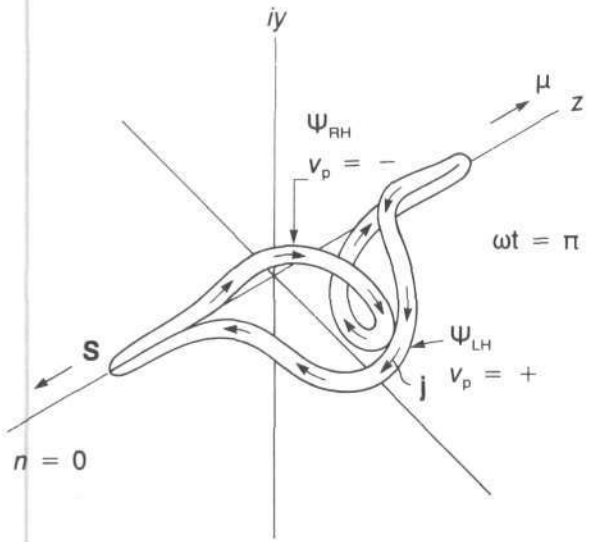

Figure 18. Perspective view of Figure 17.

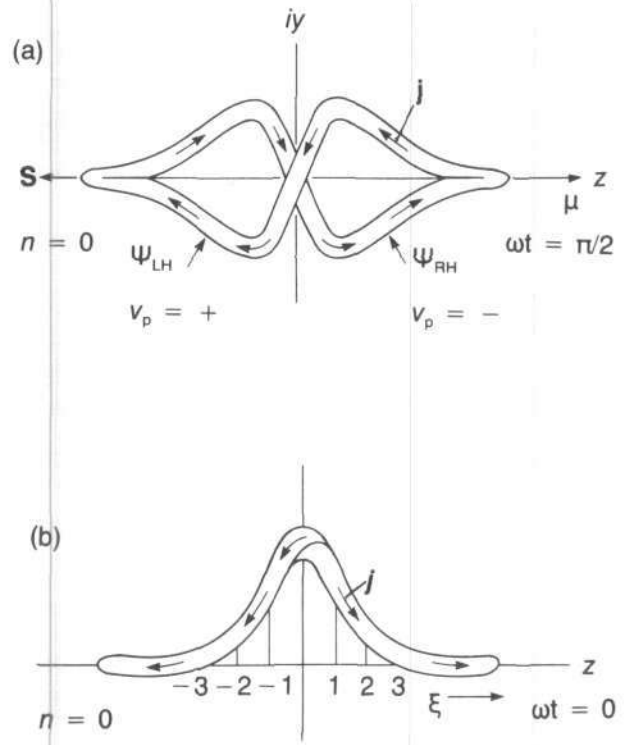

Figure 17. Lowest eigenfunction, $n = 0$ (resonating standing wave) of an electron in the one-dimensional, simple-harmonic-oscillator type of potential.

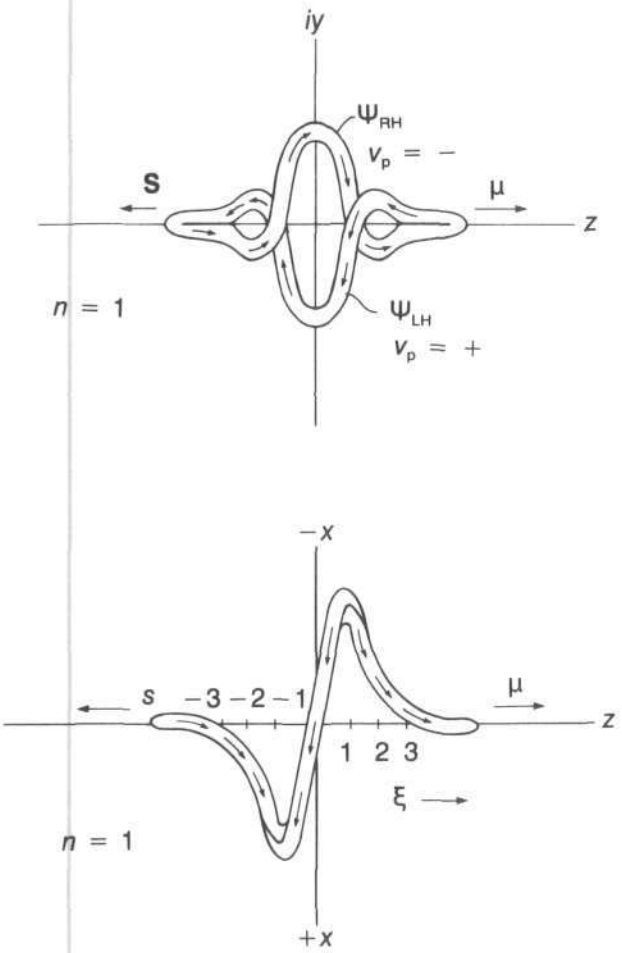

Figure 19. $n = 1$ eigenfunction for electron in potential function of Figure 17.

and **H** vectors that produce the spin-½ through the Poynting vector and the magnetic moment through the currents that flow in the filaments. In Figure 14 the directions of the resultant spin and magnetic moment are shown.

The Pauli Exclusion Principle Demystified

Even if we had never studied the subject of quantum statistics we could recognize that we could put into this same one-dimensional box an edition of our electron model that is identical to that of Figure 14 except for the fact that the current is circulating in the opposite direction, and hence the directions of spin and magnetic moment are reversed. Indeed, this second electron (see Figure 16) could be nested near the first edition to make a neat package that has *zero* spin and *zero* net magnetic moment. It is, of course, necessary to have some space-charge-neutralizing positive charge nearby to "coax" the two electrons into nesting near each other. In the helium atom this positive charge is supplied by the helium nucleus, and, naturally, the potential well is of a different form. It is difficult to imagine how we could get a third edition of our electron model to fit so neatly into this package.

If we may now borrow the language of conventional quantum statistics, we can say that we have added together in the same quantum state and the same volume two fermions with opposed spins, and we can add no more into that situation. The famous Pauli exclusion principle has thus materialized pictorially before our eyes in terms of the *chaiyah* model of the electron. The Pauli exclusion principle now becomes all the more compelling because we now recognize in terms of the *chaiyah* electron model why all fermions must have *charge, spin,* and *wavelength* to live and to have the *correct dispersion relationship.* And the de Broglie–Einstein waves that all onta apparently possess are truly physical phenomena.

For the electron in a "box" of length L (with infinitely high potential barriers), $\lambda = 2L/n = h/mv = h/p$ and $p = nh/2L$, where n is the nth harmonic or quantum number. The energy W_n (which is all kinetic) corresponding to the nth harmonic or eigenfunction is given by

$$W = mc^2 - m_0c^2 = \sqrt{(m_0c^2)^2 + p^2c^2} - m_0c^2 = \sqrt{(m_0c^2)^2 + (nh/2L)^2c^2} - m_0c^2 \quad (55)$$

for the relativistic case.

For the nonrelativistic case $\lambda = 2L/n = h/m_0v$ or $m_0v = nh/2L$,

$$W_n = \tfrac{1}{2}\, m_0v^2 = \frac{n^2h^2}{8m_0L^2}. \quad (56)$$

We are now ready to take on the case of the one-dimensional simple harmonic oscillator where the potential function is $V(z) = 2\pi^2mv_0z^2 = \frac{1}{2}m\omega_0^2z^2$, and $v_0 = \omega_0/2\pi$ is the resonant frequency for the classical simple harmonic oscillator. Figures 17 and 18 show the expected configurations of the filamentary electron for $n = 0$, where the eigenvalues for the energy are $W_n = (n + \frac{1}{2})hv_0 = W$. With the introduction of the quantities $\lambda = 8\pi^2mW/h^2$, $\alpha = 4\pi^2mv_0h$ and $\xi = \alpha^{1/2}z$, the solutions to the Schrödinger equation can be written

$$\Psi_n(z) = N_n \exp(-\xi^2/2)\, H_n(\xi) \exp(-2\pi iW_nt/h) = \psi_n(z)\, \phi(t), \quad (57)$$

where N is the normalization factor, $2\pi iW_nt/n = i\omega t$, and $H_n(\xi)$ is a Hermitian polynomial. At $-i\omega t = 0$ the projection of this solution on the x–z plane is

$$\psi_0(z) = \left(\frac{\alpha}{\pi}\right)^{1/4} \exp(-\xi^2/2) = \left(\frac{\alpha}{\pi}\right)^{1/4} \exp(-\alpha z^2/2) \quad (58)$$

and is given by Figure 17(b), for $n = 0$, $H_0(\xi) = 1$. But for $n = 1$, $H_1(\xi) = 2\xi$, and at $-i\omega t = 0$ the wave function

$$\psi(z) = \left(\frac{\alpha}{\pi}\right)^{1/4} 2^{1/2}\, \xi \exp(-\xi^2/2), \quad (59)$$

and the filamentary solutions are diagrammed in Figure 19.

The solutions of the Schrödinger equation for the Coulomb potential well of the proton ($V = -Ze^2/r$, $Z = 1$) represent a case (like the simple harmonic oscillator) where the "kinetic" energy of the electron and hence the velocity and de Broglie–Einstein wavelength changes markedly over one wavelength. The filamentary representation of the solutions of the Schrödinger equation for the hydrogen atom for the angular-momentum quantum number $l = 0$, given in Figures 20 ($n = 1$, $l = 0$) and 21 ($n = 2$, $l = 0$), is in most respects similar to those for the electron in a one-dimensional box and in a one-dimensional simple harmonic oscillator.

For example: (1) The phase velocities of the two helical filaments are traveling in opposite directions (as contrasted with the free electron, where the two phase velocities are in the same direction). (2) The resultant spin can be in either the plus or minus z direction. (3) Another electron (a fermion) can be fit into the same volume with $n = 1$, $l = 0$ (or into $n = 2$, $l = 0$) with the spin and magnetic moment in the *opposite* direction. But only these two can be fit, no more!—the Pauli exclusion principle. (4) The whole configuration rotates as shown in Figures 14 through 20 with an energy level corresponding to $\hbar\omega_i$ = constant, and the frequency of the photon radiated or absorbed in the transition is given by $W_f - W_i = \pm\hbar\omega_{\text{rad}}$.

For the electron in the one (z)-dimensional box and as a one-dimensional simple harmonic oscillator the velocities and momenta in the x and y directions are assumed to be zero. Hence the uncertainties of knowledge of position in the x and y directions, $\Delta x = \hbar/\Delta p_x$ and $\Delta y = \hbar/\Delta p_y$, turn out to be infinite because $\Delta p_x = \Delta p_y \to 0$. Thus,

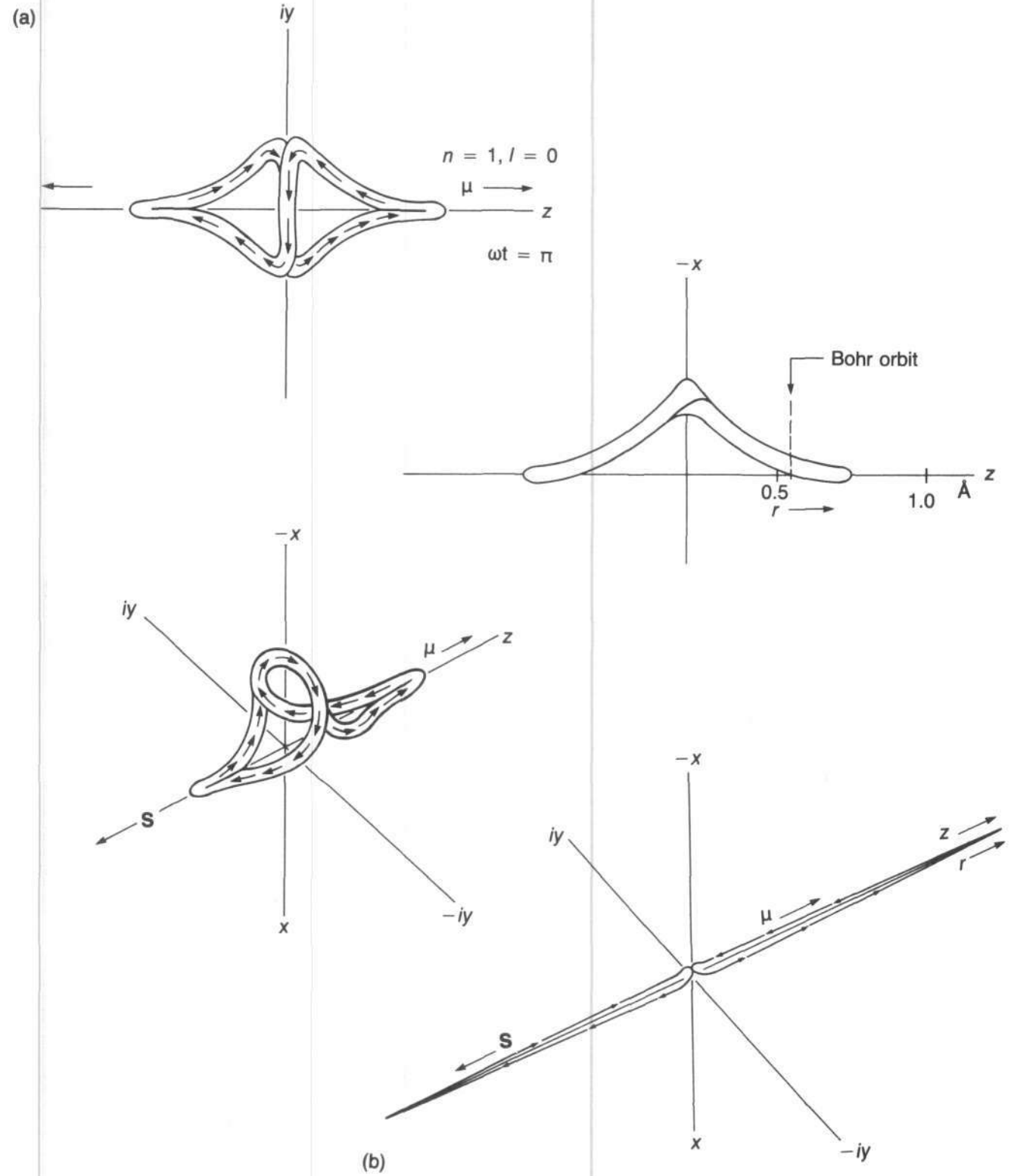

Figure 20. (a) Eigenfunction for lowest state of the hydrogen atom $n = 1, l = 0$. (b) Same state drawn with less distortion of scale.

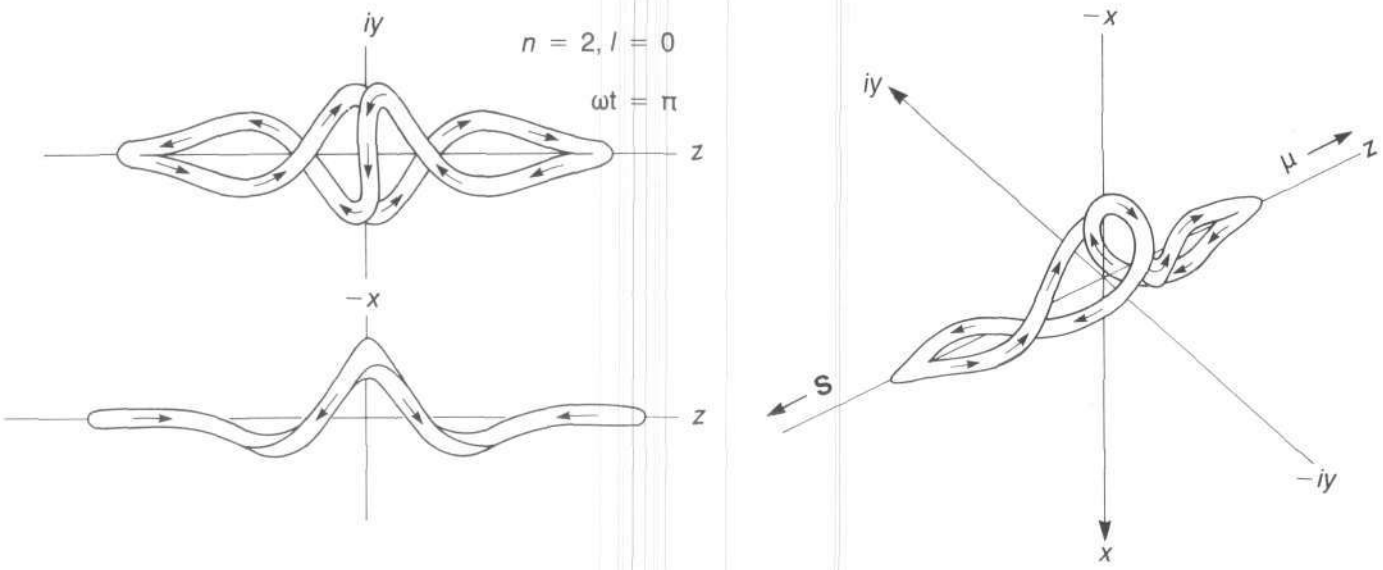

Figure 21. Eigenfunction of an electron in the $n = 2$, $l = 0$ state of the hydrogen atom.

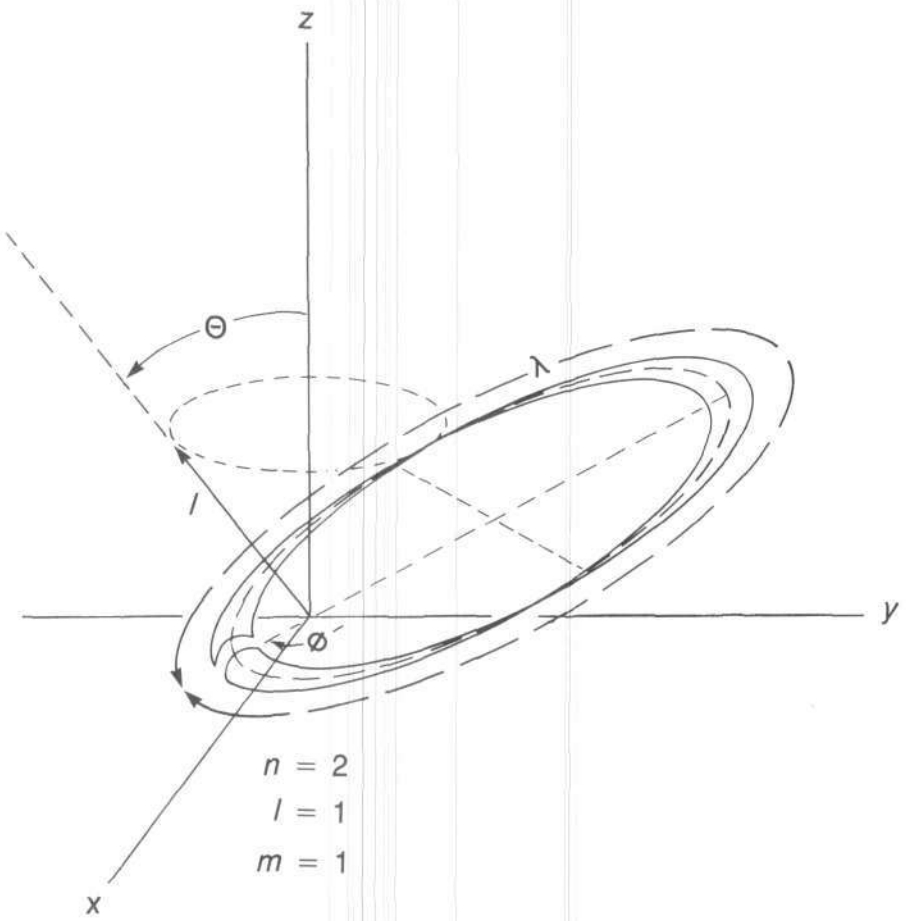

Figure 22. Eigenfunction of an electron in the $n = 2$, $l = 1$ state of the hydrogen atom.

although we know that the waves $\Psi_{RH}(z,t) + \Psi_{LH}(z,t)$ for Figures 14 through 19 are as diagrammed as a function of z,t, our uncertainty about the position of the configuration in the x–y plane means that the configuration could with equal probability be located with its axis *anywhere* in the x–y plane. Thus in the accepted language of quantum mechanics we can legitimately speak of the free-electron filamentary model in Figures 8, 9(a), 10, and 11 as being a packet of plane waves parallel to the x–y plane and traveling in the z direction. Therefore, if one should wish to employ a Huyghens principle in constructing an average or probabilistic interference or diffraction pattern when this filamentary electron with its waves encounters a double slit or crystal lattice, it is at least as legitimate to do so for this model as for the point-charge model.

The filamentary model has in addition the large philosophical advantages over the point-charge model that we have already enumerated. With the electron in the potential well of the hydrogen atom, even for azimuthal angular-momentum quantum numbers $l = 0$, there is a fundamental difference from the otherwise similar cases of the electron in the one-dimensional box and the one-dimensional simple harmonic oscillator. In the latter two cases we identified the wave propagation vectors **k** as being only in the $\pm z$ directions, but in the former case (the hydrogen atom) the **k** vector (for solutions where $l = 0$) is in the $\pm r$ direction, and the r direction can be, with equal probability, in the x, y, or z directions. Thus the volumetric probability of finding the point electron between r and $r + dr$ is $4\pi r^2\psi(r)\psi^*(r)dr$.

If one wishes to display to a viewer a black-and-white, three-dimensional model or two-dimensional photograph showing the probability (proportional to optical density) of finding the point electron at various distances from the proton, it is necessary to construct a suitable template and whirl the template with equal probability about all possible directions. Similarly, if one wishes to view a similar three-dimensional or two-dimensional photograph showing (as a function of the radius) where the average portions of energy of the filamentary electron's model lie, one must make a suitable template based upon Figures 20 and 21 and whirl it with equal probability in all directions.

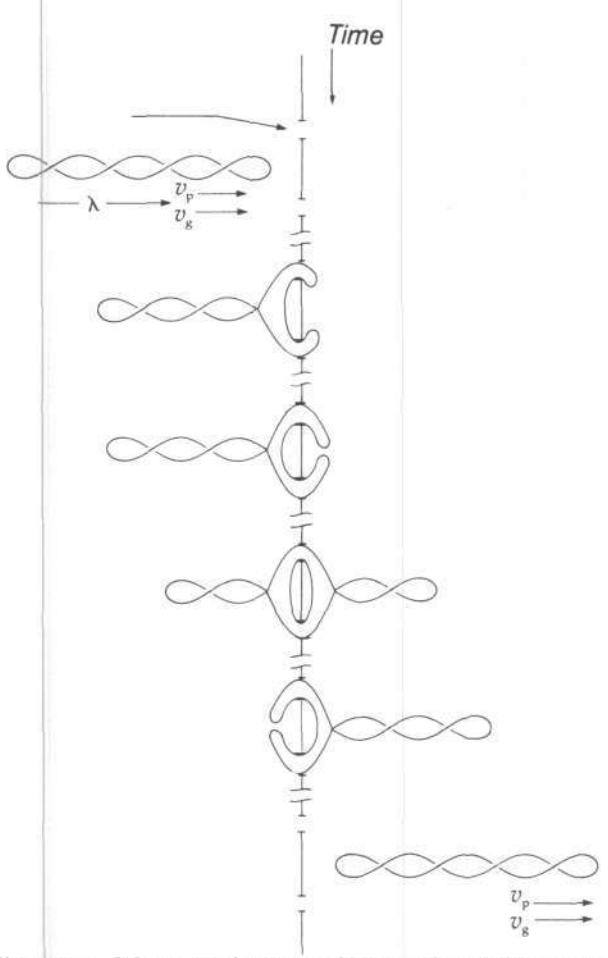

Figure 23. Schematic diagram of how a *chaiyah* filamentary electron might perform in a time sequence as it goes through a double slit (both slits at the same time) in a Thomas Young-type of double-slit experiment.

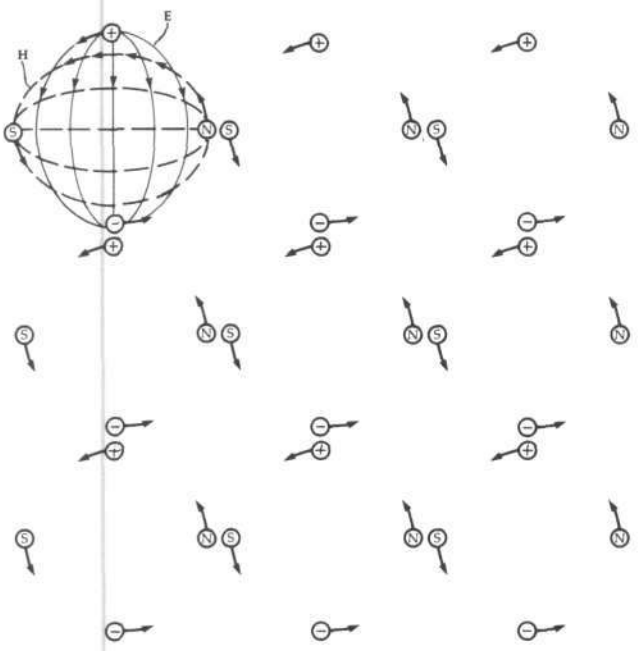

Figure 24. Schematic diagram of coherent monochromatic circularly polarized photons in a laser beam end-on as the beam recedes from the observer. If the beam is approaching the observer *either* the **E** vector *or* the **H** vector should be reversed. The photons appear as a two-dimensional array of synchronized windmills.

With the filamentary model of the electron we have thus far had a fairly easy time constructing the expected standing waves for the hydrogen atom because we have tackled only the cases where $l = 0$. Now we attempt the case where $n = 2$, $l = 1$ as shown in Figure 22. Note that instead of two filaments with waves traveling oppositely in the $\pm \mathbf{r}$ directions, there are the two filaments (RH, right hand, and LH, left hand) with waves traveling in the *same* direction parallel to the Sommerfeld elliptical "orbit." Note that the de Broglie wavelength is shorter and the amplitude of the wave near the proton is larger where the potential well is deeper and the kinetic energy greater.

The probability distribution factor $(\theta_{m,l})^2$ can be plotted (after White 1934) for various values of n, m, and l. The spin and magnetic moment of the electron do not vanish, even though the group and phase velocities now pursue the elliptical orbit instead of a straight line. The loops of the filament shown in Figure 22 adjust themselves so that the total angular-momentum quantum number $j = l + s$ can be $j = 1 + 1/2 = 3/2$ or $j = 1 - 1/2 = 1/2$.

If a *chaiyah* electron or photon of the filamentary type described in Chapter 1 encounters a double slit, how is it to produce a Thomas Young interference pattern of the type that would result from plane coherent waves of monochromatic light falling on the double slit?

We answer this question by first pointing out that filamentary onta are not mathematical points: They have geometrical extent, and their filaments are flexible enough to behave like the sensory antenna of an insect. As one of these onta encounters a double slit or a diffraction grating of N slits it can spread out and register the presence and positions of the slits on a sub-picosecond time scale. Once having this information in hand and remembering that it is really the equivalent of a plane wave propagating in the z direction, it knows what the appropriate interference pattern should be. If this particular specimen of onta repeats this exercise over and over many times it will fill out the plane-wave interference pattern. Each time the electron or photon goes through the slits it heads for a given point on the pattern that is determined by the phase as it strikes the slits and by the exact position of its centerline in the x direction as it strikes the slits. The probabilities that it heads for the various parts of the pattern are determined by the plane-wave interference pattern.

Figure 23 shows the author's rendition of how a *chaiyah* electron might look as it proceeds through the double slits, reassembles itself on the other side of the slits, and heads for the appropriate position on the interference pattern. The reader may well think of a more clever and simpler way for the electron to accomplish this mission.

It is fitting to ask the question, "What does a group of monochromatic photons in a coherent array, as in a laser beam, look like end-on as it recedes from the observer?" The answer is diagrammed in Figure 24, where these bosons appear like a lattice made up of synchronized and phase-locked, four-bladed windmills, all turning in the same sense, either clockwise or counterclockwise, to give coherent, circularly polarized light. By reversing the direction of either the **E** vector or the **H** vector (but not both), the beam will be obliged to approach the observer.

Chapter 3

Coherence of *Chaiyah* Electron Morphology With Plasma Structures Generated in the Plasma Focus and Similar Experiments

Nature has shown herself to be capable of self-organization in many contexts and on a vast range of time and distance scales. Each of the elementary onta, such as the photon, electron, proton, meson, and neutron, represents the structural organization and condensation of electromagnetic energy in a way that is not yet understood. Nuclei, atoms, and molecules represent a further self-organization of these elementary particles, and life in the form of plants and animals proliferates the structural organization of these molecules with a mind-boggling and awe-inspiring complexity and beauty. The gravitational condensation of large masses of atoms and molecules (and ions) is self-organized to produce galaxies, suns, and solar systems. Molecules swimming in a fluid state can crystallize into an organized lattice array to form a solid crystal. Even fluids and gases in flowing can organize themselves into vortices—for examples, Edgar Allan Poe's *Descent into the Maelstrom* and tornadoes.

In the less complex of these types of organization it can be perceived that the "free energy" of the system is reduced by permitting the structural organization to occur, and the result is a more stable state where destabilizing forces and processes are minimized or delayed, if not eliminated. For example, a pencil standing on its point on a table gives up its gravitational potential energy (its "free energy") and trades that free energy for kinetic energy as it falls, and then for heat energy as it strikes the table. Water droplets and soap bubbles spontaneously assume spherical shapes. It would seem that throughout Nature with its manifold structures there is a very powerful "Minimum-Free-Energy Lobby" that ensures that these stable, minimum-free-energy structures spring spontaneously into existence.

The *plasma focus* is a super "boneyard" (nomenclature borrowed from the paleontologists) wherein can be found and studied not only the laboratory-produced morphologies of solar and cosmic plasmas, such as solar flares, sun spots, and galaxies; but also the morphologies present in Type I and Type II superconductors. Moreover, this richest of all boneyards in plasma physics yields information on the processes of acceleration that produce the high-energy particles associated with solar flares, and perhaps even those found in cosmic rays. Since 1961, among all controlled thermonuclear machines, this fascinating device holds the world's record for rate of neutron production (by several orders of magnitude). Results of experiments prove that the plasma focus is every bit as much a magnetic-confinement fusion device as is the tokamak! The plasma focus, which has since 1961 been largely ignored by the U.S. Atomic Energy Commission,

the Energy Research and Development Agency, and the current Department of Energy (DOE), deserves to have this negative attitude on the part of the DOE reconsidered.

The vacuum diode and vacuum spark, which reproduce many of the effects of the plasma focus with metal-vapor plasma, are also a rich boneyard of *chaiyah* plasma.

The collision of plasma jets fired across magnetic fields produces plasmoids in the form of miniature barred-spiral and ring galaxies.

The striking morphological coherence between plasma filaments and related structures in the plasma focus, and the *chaiyah* filamentary electron presented in the preceding chapters, reflects an invariant geometrical action principle operating on all levels of the Universe—from the "micro" world of elementary onta to the macroscopic scale of galaxies. The following discussion will examine this coherence from the vantage point of a detailed review of empirical results from the plasma focus and related experiments.

Force-Free Vortex Filaments

In the middle of the 19th century, Beltrami, a mathematical physicist at Pisa, "discovered" magnus-force-free, minimum-free-energy, "Beltrami flow" in fluids. The magnus force density is the force that gives an airfoil lift, and it is equal to the vector product of the vorticity vector and the velocity vector (and -1).

In the flight of a goose, the vorticity vector points from the tip of its port wing to the tip of its starboard wing, and the velocity vector of the air flowing across those wings points from the beak of the goose toward its tail. Figure 25 shows the morphology of Beltrami's flow, where the velocity vector and the vorticity vector are *everywhere parallel*; hence the magnus force is everywhere zero, and the flow is magnus-force-free. This flow pattern in cylindrical geometry is derived from the vector equation $\nabla \times \mathbf{V} = \alpha \mathbf{V}$, where α is a constant. Beltrami, an associate of the great geometer Bernhard Riemann, showed that under certain constraints this is also a minimum-free-energy state. Lord Kelvin, who at the time was also much interested in fluid mechanics, understood the nature of this force-free fluid flow.

It was known to Gilbert, the court physician of Queen Elizabeth I, that the flow of gas burning in a flame was influenced by the presence of a magnet. Investigators of the 19th century readily recognized that an "ionized gas," which is a fluid composed of approximately equal numbers of positive ions and electrons, can conduct an electric current mostly because of the agility of the very light, free electrons. Nineteenth-century investigators also were aware that an electrical conductor carrying a current perpendicular to a magnetic field experiences a "Lorentz force," which is the force that makes an electric motor possible. The Lorentz force density is the vector product of the electric-current density vector in the conductor and the magnetic field vector in which the conductor is immersed.

In the 1950s, two astrophysicists, Chandrasehkar and Woltjer (1958), reasoned that the magnetic fields in the arms of galaxies might have a Lorentz force-free struc-

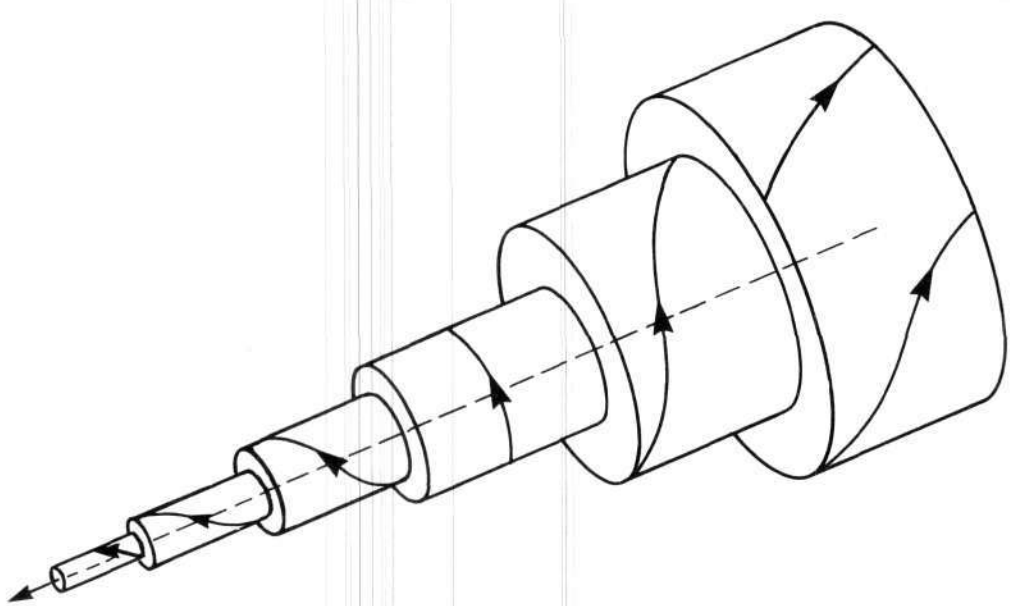

Figure 25. The directed flow pattern of Beltrami, Magnus-force-free flow, where the direction of the arrows represents not only the velocity vector **v** of the fluid but also the vorticity vector ω. In a Lorentz force-free configuration of magnetic field vector **B** and current density **j**, the arrows shown in the figure represent the directions of both **B** and **j**. In Beltrami flow, **v** and ω are everywhere locally parallel to each other. In the Lorentz force-free configuration, **B** and **j** are everywhere locally parallel to each other.

ture, and that the Lorentz force-free structure would be one where the electric current density and magnetic field are everywhere parallel. The Lorentz-force-free morphology is the same as the magnus-force-free morphology (Figure 25), where the vorticity is replaced by the current density and the negative of the velocity is replaced by the magnetic field.

This magnetic morphology is the basis of the magnetic-fusion-energy spheromak and field-reversed pinch programs, most of whose workers seem to be historically unaware of the work of Beltrami (Woltjer and Nardi 1970, 1976; Wells 1976; Bostick 1966). Instead they seem to have adopted J.B. Taylor (1975) as their primary latter-day patron saint in this subject of minimum-free-energy morphology.

In fluid mechanics the vortex filaments associated with Beltrami flow can be observed in the flow of air over the diagonal leading edge of a delta-wing aircraft. The vortices of Beltrami flow are responsible for the drilling of holes in the lee rock at the top of mountain ridges where the wind flows mainly diagonally across the ridge.

Experimental Observations of Diamagnetic And Paramagnetic Vortex Filaments

Diamagnetic Plasma Vortex Filaments

During 1954-1956, the author, on leave from Tufts University, amused himself at Lawrence Livermore National Laboratory with some small plasma guns that he had constructed. He fired them at each other across a magnetic field in a vacuum and in a gas at pressures of about 0.004 torr. The results were startling, as can be seen in the photographs in Figure 26 (Bostick 1956, 1957, 1958; Laurence 1956). It was quickly demonstrated that it is possible to produce plasma configurations that sponta-

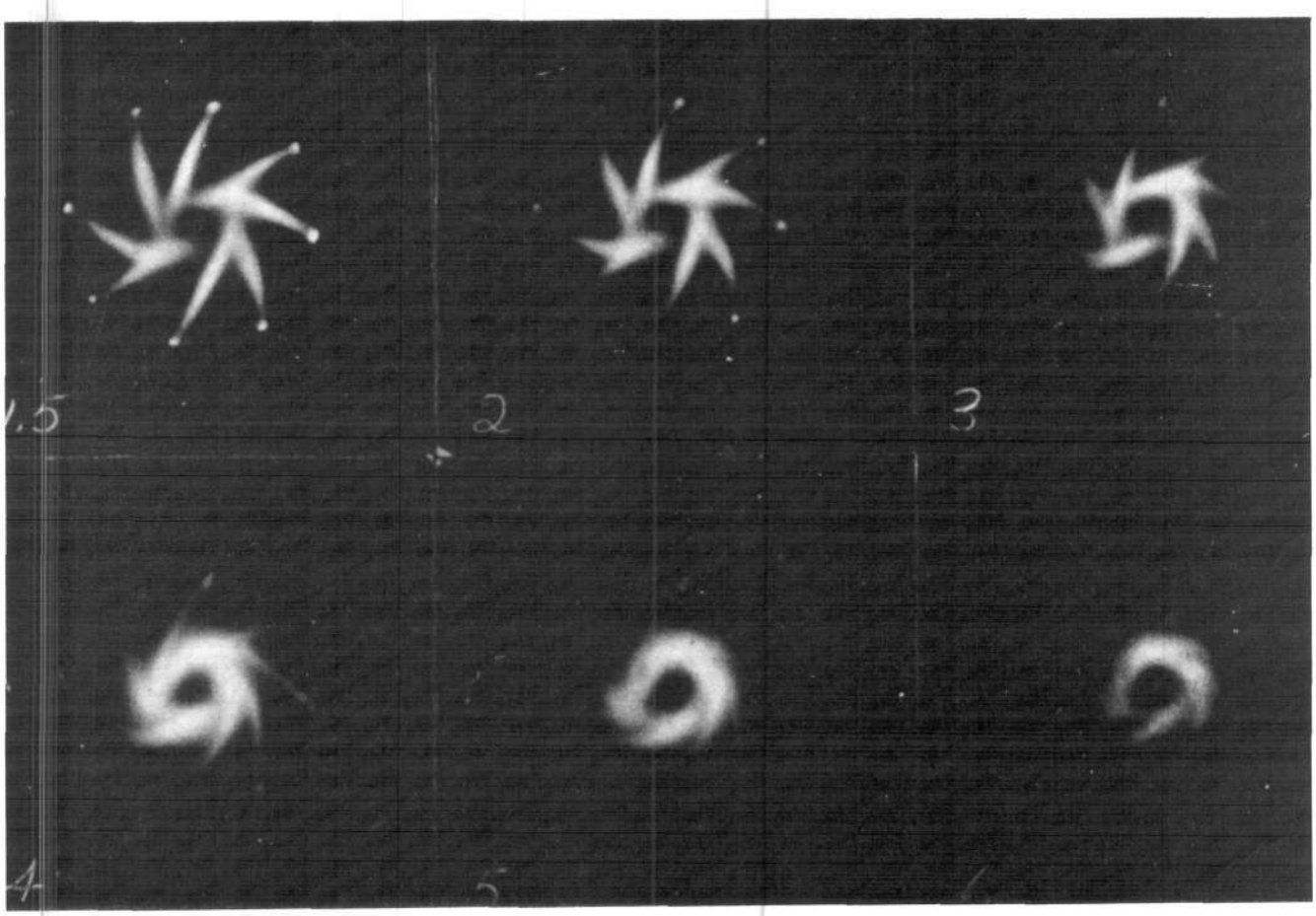

Figure 26. Chronological sequence of plasmoids (fired simultaneously from plasma focus guns) colliding with one another to eventually form a plasmoid ring. This photograph appeared on page one of the *New York Times* Dec. 12, 1956 in an article by W.H. Lawrence titled "Physicist 'Creates' Universe in a Test Tube."

neously spring into being (plasmoids) and that these plasmoids, which have incredibly sharp boundaries, can preserve their integrity as they bounce off one another, or can form new configurations as they attach to one another, depending upon the conditions of their creation and environment. The late Jim Tuck, who was the leader of the CTR program at Los Alamos, upon seeing these photographs at a "Sherwood" (CTR) meeting at Princeton in 1955, remarked, "How is it possible for these two mushy snowballs of plasma to bounce off like billiard balls?"

The diamagnetic plasmoids (diamagnetic plasma vortices of the type that bounce off one another) are basically the same phenomena that are observed in the convection rolls in the penumbra of sunspots and in the paired striations that are observed to elongate along the Earth's magnetic field after explosions of nuclear weapons or barium canisters above the Earth's atmosphere. Similar, long, cigar-shaped structures occur in the Earth's ionosphere.

Diamagnetic plasma vortices were also observed by the author in a laboratory simulation of the envelope and tail of a comet in 1955 at Lawrence Livermore: A magnetized (along the axis), sharpened bar of steel approximately 2.5 cm in diameter was placed in a vacuum chamber and a plasma gun was fired along the axis at the sharpened point of the magnetized bar. Open-shutter photographs of the self-luminous plasma showed the plasma flow to be concentrated in striations that started at the sharpened tip and continued through the tail. Similar striations are observed in astronomical comets.

Diamagnetic vortices are observed in the laboratory simulation of plasma flow (the solar wind) over the magnetosphere of the Earth (Bostick 1966).

Eventually we recognized that Nature was creating pseudo-force-free, minimum-free-energy plasmoids (*chaiyah* plasmoids!) of the diamagnetic variety: measurements at Stevens of the rotational velocity profile of these vortices showed that they rotated like rigid bodies, which is the form of rotational profile that gives minimum rotational energy for a given amount of angular momentum (Bostick 1977). The configurations in the laboratory-produced, barred-spiral-galaxy configurations are much more complicated than the simple diamagnetic plasma vortex filament that is lined up parallel to a background magnetic field in a vacuum.

The author had the pleasant fortune in 1958 to meet again Sam Allison, his old physics professor at the University of Chicago, who had read the author's papers on this work in the *Physical Review*. Sam chuckled as he remarked, "Bostick, I see that you have produced some experimental effects that have the theoreticians temporarily baffled."

When the author first reported this work at an American Physical Society meeting in Washington, D.C., in 1956 (declassification had begun), one of his slides showed plasmoids attaching to each other to produce a ring-spiral that resembled a pinwheel. The author's old boss on the MIT linear electron accelerator (microwave, standing wave), J.C. Slater, was in the audience. A friend who was sitting near Slater related later that he heard Slater remark, "These pictures must have been taken on the Fourth of July!"

David Pines, who was also attending that session, objected to the author's use of the term "plasmon" to describe these structures. Pines pointed out that "plasmon" was already reserved for the quantum of plasma oscillation energy and suggested the term "plasmoid," and plasmoids they have remained.

The spontaneous formation in the laboratory of plasma configurations (plasmoids) that resemble (in miniature) the morphology of barred-spiral galaxies by two plasma jets projected at one another across a magnetic field has prompted the author's suggestions that these laboratory barred-spirals provide an analogue dress rehearsal in miniature for the formation of astronomical galaxies. The high-fidelity quality of this analogue is underlined by the experimental laboratory observation that the plasma jets have a long-pitch helical shape that will give the spiral arms a slight helical shape. Hence if an astronomical barred-spiral galaxy (a disk galaxy as contrasted with an elliptical galaxy) is looked at in a direction parallel to the plane of the disk, the tips of the spiral arms should show themselves to be deflecting out of the plane of the disk. And this deflection of the tips of the spiral arms out of the plane of the disk is precisely what is astronomically observed in many disk galaxies. This observation thus validates not only the primacy of the role of magnetic fields in galactic genesis and morphology, but also the model presented for galactic genesis in Figure 26. The model is also applicable to star formation, and in particular binary star formation: If, in the laboratory simulation, the background plasma is too dense or the magnetic field too high, each plasma jet will curl up into a rotating "ball" without touching the plasma in the opposite jet.

Anthony Peratt (1980, 1983, 1984) has performed both experiments and computer simulation involving the attraction of parallel columns of plasma carrying current in the same direction. He describes three-dimensional "SPASH" code calculations with axial magnetic field that produce motion pictures that look similar to Figures 26 through 29. But such computer-simulated "spiral arms" cannot show any helicity.

Paramagnetic Plasma Vortex Filaments

At the 1961 International Atomic Energy Agency Conference on Controlled Thermonuclear Fusion and Plasma in Salzburg, the group of Kvartskava (Kvartskava et al. 1961) at Sukumi in the Soviet Union presented a paper showing striking framing camera pictures of filaments forming in both the θ-pinch and Zeta-pinch discharges. (In the Zeta-pinch the electric current is driven through a column of ionized gas along the direction of the axis

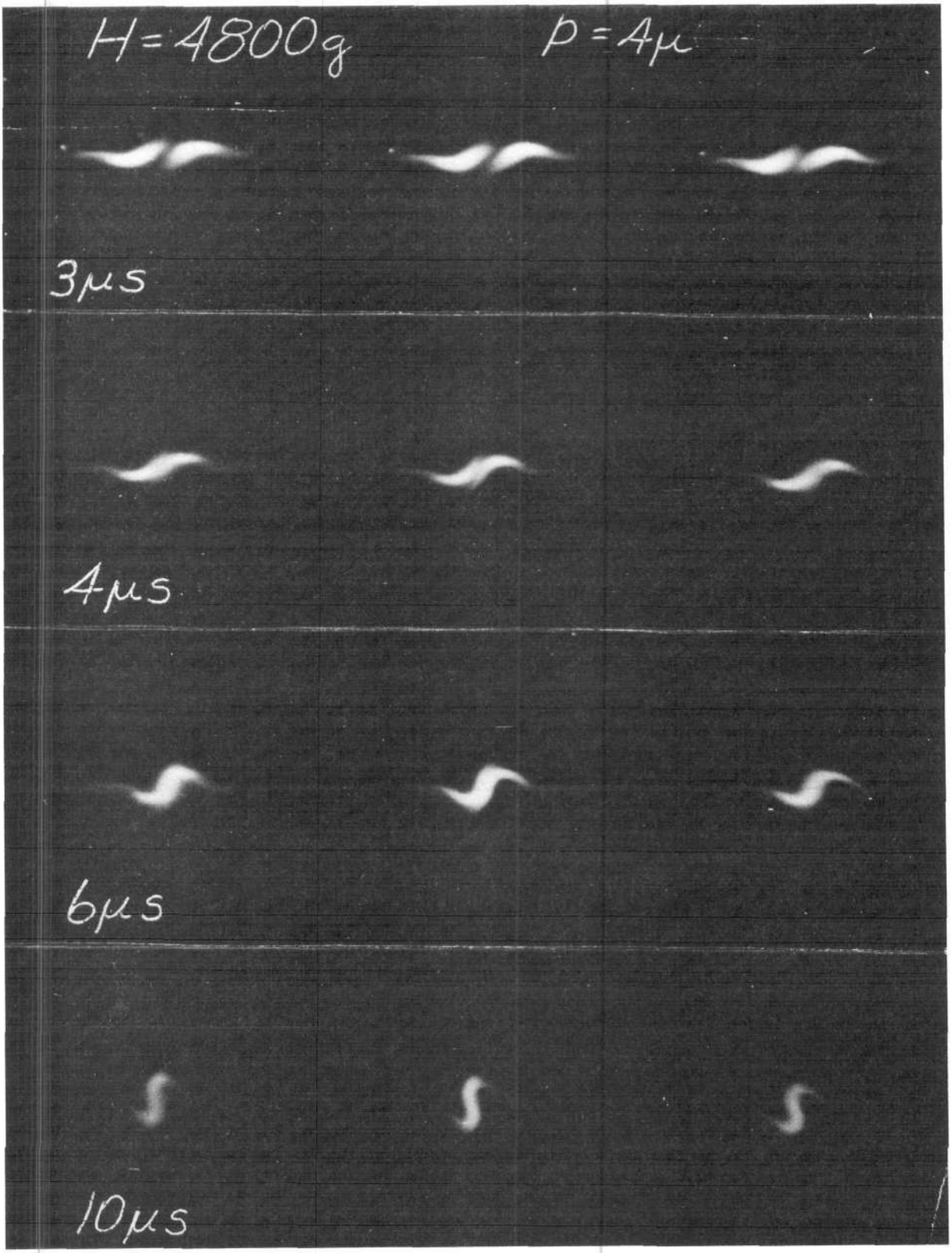

Figure 27. Two plasmoids hit head-on after their birth 3 microseconds previously in a uniform magnetic field of 4,800 gauss in a rough vacuum. The view is in the plane of the two plasmoids. A single structure is formed that after 12 microseconds has the shape shown.

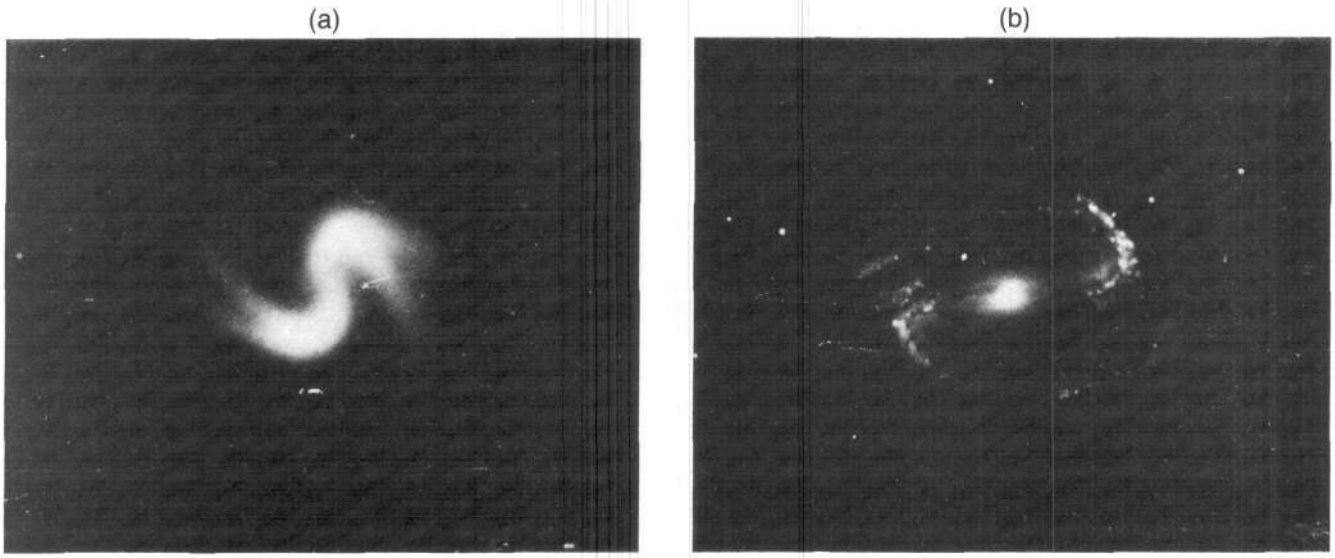

Hale Observatories

Figure 28. (a) An edge-on view of a plasmoid formed in a process similar to that in Figure 27, which resembles a barred-spiral galaxy (b). The barred-spiral galaxy shown is NGC 1300.

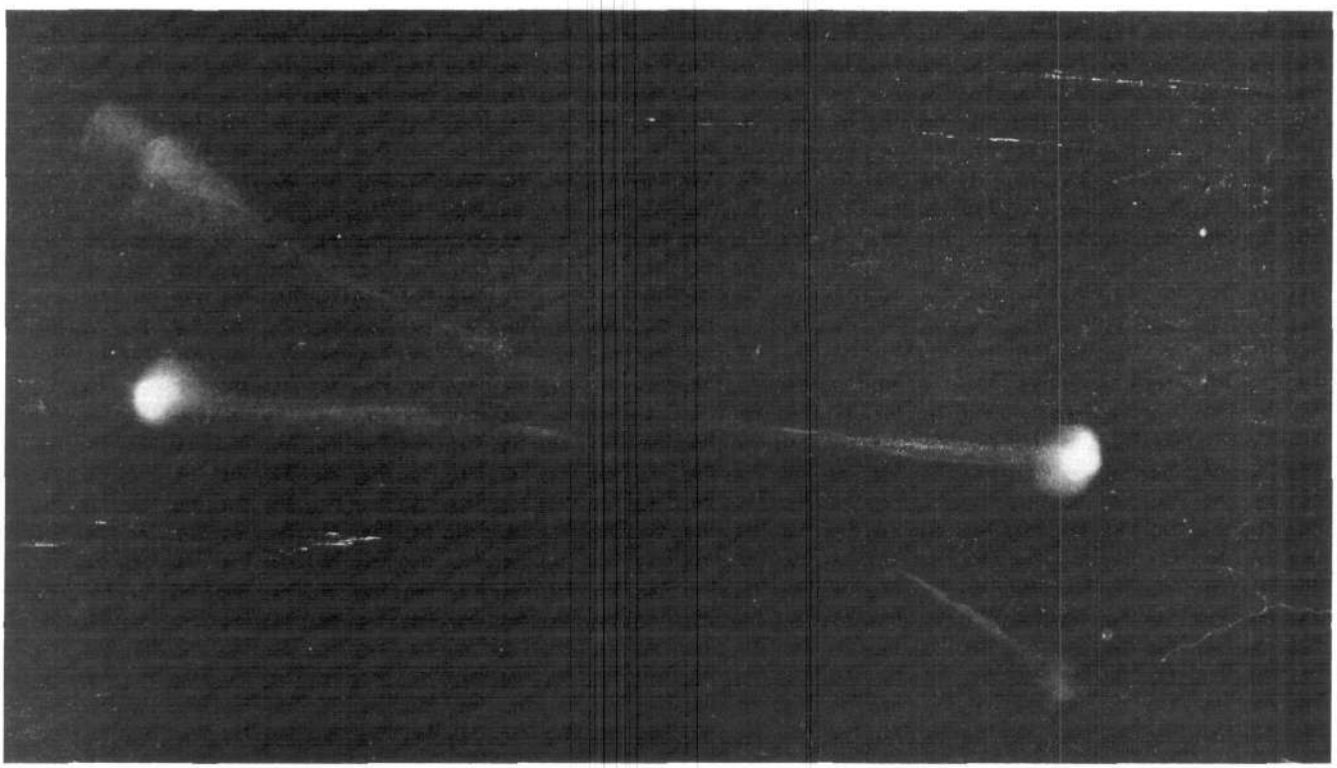

Figure 29. Two plasmoids are fired at each other in a vacuum chamber containing a strong magnetic field. The initial bursts from the guns are marked by the bright spots at left and right. The luminous streaks are the subsequent paths of the plasmoids.

of the column. In the θ pinch, the electric current is driven circumferentially around the column.)

Kvartskava used some general thermodynamic arguments to explain the existence of these filaments. It is an interesting historical coincidence that at that same scientific meeting at Salzburg, Filippov (Filippov et al. 1961) of the Soviet Union reported a high-current discharge in deuterium gas with a novel electrode structure (later to be known as a plasma-focused device; see Figure 30) in which the neutron yield of 10^{10} neutrons was a factor of 100 greater than that of the previous Zeta-pinch machines! The Zeta-pinch machines were observed about 1954 (independently in the Soviet Union and the United States) to have produced about 10^8 neutrons per discharge.

In the ensuing four years, several investigators—most importantly Joseph Mather (1971) at Los Alamos—inspired by Filippov's work, built and operated plasma-focus machines, but very few people, if any, paid any attention to the filaments that had been observed by Kvartskava. During this period Daniel Wells (the author's thesis student at Stevens), working on his experimental Ph.D thesis at the Princeton Plasma Physics Labbratory, was trying, with modest success, to create a Lorentz-force-free plasma torus with a pulsed conical θ-pinch coil (Wells 1976). The full-blown glory of the spontaneously arising force-free morphology of the vectors **B** (magnetic induction), **j** (electric current density), **v** (mass velocity), and ω (vorticity) was experimentally revealed at Stevens Institute of Technology, where investigators observed the filaments in the current sheath of the plasma focus to be produced in pairs (see Figures 31 and 32) and to have the structure shown in Figure 33 (Bostick et al. 1966, 1972, 1980; Bostick 1966). In 1965, experimenters at Stevens demonstrated with image converter photography and signals from magnetic coupling loops that the current sheath of the plasma-focus machine consisted of paired vortex filaments, the vorticity and local (axial) B_z being oppositely directed in each component of the pair. These vortex filament pairs, which act like motors since they produce their own rotation (+ and − vorticity), and like dynamos since they produce their own local B_z (+ and −), are magnus- and Lorentz-pseudo-force-free, minimum-free-energy structures that spring spontaneously into existence. Recently, Soviet investigators (Bykovskii and Lagoda 1982) have shown experimentally that similar structures form spontaneously in the current sheath (consisting of metallic ions and electrons) in vacuum sparks and diodes. It can be historically noted that there were no theoreticians [with the possible exceptions of Shafronov (1966) and Harrison (1963)] who *a priori* predicted the spontaneous arising of structures of any kind, and there are even now relatively few theoreticians who are actively interested in these spectacular, spontaneously arising experimental effects.

The heavy theoretical artillery in the magnetic fusion energy programs of the Soviet Union, United States, United Kingdom, and elsewhere had years ago predicted for the pinch effect (Bostick 1977) the sausage instability ($m = 0$), the kink instability ($m = 1$), and the characteristics of the Rosenbluth current sheath (Rosenbluth 1954) (a reinvented Ferraro current sheath of geophysical renown). Nobody, however, had predicted that the current sheath would actually consist of plasma concentrated and self-organized into pairs of right-handed and left-handed, minimum-free-energy, Lorentz-force-free, and magnus-force-free filaments. These filaments are the "blood vessels" that the plasma invented to carry its large electric current with minimum resistance. These filaments are the answer to the famous Alfvén "limiting current" of 17,000βγ A. [A column of space-charged-neutralized plasma carrying a current greater than 17,000βγ A will have its current interrupted by its own self-magnetic field because the electrons will be turned around to the opposite direction by this magnetic field. $\beta = v/c$, where v is the electron speed and c is the speed of light; $\gamma = (1 - \beta^2)^{-1/2}$.] Since even small plasma-focus machines carry about one-half million amperes in their current column, they would exceed the Alfvén limit.

The plasma changes the rules of the game by forming filaments where each electron in carrying its share of the current enjoys the Nirvana of always flowing *parallel* to a local magnetic field that is created by the collective motion of all the electrons. Thus currents of 2.5×10^6 A can be carried without submitting to the tyranny of the 17,000βγ A. Vorticity and its concomitant magnetic field are powerful instrumentalities for organization! No beehive, labor union, or automobile assembly line was ever better organized than these electrons.

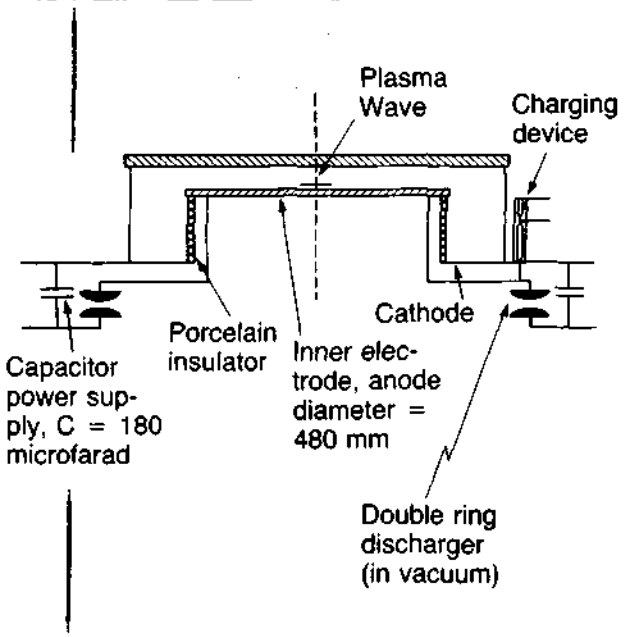

Figure 30. Schematic diagram of the Filippov electrode geometry that produced 10^{10} neutrons in 1961.

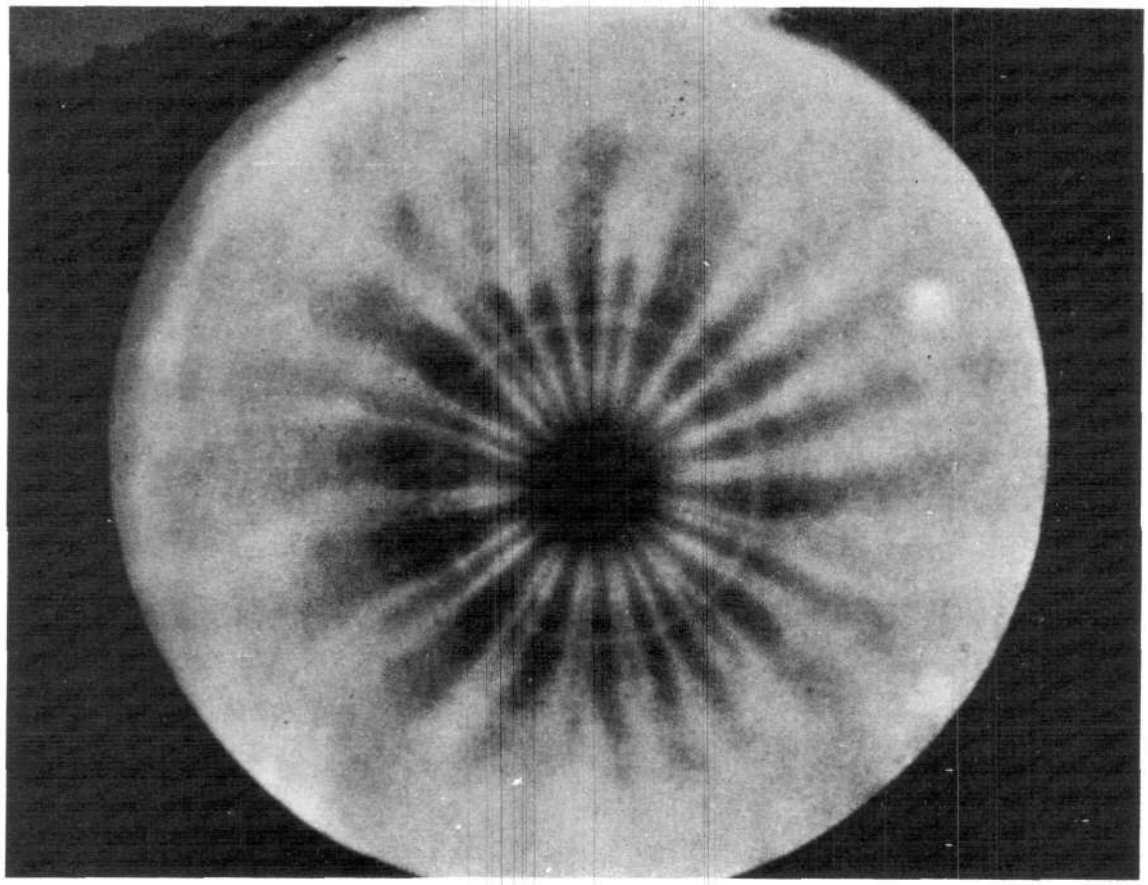

Figure 31. Image converter photo of a 5-kJ plasma focus showing the pair vortex filaments that are carrying the current in the "current sheath."

Generation of Condensed *Chaiyah* Structures

When the current sheath (composed of these filaments) forms at the end of the center conductor, a hollow column that reduces its diameter to about 5 mm (see Figure 34), the filaments are pressed close together and a rupture of one of the sorely pressed filaments occurs. The rupture is observed to spread in a few picoseconds to most of the other filaments all around the circumference of the column, like a sail ripping in a gale. Suddenly the beautifully organized force-free structure for carrying the current flow has been chopped in two as with a meat cleaver.

The magnetic fields of adjacent vortex filaments in the current sheath are antiparallel, and once the filaments are ruptured, they continue to "eat each other up" in zipper fashion as their magnetic fields annihilate each other progressively along their lengths, and the neutron-producing region moves along the filaments away from the original region of rupture. This process continues even up into the "umbrella" of the current sheath. This process of mutual annihilation of the filaments when they are ruptured is the solar flare process in miniature in the laboratory (Bostick 1977), and it is the most efficient mechanism of transforming locally stored magnetic energy into particle energy. As such this mechanism should even be considered on a cosmic scale as a candidate for acceleration of the onta that form the cosmic rays. (What a "boneyard," the plasma focus!)

The electrical resistance of the cloven region increases in a few picoseconds by a factor of several hundred ("anomalous resistance"!). The magnetic energy stored in the filaments of the plasma column, around the plasma column, and in the inductance of the entire circuit sends the voltage across this cloven region (a "plasma diode") up to a factor of 1,000 greater than the original voltage on the capacitor that drove the current in the plasma focus. The power from the current driven across this high resistance by this high voltage accelerates electrons (through the hollow-anode center conductor) and deuterons (if the filling gas is deuterium) to a spectrum of energy from a few thousand electron volts to 13 MeV.

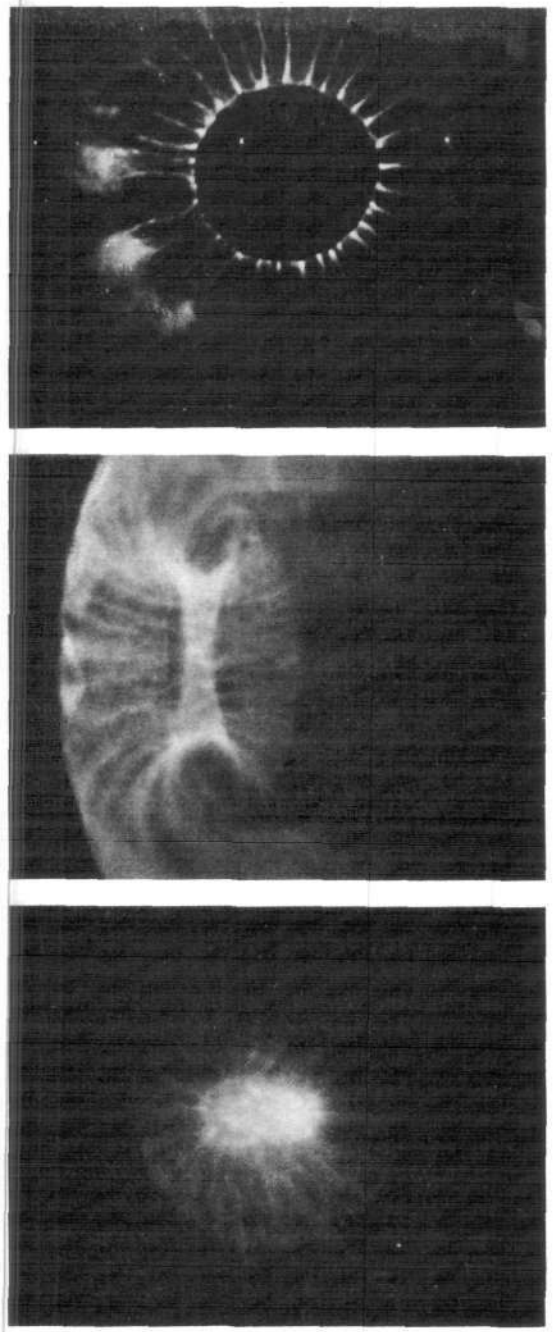

Figure 32. (a) Image converter photographs of vortex filaments. A 5-nsec axial view of the vortex filaments lying in the grooves of the corrugations of the current sheath. The edge of the 3.4-cm-diameter positive center conductor can be seen. Note how filaments fray at the outside end. Filaments (with pairing) can be detected. Center conductor (anode) is solid.

(b) Oblique view of current sheath with filaments with a hollow center conductor (anode).

(c) Same as (b), but at a later time when vortex filament destruction is proceeding in the halos. Hollow center electrode (anode).

In all three discharges, the background filling pressure is 8 torr of deuterium; peak current is ~ 0.5 MA.

The process might well be described by the term "electronic ram" (Raudorf 1951, 1974; Farynski 1983; Noll 1983)—or more appropriately, "magnetic ram"—because of the magnetic energy stored around the electrodes in transmission lines and the nearby Beltrami-filamented current sheath, which insists that the current across the cloven gap not be changed. As the conduction current across this cloven gap drops to essentially zero in a few picoseconds, the displacement current takes its place.

It is the "magnetic insulation" provided by this displacement current that now stops the flow of electron current across this gap in every region except the geometrical center of this displacement-current column, where the insulating magnetic field is zero. This displacement current effectively charges the "diode capacitor" to a voltage of about 13 MeV, which accelerates electrons and deuterons to that energy. The displacement current drops to zero and reverses sign, whereupon a flood of conduction current is released and the capacitor discharges rapidly. This process repeats itself with a period of about 20 psec and a duration of the pulse of the electron beam of about 3 psec. The train of pulses endures for about 200 psec.

The high energy of the plasma-focus-produced deuterons preanoints the plasma focus as the heir apparent to the controlled-fusion throne when the profession recognizes that the change to the clean, no-neutron fuel, ^{11}B plus ^{1}H, is to be made. Recent experiments at Stevens (May 1984) show an energy spectrum of the deuterons that is a straight line on a log–log plot with an exponent

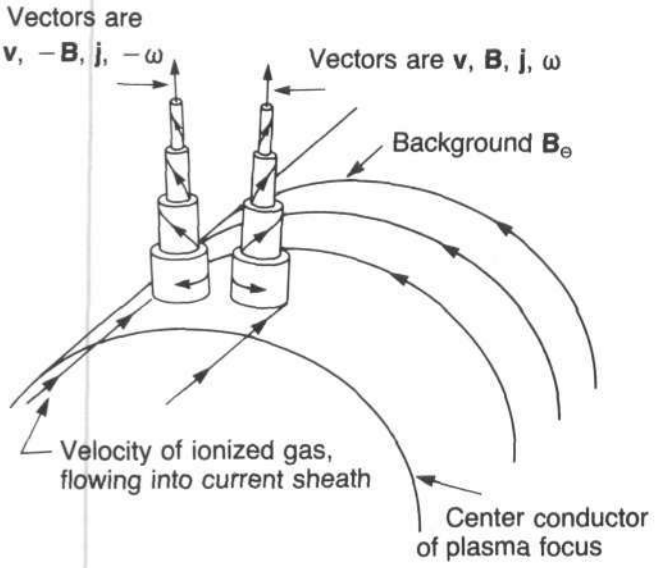

Figure 33. Dissected diagram of the vector configurations of a pair of paramagnetic vortex filaments formed in the current sheath of the plasma focus; **v** is mass flow velocity, **B** is local magnetic induction, **j** is current density, ω is vorticity, $\mathbf{B}_e$ is background magnetic field caused by flow of current in the coaxial electrodes.

of −2.7, which is similar in form to that of the high-energy primary component of the cosmic rays! Some of the 2.45-MeV neutrons produced by the ${}_1^2D + {}_1^2D \rightarrow {}_2^3He + {}_0^1n$ reaction are observed to be produced in the volume of deuterium gas extending about 30 cm in front of the center conductor, but the larger portion (about 65 percent) of the D–D neutrons are observed, by neutron collimation techniques, to be produced in a volume less than 1 cm in diameter in the region where the column was ripped by the tearing of the filaments. It appears from X-ray pinhole camera photos that some of the filaments may survive to carry a large portion of the current all by themselves, become knotted, and reconnect themselves into individual plasma "nodules" (Bostick et al. 1978), as shown in Figure 35.

These individual plasma nodules have electron and ion densities of 10^{19} to 10^{20} cm^{-3}, perhaps as high as 10^{22}, a factor of 100 to 1,000 greater than the filling ion density of deuterium! They have magnetic fields up to 200 MG, the highest magnetic fields known to be produced in a laboratory! The pressures of these magnetic fields go up to 2,000 Mbar, far higher than the pressures existing in the interior of an exploding nuclear weapon. The dimensions of the diameters of the columns are observed to be as small as 40 μm, and they carry circulating currents of 5 MA. Recent Soviet work by Bykovskii and Lagoda (1982) and Korop et al. (1979) with laser-induced "vacuum" discharges that use metallic plasma from the electrodes confirm the results on plasma nodules reported by the Stevens investigators. Indeed, Bykovskii and Lagoda claim to have densities in the nodules up to 10^{22} cm^{-3}.

When the high currents in the nodules are self-interrupted they also generate high-energy electrons (average

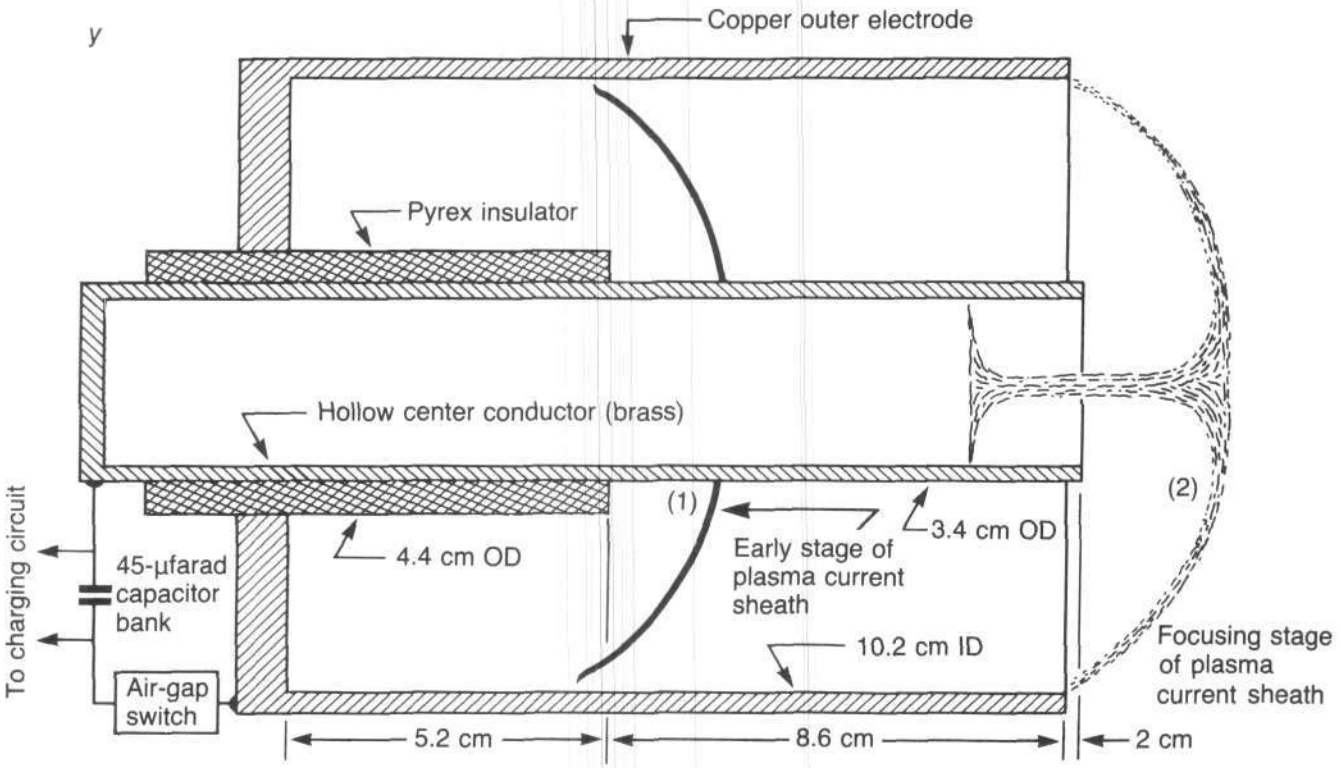

Figure 34. Schematic cross section of coaxial accelerator with a hollow center electrode. The current sheath is shown (1) during motion between the electrodes and later (2) at the time of halo formation, when neutrons and X-rays are formed. (OD is outside diameter; ID is inside diameter.)

energy 5 keV at densities of approximately $10^{20}/cm^3$) that produce the X-ray pinhole images by bremsstrahlung on the deuterons, and high-energy deuterons that not only produce the 2.45-MeV neutrons from the D–D reaction, but also produce the 14.1-MeV deuterons from the ${}^2_1D + {}^3_1H \rightarrow {}^3_2He + {}^1_0n$ reaction, the tritons (${}^3_1H$) being produced by the ${}^2_1D + {}^2_1D \rightarrow {}^3_1H + {}^1_1p$ reaction, and *being present in sufficient numbers only because of the highly local magnetic confinement* of the ${}^3_1H$ in these nodule structures (Bostick et al. 1975)! The highly definitive X-ray pinhole photos of the plasma nodules, one of the highest spatial-resolution diagnostic techniques available in the plasma-focus research so far, can thus pinpoint the sources of a fairly large fraction of the neutrons to these plasma nodules whose structural dimensions go down to 40×200 μm. In a small (~10 kJ) plasma-focus machine there may be about two to four clearly observed strong nodules. In a large plasma-focus machine (200 kJ) there may be so many nodules superimposed that it is difficult to count them. It may be that these plasma nodules observed in the X-ray pinhole photos are actually the sites of the most intense acceleration of electrons and deuterons by the magnetic-ram–diode process.

The investigators at Stevens have used thin films of CR-39 etchable-plastic track-detector material in front of the X-ray film for pinhole-camera photography of the dense plasma nodules. The CR-39 records the tracks of positive ions produced in the range of about 1 to 3 MeV. A permanent magnet is placed at the pinhole to deflect the images of charged positive ions having a large enough *e/M* ratio. The results show that there are deflected images composed mostly of singly charged deuterium atomic ions. The undeflected image is formed of tracks corresponding to a small *e/M* ratio, perhaps a net electronic charge of 1 or 2, but a large number of deuterons, 10 to 1,000! The author has observed similar particle tracks with pinhole photography on CR-39 track detectors from the first "betatron focus" in air at 1 torr after the anode foil on the FX-25 REB machine at the Air Force Weapons Laboratory. These gigantic "molecules" (or "minute plasmoids") represent an assemblage of electrons and deuterium ions, almost space-charge-neutralized, where the thermal energy of the electrons and deuterium ions is very small compared with the organized energy. The density of electrons in the cluster probably approaches solid density of $10^{23}/cm^3$. By inference we can say that this is evidence that the ion and electron densities in the plasma nodules themselves approach the same high values. We can point out that this condensation represents essentially a *phase transition to a degenerate state*. The ordered circulation pattern within these clusters is not known, but they must be some kind of minimum-free-energy, force-free configuration. These clusters emanate from the nodules in all directions. These clusters represent yet another form and size of plasmoid that Nature adds to its already long list of *chaiyah* plasmoids.

Phase Transition into Coherent Condensed States: Analogy with Superconductors

The paired vortex filaments in the current sheaths of the plasma focus are the macroscopic embodiment of the paired flux tubes formed by minimum-free-energy Cooper-paired electrons (bosons) in Type II superconductors at a few degrees Kelvin, where condensation of these bosons into a well-regimented blanket produces the resistanceless vortex flow around the "flux tubes." In Type II superconductors the docility of these condensed, degenerate, well-organized bosons is induced by the low temperature and the Coulomb neutralizing effect of the positive ions of the metallic lattice of the superconductor material. This condensation of the boson gas is viewed as a phase transition phenomenon.

In the current sheath of the plasma-focus machine (or the "vacuum" diode) the electron temperature is at least a few electron volts (certainly not ~1°K!). So we ask, "What induces the phase-transition condensation into paired vortex filaments in the current sheath of the plasma focus? What induces these electrons to behave like degenerate, Cooper-paired bosons?" The only answer that we can supply is that the organized, vortex energy of the positive ions (~100 eV), and the electron energy parallel to the Lorentz-force-free magnetic field, *ab initio* and on a continuing basis (for ~2 μsec), far outweigh the disrupting effects of any ion temperature T_i or electron temperature T_e. We know that T_e (perpendicular),

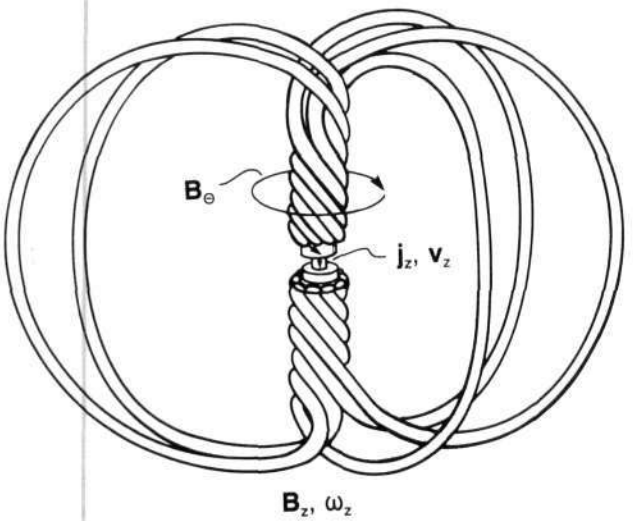

Figure 35. Diagram of a hypothesized plasma nodule, a toroidal solenoid wound with a force-free core carrying current density **j**, vorticity ω, magnetic field **B**, and mass velocity **v**, as deciphered from the appearance of a photograph of a plasma module taken by means of an X-ray pinhole camera.

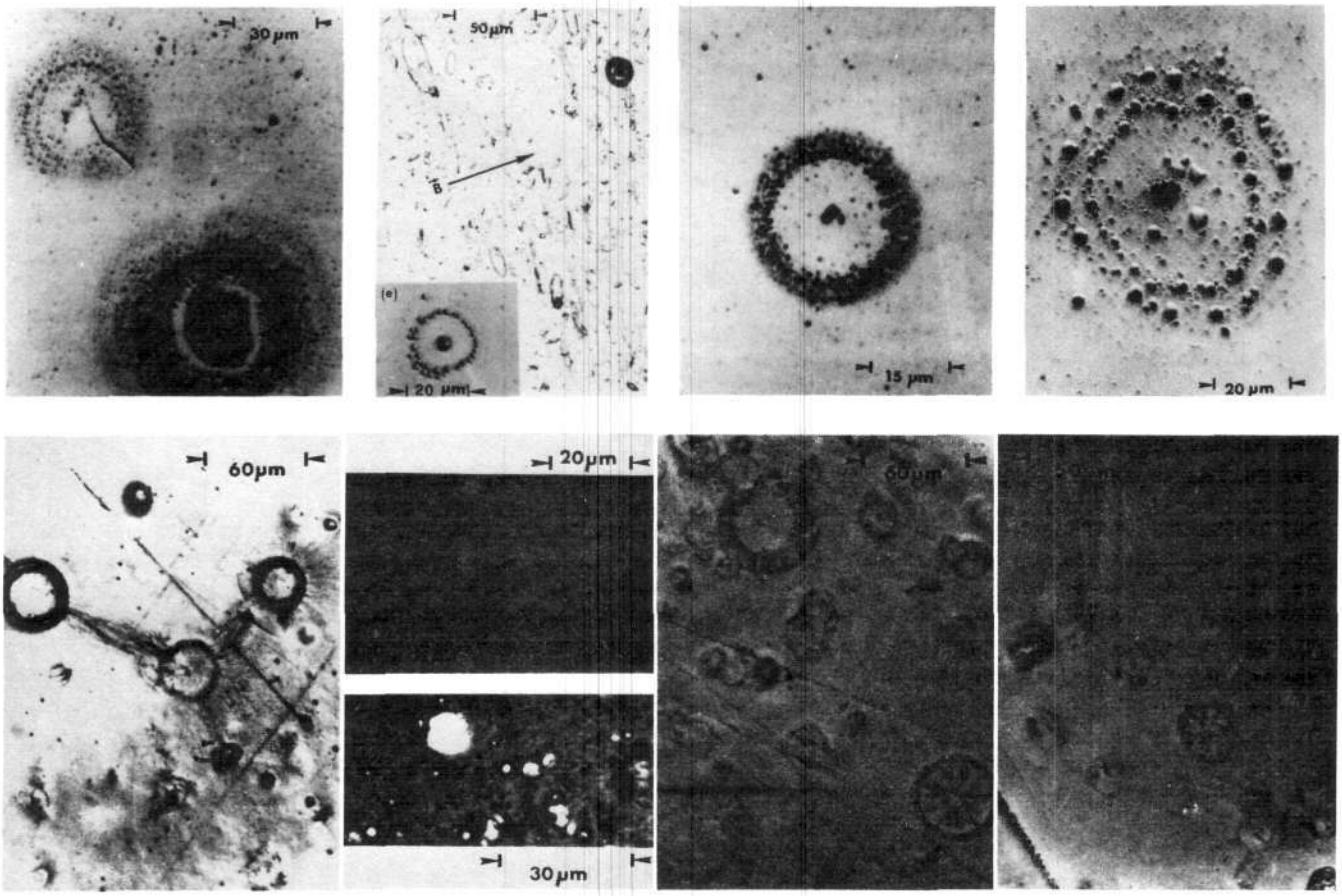

Figures 36 and 37. Observed damage patterns produced on polystyrene witness foils and target witness surfaces that show that the relativistic electron beam proceeding through the background gas of 3 torr pressure of deuterium was condensing into filaments of 2- to 300-micron diameters. There is no magnetic field.

electron energy perpendicular to the local B, will be subject to synchrotron radiation, but T_e (parallel) will not. There is thus a tendency for the electrons to retain only that energy that is parallel to the local B, and the electrons will eventually flow everywhere parallel to the local B. There may be other more subtle effects, not yet understood, that continually convert T_e (perpendicular) to electron energy parallel to the local B, which is a pseudo-Lorentz force-free configuration.

Meirovich and Sukhorukov (1975) have noted that in the classical Bennett pinch, if the theory is carried correctly to its logical conclusion, the electron (and positive ion) densities on the axis will approach infinity. Before this can happen the electrons will become degenerate, and therefore one can expect degeneracy in the pinch. Meirovich predicts degeneracy for electron densities greater than $10^{30}/cm^3$. He predicts the formation of a gigantic "linear atom" within which thermonuclear reactions can occur because the deuterons can pick up the high degenerate energy of the electrons, and at $n = 10^{30}/cm^3$ the Lawson criterion $n\tau \geq 10^{14}$ might be achieved. However, Meirovich does not take into consideration the filamentation of the current sheath that prevents the Bennett pinch from forming. And he has not considered the formation of nodules, which in themselves are a kind of degenerate condensation with $n \cong 10^{20}$–10^{23}, vorticity, and pseudo-force-free magnetic fields up to hundreds of megagauss. But nevertheless, we should heed his seminal suggestion that these degeneracies should be considered as a possible aid to the controlled thermonuclear process.

It may be that the currents in the central column of the nodule can exceed the Pease–Braginski current (Peratt et al. 1980, 1983, 1984; Braginski 1958), and that the radiation loss (by bremsstrahlung and synchrotron radiation) will exceed the joule heat developed by collisions between electrons and positive ions, and that a degenerate collapse to very high densities can occur.

But the Pease–Braginski critical current concept was not developed for the self-consistent, force-free type of magnetic fields and current density patterns we believe to be present in the plasma nodules. No one really knows

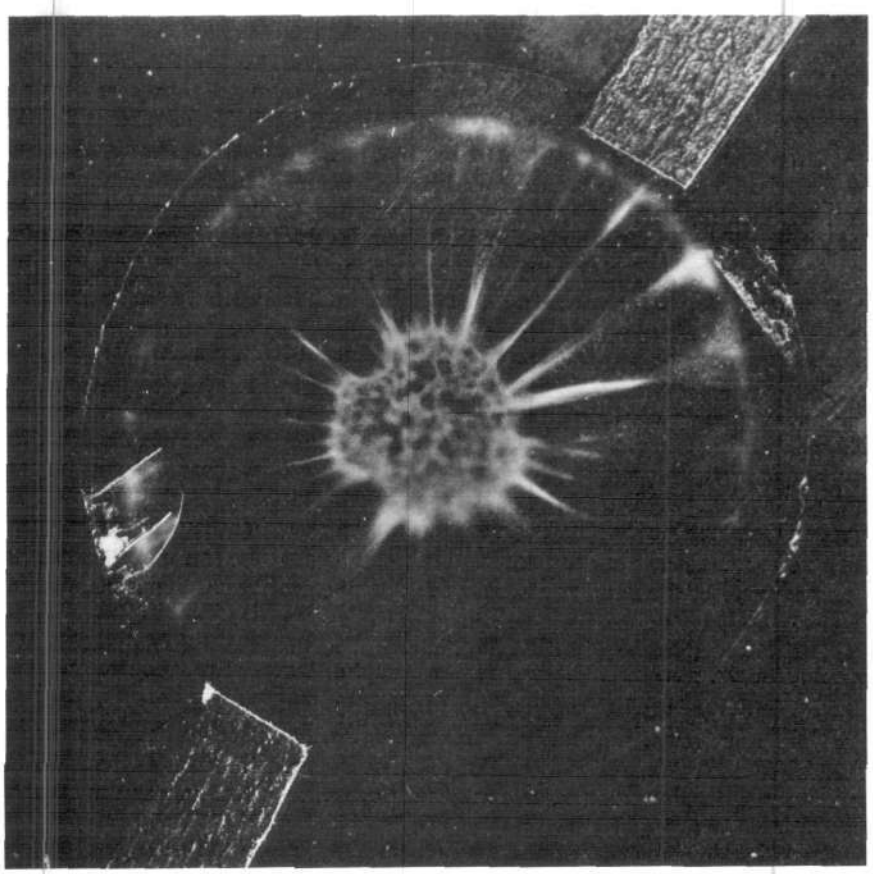

Figure 38. Bleach pattern produced on blue cellophane placed against the downstream side of an .001-inch titanium anode foil by the relativistic electron beam, at 1.5 MeV energy from the half-inch-diameter carbon cathode in the FX-25 relativistic electron beam machine (25 kA, 40 μsec). Radial striations are engraved by the pairs of vortex filaments of electrons that are formed with the help of some plasma that evolves from the electrodes and the background gas in the so-called vacuum diode. The space charge neutralizing effect of the evolution of plasma permits the vortex filaments to be, as a group, pinched toward the center of the pattern. The flux-tube character of each current-carrying vortex filament is evidenced by the center region where the incoming filaments collide with each other. The magnetic flux along the axis of each incoming flux tube is brought into this center region by the inward radial transportation of the flux-tube-bearing filaments.

One interpretation of the unbleached islands in the center is that there are regions where the local $\mathbf{B}_z$ flux tubes are trapped. Another possible interpretation is that the unbleached areas represent regions of "return current" of plasma electrons with a surrounding sheath of unpinch. What is most likely is that both effects are occurring in the same region to produce the islands of unbleach. The photograph shows regions where the unbleached islands or cells are packed in a regular hexagonal pattern like a honeycomb. Here we see what is very likely the most efficient two-dimensional packing of "Beltrami cylinders." Each Beltrami cylinder contains relativistic current (and local $\mathbf{B}_z$) flowing cathode-to-anode axially at its periphery and, perhaps, plasma electron current flowing axially (and local $\mathbf{B}_z$) anode-to-cathode at its axis.

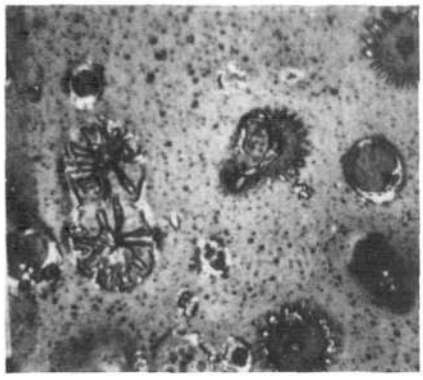

Figure 39. In 1982, Vittorio Nardi of the Stevens Institute group, working with the relativistic electron beam from the plasma focus, studied the behavior of vortex filaments as they passed from a dielectric (glass) drift tube of 0.5 cm diameter. Within a few millimeters downstream, the damage pattern showed that the filaments were increasing their surface energy by serrating their peripheries and by fissioning.

what is happening in the plasma nodules to produce the condensation to high densities, high current densities, and enormous magnetic fields. It does not seem to be known what brings about an interruption of these currents to produce a picosecond conversion locally of this magnetic field energy into electron and positive ion energy.

Now the "plot thickens": In 1977, at Stevens where the relativistic electron beam (REB), ~0.7 MeV, generated by the plasma focus was being studied (Bostick et al. 1980), Vittorio Nardi observed damage patterns produced on polystyrene witness foils and silicon witness surfaces which showed that the REB proceeding through the background gas of 3 torr of deuterium was condensing into filaments of diameters 2 to 300 μm (see Figures 36 and 37). The larger-diameter patterns were made up of the 2-μm filaments arranged in spiral patterns, looking very much like tight-packed, concentric-circle configurations. The damage is produced by positive ions (~2 MeV) that are well organized and collectively accelerated by the filamentary structure. The entire structure involves the positive ions and the electrons, and, we believe, the flux-tube morphology of the pseudo-Lorentz-force-free structure and the vorticity. These structures were called filaments, but it was really not known whether they were shaped like cigars (that is, long and filamentary) or like washers or doughnuts (that is, short, closed circles).

These Stevens experimental results on filamentation in REB were confirmed in 1979 by the author, on leave from Stevens at the Air Force Weapons Laboratory: With a 1.5-MeV, 25-kA, 40-nsec electron beam from such a vacuum-diode machine, the FX-25 REB machine, the same type of damage patterns that were observed at Stevens were observed in air at 1 torr. The roles of vorticity and local, self-manufactured B_z in the REB patterns, as hypothesized by the Stevens group, were royally confirmed in 1981 by the bleach patterns produced on blue cellophane placed against the downstream side of the 0.001-inch Ti anode foil of the FX-25 REB machine (see Figure 38): The paired radial striations observed are engravings of the pairs of relativistic electron vortex filaments that form in the current sheath that develops in the pinching process as a plasma in the "vacuum" diode is evolved from the Ti anode foil and the carbon cathode.

The flux-tube nature of these filaments is beautifully portrayed by the spots of "no-bleach" that occur near the center of the pattern: These no-bleach spots are, without a doubt, concentrations of local B_z, of one sign or the other, that have been created and transported by the paired vortex filaments as they move from the periphery of the pattern toward the center. These "no-bleach" islands may also be sites of "return" plasma electron current. In the REB filaments we have the spectacle of 1.5-MeV electrons and collectively accelerated 1–2-MeV positive ions collaborating to perform the same morphology and current-carrying function as the Cooper-paired electrons, condensed by phase transition into a degenerate gas that flows as a regimented, resistanceless blanket vortically to form the paired flux tubes of Type II superconductors.

Again, the only explanation for this degenerate super-organized type of behavior on the part of the 1.5-MeV electrons and the positive ions is that the disorganized, perpendicular-to-local-B electron energy is (and remains) negligible compared to organized, parallel-to-local-B electron energy. And the organized energy of the positive ions overwhelms their own disorganized energy. The spontaneous formation of these vortex filaments in both the REB machines and the current sheath of the plasma focus represents a densification (condensation or compression) of mass, magnetic energy, and organized (or directed) kinetic energy *without* the increase of temperature (or random kinetic energy), and such a process is typical of a phase transition from a classical state (like a perfect gas) to a degenerate state (like Cooper-paired electrons-bosons in Type II superconductors).

In 1982, Vittorio Nardi of the Stevens group, working with the REB from the plasma focus, studied the behavior of the vortex filaments as they passed from a dielectric (glass) drift tube of 0.5 cm diameter to one of larger diameter. Within a few millimeters downstream the damage pattern showed that the filaments were increasing their surface energy by serrating their peripheries and by fissioning (see Figure 39). If we can assume that the head of the filament is moving as fast as the measured speed of the head of the beam ($\beta = 0.7$), we can calculate that this deformation of the periphery (which increases the surface area) takes place in a time $0.3/(0.7 \times 3 \times 10^{10}) \approx 0.15 \times 10^{-10}$ sec $= 15 \times 10^{-12}$ sec $= 15$ psec, which suggests that the relativistic vortex filament possesses an incredibly fast "nervous system." This tendency to increase surface means that the filament has a negative surface energy, similar to the flux tubes of Type II superconductors. The smaller dielectric drift tube has been carrying a substantial portion of the return current for the filaments, which are carrying some of the return current on their own surfaces. When suddenly the drift tube wall is removed to a larger distance from the filaments, the drift tube carries less return current, and the filaments must enlarge their surface areas to be able to carry more return current on their own surfaces.

Finale

This article has set forth a conception of the electron and photon as composed of highly concentrated self-gravitational electromagnetic fields. The frantic search for "grand unification of all forces"—electromagnetic, strong, electroweak, and gravitational—"The Holy Grail," so to speak (or perhaps more appropriately, "The Golden Fleece"), is now in principle essentially solved: All forces are electromagnetic in character; the differences depend only upon the morphology and dimensions. The mysterious strong, short-range forces of nuclear physics will go the way of the epicycles of Ptolemaic geocentric cosmology and the phlogiston of the 18th century.

Aristotle preached that there was one set of physical laws for heavenly bodies and another set of laws for earthly bodies. The Copenhagen interpretation of quantum mechanics preaches that there is one set of physical laws for macroscopic-land but another law-of-the-land for atomic-land. This present work is the author's way of showing that this Aristotelian and Copenhagen School logic is philosophically flawed, that the quantum-mechanical wave function is a physical wave on an electromagnetic filament, that a unification (comparable to the return of the prodigal son) is taking place between quantum mechanics and classical physics. Aristotle also stated that women would never be able to compete in strenuous sports such as the Olympic Games (one set of laws for male bodies, another set of laws for female bodies). The recent performances by women in the Olympic marathon further belie his logic.

Aristotelian and Copenhagen School logic are examples of the "apartheid" syndrome in scientific thought. The adjective *apartheid* applies, for example, to the law imposed by the Spanish Conquistadores, which forbade the Indians in the New World to own a horse.

In this article we strike a blow for freedom from the tyranny of the apartheid syndrome in scientific thought, not only in the matter of the morphology of and cosmology of the electron, but also in the matter of Department of Energy funding for the plasma focus as a fusion device: The same basic laws apply to the plasma physics from the largest tokamak devices down to the smallest plasma-focus devices. There should be a sense of community, understanding, and brotherhood among the people working on these disparate devices. The Department of Energy should not continue to refuse to support plasma-focus fusion research because the plasma focus is small and not understood by the department's proposal reviewers. The plasma focus is as well understood by the people who work with it as the tokamak is by its workers.

The philosopher Descartes said, pretentiously and with considerable flippancy, "*Cogito, ergo sum*" (I think, therefore I am). The onta and the plasmoids can make more profound and modest statements about their lives: The onta and plasmoids could say, "Our free energy strives to become a minimum" (*unsere freie Energie strebt nach minimum*). The onta and plasmoids could say, "In doing so we are obliged to create filaments with charge, current, Poynting-vector spin, and waves in order that we may spring into life and live." The onta may also add, "To achieve this stable, equilibrated, force-free, free-energy-minimum *chaiyah* silhouette we have faithfully adhered to a strict diet of natural, distributed-source **E** and **H** vectors, and have religiously eschewed concentrated gourmet sweets like Newtonian lump-point mass and point charge, so dear to the palates of the practitioners of quantum electrodynamics. And by eschewing the gourmet effects of lump-point mass and charge it is not necessary for us to endure the mental and physical agony of the deceitful corsets and girdles of renormalization."

And with this declaration against the tyranny of Aristotelian logic, all onta and plasmoids in the entire Universe raise their glasses (filled only with natural, unadulterated juices) as they join in the toast, "*L'chaim!*"

And as they turn their backs on the Pied Pipers from the Copenhagen Schoolhouse and march toward the light of a new scientific renaissance appearing on the horizon, they exultingly raise their voices in song to Friedrich Schiller's "Ode to Joy" and Beethoven's Ninth Symphony:

Freude, schöner Götterfunken,
Tochter aus Elysium,
Wir betreten feurtrunken
Himmlische, dein Heiligtum.

Joy, immortal spark of Deity,
Daughter of Elysium,
Filled with fire-drunken gaiety,
To thy temple-ground we come!

References

Beltrami, E. 1889. "Considerazioni Idrodinamiche" [Hydrodynamic Considerations]. Rendiconti del Reale Instituto Lombardo. Serie II. Tomo XXII, pp. 121-130.

Born, M.H. 1971. *The Born-Einstein Letters*. New York: Walker.

Bostick, W.H. 1956. *Phys. Rev.* **104:** 292.

————. 1957. *Phys. Rev.* **106: 404**; "Plasmoids," *Sci. Amer.* **197: 81** (Oct.).

————. 1958. *Rev. Mod. Phys.* **30(3)**: 1090.

————. 1958 and 1961. "The Gravitationally Stabilized Hydromagnetic Model of the Elementary Particle." Gravity Research Foundation Essay Contest, New Boston, New Hampshire: First prize 1961, fourth prize 1958.

————. 1977. "The Pinch Effect Revisited." *Intl. J. Fusion Energy* **1**: 1 (March).

————. 1978. "Toward Understanding the Nature of Fusion Energy." *Fusion* **2**: 42-54 (May).

Bostick, W.H., Nardi, V., and Prior, W. 1971. *Proc. Conf. on Cosmic Plasma Physics, ESEIN. Frascati, Italy, Sept., 1971*. New York: Plenum Press, p. 175.

————. 1972*a*. *J. Plasma Physics* **8**: 7.

————. 1972*b*. *Proc. of International Symposium on Dynamics of Ionized Gases, IUTAM, Tokyo, 1971*. Tokyo: Univ. Tokyo Press. p. 375.

————. 1975. *Proc. IAEA Conf. on Plasma Physics and Controlled Nuclear Fusion Research*. Tokyo (Nov.) 3: 109.

————. 1980. *Phys. Rev. A* **22**(5): 2211.

Bostick, W.H., et al. 1966. *Phys. Fluids* **9**: 2079.

————. 1983. *Second International Conference. on Energy Storage Compression and Switching, Venice, Italy*. New York: Plenum Press.

Braginski, S.I. 1958. "The Behavior of a Completely Ionized Plasma in a Strong Magnetic Field." *Soviet Phys. JETP*. 6(33): 494 (March 1958, No. 3).

Bykovskii, Yu.A., and V.B. Lagoda. 1982. "Local High-Temperature Plasma Formations in a High-Current Pinching Discharge." *Sov. Phys. JBTP* **56**(1): 61 (July).

Chandrasekhar, S., and E. Fermi. 1953. *Astrophys. J.* **118: 116**.

Chandrasekhar, S., and L. Woltjer. 1958. *Proc. Natl. Acad. Sci.* **44**: 285.

Conant, D. 1978. *Unified Quantum Field Theory*. St. Louis, Mo.: Los Alamos Consultants.

Einstein, A. 1953. *The Meaning of Relativity*. Princeton, N.J.: Princeton Univ. Press, p. 107.

Farynski, A., et al. 1983. "A Diode Model of High-Energy Charged Particle Emission in the Plasma Focus Device," 11th European Fusion Conference, Aachen, 1983, p. 497.

Filippov, N., T. Filippova, and B. Vinogradov. 1961. *Proc. 1st IAEA Conf. on Plasma Physics and Controlled Thermonuclear Research, Salzburg*, p. 577.

Harrison, E. 1963. *Plasma Phys.* **5**: 23.

Hasimoto, G.H. 1972. *J. Fluid Mech.* **51**(part 3): 477.

Komelkov, V.S., et al. 1960. *Proc. 5th Int. Conf. on Ionization Phenomena in Gases, Munich* **2**: 2191.

Korop, E., B. Meierovich, Y. Sidel'nikov, and T. Sukhorukov. 1979. "Micropinch in a High-Curent Diode." *Sov. Phys.* **22(9)**: 727 (Sept.).

Kvartskava, I., et al. 1961. *Proc. 1st IAEA Conf. on Plasma Physics and Controlled Thermonculear Research, Salzburg (1961)*, p. 533.

Laurence, W.H. 1956. "Physicist 'Creates' Universe in a Test Tube." *New York Times* (Dec. 12), p. 1.

Jiménez, J.L., and R. Montemayor. 1983. "The Classical Motion of an Extended Charged Particle Revisited," Nuovo Cimento **75**(1): 87 (11 May 1983).

Mather, J. 1971. "Dense Plasma Focus." In *Methods of Experimental Physics*. Vol. 9, Part B, Plasma Physics, ed. R. Lovbora and H. Orien, p. 187. New York and London: Academic Press.

Meirovich, B. and Sukorukov, S. 1975. "Equilibrium Structure of Relativistic Beams," *Soviet Phys. JETP* **41**: 895 (May).

Nardi, V. 1976a. *Proceedings of the First International Conference on Energy Storage, Compression and Switching, Asti-Torino, Italy, Nov. 1974*. New York: Plenum, p. 173.

————. 1976b. *Phys. Rev. Lett.* **25: 718**.

Noll, R., et al. 1983. *Phys. Lett.* **99A**(9): 435 (26 Dec. 1983).

Pais, A. 1983. *Subtle Is the Lord*. Oxford: Oxford University Press.

Pauling, L., and E. Wilson. 1935. *Introduction to Quantum Mechanics*. New York: McGraw-Hill.

Pease, R.S. 1957. "Equilibrium Characteristics of a Pinched Gas Discharge Cooled by Bremsstrahlung Radiation." *Proc. Roy. Soc. B.* **70:1445**.

Peratt, A., et al. 1980. *Phys. Rev. Lett.* **44**: 1767 (June).

————. 1983a. *Astrophys. and Space Sci.* **91**: 19-33.

————. 1983b. *J. Appl. Phys.* **54**: 11 (Nov.)CHECK PAGE NO.

————. 1984. *Sky and Telescope*. (Aug.), p. 118.

Raudorf, W. 1951. "An Electronic Ram." Wireless Engineer. **1951:** 215 (July).

————. 1974. "Acceleration of Electrons by an Electrodynamic Space-Charge Effect." In *Proceedings of the International Conference on Energy Storage, Compression and Switching, Asti-Torino, Italy, Nov. 1974*. New York: Plenum, p. 381.

Rosenbluth, M. 1954. *Infinite Conductivity Theory of the Pinch*. Los Alamos Scientific Laboratory. Report LA-1850, (Sept.).

Schwarz, J.H. 1975. "Dual Resonance Models of Elementary Particles." *Sci. Amer.* (Jan.), p. 61.

Segré, E. 1959. *Experimental Nuclear Physics* Vol. III. New York: John Wiley.

Shavronov, V.P. 1966. *Reviews of Plasma Physics*, Vol. 2, ed. M.A. Leontovich. New York: Consultants Bureau.

Taylor, J.B. 1975. "Relaxation of Toroidal Discharges." *Proceedings of Conference on Pulsed High Beta Plasmas*. Culham: PUBLISHER?, p. 59.

Wells, D. 1976. *Proceedings of the International Conference on Energy Storage, Compression and Switching, Asti-Torino, Italy, Nov. 1974*. New York: Plenum, p. 197.

White, H. 1934. *Introduction to Atomic Spectra*. New York: McGraw-Hill.

Yadava, K.S. (1976), "On the Stability and the Genesis of the Electron." *Nuovo Cimento* 32(2): 273 (11 April 1976).

Missing Energies at the Pair Production by Gamma Quanta

by Erich R. Bagge

Institute for Pure and Applied Nuclear Physics,
University of Kiel
Kiel, West Germany

Abstract—If the electron states of negative energy in the fully occupied Dirac-sea are included in the normal conservation laws for the energy and momenta, then the theory of pair creation by gamma-rays says that the spectra of the produced positrons and electrons are totally different from each other. Gamma-ray experiments with a helium-filled Wilson cloud chamber in a magnetic field of 700 G confirm this theoretical result.

Introduction
The Missing Solar Neutrinos and the New Conservation Laws in Particle Physics

When Davis published his fascinating results concerning the missing solar neutrinos in the late 1960s (Davis and Evans 1973), there was a real chance that such particles did not exist at all. At that time the experimental error for the observation of solar neutrinos was higher than that for the observable effects.

This was the motivation for the author to develop a theory of β-decay without neutrinos. Starting with Dirac's ideas on the fully occupied electron states at negative energies (Dirac-sea), in which these particles behave as massless and chargeless quantas, it was possible to explain the shapes of the allowed continuous electron spectra in β-decay of nuclei. One obtains practically the same formula as in Fermi's theory of β-decay for the energy spectra of the electrons.

There is no need to assume that neutrinos exist at all. The conservation laws for the energies and all sorts of the momenta can be fulfilled without those particles. To do so it is only necessary to attribute the character of real existence to energies and momenta of the electrons in negative states. This means that the conservation laws for energy and momenta should be fulfilled for the positive states (world) and negative states (antiworld) together as if there is a superworld for the two types of universes, like the two sheets of a Riemannian plane.

To then calculate the quantum-mechanical probabilities for the β-decay, one has to look for interacting forces that are producing these transitions. It is not difficult to find them: The magnetic momenta of the electrons in the antiworld cannot be compensated for in the same way as the Coulombian forces; their multipole character does not allow it. In this way the electrons of the antiworld react directly with the magnetic momenta of protons and neutrons in the nuclei, producing thus the β-decay if energetically possible.

Using Dirac's formula for the transition probabilities, one easily obtains not only the β-spectrum, for instance, of the neutron, but also its lifetime (~1,000 sec), without introducing a new physical constant g (as in Fermi's theory). Obviously, other well-known constants are involved. Comparing this theoretical result with Fermi's theory, it is possible to express Fermi's g by a combination of these constants as follows:

$$g = 2\pi/3 \cdot e^2/\hbar c \cdot m/M \cdot \mu \cdot R^3 \cdot mc^2 \approx 10^{-49} \text{ erg} \cdot \text{cm}^3;$$

where $e^2/\hbar c$ is Sommerfeld's constant of fine structure and equals 1/137.04, m is the mass of the electron, M is the mass of the neutron, and R is the range of nuclear forces, equal to 2×10^{-13} cm.

The value of g is practically the same as that derived in Fermi's theory by adapting the observed lifetimes in β-decay. However, while in Fermi's theory the constant g plays the role of a new physical quantity, in our case

its value is determined directly by well-known constants of atomic and nuclear physics.

To believe that g is a physical constant of a new and individual character that is necessary to determine the strength of the so-called weak interactions is no longer justified; it is a heterodoxy that should be given up as soon as possible. At least the younger generation of students should be informed correctly about this curious situation by which they have been misled now for a long time. To avoid misunderstandings, let me state that Fermi's theory played an essential and very useful role in the past, and its constant g could be regarded then, for well-founded reasons, as a new physical constant; now, however, Fermi's theory is no longer correct.

The so-called weak interactions are nothing else but quite normal forces between the magnetic dipoles of elementary particles and those of the electrons in negative states of energy. Perhaps for most of the community of physicists, the fully occupied antiworld with its not-directly-observable particles has an unacceptable or even uncanny character. But at this time, it is the best way to describe the basic phenomena for particle production in conformity with the real events in physics. The following part of this paper will show this for another type of physical process; namely, the pair production of positrons and electrons by light quanta.

The Pair Creation by Light Quanta in a World of Positive And Negative Energy States

The reason that the process of pair production has to be discussed under the auspices of the newly interpreted conservation laws for energy and momenta was raised in a discussion during a physics meeting in 1977. The author referred there to the above-described theory of β-decay, to which well-known physicists raised two serious objections. One said: "In quantum electrodynamics there is no need for states of negative energies. We get good results without them. They do not exist." The other physicist added: "If your theory were correct, the whole system of elementary particle physics would have to be changed completely. Neutrinos play such a big role in the group-theoretical aspects of elementary particle physics that we cannot do without them."

It was not easy for me to answer convincingly in defense of my theory, because I had only one good theoretical result compared to a legion of experimental and theoretical successes in the realm of nuclear particle physics. Nevertheless, I had behind me the possibility of determining the lifetimes of atomic nuclei for β-decay correctly without introducing ad hoc a new physical constant. Therefore, I was forced to search for other physical processes that show that Dirac's states of negative energies are of more than purely academic interest.

The process of pair production provides such a demonstration, as I shall show.

In 1934, two theoretical physicists, Bethe and Heitler, developed the famous quantum-electrodynamical theory of pair creation by energetic light quanta (Bethe and Heitler 1934; Heitler 1954), which has since become the basis for so many theories on electron-positron cascades in cosmic radiation, in elementary particle physics, and, last but not least, in nuclear energy. Often, but not in all cases, the theoretical statements and the experimental results came together relatively well. Nevertheless, a fully convincing confirmation that this theory describes absolutely correctly the pair production by light quanta was never given by corresponding experiments.

The reason for this situation may be that fundamental assumption in Bethe and Heitler's theory that says that the energy $h\nu$ of the light quantum is strongly equal to the sum of the total energies of positron E^+ and the electron E^-:

$$h\nu = E^+ + E^-. \tag{1}$$

In this way the energy conservation law seems to be fulfilled. But is it also correct?

The first objection raised is that the negative energy of the electron before its appearance in the world of positive states has not been taken into account. The second objection is that in Bethe and Heitler's theory there is no interconnection between the energies and the momenta of the three interacting partners. There is no freedom for a more general, four-dimensional energy-momentum exchange. The momentum of the positron in the normal world is that of the electron in the antiworld with a negative sign, and it is strongly bound to this situation. There is no obvious or real, well-founded reason to introduce such a hard physical restriction for the motion of one of two particles in a three-partner reaction.

These viewpoints may be enough to justify a quite different description of the pair creation by energetic light quanta stimulated by the success of the same ideas in β-decay.

If $E = -|E|$ is the negative energy of the electron in the antiworld, then the conservation law for the energies at pair creation should be formulated as follows:

$$h\nu + E = E^+ + E^-. \tag{2}$$

Since the electron of the antiworld behaves like a massless quantum, one has to attribute to it a momentum $\mathbf{p} = \mathbf{E}/c$. The momentum of the positron may be $\mathbf{p}_+$ and that of the electron $\mathbf{p}_-$.

Then the conservation of the momenta postulates the equation:

$$\mathbf{h}\nu/c + \mathbf{E}/c = \mathbf{p}_+ + \mathbf{p}_-. \tag{3}$$

Equations (2) and (3) are the basic changes in a new theory of pair production published in 1977 by the author (Bagge 1975, 1976, 1977, 1978). One of the interesting statements of the new theory says that the energy spectra of positrons and electrons are completely different from those of Bethe and Heitler.

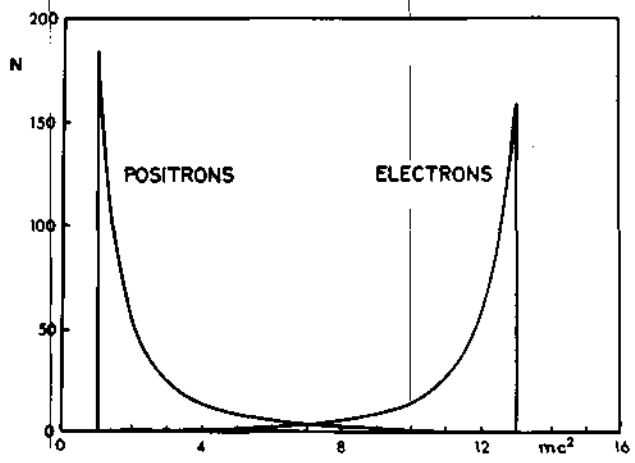

Figure 1. The theoretical energy spectra of the positrons and the electrons at the pair creation by gamma quanta of 7.15 MeV, according to this theory (Bagge).

Figure 1 represents the two spectra of the positrons and of the electrons produced in pair creation by 6.14-MeV gamma quanta. The spectra are clearly not identical, but in a certain sense are complementary to each other. While the positrons are generated at low energies (maximum near-zero kinetic energy), the electrons prefer to have high energies (maximum near the full energy of the primary gamma quantum).

This is a theoretical result on the basis of the above-described generalized conservation laws. In a certain sense, it already includes as a consequence of the negative energy E in Eq. (2) the statement that there are missing energies for the two created particles, the positron and electron. In Bethe and Heitler's theory the two spectra of these particles have identical shapes.

This situation opened the possibility of proving which type of theory is better adapted to the true physical pair

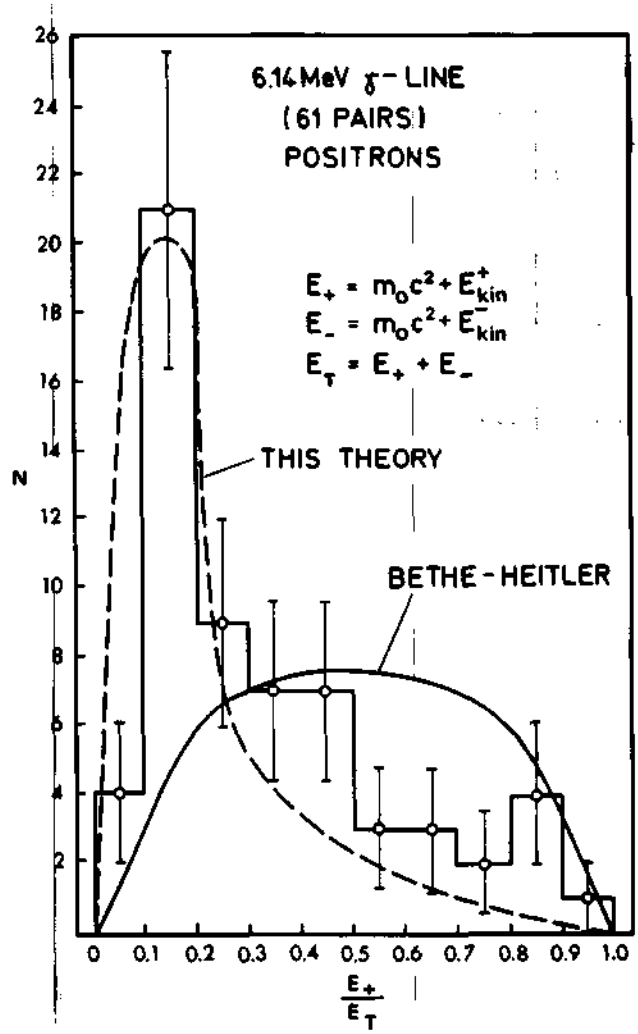

Figure 2. The measured energy spectrum of the positrons at the pair creation by gamma quanta of 6.14 MeV (histogram), compared to the Bethe–Heitler Theory (curved line). The Bagge Theory is the dashed line.

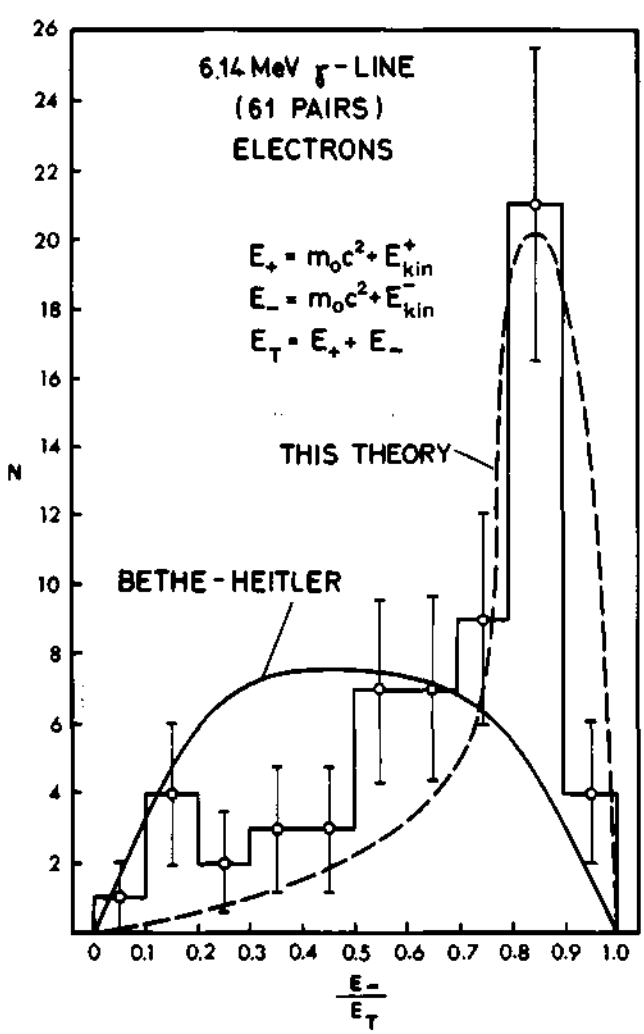

Figure 3. The measured electron spectrum at the pair creation by gamma quanta of 6.14 MeV.

creation. Therefore, the following experiment was performed working closely with my Egyptian collaborator Abu El-Ela, partly at the reactor-station of Geesthgacht near Hamburg and partly at the Institute of Pure and Applied Nuclear Physics at the University of Kiel (El-Ela and Bagge 1984). A short letter of some of the main results is already in press in the journal *Atomkernenergie/Kerntechnik*, and the results are published in more detail in Abu El-Ela's thesis at Kiel University (El-Ela 1984).

Wilson Cloud Chamber Experiments For Investigation of Positron and Electron Spectra in Pair Creation

A cylindric Wilson cloud chamber of the Blackett type, originally used for cosmic ray studies (30 cm in diameter and 6 cm illuminated depth), was filled with helium at about 1.2 bar and the vapor of a water-alcohol mixture. Two Helmholtz coils produced within the illuminated part of the chamber an almost homogeneous magnetic field of 703 G throughout the whole volume. The magnetic vector was orientated perpendicularly to the plane of the chamber.

On one side of the chamber was a 1-cm^2 gold target, 25 μm thick. The gamma-rays came through a Plexiglas foil covering the 1-cm^2 hole in the glass ring of the chamber, nearly perpendicular to the magnetic field vector.

The gamma-rays were produced by reactor-activated nitrogen-16 (^{16}N), decaying in about 7 sec to ^{16}O, which in addition to gamma-rays of 6.14 MeV, emits others of higher energy (6.91, 7.11, and 8.87 MeV). The Wilson cloud chamber is installed about 6 m distance from the center of the reactor. A cartridge with enriched ^{15}N in urea was irradiated by neutrons in a tangential tube of the reactor facility. At every expansion of the chamber, the irradiated cartridge was shot for about a second by a pressurized pipeline to a lead cavity with a 1-cm hole for focusing the gamma-rays on the target.

About 2,000 stereoscopic photographs have been taken with two Hasselblad cameras, and every tenth photo contained a good, measurable electron–positron pair.

The curvatures of the particle paths in the chamber could be measured by a Pulfrich stereocomparator by point-to-point determination of the coordinates. The evaluation was done by a computer (normally 10 to 20 points per path). Every pair was recognized by its origin on the target, where the two paths of positron and electron meet each other. In this way, we obtained for every event the energy of the positron and the electron separately and thus the total energy of the pair.

Figure 2 shows the spectrum of the positrons for pair energies in the neighborhood of 6.14 MeV, and Figure 3 shows the same for the electrons.

One sees that the two particle spectra show the same features as the theoretical spectra in Figure 1: The maximum for the positrons appears at low energies and for the electrons at high energies. If the theoretical curves of Figure 1 are averaged over the same intervals as is done for the experimental values (the dotted curves in Figures 2 and 3), then these curves and the experimental ones come together in good conformity, while the corresponding Bethe-Heitler curves differ so greatly from them that it is very hard to believe that mere statistical fluctuations have generated such discrepancies.

Obviously, better statistics are still necessary to be absolutely sure that the experiments support the new interpretation for pair creation, but all new observations show the same behavior.

In this way, another small step is taken to include the negative energy states in the antiworld more directly and also more fruitfully than has been done up till now.

References

Bagge, E. R. 1975*a*. *Atomkernenergie* **25:** 251-256.

———. 1975*b*. *Atomkernenergie* **26:** 70-73.

———. 1976. *Atomkernenergie* **27:** 253-256.

———. 1977. *Izvestia Academia Nauk USSR*, ser. fiz. **41:** 1960–1968.

———. 1978. *Proc. X. Leningrad Seminar*, 372–386.

Bethe, H. and Heitler, W. 1934. *Proc. Roy. Soc. A.* **146.**

Davis, R. and Evans, I.C. 1973. *13th International Cosmic Ray Conference, Denver, Colo.* (Aug. 1973), p. 2001.

El-Ela, Abu and E. R. Bagge. 1984. *Atomkernenergie* **45** (in press).

El-Ela, Abu. 1984. Doctoral Thesis (Dr. rer. nat.). University of Kiel, West Germany.

Heitler, W. 1954. *The Quantum Theory of Radiation*. Oxford: Clarendon Press.

The Relation between Angular Momentum and Star Formation In Spiral Galaxies

by L. Carrasco and A. Serrano

Instituto de Astronomía
Universidad Nacional Autónoma de México
Apdo. Postal 70-264
Mexico City, D.F., 04510
Mexico

Abstract—We derive the radial distribution of the specific angular momentum, $j = J/M$, in M31, M51, and the Galaxy, objects for which well-observed rotation curves are available. We find that the specific angular momentum varies inversely with the present star formation rate; that is, minima of spin angular momentum correspond to the loci of spiral arms. We also find that stellar formation rate is approximately an inverse function of j. These results indicate that the morphological difference between spiral and elliptical galaxies might be understood in terms of different amounts of j in the protogalactic clouds. New values of Oort's A constant are estimated for the arm and interarm regions in our Galaxy.

Introduction

Recently the authors discussed the relationship between specific angular momentum, j, and mass, M, for a wide variety of astronomical objects (1982). We concluded that the observed relation $j \propto M^a$, with a between ⅔ and ¾, is consistent with the assumption of mechanical equilibrium, scaled by the mean density of the system, as Ozernoy (1967) had suggested for spiral galaxies. Moreover, we showed that spheroidal systems such as elliptical galaxies and bulges also follow a $j \propto M^{2/3\text{-}3/4}$ power law. However, these systems have an amount of specific angular momentum j about one order of magnitude below the equilibrium line, as defined by spiral galaxies.

The initial star formation rates (ISFR) must have played a very important role in determining the overall morphological characteristics of galaxies: In ellipticals the ISFR was very large, while in spirals and particularly in Magellanic-type irregulars, this rate has been very small. On the other hand, it has been suggested that the Hubble sequence represents also a sequence of angular momentum (Brosche 1970, Strom 1980). If so, the ISFR and specific angular momentum could be two inversely correlated quantities, as Sandage has suspected (1975). If indeed j plays a role in determining the ISFR at the time of formation of galaxies, it is likely that j can play a role in determining the present star formation rates in spiral galaxies; that is, systems that are currently forming stars at high rates on a large scale.

In this paper we investigate, from an observational point of view, the relation between specific angular momentum and stellar birthrates in two nearby spiral galaxies and in the Milky Way. For these galaxies, well-observed HI (21 cm) or HII (Hα) rotation curves are available in the literature. In the next two sections, we discuss the radial distribution of j and the stellar birthrates, respectively; then we discuss the observational evidence, with conclusions drawn in the last section.

The Radial Distribution Of j in Spiral Galaxies

A direct method to derive the radial distribution of specific angular momentum of the gaseous components in galactic disks is the analysis of high-quality Hα or 21-cm rotation curves of galaxies: V_t as a function of r [$V_t = f(r)$]; V_t being the tangential velocity and r the galactocentric distance. From these data, the radial trend of the angular velocity $\Omega(r)$ can be derived. Finally, through numerical differentiation of $\Omega(r)$, one obtains the curve $A(r) = -r/2\ [d\Omega(r)/dr]$, as a function of r. One should recall that Oort's constant A describes locally the spin-specific angular momentum or shear of the gaseous disk, which is in fact that relevant quantity when considering the spin angular momentum of interstellar clouds. For a given cloud, A times its square radius is the specific angular momentum. Under the assumption that the mean radius of interstellar clouds is not a strong function of galactocentric distance, A is a good estimator of j. Hence, hereafter we will refer interchangeably to the specific angular momentum as A or j.

We have derived the radial distribution of j by applying the above outlined method to the galaxies listed below. The sources of rotational data used in this paper are:

(1) *The Galaxy*: 21-cm rotation curve by Burton and Gordon (1978) for $r < R_0$ and Jackson et al. (1979) for $r > R_0$;

(2) *M31*: 21-cm rotation curves by Roberts and Whitehurst (1975) and Emerson (1976); and

(3) *M51*: Hα Fabry-Pérot rotation curve by Tully (1974a).

Our results are summarized in Figures 1(a), 2(a), and 3(a). There we have plotted A as a function of r [$A = f(r)$] for the systems studied. In every case we find, in the mean, first a sharp increase near the nucleus of a given galaxy and farther out a smooth decrease of A in the outward direction; however, superimposed on this general trend there are sharp local minima of specific angular momentum. These minima only reflect a fact already present in rotation curves: For a long time, rotational data of different galaxies have been smoothed in order to obtain the general trend in rotation curves (a most important result for mass determinations). By doing so, significant information contained in undulatory variations of the rotation curves has been overlooked. These variations (also called "wiggles") have been suspected by some authors to be real and not caused by observational errors (see, for example, Pismis 1965, 1975). In these undulations, there is a region in which the tangential velocity increases with radius; that is, $V_t \propto r$ locally. This condition implies that A would be small in these regions, and there, the gas rotates about the center of the galaxy in a nondifferential manner. The minima in the case of M31 are not as deep as in the case of the galaxy or M51; we suspect that this is largely the result of an angular resolution effect of the 21-cm rotational

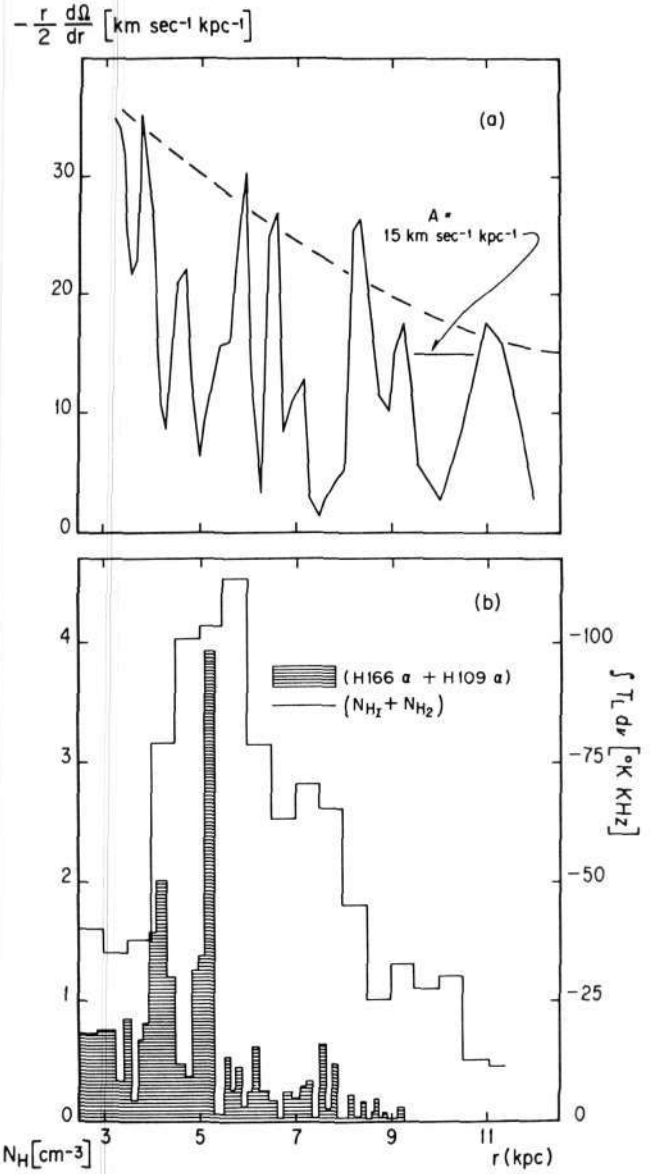

Figure 1(a). The derived values of Oort's constant ($A = \frac{1}{2} r\, d\Omega/dr$) are plotted as a function of galactocentric distance r for the Milky Way. The dashed curve represents the value of A associated with a differentially rotating disk with a velocity dispersion $\sigma \cong 8$ km/sec. The IAU adopted value of A for the solar vicinity is plotted as reference.

Figure 1(b). A histogram of the radial distribution of gas (solid line), together with a histogram of the radial distribution of HII regions (hatched area) for the Galaxy, the latter being proportional to the stellar formation rate. In our Galaxy, this can be obtained from the general distribution of the emission measure of H166α and H109α hydrogen recombination lines.

N is the rate of star formation as inferred from the density of the indicated specific spectrum of the hydrogen gas, HI, HII, the sum of HI and HII, H166α and H109α.

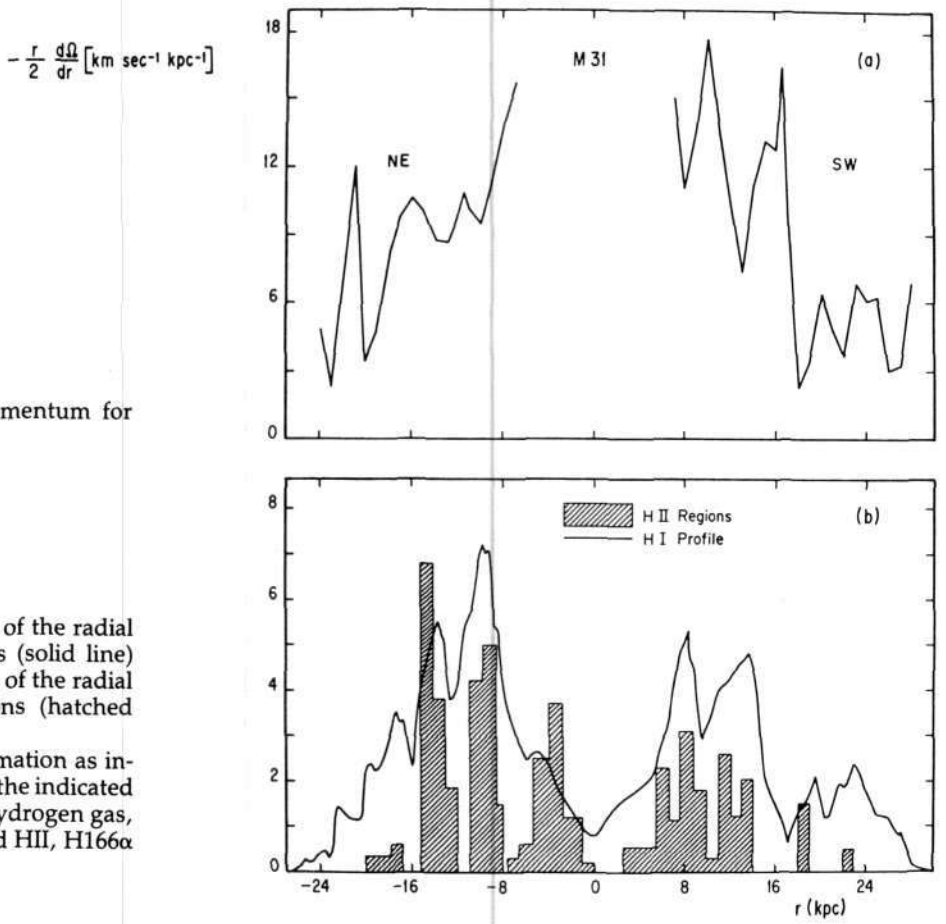

Figure 2(a). Angular momentum for M31 (NGC 224).

Figure 2(b). A histogram of the radial distribution of HI regions (solid line) together with a histogram of the radial distribution of HII regions (hatched area) for M31.

N is the rate of star formation as inferred from the density of the indicated specific spectrum of the hydrogen gas, HI, HII, the sum of HI and HII, H166α and H109α.

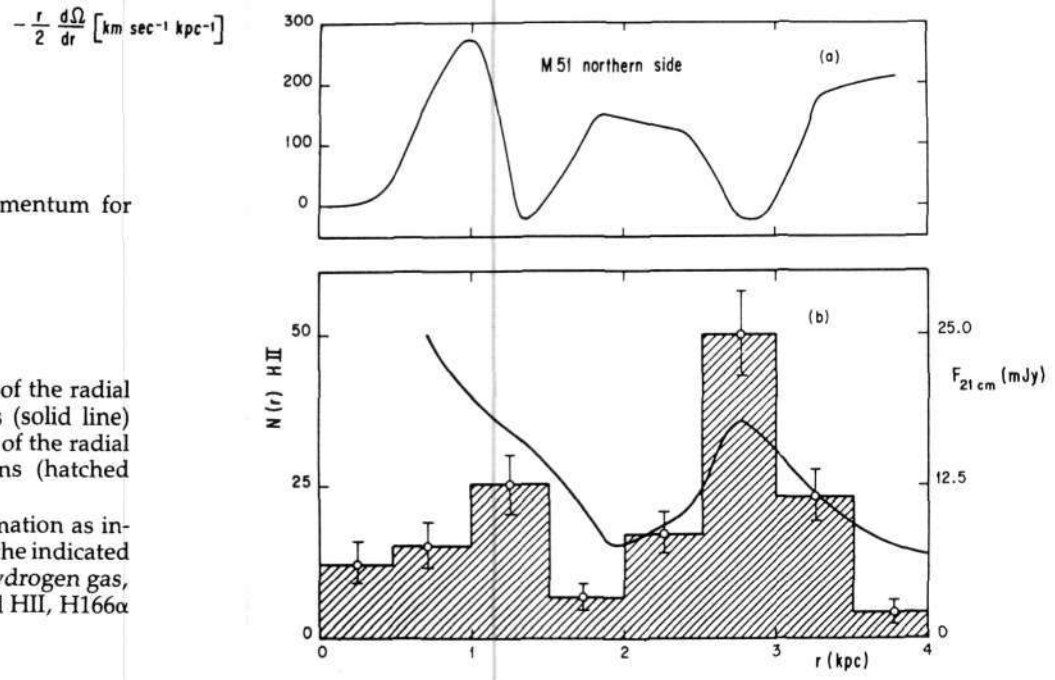

Figure 3(a). Angular momentum for M51 (NGC5194).

Figure 3(b). A histogram of the radial distribution of HI regions (solid line) together with a histogram of the radial distribution of HII regions (hatched area) for M51.

N is the rate of star formation as inferred from the density of the indicated specific spectrum of the hydrogen gas, HI, HII, the sum of HI and HII, H166α and H109α.

data available for the former. In the last two cases, with better specific resolution, the minima are in fact zeros of the A as a function of r curves.

The Radial Distribution Of Stellar Formation

It is generally accepted that the frequency distribution of HII regions as a function of radius provides us with a good relative measure of the stellar birthrate of hot, young stars in galaxies (Metzger 1978). In external galaxies, this distribution can be inferred from direct counts of HII (ionized hydrogen) regions; in our Galaxy, on the other hand, it can be obtained from the general distribution of the emission measure of H166α and H109α hydrogen recombination lines. Histograms representing the relative radial distributions of star formation rates together with the distribution of the gas are shown in Figures 1b, 2b, and 3b, for the Galaxy, M31, and M51 respectively. The data were taken from:

(1) *The Galaxy*: Gordon and Burton (1976) for the neutral gas; Lockman (1976), Hart and Pedlar (1976) for the hydrogen recombination lines;

(2) *M31*: Rubin and Ford (1970) for the HII regions' distribution, and Guibert (1974) for the neutral gas; and

(3) *M51*: Tully (1974a) for the HII regions, and Segalovitz (1977) for the 21-cm data.

We would like to point out that the distributions under consideration refer to sectors 30° wide centered about a certain radial direction and are *not* averages over concentric rings. In M31 and M51, they refer to the distribution of HII regions along the major axis, while in the Galaxy they refer to the longitudinal distribution. In each case we see a rather discontinuous distribution with local maxima, every time a spiral arm is crossed along a chosen radius.

Discussion

From a direct comparison of the radial distributions of (1) specific spin angular momentum of the gas and (2) stellar formation rates [Figures 1(a) and (b), 2(a) and (b), and 3(a) and (b)], the high degree of inverse correlation that exists between these two quantities can easily be noticed. Whenever the spin specific angular momentum drops to a local minimum there is an occurrence of efficient star formation. The inverse correlation is not perfect, judging from the figures; however, this is not surprising, since the rotational data are not free of observational errors, which cause the appearance of spurious "wiggles" in the A as a function of r curve. Nevertheless, the observed minima of specific angular momentum usually do coincide with the loci occupied by the spiral arms. This relation is indicative that the gas located in spiral arms is rotating—to a first approximation—as a rigid body.

Further evidence of nondifferential rotation of the gas within spiral arms is present in the kinematic data published by Rickard (1968) for the gaseous component of the Perseus arm, where he has found a constant Ω for $10.5 > r > 12$ kpc (kiloparsecs). This result has been confirmed by Humphreys (1976) in a study of the optical spiral tracers in this region of the sky. The spiral density wave theory does predict velocity fields (streaming) in the arms that show a tendency toward rigid body. This is to be expected, since the spiral pattern itself must rotate rigidly. However, as Humphreys already pointed out (1976), the streaming motions expected from the density wave theory (Lin, Yuan, and Shu 1969; Yuan 1969) can account, in the best of cases, only for about half of the observed effects in the Perseus arm. Still another impressive example of the rigid-body rotation within spiral arms is evident in the wavy rotation curve of M51, to judge from the observations by Tully (1974a) and by Goad et al. (1979). For this galaxy, Tully (1974b) claims density wave streaming with amplitudes of 25 km/sec as derived from his smooth fit to the data, while the observed departures from circular motions have semiamplitudes of the order of 100km/sec to judge from the data presented in his Figure 3.

The presence of minima in the A as a function of r curve for (1) the gas in the Galaxy and (2) in the young stars—at least for those in the Perseus arm—is supported also from the analysis of the velocity ellipsoid for extreme Population I objects. As Lindblad (1927) and Oort (1928) have shown, the ratio of the velocity dispersions in the tangential and radial directions is related to Oort's A and B constants according to:

$$\sigma_\theta^2/\sigma_r^2 = -B/(A - B).$$

For OB stars, the average values of these dispersions are 11.2 and 12.9 km/sec for the tangential and radial directions, respectively (Parenago 1951, Filin 1959, Stone 1978). The ratio of their squares $\sigma_\theta^2/\sigma_r \cong 0.75$ is indicative of rather small values of A for these objects; that is, $-A/B \cong 0.33$. This is to be compared with the canonical ratio $-A/B = 1.5$. Given that the gas in spiral arms has $A \cong 0$, we expect young OB stars also to have small values of A.

Figure 1(a) also yields important information about the kinematics of the disk of the Galaxy. If one identifies the upper envelope of the A versus r curve with the interarm regions (dashed curve), and assumes that the gas in those regions is not perturbed by the spiral pattern, then this envelope should describe the kinematics as a gaseous disk with a velocity dispersion of $\cong$ 8 km/sec. From this envelope we derive a value $A \cong 18$ km/sec kpc for the solar vicinity, in good agreement with the determination of A from proper motions, cepheids, or secular parallaxes (Morgan and Oort 1951, Joy 1939, Stibbs 1956, Gascoigne and Eggen 1957, Walraven et al. 1958).

In any reasonable theory of star formation, the spinning of interstellar clouds, out of which stars are formed, inhibits the contraction of the cloud by centrifugal force.

If differential rotation is the main cause of spinning of interstellar clouds, then it is quite clear from the derived A as a function of r curves that clouds within the spiral pattern spin much more slowly than those in the interarm regions. Therefore, spiral arms are not only regions of enhanced gas density, but also regions where clouds rotate slowly, consequently providing the most favorable physical conditions for star formation.

As to the main cause of the slower spin of interstellar clouds within spiral arms, it is quite attractive to think of magnetic fields, associated with the spiral structure, to stop rotation, since we know that the mean field B is concentrated along the arms in a coherent manner, as can be inferred from the radio polarization maps of external galaxies by Beck et al. (1980), Segalovitz et al. (1976), and Sofue et al. (1980). Furthermore, Mouschovias (1979) and Mouschovias and Paleologou (1979) have shown that the time scales for magnetic transport of angular momentum of an interstellar cloud are extremely short ($\tau \cong 10^4$–10^5 yr), for values of magnetic field strength comparable with those observed.

The inverse relation between series (a) and (b) in the figures suggests a function for the stellar formation rate of the form

$$dN/dt^* \propto \rho^{\alpha} j^{-s}.$$

The dependence of the stellar formation rates upon the gas density is likely to be similar to Schmidt's law (Schmidt 1959, Smith et al. 1978, Guibert et al. 1978). However, from the data presented here, it is clear that density alone cannot describe in detail the radial trend of the star formation rate (SFR). Hence, we have carried out linear regressions for log (SFR)—α log ρ as a function of log j for the galaxies studied here. The table presents our results for s, for different values of α.

The results presented in the table for the exponent s indicate that star formation rates in spiral arms vary as the inverse of the specific angular momentum j. This result strengthens the suspicion that the initial star formation rates in galaxies might have been controlled by their angular momentum per unit mass j. In the authors' 1982 paper, we have shown that elliptical galaxies have angular momenta about one order of magnitude smaller than spirals of comparable mass, and yet ellipticals follow an $M^{2/3}$ power law for j. This latter fact indicates that elliptical galaxies were in gyrogravitational equilibrium at the time of formation. This leads us to suggest that their morphological differentiation could be the result of a higher efficiency for the removal of angular momentum in protoellipticals than in protospiral galaxies, because of environmental conditions. This could be the case if the torque mechanisms responsible for the removal of angular momentum in protogalaxies are density dependent, as in the case of tidal or magnetic interactions. This suggestion is supported by the correlation between richness and type content in clusters of galaxies (Arp 1963, de Vaucouleurs 1975, Abell 1975) and the correlations derived by Dressler (1980) between galaxy morphology and ambient matter densities.

Regression Values for the Exponent s and Correlation Coefficients

Galaxy	α	s	Corr. Coeff.
Milky Way	1	1.21 ± 0.42	0.67
	2	1.26 ± 0.45	0.66
M31	1	0.70 ± 0.43	0.57
	2	1.12 ± 0.29	0.74
M51	1	0.66 ± 0.32	0.77
	2	0.51 ± 0.33	0.68
		$\hat{s} = 0.91 \pm 0.28$	

The results indicate that star formation rates in spiral arms vary as the inverse of the specific angular momentum.

Conclusions

From the results discussed above, we conclude:

(1) The stellar formation rates in spiral galaxies are inversely correlated with the spin-specific angular momentum of the gas. This rate can be expressed as

$$dN/dt^* \propto \rho^{\alpha} j^{-s};\ 1 > \alpha > 2 \text{ and } 0.5 < s < 1.2.$$

(2) The spiral structure is coincident with loci for the minima of spin angular momentum.

(3) The likely value of Oort's constant A is 18 km/sec kpc for an interarm region at the solar galactocentric radius, and $A = 3.5$ km/sec kpc for the local arm. The latter result is consistent with the near equality of the velocity dispersions in the tangential and radial directions for extreme Population I objects.

(4) The Hubble sequence might indeed represent a sequence of specific angular momenta, since differences in j will show up as differences in the initial star formation rates. The observed values of j depend upon the environmental history of a given galaxy, and further study of the plausible torque mechanisms is desirable.

References

Arp, H.C. 1963. *Scientific American*, p. 70.
Beck, R., Berkhuijsen, E.M., Wielebinski, R. 1980. *Nature* **283**:272.
Brosche, P. 1970. *Astron. Astrophys.* 6:240.
Burton, W.B., Gordon, M.A. 1978. *Astron. Astrophys.* 63:7.
Carrasco, L., Roth, M., Serrano, A. 1982. *Astron. Astrophys.* **106**:89.
Dressler, A. 1980. *Astrophys. J.* **236**:351.
Emerson, D.T. 1976. *Monthly Notices Roy. Astron. Soc.* **176**:321.
Filin, A.J. 1957. *Astron. J. USSR* **34**:838.
Gascoigne, S.C.G., Eggen, O.J. 1957. *Monthly Notices Roy. Astron. Soc.* **117**:430.

Goad, J.W., de Veny, J.B., Goad, L.E. 1979. *Astrophys. J. Suppl.* **39**:439.
Gordon, M.Z., Burton, W.B. 1976. *Astrophys. J.* **208**:346.
Guibert, J. 1974. *Astron. Astrophys.* **30**:353.
Guibert, J., Lequeux, J., Viallefond, F. 1978. *Astron. Astrophys.* **68**:1.
Hart, L., Pedlar, A. 1976. *Monthly Notices Roy. Astron. Soc.* **176**:547.
Humphreys, R.A. 1976. *Astrophys. J.* **206**:114.
Jackson, P.D., Fitzgerald, M.P., Moffat, A.F.J. 1979. in *The Large Scale Characteristics of the Galaxy*, IAU Symposium No. 84, ed. W.B. Burton. Dordrecht: D. Reidel, p. 221.
Joy, A.H. 1939. *Astrophys. J.* **89**:396.
Lin, C.C., Yuan, C., Shu, F.H. 1969. *Astrophys. J.* **155**:721.
Lindblad, B. 1927. *Monthly Notices Roy. Astron. Soc.* **87**:553.
Lockman, F. 1976. *Astrophys. J.* **209**:429.
————. 1979. *Astrophys. J.* **232**:761.
Mezger, P.G. 1978. *Astron Astrophys.* **70**:565.
Morgan, H.R., Oort, J.H. 1951. *Bull. Astron. Inst. Netherlands* **11**:379.
Mouschovias, T. Ch. 1979. *Astrophys. J.* **228**:159.
Mouschovias, T. Ch., Paleologou, E.V. 1979. *Astrophys. J.* **230**:204.
Oort, J.H. 1928. *Bull. Astron. Inst. Netherlands* **4**:269.
Ozernoy, L.M. 1967. *Astron. Tsirk.* **407**:422.
Parenago, P.P. 1951. *Pub. Sternberg Inst.* **20**:26.
Pismis, P. 1965. *Bol. Obs. Tonantyzintla y Tacubaya* **4**:8.
————. 1975. *Proc. First European Astr. Meeting*. eds. B. Barbanis and J.D. Hadjidemetriou. Berlin: Springer, p. 319.
Rickard, J.J. 1968. *Astrophys. J.* **152**:1019.
Roberts, M.S., and Whitehurst, R.N. 1975. *Astrophys. J.* **201**:327.
Rubin, V.C., and Ford, W.K., Jr. 1970. in *The Spiral Structure of Our Galaxy*, IAU Symposium No. 38. Eds. W. Becker and GI Contopoulos. Dordrecht: D. Reidel, p. 61.
Sandage, A. 1976. *Galaxies and the Universe*. Eds. A. Sandage, M. Sandage, and J. Kristian. Chicago: The University of Chicago Press, p. 32.
Schmidt, M. 1959. *Astrophys. J.* **129**:243.
Segalovitz, A., Shane, W.W., and de Bruyn, A.G. 1976. *Nature* **264**:222.
Segalovitz, A. 1977. *Astron. Astrophys.* **54**:703.
Smith, L.F., Biermann, P., and Mezger, P.G. 1978. *Astron. Astrophys.* **66**:65.
Sofue, Y., Takano, T., and Fujimoto, M. 1980. *Astron. Astrophys.* **91**:335.
Stibbs, D.W.N. 1956. *Monthly Notices Roy. Astron. Soc.* **116**:453.
Stone, R.C. 1978. *Astron. J.* **83**:393.
Strom, S.E. 1980. *Astrophys. J.* **237**:686.
Tully, B. 1974a. *Astrophys. J. Suppl.* **27**:434.
————. 1974b. *Astrophys. J. Suppl.* **27**:449.
Walraven, T., Muller, A.G., Oosterhoff, P.T. 1958. *Bull. Astron. Inst. Netherlands* **14**:81.
Yuan, C. 1969. *Astrophys. J.* **158**:871.

New Frontiers in Biophysics

by James Frazer, PhD

Houston Medical Center
M.D. Anderson Hospital
6723 Bertner
Room AG. 302
Houston, Tex. 77025

Abstract—The absorption and emission spectra of a variety of biological surfaces suggest the presence of long-range coherence in electromagnetic action as the basis for numerous basic biological processes, from membrane activities to DNA replication.

A line of experimental evidence points to a close connection between self-similar geometries found in biological contexts and biological work. That is, organisms or tissues do useful work by creating certain kinds of transformations, and these transformations have a geometric quality that is best described as self-similar in form. The specifics of this should become clearer as some of the experimental findings related to these geometries are described.

The series of experiments started out several decades ago with observations that organelles in cells, such as mitochondria, swell and shrink as part of their normal functioning and that this swelling and shrinking is associated with energy utilization and production (Frazer 1966). There has not been much controversy about this. However, since swelling and shrinking is a generalized process that goes on in numerous parts of the living cell, it cannot simply be the result of shifting of water or ions, but may involve proteins that contract, similar to muscle contraction. Furthermore, since proteins generally have numerous areas of charge on their surfaces, the motion of these contracting proteins (their changes in shape with contraction and relaxation) causes a varying electromagnetic field, a point that is still surrounded by controversy.

An electron spin-resonance spectrometer was used to measure the expected electromagnetic waves, and a rather healthy infrared emission spectrum was obtained when the samples were passed through resonant frequencies. This, of course, was all very exciting, but a few years ago the funder of the research, the U.S. Air Force, decided that biophysics did not exist any more, and suddenly closed the research project, carrying the laboratory furniture out the door as part of the same operation that shut down the manned space exploration project (Frazer 1970).

The idea was that electromagnetically active surfaces occur in all body tissues, that these surfaces can be affected by imposed fields, and that such surfaces emit their own fields and thereby affect their neighboring surfaces as well as distant ones. Furthermore, the kinds of frequencies observed, and particularly the strong resonances involved, suggested that the surfaces were absorbing and emitting coherently over moderately long ranges (micrometers) of surface distance, a very, very interesting possibility. This means that the kind of work performed by the biological substrate is properly characterized as geometrical reordering, rather than traditional alteration of collision probabilities in a high-entropy gas.

Considering something like the brain or the immune system, we are dealing with biological tissues and organs that have a staggering number of such surface relations, and our approach to coherence in their functioning should be the kind of orientation that will make sense of the otherwise appalling amount of complex activity being performed.

Returning to the story of my own line of research: Studies of the spectrum of absorption and emission of

some very pure proteins were performed together with Dr S. Klainer of Block Engineering Research Company (Klainer 1975). Solutions of those substances were exposed (while the spectra were being made) to strong electromagnetic fields. I was able to show that the backbone (amide bond) portion of the protein chymotrypsin was strongly altered by the electromagnetic fields. We had to be very careful to control the temperature to be sure of this effect. And the effect was reversible—the protein reverted to normal when the external field was shut off. So we found the importance of electromagnetic fields in both directions of effect: The molecules or biological surfaces can emit the field, and a field can be applied to shift the resonant frequency of the biological entity.

If that could be done, the next thing, then, was why not steer fields so that a desired property would occur in tissues? That is exactly what we did. We steered fields into fairly small volumes of tumors—very well-defined tumors that had been injected into animals and were growing—using a particular kind of field steering that creates extreme hyperthermia (high temperatures). I am glad to be able to report that we have not had a tumor recurrence since we began this particular experiment last January—that is about 130 animals so far over the past six months (Yamanashi 1984).

At M.D. Anderson Hospital in Houston, Tex., our hyperthermia clinic is using a similar technique to treat human cancer patients. For each different type of tumor, we use the particular kind of hyperthermia that is applicable to the patient. Depending on the type of tumor, its location, and its size, the applicators are designed to place fields as nearly as possible in the vicinity of the tumor and not in the surrounding normal tissue. For some patients who are very hardy and who have need for it, whole body hyperthermia is administered. Hyperthermia, when used, often accompanies chemotherapy and radiotherapy. It has been found that hyperthermia potentiates the beneficial effects of either chemotherapy or radiotherapy. This offers a promising modality for the control of cancer when it occurs, though it is still very much a beginning research entity and not to be undertaken lightly, or certainly not to the exclusion of other forms of treatment.

Another interesting aspect of heat treatment is the use of nuclear magnetic resonance imaging (NMR), which is becoming more and more prevalent among major medical institutions across the country. NMR involves imposing a strong magnetic field on the tissue or organism (which according to theory aligns the spins of the hydrogen protons in water and other substances) and then observing the absorption and emission characteristics of these protons. Generally speaking, the more regularly periodic the protons are arranged, the more rapid the emission of radiation occurs in this situation. Therefore, NMR measures something akin to long-range coherence of water and other substances present in living tissue. By localizing the different degrees of ordering of the protons throughout a tissue, an image can be made from this predominant entity of biological tissue. Tumor tissue absorbs and emits at frequencies and with time distributions slightly different from normal tissue. If the right signal is sent into the organism, and the right time to "listen" is chosen, we can "see" any tumor present. Once we have the tumor in our sights, we can then insert a particular kind of probe, turn up the power of the NMR machine, and heat up the tumor area to treat the disease with the same machine!

Dr. William Yamanashi, at the City of Faith Hospital in Tulsa, Okla., is at present putting some of our tuned probes into models of animals, imaging those models in an NMR field, and measuring the temperature at the same time. However, routine use in clinical settings is still, unfortunately, far in the future.

Our hope for the future is to study the metabolism of the tissue from a geometric standpoint. A crucial promising area is the comparison of absorbed to emitted frequencies of electromagnetic radiation in such substances as DNA and chlorophyll. There is already preliminary evidence that there is a sizable upshift of the photon frequencies under certain conditions, and this is likely to be related to the notion of biological work.

We must then attempt to pinpoint some of the crucial differences between the metabolic geometry of cancer and normal tissue. This is likely to be of great advantage in helping us design treatment and, ultimately, prevention strategies.

The Importance of Surface Relations in Biology

I will now review some aspects of the relationship of physics to biology, and lead into some more detailed aspects of my own work and that of several others who are looking at biology from a similar standpoint.

While it is tempting to write such histories in sweeping, breakthrough-to-breakthrough fashion, the actual practice has been more like trench warfare, with the achievement of one small objective at a time, followed by periods of application and consolidation accompanied by undercurrents of extreme skepticism. Most such developments are accompanied by instrumental developments. In a very broad view, the chief implication of the recent history of this diffuse area is the humbling prospect of biological action accomplished by multiple layers of *complementary topological organization*.

The best-known example of complementarity is the base pairing in the double helix of DNA. We must approach these types of apparent "similarity" in complementarity as instances of self-similarity more readily seen in logarithmic spiral work-function-type geometries, rather than in the more usual mental models, though such models are based on X-ray diffraction distances. Further examples similar to the DNA complementarity

include the more gradual accretion of knowledge concerning the presence and activities of messenger RNAs; the control of protein synthesis; and knowledge of the vast number of enzyme systems, genome-controlled, acting cooperatively in maintaining visible cellular level structural integrity and metabolic functions. Some aspects of the processes by which such genome expression is controlled or modulated are beginning to be uncovered, but the processes by which external influences can modulate this activity are, at present, fairly speculative. There are a large number of investigations of ionic content, protein phosphoryllation activity, the activities of cyclic nucleotides in directing genome expressions, but, as yet, there are very few unifying principles of the nature of genetic action (Koshland 1981, Gorenstein 1981).

Studies of the process of enzyme (protein catalyst) action have similarly indicated the importance of specific conformation of both enzyme and substrate (the substance acted upon by the enzyme). More recently, measurements of tertiary (higher-order) structure alteration of enzymes have been investigated both practically and as computer reconstructions (Gelin 1975). Theories of catalysis have undergone some advance also by increasing precision of knowledge of the topological distribution of charge at catalytic sites. Multiple sites on enzymes are frequently involved in catalysis. Analysis of tertiary structure changes during catalytic processes, which involve frequently the temporary redistribution of charge in the enzyme, has indicated that fairly large energy transitions occur with this redistribution of charge, allowing rapid reaction kinetics otherwise forbidden (Peticolas 1979).

Cell contacts are involved in a wide range of crucial activities. For example, cells in developing tissues grow rapidly during the phase of tissue formation in the embryo and the growing young, but in the adult the rate of multiplication decreases as the tissue achieves its mature size. What regulates this change in rate? One hint comes from growing cells in culture plates in the laboratory. Most types of cells will multiply over the surface of the petri dish until they form a one-cell-thick confluent surface of cells over the entire dish. They then stop multiplying. It appears that the contact between cells inhibits further cell division.

Some similar inhibition may operate in normal tissues. This phenomenon is seen not only in embryos, but also in the spatial relationship of nerve cells, in blood platelets during the formation of blood clots, in the adherence of cells forming intact blood vessel walls, and in the activities of certain immune cells that engulf bacteria by first forming certain kinds of attachments to them. Other contact relationships implying a very sophisticated topological recognition process regularly take place in immunological recognition processes and antibody formation, where it appears that cell surfaces and small portions of immunoglobulin control can result from gene action. Parenthetically, cancer cells grown in laboratory cultures typically do not stop after they cover the plate with a one-cell-thick layer, but continue to multiply, producing irregular clumps. Thus, they apparently are not inhibited by contact the way normal cells are.

All of these are multicellular processes implying cell-to-cell action on a most sophisticated level.

Improvements in Understanding

Several other examples of the recent improvement in understanding of cell surface activity come to mind. Several years ago, it became apparent that cell organelles such as mitochondria (mitochondria oxidize carbohydrates and produce ATP) drastically altered their shape and volume in different metabolic environments at a rate consistent with activities of their oxidizing enzymes. Proton displacement across the membrane of the mitochondrion and ion redistribution accompanied the process. About the same time, proton displacement was recognized as a fundamental activity of several kinds of epithelial cells and also as a regular accompaniment to photosynthetic phosphorylation (the addition of phosphate to an entity). A short time later it was proposed, and it has now been partially demonstrated, that proton-displacing oxidation-reduction enzymes could be located within and penetrating through the mitochondrion membrane. These or other similar proteins have been hypothesized to be the euphemistically termed "pumps" or channels that translocate ions across the membrane (DePierre 1977, Wickner 1979).

Studies on several different types of membranes have shown that a repeatable topological distribution of certain glyco- or lipo-proteins (proteins covalently linked to carbohydrates or lipids) with several known enzymes does occur in most membrane systems studied. Indeed, this arrangement has an important relationship to the energy "gain" in photosynthesis and in mammalian eye pigments (photoreceptor substances).

The investigation of each of the broad areas mentioned in the above several paragraphs has come about in large part because of the development of appropriate laboratory technology, almost all of it intended as physical experiments in their inception. Such developments have had their clumsy beginnings, followed by commercial development and finally wide use among researchers. One need only recall centrifuges of 30 years ago (the old PR-1) and compare it to the modern gradient centrifugation techniques to appreciate the awe-inspiring number of physical and engineering advances necessary for this technique alone. The electron microscope, developed in the 1930s, which multiplied magnification power by a thousandfold and gave us our first ultrastructural pictures of the cell, was a product of de Broglie's idea that the electron has a wave activity associated with its propagation, an idea that rocked the entire basis of physics and that is still not completely understood. (Winston

Bostick elaborates on this wave particle idea in this issue of the IJFE.)

Similarly, wedge single-beam spectrometers have given way to multiple wavelength grating spectrometers allowing computer reduction of multiple wavelength data that formerly would have taken months or years to accumulate. New methods of high-precision liquid or gas chromatography with drastically improved detector systems have appeared and have supplanted many older methods. Particle counters and pulse height analysis have revolutionized the use of isotopes, and mass spectrometry has made the use of nonradioactive isotopes feasible in certain instances.

While these applications of physics have led to impressive advances in biology, the new area of diagnostics mentioned above, nuclear magnetic resonance, promises to profoundly alter our way of thinking about biology. Furthermore, this technology is opening up the possibility for biology to actually revolutionize the ideas of physics. First of all, NMR has highlighted the importance of coherence among physiological structures. This coherence even extends to the fascinating area of water itself. When we can say what water actually "is," in a variety of circumstances, we will be a long way toward understanding life. Another similar area is the study of membrane systems and states of water, which involves nonlinearities flying in the face of the usual notion of thermodynamics (Damadian 1976).

Most current models of biological processes have not, as yet, paid sufficient attention to the nature of cell surfaces. Most of us biologists have a picture of a "bilipid leaflet with protein inclusions" burned into our brain, but electron micrographs stubbornly insist on the existence of an external glycolipid structure attached to those proteins which, seemingly, is also the binding site for several types of divalent metal and many other substances. It would appear that such surfaces present a topological charge distribution alterable in some way by the presence of such binding agents, and that such agents can be translocated. Adequate description of surfaces has not yet been worked out, much less the charge distribution, so it is not possible at present to draw an other-than-conceptual picture of surface charge contours. We know there are group-specific vibrational states leading to absorption and emission of photons of infrared-to-millimeter wavelength waves. The extent of coherence of these emissions on the microscopic level has been attacked only in the case of DNA homopolymers (DNA composed of identical subunits). Certainly close approach fields should have perturbing effects on nearest neighbor molecules, but the nature of such perturbation seems not to have been investigated. That net surface charges exist has long been known from studies of electrophoretic activity (directed molecular movement when placed in an electric field) and studies of surface potentials, but the exact time variant distributions of such charges and their associated fields is a matter of conjecture. Macroscopic emissions from most biological systems resemble those of water or other nearly blackbody radiators at equivalent temperatures. The study of infrared emissions on a microscopic scale seems to have been ignored (Mei 1981).

It is known that much of the measured net surface charge is the result of organic acids and bases as expected from the analytical composition of surface glycolipids and glycoproteins. Also known is the spectral and acoustic wave selectivity of such groups, and that charge shifts along long chain molecules can alter potentials at distances long enough to penetrate membranes, thus inducing alterations of intracellular ion dissociation potentials. With spatial patterns of such potentials evident, the possibility of an extracellular-induced intracellular geometric coding system becomes apparent. Cooperative behavior such as this is already known for oxygen transport in muscle, proton translocation, and calcium translocation across membranes.

An Organizational Supercode

Levels of complementarity applied at the enzyme level, or the topological distribution of enzymes, and the dramatic effects of surface contact phenomena as reflected in qualitative and quantitative alterations in genome expression, bespeak an organizational supercode only now being somewhat dimly perceived in fields as diverse as embryogenesis, tumor biology, enzymology, immunology, and nerve cell membrane function. The pervasive influence of a topological code will probably be a profitable area of study for some time to come.

It can already be speculated, with some basis, what are some of the processes such a code would encompass. One, certainly, would require inductive effects to alter dissociation constants of acids or bases when the free groups interacted with cations (positively charged ions). Large uncertainties exist for the next order of complementarity, or the exact mechanisms by which a pattern of such events could entrain cellular reactions.

It is known that a cytoskeleton (a network structure within the cell) in contact with a layer of actin (muscle protein) just under cell lipid membranes is capable of causing dramatic lateral movements of the whole membrane. Newer studies have shown that calcium-dependent proton phosphorylation can rearrange receptor sites in nerve synaptic surfaces. Older work has shown that there may be as many as 100 different neurotransmitter substances in the brain, whose receptors are modulated by calcium-dependent rearrangements. We already know that calcium fluxes are influenced by low-frequency fields and that receptors for calcium itself possess strong steric (surface geometry) requirements.

Unknown steps in these kinds of processes are the relationships of such surface events to shifts in control of enzyme synthesis. It is already known that specific receptor groups are "uncovered" by repeated electrical

activity, but it is also known that shifts in proteins synthesized from DNA templates occur on application of different neurotransmitters. On the other hand, we also know of the hypervariable portion of immunoglobulin molecules so that the immune response also indirectly produces alteration in a small portion of a protein molecule in response to some sort of trigger, while the rest of the molecule remains constant—a "difference amplifier"!

The exact relationship of triggers to the control of synthesis of regional and specific receptors is also unknown.

Our hypothesis is that the approach of a surface with a topological/time variant charge distribution is accompanied by a "broadcast" of particular bands of frequencies detectable at microscopic separation distances. Calcium and other divalent ions serve to stabilize particular configurations of this topology. Activation of contractile activity and other actions such as enzymatic digestion of contents within cells occurs by alteration of ion dissociation constants liberating locally high concentrations of stabilizing ions. This activity also results in a geometric pattern of specific release of nucleotides forming a reverse messenger (that is, a messenger to the DNA rather than the reverse), perhaps related to cyclic nucleotide activity, and this process then alters the expression of (or otherwise changes) the genetic content.

Whether or not the hypothesis is correct, such a system could have coding possibilities ample for 10^{55} events/second/brain. The possibility of such an awe-inspiring coding system certainly is worth examining very carefully in a system whose normal genetic expression is well known. The relationship to be studied would be known topological perturbations resulting in repeatable alterations of cytogenetic expression.

Within this context, the recent progress in genetic engineering and use of bacteria and mammalian cells to incorporate genomes for transcription of specific proteins is one of the more important events of biological research in the past half century. The full implication and use of this methodology extend far beyond our present imagination. I, for one, would like to see it applied to the study of higher-order coherence of electromegnetic activity of the genome, for which this technology is eminently suitable.

References

Damadian, R., Minkoff, L., Goldsmith, M., Stanford, M., Koulther, J. 1976. "Field Focusing Nuclear Magnetic Resonance (FONAR), Visualization of a Tumor in a Live Animal." *Science* **194:** 1430-01.

DePierre, J.W., and Ernster, L. 1977. "Enzyme Topology of Intracellular Membranes." *Annual Review of Biochemistry* **46:** 201-62.

Frazer, J.W. 1970. *Presentation to Marking and Tracking Group.* Edgewood Arsenal, Maryland.

Frazer, J.W., Breemen, V.L., Langlinais, P.C., Martin, C. 1966. "Morphological and Spectral Differences Between Oxidized and Reduced Rat Kidney Slices in Vitro." *Anatomical Record* **154:** 461.

Gelin, B.R., and Karplus, M. 1975. "Sidechain Torsional Potentials and Motion of Amino Acids in Proteins; Bovine Pancreatic Trypsin Intubation." *Proceedings of the National Academy of Sciences* **72:** 2002-06.

Gorenstein, D.G. 1981. "Nucleotide Conformational Analysis by 31 P Nuclear Magnetic Resonance." *Annual Review of Biophysics and Bioengineering* **10:** 355-81.

Klainer, S.M., and Frazer, J.W. 1975. "Raman Spectroscopy as an Analytic Technique for Biological Damage Studies: Raman Spectroscopy of Molecular Species During Exposure to 100 Megacycle Radio Frequency Fields." *Annals of the New York Academy of Sciences* **247:** 323-26.

Koshland, Jr, D.E. 1981. "Biochemistry of Sensing and Adaptation in a Simple Bacterial System." *Annual Review of Biochemistry* **50:** 765-82.

Mei, W.N., Kohli, M., Prohofsky, E.W., Van Zandt, L.L. 1981. "Acoustic Modes and Nonbonded Interactions of the Double Helix." *Biopolymers* **20:** 833-52.

Peticolas, W.L. 1979. "Mean Square Amplitudes of the Longitudinal Vibrations of Helical Polymers." *Biopolymers* **18:** 747-55.

Wickner, W. 1979. "The Assembly of Proteins into Biological Membranes: The Membrane Trigger Hypothesis." *Annual Review of Biochemistry* **48:** 23-45.

Yamanashi, W.S., Boddie, A.W., Frazer, J.W., McBride, C.M., Martin, R.G. 1984. "Observations on Tissue Heating Using an Invasive Ground Probe with an R.F. Hyperthermia System." *Medical Instrumentation* **18:** 220-23.

Reports

Recent Experimental Results of The Plasma-Focus Group at Darmstadt, West Germany: A Review and Critique

by Winston Bostick

Editor's Note: Much attention has been given in recent years to the problem of constructing sources of coherent electromagnetic radiation at very short wavelengths. The extension of laser technology into the X-ray and gamma-ray range—already begun with the first successful test of a nuclear-bomb-powered X-ray laser by Lawrence Livermore National Laboratory—will assuredly have far-reaching consequences for every branch of theoretical and experimental science. The X-ray laser is one of the key components of the antimissile defense system being developed under the U.S. Strategic Defense Initiative. Applications of X-ray holography to the study of living processes have already been explored theoretically, and promise to revolutionize molecular biology. The development of a gamma-ray laser (graser) will do the same thing for nuclear and particle physics.

Many schemes have been proposed for the construction of very-short-wavelength lasers, ranging from accelerator-driven, free-electron lasers and the use of high-power, visible-wavelength lasers, synchrotron radiation, and nuclear explosions as pumping sources, to colliding matter-antimatter beams. The central problem addressed by these schemes is the need to achieve extremely high power densities in the lasing medium, while at the same time avoiding the dissipation of pumping power in various "parasitic modes."

In this context, the detection of monochromatic X-ray radiation from the plasma-focus device at Darmstadt University is of extraordinary interest. It has been known for some time that the plasma discharges created in focus machines are capable of achieving energy flux densities beyond those reached even in nuclear explosions—in a device small enough to fit onto a desktop. Careful experimental work at the Institute for Applied Physics at the University of Darmstadt points to the generation of high-intensity, picosecond-pulsed electron beams within the focus discharge, which in turn generate monochromatic X-rays through interaction with the plasma. There is reason to expect that actual X-ray laser action either occurs or can be made to occur in this type of device.

In the following report, the author reviews the results of the Darmstadt group and offers a new interpretation of the mechanism for the observed, pulsed electron beam generation in the plasma-focus discharge.

* * *

Experimental work with the 1.6-kJ, Mather-type plasma focus at the Technische Hochshüle in Darmstadt has employed high-resolution instrumentation to bring forth results that show the plasma focus to be an even greater creator of fine-structural and self-organizational surprises than has heretofore been suspected (Krompolz and Herziger 1981; Schmitt et al. 1983; Noll et al. 1983; Herziger et al. 1983; Haas et al. 1983; Krompolz et al. 1980a, 1980b, 1981). The experimenters there are to be congratulated on the ingenuity and skill with which they have mustered a wide range of diagnostics to achieve these remarkable results, which are summarized here.

(1) The electron beam produced by the Darmstadt plasma focus is found to be chopped into a series of short pulses or segments that are spaced by 25 psec between centers, the duration of the train of pulses being 200 psec. These observations involve measuring the temporal fluctuations in Cherenkov radiation produced by the electron beam as it enters a plastic target where the speed of light is less than the electron speed. The fluctuation cycle (too fast for an oscilloscope) is measured with a streak camera (Hamamatsu C979). When the observed streak-camera pattern is corrected for velocity dispersion of the electrons, the individual electron pulses are estimated to be about 0.1 of the spacing between the centers of the pulses. Microwave emission frequencies measured by time of flight of the group velocity in a suitably long waveguide give a first harmonic of 40 GHz, which corresponds to the spacing of 25 psec, and a harmonic structure that suggests that the FWHM (full width at half-maximum) of the individual pulses is ~1–3 psec.

(2) The experimenters report an energy spectrum of protons (with hydrogen filling of the vessel) up to 3.2 MeV, with a magnetic spectrograph, and a fine structure in the energy spectrum with spacings between intensity "lines" of 50-5 keV. Time-of-flight spectra of protons also showed a somewhat similar fine structure.

(3) A phosphor screen, shielded from the light from the plasma focus by a thin aluminum foil, is used to register the soft X-ray (8–13-Å) pattern emitted in a cone at an angle θ with the direction of the electron beam. A relativistic electron beam propagating in a periodic potential or density structure of spacing λ_0 should radiate electromagnetic radiation of wavelength λ at an angle θ given by $\theta = 1/2\gamma$, $\lambda = \lambda_0/2\gamma^2$, where $\gamma = (1 - \beta)^{-1/2}$, $\beta = v/c$, and the kinetic energy of the electrons is $(\gamma - 1)m_0c^2 = E$. The value of λ (with a quantum of energy ~1 keV) is measured by a bent-crystal von Hamos spectrometer, where the resolution of the instrument provides a measured value of $d\lambda/\lambda = 0.003$. This monochromatic radiation provides a value of the spacing λ_0 of the periodic structure of ~170 Å = 17 nm; $1 < \gamma < 4$. In the compression phase, periodic structures with spac-

ings of 40–100 nm were measured with Schlieren diagnostics. But 17 nm is beyond the resolution of optical Schlieren. This monochromatic coherent X-ray emission is essentially an X-ray free-electron laser and as such should be of great interest to the scientific and military communities.

The Darmstadt Plasma Focus has high reproducibility with control through a precisely triggered switch.

Interpretations of Experimental Results

Spatial Density Modulation of Plasma Electrons In the Current Sheath and in the Electron Beam Channel at 'Focus Time'

The Darmstadt group report that their Schlieren images during the collapse phase when the diameter of the current sheath column is about 1 cm show electron density bunches that are spaced (along the axis direction) by $L = 40$–$100\ \mu m$. At this point in time strong microwave emission at frequency $f = 10$ GHz is observed. They interpret the spatial modulation of electron density as being due to the onset of a lower hybrid drift instability that should fit these values of L and f. The lower hybrid frequency $\omega_l = (\Omega_e \omega_e)^{1/2}$, where $\Omega_e = eB/M_i$ and $\omega_e = eB/m_e$. They also state that enhanced light scattering at a **k** vector of 1.1×10^{-4}/cm, corresponding to a $\lambda = 6\ \mu m$, also confirms the existence of microinstabilities (of the lower hybrid drift variety) when the collapsing plasma is nearer the focus stage. The regular, spatially modulated electron density pattern along the axis during the final focus stage, inferred from the highly collimated, monochromatic ($\lambda = 13$ Å) soft X-ray emission at $\theta = 1/2\gamma$ ($\lambda_0 = 170$ Å $= 2\lambda\gamma^2$), is attributed to strong Langmuir turbulence (electrostatic plasma electron oscillations) that produces this self-organized pattern. They also affirm that simultaneous to the occurrence of this regular electron-density modulation pattern with $\lambda_0 = 170$ Å, a strong infrared emission at 12 μm (= 120,000 Å = 12,000 nm) is observed. They state that these values indicate the oscillation of an electron-cyclotron drift instability, the wavelength λ_0 and frequency of which are given by $\lambda_0 > \max[2\pi(m_e/m_i)^{1/2} r_{ce}, \lambda_D]$; $\omega_{ce} = eB/m_e c$, where m_e/m_i denotes the mass ratio of electrons to ions, $r_{ce} = mvc/eB$ = the electron gyroradius, and λ_D is the Debye radius of the plasma. They conclude that the periodic density modulation is generated by a heavily oscillating electron cyclotron drift instability, and that this particular instability induces a powerful particle acceleration owing to its variable phase velocity, which, in turn, depends upon the strength of B.

Intensity Modulation of Ion Energy Spectrum And Periodic Emission of Electrons (to Produce A Chopped Beam)

Both of these effects are attributed to the presence of a nonlinear three-wave interaction in the focus plasma. The Darmstadt researchers suggest that this process can lead to simultaneous repetitive oscillations of the wave amplitudes, provided that one of the interacting waves has negative energy and is able to release energy while growing in amplitude. They state that the slow space charge wave during a beam plasma interaction is of this type. During the rising part of the amplitudes, electrons and ions can be captured and accelerated in the potential wells of the waves, and subsequently released during the falling part of the wave amplitudes. They claim that this assumption leads to a close relationship between the observed periodic emission of the electrons and the peaks in intensity ("spectral lines") in the ion spectra. They construct by this assumed three-wave interaction a temporal evolution and decay of the wave amplitude over a span of 200 psec, where the spacing between wave peaks is 10 psec and the FWHM of each wave peak is 1 psec.

Critique and Remarks

This author has already paid a rather glowing compliment to the Darmstadt experimental work, and he now also congratulates the workers on their ingenuity and resourcefulness in attempting to explain self-consistently the experimental results in terms of various kinds of self-organizing, large-amplitude drift waves and Langmuir turbulence that eventually create the plasma structures that "do the job." This author has a warm spot in his heart for investigators who recognize the importance of self-organizing plasma structures. May we remind the readers (including the Darmstadt group) that he himself was one of the first investigators to set the stage, by accident, for nature to produce such structures in the laboratory, 30 years ago at Lawrence Livermore National Laboratory (Bostick 1956a, 1956b, 1957). These structures came to be called plasmoids, which are force-free, minimum-free-energy plasma structures of spectacular morphology that spontaneously spring to life. Solar flares, radio stars and galaxies, galactic arms, filamentary cluster structures of galaxies, twinkling of radio stars, and so on have been engaged in producing these structures for at least 30 billion years. In fact, the Universe itself is probably one gigantic plasmoid.

During the intervening years since 1956, the author with his colleagues (principally V. Nardi and W. Prior and students at the Stevens Institute of Technology in New Jersey) has pursued the study of these structures at the Stevens Institute, where the plasma-focus research has yielded an incredible variety of Beltrami-style vortex filaments. Lyman Spitzer in his book was supposed to have taught us everything we ever needed or wanted to know about the conduction of electric current by plasmas. But his book neglects to mention the very important fact that electrons prefer to carry current parallel (not perpendicular) to a magnetic field, and that they will therefore collectively create a Beltrami, force-free type of magnetic morphology, where electrons everywhere are flowing parallel to the local magnetic field. To create this beautifully self-organized magnetic configuration it is re-

quired that mass velocity and vorticity all be parallel (or antiparallel) to the magnetic field and current density vectors of the Beltrami morphology. The paired flux-tube morphology of these vortex filaments is a macroscopic, classical manifestation of Type II superconductivity. In the matter of complexity of self-organization, this type of intricate, geometrical, Beltrami self-organization is to a self-organized Langmuir (or lower hybrid) wave pattern as the vertebrates are to the protozoa.

The current sheath of the Darmstadt plasma focus is driven faster than that at Stevens and the vortex filaments are on a much finer scale (smaller in diameter, closer together), not nearly so easily resolved, *but they are there!* The Darmstadt plasma-focus current sheath cannot carry the current, Lyman Spitzer notwithstanding, if the sheath is not made up of these paired vortex filaments (Bostick 1966). The Russian vacuum spark physicists and the Polish plasma-focus physicists recognize the important role of these paired vortex filaments. Relativistic electron-beam "vacuum" diodes had been in use for 20 years (millions of dollars of computer simulation time!) with few if any of the workers in that field recognizing that the current in the diode was carried by paired vortex filaments. The major recognition came via a plasma-focus physicist.

The basic interruption of the plasma-focus current that leads to the spatially (<0.3 mm diameter, <1 mm length) and temporally (<20 psec) compressed acceleration process of the electron beam and the ion beam when the current column becomes <10 mm in diameter is a stimulated, sudden (~10 psec) ripping of all of these filaments at one value of the coordinate z (the axis coordinate), all around the circumference of the ring of vortex filaments. The plasma whose electrons (primarily) were carrying a current of 0.5 MA in its organized filaments now must face the magnetic-insulating tyranny of the Alfvén limit in the gap where the filaments have been severed. If plasma-focus physicists persist in describing this process with the Neanderthal language of "Kruskal-Schwartzchild, MHD, $m = 0$ instability," they do so at peril of their own eventual intellectual embarrassment. The plasma electrons apparently know how to accommodate to this sudden confrontation by the Alfvén limit. It is and has been a challenging puzzle for us to divine how Nature tells the plasma what to do. Our acronym for the process can be designated by the letters *p-a-s-e-r:* particle acceleration by stimulated eruption of resistance.

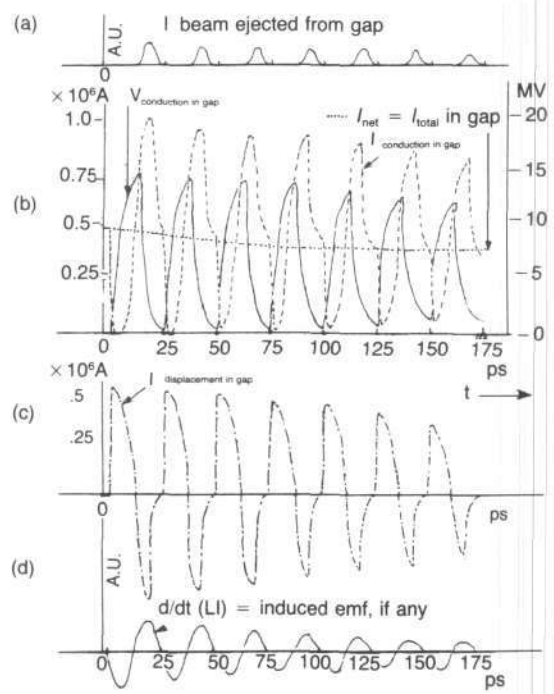

Figure 1. Estimated wave forms produced by plasma focus as a shuttering electromagnetic ram. A.U. is arbitrary units.

The chopping of the electron beam from the plasma focus is, in this author's opinion, the most important result that the Darmstadt group has brought forth. The author, therefore, addresses his remarks primarily to analyzing this result, and he now offers up for dialogue and criticism a qualitative solution to this puzzle. In doing so, he invokes, at the beginning, a paraphrasing of lines from the poem about Barbara Fritchey of Civil War renown, "Shoot if you will at this old gray head, but spare your historical scientific accuracy and scientific integrity instead."

To explain the segmenting of the electron beam and the acceleration of electrons and ions to high energy we advance the hypothesis that the cycle is produced and reproduced many times over by an "electronic ram" (Raudorf 1951, 1974) (perhaps more appropriately a "magnetic" or "electromagnetic" ram) with an oscillating effect akin to a blocking oscillator circuit.

With the sudden interruption at $t = 0$ (see Figure 1) of the plasma electron current, which, scant picoseconds before, had been blithely flowing in continuous force-free filaments, the magnetic insulating effect of the gross B_θ, now being generated by a displacement current I_{displ} (previously generated by the continuous conducting current in all the filaments) flowing into a "plasma capacitor" (the gap where the filaments are cut), permits the capacitance to be charged with the voltage wave form V_c as shown.

The insulating effect of the displacement-current-produced B_θ occurs everywhere in the gap of the capacitor except near and at the geometrical center line, where B_θ becomes small enough (or zero) to permit electrons and ions to be accelerated along the axis to energies corresponding to the voltage V_c on the capacitor. The very small diameter of the electron and ion beam so restricted at this time by the form of B_θ corresponds to the insertion of a very high equivalent-circuit resistance across the capacitor at this symmetry axis, and as current is driven

through this effective equivalent-circuit resistance by the voltage V_c, electrons and ions in this small-diameter beam are actually being accelerated to the high voltage attained by V_c. One must not lose sight of the fact that for the relatively few ions and electrons that are in these small-diameter beams there is a strong focusing effect brought about by the form of B_θ. This strong focusing effect will serve to give the beams generated during this phase greater concentrations on the axis than they would otherwise have. The small diameter of the electron beam at this stage also corresponds to an inductance in series with the high resistance. The effect of this inductance is to slow down initially the onset and rise of the conduction current.

The "ram" effect of the magnetic energy stored by the total current, I_{total}, flowing in the plasma column and electrodes and transmission lines ensures that the $I_{\text{net}} = I_{\text{total}}$ in the gap does not change much in these 12 psec, but I_{total} will drop to about 0.5 of its initial value in about 200 psec (after many cycles of beam segmentation), giving rise to the well-known dI/dt_{total} signal at the breach of the electrodes.

The displacement current I_{displ} that produces the magnetically insulating B_θ at the gap (the capacitor) decreases as V_c approaches its maximum, and the conduction current (made up of accelerated electrons and ions in a beam that is probably increasing somewhat in diameter) increases concomitantly as the I_{displ} decreases, all the while $I_{\text{total}} \equiv I_{\text{cond}} + I_{\text{displ}}$. Even at this stage the new-conduction-current electrons are probably beginning to fashion themselves into a group of Beltrami-type, force-free filaments that will enable them to circumvent the Alfvén limit.

The value of I_{displ} becomes zero when V_c reaches its peak and goes negative (as V_c decreases), thereby canceling much of the B_θ that at this point is being produced by the conduction current. The area near the axis available to a beam current increases as magnetic insulation is constantly sabotaged by the increasing magnitude of the reversed B_θ from the reverse I_{displ}. The increase of the cross-sectional area available to the beam brings about a rapid RC decay of the charge and voltage, V_c, on the capacitor. It is during this decay phase of the voltage on the capacitor that most of the electrons and ions are accelerated and the greater part of the energy spectra of the ions and electrons is developed. The high-current electron beam that flows at this time must develop force-free filamentary structures in order not to be magnetically cut off by its own gross B_θ. These structures interrupt themselves sharply at 25 psec, and the cycle begins again with I_{cond} plummeting toward zero, its place being taken by I_{displ}, and V_c rising again because of I_{displ}.

As just suggested, the accelerated segments of the electron beam in order to propagate when their currents approach or exceed the Alfvén limit (a limit imposed *by their own* B_θ) must resort to some form of Beltrami, force-free vortex configuration, and indeed the damage on targets (Nardi 1980, 1983) bears ample witness to the production of such structures with small diameters of about 3 μm. The smaller vortex structures organize themselves into larger spiral patterns with diameters as large as 300 μm. If, as the Darmstadt data suggest, the duration of an electron pulse is about 3 psec, and if the group velocity of the structures (as measured at Stevens) is about 1.5×10^{10} cm/sec, the upper limit to the length of the vortex structure will be $3\times10^{-12} \times 1.5\times10^{10} \sim 0.5$ mm $= 500$ μm.

If we take the peak current in the plasma focus as that for the Stevens machine, 0.5 MA, and with the spacing between pulses of 20 psec $= 20\times10^{-12}$ sec, the number of electrons in each segment of the beam is $(5\times10^5\times20\times10^{-12})/(1.6\times10^{-19}) = 6\times10^{13}$. One segment may contain perhaps 100 vortex structures similar to that of Figure 1, so that one of these structures would contain about 6×10^{11} electrons, carrying a group current of about 5×10^3 A. However, the current circulation pattern down the center of the vortex would be approximately given by $(6\times10^{11} \times 1.6\times10^{-19} \times 3\times10^8)/(2\times10^{-4}) = 14\times10^4 = 1.4\times10^5$ A, if we take the length of the vortex structure of Figure 1 to be 100 μm $= 10^{-4}$ m. If the radius of the core carrying this longitudinal current is 1 μm (10^{-4} cm), the B_θ surrounding this core is $2I/10r = (2\times1.4\times10^5)/(10\times10^{-4}) \approx 3\times10^8$ G $= 300$ MG!

The magnetic stored energy will be

$$\frac{B_\theta^2}{8\pi} \times \text{Volume} \equiv \frac{9\times10^{16}}{8\pi} \times 10^{-2} \times 4 \times 10^{-8} \equiv 10^{-6}\ \text{erg} = 0.1\ \text{J}. \quad (1)$$

The stored kinetic energy (of one of these vortices) in the electron's velocity in the laboratory frame of reference is, if we take an effective average kinetic energy for an electron of 3×10^5 eV $\approx 5\times10^{-7}$ erg $= 6\times10^{11}\times5\times10^{-7} = 30\times10^4$ erg $= 0.03$ J, which is about one-third of the magnetic energy. The magnetic energy is comparable to or greater than the rest energy of the electrons that compose the structure.

Luce and Nardi (Luce 1978, 1983; Nardi 1980) have observed that these structures prefer to travel along dielectric surfaces and through small cracks in dielectrics, where the electrons composing the structure can presumably enjoy some space-charge neutralization through the proximity of polarization charges in the dielectric. There will also be return currents that flow back along the dielectric surface and through any plasma that is provided by the ionization of a low-pressure background gas.

The energy deposition density on a target by one of these vortex structures is $0.1/(4\times10^{-8}) \approx 2.5\times10^6$ J/cm^2. The power deposition on a target is $0.1/(4\times10^{-8} \times 0.3\times10^{-12}) \approx 10^{19}$ W/cm^2 $= 10^7$ TW/cm^2.

As these structures (such as Figure 2) proceed through a background gas of 3 torr of deuterium (for example, in the electron beam from a plasma focus) and near a

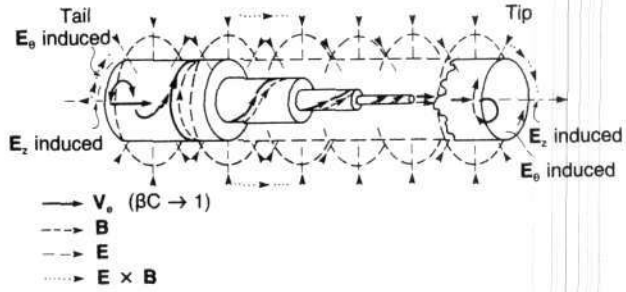

Figure 2. Propagation of a cigar-shaped electron vortex structure as viewed from the laboratory frame of reference.

dielectric surface, their electron circulation is roughly like that of a wide rubber tire doing a "poloidal roll" with the outside perimeter in contact with the background ionized gas and perhaps "in contact with" a dielectric surface. The degree of "skidding" on the dielectric surface and background gas is unknown. The electrons in the center proceed forward in the z direction with speeds (in the laboratory frame) that are larger than those at the periphery.

Although the electrons of the vortex structure can enjoy some space-charge-neutralizing comfort from the polarization charges of their dielectric and ionized-gas environments as they proceed on their journey, they cannot be entraining positive ions into their structures: any positive ions—deuterons, for example—entrained into the structure would be obliged to have speeds equal to that of the structure, whose speed can be $\sim c/2 = 1.5 \times 10^{10}$ cm/sec. The positive ions would acquire energies of hundreds of millions of electron volts, and these energies are not observed. It must be concluded that the vortex structure of Figure 2 is composed almost entirely of electrons.

As the vortex structure of Figure 2 proceeds with a group velocity in the z direction it produces an overall surrounding B_θ that must travel along with the structure. As the head of the structure continuously establishes this ongoing B_θ it induces an electric field E_z at the forward end, which accelerates positive ions forward. As the tail of the structure disestablishes the surrounding B_θ at the tail end, it induces an electric field that accelerates positive ions in the $-z$ (backward) direction. The kinetic energy imparted to positive ions (provided by ambient plasma) at the head of the structure is returned to the structure at its tail as these same ions are overtaken by the tail. The structure can thus proceed through the background medium with very little loss, almost like a smooth sphere proceeding at low speeds through an inviscid fluid. The damage produced when the structure hits a witness plate is due primarily to the positive ions accelerated forward at the head and to the ions and electrons that are accelerated by the destruction of the 0.1 J of stored magnetic energy in the structure, that is, the high-density B_θ around the core and the high-density B_z at the core.

The reaction forces produced by these induced electric fields at the head and tail tend to shorten the length of the structure (blunted at the nose, kicked in the tail). It is not known *a priori* what the equilibrium aspect ratio of the structure will be. The length may shrink to less than 100 μm.

The overall picture of the beam-producing mechanism in the plasma focus is that of a shuttering magnetic ram launching from the gap (the "capacitor") a train of beam pulses, as suggested by Figure 1. The electron beam pulses proceed at 180° along the z axis through the hollow center-electrode (anode) structure of the plasma-focus machine. Each pulse or segment of the electron beam is made up of many electron vortex structures of the type shown in Figure 2. As the electron beam consisting of a train of these pulses (each pulse consisting of many electron vortex structures) proceeds through the background gas of about 3 torr of deuterium, in a drift tube with either metallic or dielectric walls, a return current is carried along the drift tube walls and through the ionized background gas.

A segmented train of positive-ion (deuteron) beam pulses proceeds simultaneously in the 0° direction, away from the anode.

There is substantial evidence that a similar gap and launching process of electron beams occurs in the "first betatron focus" of relativistic electron-beam machines after the beam penetrates the anode foil into a drift tube containing a gas (for example, air or hydrogen) at a pressure of about 1 torr: One can observe with open-shutter photography a sharp (~1 mm diameter) beam emanating from this "focus." Pinhole photographs of this region with etchable plastic (CR-39) show images composed of ion tracks corresponding to energies of about 2 MeV, coming from such a focus spot as they do in the plasma-focus machines. I suggest that a shuttering "magnetic ram" or "electronic ram" process is in operation at this point in REB machines.

The size of the emitting source of the plasma-focus deuteron beam at Stevens as imaged by a pinhole (300 μm diameter) at 0° with the axis with CR-39 etchable plastic to record the deuteron tracks is equal to or less than 300 μm. One expects a small diameter of this beam during the phase of high I_{displ} if one recognizes that the magnetic insulation of the displacement current is effective except at the geometrical center of this displacement-current carrying column (which flows across the gap), where B becomes zero. As we have already stated, there will always be some beam current (very small in diameter) at this center even when the displacement current is high.

During this phase of high I_{displ} the radially inward $\mathbf{E} \times \mathbf{B}/B^2$ cycloidal drift of both deuterons and electrons at the surfaces of the gap, from the B_θ produced by I_{displ} and the E_z produced by V_c, will concentrate the plasma density at the center of the gap, distorting the center of the negative "plate" of the "capacitor" into a locally high-

density plasma point, which can act like a field-emission cathode point. The high-plasma-density anode plate of the capacitor also will be distorted at its center into the shape of a small-diameter point or "needle." During this phase the small-diameter electron beam is very likely emitted from this cathode point. It is to be expected that this cathode point remains at the center of the emitted electron beam, even after I_{displ} has reversed sign and the beam is expanding in diameter. Mach-Zender interferometry photos (1 nsec exposure time; also X-ray, and to a certain extent, pinhole photos) of the profiles of the Stuttgart plasma focus (Herold 1984) show quite dramatically a morphology in which the two plates of the capacitor are rather clearly delineated, with the beam acceleration column joining the two plates in the geometrical center of the plates (Figure 3).

It is instructive to evaluate the capacitance from the shape and dimensions of the "plasma capacitor" as seen with Mach-Zender interferometry (1 nsec) in the Stuttgart plasma-focus machine [280 kJ, 60 kV, 1 MA—Figure 3(a)] and the Stevens machine (5 kJ, 20 kV, 0.5 MA) as seen with the image converter [5 nsec—Figure 3(b)]. If the dielectric of the capacitors were vacuum the capacitance would be given by $C = \varepsilon_0 kA/d$, where $\varepsilon_0 = 8.85\times10^{-12}$, $k = 1$, A = area in square meters, and d = spacing in meters. For Figure 3(a), $C = (8.85\times10^{-12} \times 4.5\times10^{-4})/(0.5\times10^{-2}) = 80\times10^{-14} = 0.8\times10^{-12}$ F. For Figure 3(b), $C = (8.85\times10^{-12} \times 0.78\times10^{-4})/(0.3\times10^{-2}) = 23\times10^{-14} = 0.23\times10^{-12}$ F.

The value of the dielectric constant of a plasma $\varepsilon/\varepsilon_0 = k = 1 + 4\pi\rho c^2/B^2$ (B in gauss, ρ in gram-meter-seconds per cubic centimeter). If the electron-ion density n of the deuterium plasma is 10^{17}, and the average value of B is 10^5 G, the value of k will be 3.8×10^5. For example, the Stevens machine, with a current of $I = 0.5$ MA $= 5\times10^5$ A, should charge C up to $V_c \cong 10^7$ V in about 12 psec (12×10^{-12} sec). Thus $Q = 5\times10^5 \times 12\times10^{-12} = 6\times10^{-6}$ $C = CV = C\times10^7$, and C should be $C = 6\times10^{-6}/10^7 = 5\times10^{-13} = 0.5\times10^{-12}$ F, which is the correct order of magnitude (compare with $C = 0.23\times10^{-12}$ F) for $k = 1$, not for $k \geq 3.8\times10^5$. We conclude that either the effective value of n must be $2.5\times10^{11}/\text{cm}^3$ between the plates or that the plasma as a dielectric in the presence of B cannot respond rapidly enough in the 12-psec time interval to make k appreciably different from 1.

We now attempt to establish a rationale that connects the electronic-ram (or magnetic-ram) model of the plasma focus with the deuteron energy spectrum that has been measured recently at Stevens by two methods: (1) magnetic spectrometer and (2) time of flight. These two methods give experimental results that are in good agreement. They show a spectrum of $N(E)$ as a function of E on a log–log plot that is a straight line with an exponent of -2.7; that is, $N(E)dE = kE^{-27}dE$, where k is a constant. This spectrum is measured up to an energy of 13 MeV.

The charge–discharge cycle of the electronic-ram model of Figure 1 suggests that, to a first approximation, the

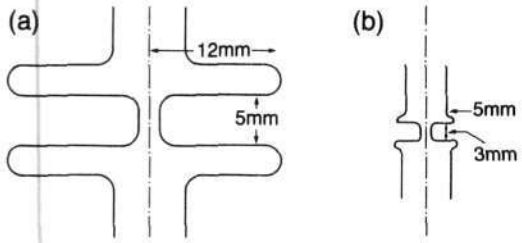

Figure 3(a). Typical approximate plasma density profile of the Stuttgart plasma focus, as inferred from a 1 ns Mach Zender interferogram.

Figure 3(b). Typical approximate plasma density profile as inferred from a 5 ns image converter photo of the Stevens plasma focus.

discharge of the plasma capacitor looks like an RC decay where the energy lost in the resistance R is actually represented by the electrons accelerated (at 180°) to a beam in the gap and the positive ions accelerated (at 0°) to a beam in the gap. Thus $V_c = V_0 \exp(-t/RC)$, or the energy E to which positive ions (and electrons) would be accelerated can be written $E = E_0 \exp(-t/RC)$, where V_0 in volts is equal to E_0 in electron volts. During this RC-decay phase of the capacitor $dV_c/dt = (-V_0/RC) \exp(-t/RC)$, or we could write $dE/dt = (-E_0/RC) \exp(-t/RC)$, and $dt = (-RC/E_0) \exp(t/RC)dE$. Now for a constant value of the increment dE the number of deuterons (and electrons) that are accelerated will be proportional to $|dt|$. We can therefore make an initial suggestion that $N(E) \sim \exp(t/RC)$, $E \sim \exp(-t/RC)$ and the slope of the log–log plot of $N(E)$ as a function of E would be a straight line with the slope

$$\frac{(d/dt)\ \ln N(E)}{(d/dt)\ (\ln E)} = \frac{(d/dt)\ (t/RC)}{(d/dt)\ (-t/RC)} = -1, \qquad (2)$$

and the spectrum would be given by $N(E)dE = \text{const} \times E^{-1}dE$. However, we should recognize that $N(E)$ in the beam spectrum is not only proportional to dt, but that it must also be proportional to the cross-sectional area of the beam that is permitted to flow near the geometrical center of I_{displ}, where B_θ is low enough to admit the beam. As I_{displ} becomes negative after V_c starts to falls and the capacitance is discharging and B_θ from I_{displ} is increasing in the opposite direction, the radius of the admitted beam would be expected to increase as $1/\exp(-t/RC)$ and its area as $1/\exp(-zt/RC) = \exp(zt/RC)$. Thus we might expect

$$N(E) \cong \underbrace{\exp(t/RC)}_{\text{contribution from } dt} \times \underbrace{\exp(2t/RC)}_{\text{contribution from increased channel area for the beam}} \cong \exp(3t/RC) \qquad (3)$$

Thus the ln $N(E)$ as a function of ln E plot should be a straight line with a slope of

$$\frac{(d/dt)\ \ln N(E)}{(d/dt)\ (\ln E)} = \frac{(d/dt)\ (3t/RC)}{(d/dt)\ (-t/RC)} = -3.$$

The spectrum would then be given by $N(E)dE = \text{const} \times E^{-3}dE$. Within the crude approximations made here the exponent -3 (usually called γ) is reasonably close to the experimental -2.7. It can be pointed out that the primary cosmic ray spectrum for $E < 10^6$ GeV has $\gamma = 2.73$ and for $E > 10^6$ GeV, $\gamma = 3.34$. If our plasma-focus model as an electronic ram proves to be correct, and if its expected spectrum from a more rigorous theoretical analysis bears out the sketchy foregoing analysis, we can enter this model into the horse race concerning the question as to how the cosmic rays acquire their energies, which go as high as 10^{21} eV.

It is interesting to note that the electron energy spectrum from Raudorf's electronic-ram experiment is a straight line on a log–log plot with a slope of about -3 between the energies of 1 and 10 MeV.

References

Bostick, W.H. 1956. *Phys Rev.* 104: 292; *New York Times*, Dec. 12, p. 1; "Experimental Study of Plasmoids," *Electromagnetic Phenomena in Cosmical Physics*, IAU Symposium Number 6, Stockholm, 1956 (Cambridge: Cambridge University Press).

Bostick, W.H., Prior, W., and Farber, E. 1965. *Phys. Fluids* **8:** 745.

Bostick, W.H., Prior, E., Grunberger, L., and Emmert, G. 1966. *Phys. Fluids* **9:** 2079.

Herziger, G., et al. 1983a. "Observation of Nonlinear Phenomena." Plasma Focus Workshop, Stuttgart, (Sept.).

Herziger, G., et al. 1983b. "Radiation and Particle Emission from a 1.6 J Plasma Focus," Plasma Focus Workshop, Stuttgart, (Sept.).

Haas, C.R. et al. 1983. "Dynamics of Microstructures." Plasma Focus Workshop, Stuttgart (Sept.).

Krompolz, H., and Herziger, G. 1981. "Phenomena of Self-Organization in Dense Plasma." *Chaos and Order in Nature*. Ed. H. Haken (Berlin: Springer-Verlag), p. 131.

Krompolz, H. et al. 1980a. "Periodical Modulations in High Energy Spectra in the Plasma Focus Device." *Phys. Lett.* **76A:** 255 (March 31).

Krompolz, H. et al. 1980b. "Formation of the Plasma Layer in a Plasma Focus Device." *Phys. Lett.* **77A:** 246 (May 26).

Krompolz, H. et al. 1981. "A Scaling Law for Plasma Focus Devices." *Phys. Lett.* **82A:** 82 (March 9).

Luce, J.S., and Bostick, W.H. 1983. "LLL Experiments in Collective Field Acceleration." *Second International Conference on Energy Storage, Compression and Switching, Venice 1978*. (New York: Plenum), p. 437.

Luce, J., Bostick, W.H., and Nardi, V. 1979. Lawrence Livermore Laboratory Report No. UCID-17232, in *Collective Methods of Acceleration*. Ed. Rostoker and Reiser (New York: Harwood), p. 493.

Nardi, V. et al. 1980. "Internal Structure of Electron-Beam Filaments." *Phys. Rev. A* **22:** 2212 (Nov.).

Nardi, V. et al. 1983. "Structure and Propagation of Electron Beams." *Second International Conference on Energy Storage, Compression and Switching, Venice 1978*. (New York: Plenum), p. 449.

Noll, R., et al. 1983. "Observation of Picosecond Modulated Electron Beams from the Plasma Focus." *Phys. Lett.* **99A:** 435 (Dec. 26).

Raudorf, W.R. 1974. "An Electronic Ram." *Wireless Engineer, Proceedings of First International Conference on Energy Storage, Compression and Switching* (New York: Plenum), p. 381.

Schmitt, K., et al. 1983. "High-Power Narrow-Band Millimeter Waves Generated by the Electron Beam Emitted from the Plasma Focus," *Phys. Lett.* **95A:** 239 (May 2).

The Polarized Fusion Program at LLNL

Numerical simulations have shown that using spin-polarized fusion fuel can reduce the required driver energy to attain a specific energy gain (total fusion energy generated divided by driver energy input) by as much as a factor of 7 in inertial confinement fusion (Moore 1983, Nuckolls 1984). This means that the cost of electricity generation by inertial confinement fusion could be greatly reduced. The Lawrence Livermore National Laboratory has initiated a program to experimentally confirm these numerical projections.

According to Dr. Eric Storm, the program is currently operating with a budget of about $500,000 per year. Its primary goal is to explore "brute force" techniques for preparing spin-polarized deuterium-tritium (DT) fuel for inertial targets that would be tested with the 100-kJ Nova laser system within the next three years. The specific goals are to attain a better than 80 percent spin polarization of a 50-50 DT mixture and to maintain it in the polarized state for more than 10 seconds.

Given the rapid rate at which deuterium molecules (^{2}D) depolarize tritium molecules (^{3}T) the program is first exploring the preparation of D-T molecules and their spin polarization. Although pure-deuterium spin-polarized fuels are not being explored at this time, possible future experiments with pure-deuterium polarized fuel targets are not being excluded at this time. Various university and outside consultants are being brought into the program to facilitate development of the expertise needed to achieve the spin-polarization requirements.

—*Charles B. Stevens*

References

Moore, R.M. 1983. *Phys. Rev. Lett.* **51:** 396-399.

Nuckolls, J. 1984. "Das wirtschaftliche Potential der Tragheitsfusion." *Fusion* [German-language edition] **5:** 27-32 (Feb.).

Muon Approach to Cold Fusion Makes Progress

by Charles B. Stevens

Scientists from around the world gathered at Jackson Hole, Wy., in June 1984 for the "Muon-Catalyzed Fusion Workshop." The recent experimental results reported there open up the possibility of practical applications for this "cold" approach to harnessing nuclear fusion energy. The development of particle-beam technologies within President Reagan's Strategic Defense Initiative promises to greatly accelerate this alternative approach to igniting fusion reactions.

The most general approach to achieving nuclear fusion, such as that pursued in magnetic and laser fusion research, involves raising the hydrogen fusion to extremely high temperatures on the order of 100 million degrees Celsius. At these temperatures the hydrogen nuclei will have sufficiently high relative velocities so that in their collisions with one another they can overcome their mutual electrical repulsion and fuse. The idea here is that the relative velocity is great enough so that the nuclei come within such a short distance of one another that the strong nuclear force overcomes the repulsive electrical force.

Since the 1950s, it has been known that an entirely different, low-temperature (less than 1,000°K) approach —muon-catalyzed fusion—could produce nuclear fusion. However, this approach did not appear to be capable of producing net energy; more energy would be consumed in generating muons than the output of the fusion reactions they would catalyze. Now, recent experimental results are changing this prognosis.

Muons are generated when extremely high-energy particle beams collide and their nuclear ions disintegrate. The muon is a short-lived particle that has the same negative electric charge as an electron, but has several hundred times its mass. In fact, after it decays, within 2 μsec, the muon becomes an electron.

When a muon is directed into a container of hydrogen gas, it will be slowed down by collisions with the hydrogen molecules, and it takes the place of an electron in one such molecule. However, since the muon is much heavier than ordinary electrons, its orbit is much closer to the nucleus.

When a muonized hydrogen molecule consists of two hydrogen atoms (in particular the two heavy isotopes of hydrogen, deuterium and tritium), then the muon will orbit both nuclei of these atoms at close range. The negative charge of the muon at this close range shields—balances out—the positive repulsive electric charges of the two nuclei so that they can come much closer together. In fact they come close enough for nuclear fusion, and the muon therefore acts as a catalyst. In this way nuclear fusion can be achieved without the high relative velocities (high temperatures) needed in magnetic and laser fusion.

The original analysis by U.S. scientists was that much more energy would be needed to generate muons than would be produced by muon-catalyzed reactions. The energy needed to generate a muon appears to be at least 100 times that produced by a single fusion reaction, and therefore each muon would have to catalyze more than 100 fusion reactions as a minimum requirement for net energy generation. In the 1950s, U.S. scientists projected that the muon deuterium-tritium molecular formation would take on average about 30 μsec; since the muon decays within less than 2 μsec, very few muon-catalyzed fusion reactions would be achieved by each muon.

While U.S. scientists, therefore, gave up muon-catalyzed fusion research, Soviet scientists continued to explore it. In the late 1960s and into the mid 1970s, Soviet scientists theoretically discovered that muons could first combine with a single tritium nuclei and that this muonized atom would then rapidly penetrate and combine with a deuterium molecule. This rapid molecular formation path is called a "resonance" model, and it was projected that it could take place at a rate up to 30,000 times faster than the previous 1950s calculations. Therefore, each muon could theoretically catalyze hundreds of fusion reactions.

At the Jackson Hole workshop, experimental results were presented that not only confirmed these theoretical projections, but also showed that the dynamics of muon-catalyzed fusion are much more promising: The rate of molecular formation increases faster than projected with increasing temperature and density of the hydrogen gas. Furthermore, one path for losing muons from the reacting gas—the muon sticking to the fusion reaction-product nuclei—has been found to be seven times less severe then previously thought.

The Prognosis

Many questions remain to be addressed before the prospects for economic power can be fully determined, and the same prerequisite holds for both scientific and economic demonstration: development of a sufficiently high-current, high-energy particle beam. Such high-current accelerators are one of the technologies being pursued as defensive beam weapons, and the technology to achieve such devices already exists. A high-current accelerator will produce a sufficient number of muons to provide a full-scale demonstration of muon-catalyzed fusion energy generation. Also, such an accelerator will permit the determination of the efficiency by which muons can be generated.

If muon-catalyzed fusion is found not to be capable of economical net energy generation on its own, it could still be combined with the breeding of fissile fuel for nuclear fission power plants to provide an economically feasible facility.

Among the more interesting, speculative ideas brought up at the workshop were the possibilities of using muon-catalyzed fusion to help ignite hot fusion as well as combining muon-catalyzed fusion with the spin polarization of fusion fuel.

Radiative Collapse to Super Densities: A Review of the Work of B.E. Meierovich

by Charles B. Stevens

Over the past several years, Dr. B.E. Meierovich of the Soviet Academy of Sciences Institute for Physical Problems in Moscow has published several intriguing papers on the theoretical aspects of radiative collapse of relativistic beams to super densities and an extension of this analysis to plasma pinches, such as those seen in the plasma focus. This report reviews Meierovich's recent work.

Meierovich's work on radiative collapse to super densities first came to our attention in a private communication from F. Winterberg. Meierovich had written a brief comment on a 1979 work by Winterberg on the question of radiative collapse. Meierovich noted that in his own analysis he utilized the quasiclassical approximation where gamma is not too large, while Winterberg had taken the ultraquantum approach where the beams involved are highly relativistic, having high gammas.

Meierovich noted (1981) that investigation of self-focusing streams of charged particles, started by Bennet and revived by Budker, had resulted, in recent years, in the formation of a special trend in the physics of non-neutral plasmas and powerful electron-ion beams. A far-from-complete list of projects using strong-current devices—including items from proposals for solving the problem of controlled thermonuclear fusion, the construction of lasers in the X-ray and gamma-ray ranges, and collective acceleration of charged particles—provides one with an idea of the effect of the impact of this subject on the modern development of physics.

A study of the pinch systems shows that the most interesting experimental phenomena arise in the process of strong compression (a burst of X-ray radiation, high temperature, high density and multiplicity of the atomic ionization, acceleration of electrons and ions, appearance of neutrons, and a blasting character of the electronic emission). The nontraditional approach to the pinch effect, based on the analysis of the equilibrium and radiation of the plasma in the proper magnetic field of the current, enables one to describe in a unified manner the phenomena accompanying the pinch effect, and to some extent fills the gaps resulting from attempts of uncorrelated explanations of isolated properties of the pinch.

Micropinch Regions and Sparks

Korop et al. (1979) note that one of the most interesting effects observed in sparks and pinches is the formation of a micropinch region in which the state of the matter approaches that in stars, which was discovered in 1968 by Cohen et al. in experiments with a low-inductance vacuum spark. Levedev et al., Plyutto et al., and Handel et al. all came close to discovering this unique property of sparks. Today, Meierovich says, we also know that the physical nature of this effect has much in common with that of the plasma focus of Filippov and Mather.

The first scientific conference on spark discharges was held near the end of the last century, just after the discovery of X-rays. At the time, physicists had probably not yet run into this phenomenon, which, although very interesting from the experimental standpoint, is very awkward to deal with theoretically: Despite constant study of the nature of the spark for more than half a century, not a single one of the properties of sparks that were observed experimentally had been predicted theoretically. Among these properties are the X-ray burst, the high temperature and the multiple ionization of atoms, self-contracted electron beams, fast ions, and the explosive nature of the electron emission. Recent research has shown that there is still much to learn about this type of discharge, although the spark is almost the most common type of naturally occurring discharge.

By "spark" is meant a brief stage (lasting about 0.1 μsec, according to experiments) in the formation of those conditions that are required for a stable arc. Clearly, all types of vacuum breakdown, including the explosive emission in the diodes of high-current electron accelerators, are sparks. Events characteristic of sparks also precede the establishment of an electric arc at atmospheric pressure.

Meierovich pointed out (1981) that the analysis of the plasma equilibrium in the collective interaction electromagnetic field, created by the charges, shows that in addition to the well-known equilibrium configurations of the plasma as a classical ideal gas, there is a substantially wider class that contains the structures compressed by collective interaction forces up to the electronic degeneracy. A practical realization of peculiar equilibrium states depends substantially on their stability. Thus, after an analysis of the possible equilibrium structure of the beams, the stability problem becomes primary.

A kinetic approach to the problem of stability of pinch systems was advanced in the work by Buneman. However, this approach is generally not realizable in principle because of mathematical complications, and because it is impossible to take into account the total multitude of phenomena occurring in the plasma of a high-current channel.

A Nontraditional Approach

In addition to reviewing the standard concepts, Meierovich outlines (Korop et al. 1979) a nontraditional approach to the theory of the micropinch, based on an analysis of equilibrium of a plasma in the magnetic field produced by the current. The results show that conditions can be created in the course of the micropinch such that the magnetic forces caused by the current compress the hot plasma to the point of electron degeneracy; that is, to a condensed state. At maximum compression, the micropinch is similar to a Thomas-Fermi "linear atom,"

consisting of ions that are at rest on the whole and drifting electrons that carry the current. This state of matter, which has never arisen before, would seem to be a unique example of a macroscopic quantum object at high temperatures. The emission observed experimentally can be explained in a natural way as the collisionless emission resulting from electron transitions between quantum levels in the course of the filling of the states of the linear atom and the subsequent radiative cooling of this linear atom.

Pinch Theory Needed

An accurate quantitative description of the initial stage of the rapid contraction of the micropinch requires a theory for the evolution of the plasma in the course of a pinch—a theory that is not available. The question becomes even more complicated when one takes into account the effect on the contraction of the synchrotron radiation of the electrons in the magnetic field produced by the strong current. To a large extent, the difficulties stem from the fact that the micropinch is optically dense for the synchrotron radiation of the plasma, but at the same time (during the contraction stage) is a very nonequilibrium formation. Under these conditions, the radiation transport is not simply radiative heat transfer, as it is in the usual physics analysis of stellar atmospheres. Because of the large number of photons (the radiation is trapped) and the nonequilibrium energy distribution of the electrons during the fast contraction stage, the induced synchrotron radiation must be taken into account.

In contrast with atoms, ions are not localized at the center as in a nucleus in the micropinch; their radial profile is also determined from the equilibrium conditions. Generally speaking, the size of the volume occupied by the electrons is of the same order of magnitude as that of the volume occupied by the ions. Furthermore, the electrons are drifting along the discharge channel with respect to the ions. The state of maximum compression can be thought of as a "linear atom" consisting of ions that are at rest on the whole and drifting electrons. Different electrons transverse the micropinch region at different times, while the radial profile of the electron density is approximately a steady-state profile. If the micropinch contracts to the point of electron degeneracy, then the micropinch region would be a laboratory case of condensed matter at high temperatures; that is, matter in a similar state to that of the interior of stars.

Insofar as the fusion problem is concerned, the pinch in a high-current diode attracts interest because of the possibility of heating to fusion temperatures a strongly compressed plasma, whose expansion is prevented by collective interaction forces. The idea of using a self-contracting relativistic beam as a fusion reactor can be credited to Budker. The primary objection to this idea is the pronounced radiative energy loss of the very hot electrons. Since the intensity of the emission by the electrons falls off in the course of the radiative cooling because of Fermi condensation of the electrons, it may be worthwhile to reexamine this objection.

It is natural to attempt to make use of the very nonequilibrium contraction in the initial stage of the pinch to pump high-power sources of induced synchrotron radiation over the spectral range from microwaves to hard X-rays.

Aside from its practical applications, the contraction of a plasma to the point of electron degeneracy in a high-current device is of much physical interest in itself, since this effect makes it possible in principle to produce in the laboratory condensed matter at high temperatures; that is, matter in a similar state to that of the interior of stars.

However, despite the fact that the experimental results on micropinches are consistent with, and in fact find a natural explanation in, the theory of the equilibrium and collisionless emission of a plasma heated to the point of electron degeneracy, there is still not enough evidence to prove definitely that linear atoms are present in a micropinch. Direct experiments are required to detect the strong electromagnetic fields and the high densities of matter in regions with dimensions measured in angstroms.

The initial thinking of Meierovich can be seen in his 1976 work, and more recent developments in his analysis can be found in his 1983 and 1984 papers. He notes in the 1984 paper that it cannot be excluded that for some reasons the self-compression of matter does not lead to the degeneracy of electrons in the presently available devices. In this regard, Meierovich takes special note of the possibilities of filamentation and the experimental and theoretical work of Winston Bostick and Vittorio Nardi et al. (1980 and 1974).

References

Bostick, W.H., V. Nardi, and N. Prior, 1972. *J. Plasma Phys.* **8:** 7.

Korop, E.D., B.E. Meierovich, Yu.V. Sidel'nikov, and S. Sukhorukov. 1979. "Micropinch in a High-Current Diode." *Sov. Phys. Usp.* **22(9):** 727-741 (Sept.).

Meierovich, B.E. 1976. "Collisionless Emission of Radiation by an Inhomogeneous Plasma." *Sov. Phys. JETP* **44:** 546-553 (Sept.).

———. 1981. "Hydrodynamics of Plasma in a Dense Pinch." *Physica* **105A:** 313-329.

———. 1983. "Oscillations and Analysis of Stability for Pinch Systems." *J. Plasma Physics* **29:** 361-381 (part 3).

———. 1984. "Electromagnetic Collapse: Problems of Stability, Emission of Radiation, and Evolution of a Dense Pinch." *Physics Reports* **104:** 259-347.

Nardi, V. 1974. *Proc. Int. Conf. Asti-Torino (Italy)* (Nov. 5-6).

Nardi, V. et al. 1980. *Phys. Rev.* **A22:** 2211

Winterberg, F. 1979. "Radiative Collapse of a Relativistic Electron-Positron Plasma to Ultrahigh Densities." *Physical Review A* **19:** 1356-1362 (March).

Overview on Aging of Tissue

by John Grauerholz, M.D.

Theories of aging fall into two general categories: one postulating an accumulation of "wear-and-tear" changes leading to eventual loss of function, and the other postulating some sort of program or "clock" that necessitates the ultimate demise of an organism. The locus of these changes can be the molecular, cellular, tissue, organ, or systemic level. The argument then turns on which, if any, are the primary (etiologic) changes and which the secondary (pathogenetic) consequences. Most of these arguments are posited in a context that attempts to apply the Second Law of Thermodynamics to living processes. The dominant paradigms are those of Darwinian selection or systems analysis applied to molecular biology.

This article provides an overview of existing research activities and the leading hypotheses, summarizing relevant articles as they apply at the previously defined levels of biological organization, but without detailed critique of any particular theory. The limitations of the present approaches and the most promising areas are discussed in the summary section.

Molecular Level

At the level of macromolecules, functional impairment can result from insufficient production, production of impaired molecules, or increased destruction of the species in question. Insufficient production and production of impaired molecules are usually related to problems with DNA transcription to RNA or RNA translation to protein.

The following summary of the article by D. Gershon, "Character and Possible Effects of Age-Associated Alterations in Enzymes and Proteins," illustrates the production of impaired macromolecules:

> Most enzymes studied show accumulation of modified inactive or partially active molecules as a function of age. These differences occur only in heat stability and specific catalytic activity per unit, and do not affect affinity for substrate, affinity for specific inhibitors, electrophoretic mobility, molecular weight, or antigenic identity. The preservation of the majority of the characteristics rules out major structural alterations, such as amino acid substitutions.
>
> Oxidation of the SH group and methionine does not involve change in the electrical charge of proteins, and oxidation of methionine to methionine sulfoxide occurs in human lens protein during cataract formation. If this occurred at the active site of an enzyme it could affect enzyme function without significantly altering substrate binding or overall configuration. An enzyme that reduces methionine sulfoxide to methionine is present in liver cells and declines with age, and may thus provide less protection to proteins in aging cells.
>
> Decrease in specific activity per unit of enzyme may range from 30 to 70 percent in aging cells. This can lead to both decreased synthesis of new protein and impairment of the ability to degrade and recycle old protein, with consequences for the following cellular functions:
>
> 1. Supply of amino acids during starvation.
> 2. Contribution to the control levels of inducible and constitutive enzymes.
> 3. Disposal of altered proteins by discriminately rapid hydrolysis.

Although the foregoing describes an age-associated molecular change that leads to diminishing function over time, it does not postulate a formal "clock." The following summary of part of an article, "Molecular Clocks, Molecular Profiles and Optimum Diets: Three Approaches to the Problem of Aging," by Arthur B. Robinson (1979), illustrates a molecular clock theory.

> It has been hypothesized that the deamidation of glutamyl and aparaginyl residues serves as a molecular clock for many processes, including protein turnover, development and aging. When the *in vivo* deamidation of cytochrome *c* was proved, the author became curious about glutaminyl and asparaginyl, two residues which are inherently unstable in physiologic solvents.
>
> It was hypothesized that their instability was their principal function, enabling deamidation to function as a biological clock, providing a means for the predetermined alteration of peptide and protein stucture at specific intervals after synthesis.
>
> Development of organisms requires molecular clocks so that the development process occurs with correct timing and duration. These processes may be timed by deamidation.
>
> Aging is, in some respects, analogous to protein turnover and if intrinsic life span is actively planned through evolution or other means, deamidation is a likely candidate for the timing mechanism.
>
> The principal evidence about deamidation and aging relates to *in vivo* accumulation of various deamidated proteins with age.
>
> Deamidation is under simple genetic control, is adjustable to most biologically useful time intervals, and can easily implement changes in biological processes through changes in peptide and protein charge and structure. Amides cause changes of most proteins *in vivo*, and if these changes were not useful, they would have been evolutionarily eliminated.

Another cause of enzyme dysfunction is lack of certain trace elements such as zinc, copper, manganese, magnesium, and selenium, which form either tightly bound

complexes, called metalloenzymes, or more loosely bound metal-enzyme complexes. Interestingly, many of these enzyme systems are important in immunologic function.

Cellular Level

The Nucleus

Most etiologic theories ultimately base themselves on random or programmed alterations in the genetic program contained in deoxyribonucleic acid (DNA). The extremes are represented by postulating a totally random accumulation of errors in the form of point mutations, to the concept of a totally programmed reading out of genetic information related to development, maturation, aging, and ultimate life span. In the middle of these extremes is the theory that there is accumulation with age of chromosomal mutations whose lost functions are replaced by redundant (reserve) sequences until the reserves are depleted and senescence ensues.

Studies on fibroblasts by Hayflick (1977) indicate that normal cells in culture undergo a finite number of cell divisions and then stop (the "Hayflick limit"). If old nuclei are placed in young cytoplasm, the number of remaining divisions appears to be influenced by the nucleus and not the cytoplasm. These studies are taken to indicate that there is a "clock" in the nucleus that regulates life span. Recent experiments have indicated that this limit can be exceeded by adding certain factors to the medium. Some researchers, such as Robin Holliday of Britain, contend that there is a population of potentially immortal cells that are simply diluted out by standard culture conditions such that the remaining cells are so-called committed cells with a finite life span.

The finite-multiplication characteristic of normal cells in culture does not apply to transformed (malignant) cells, which will divide infinitely as long as they are fed. In the process of transformation, whatever factor is responsible for stopping replication in normal cells is lost. When a normal old (nondividing) cell is fused with a transformed cell, the nucleus of the old cell will synthesize new DNA. This indicates that the DNA of the old cell may not be irreversibly altered by age.

Hart and Setlow (1974) studied the ability of fibroblasts from various species (shrew, mouse, rat, hamster, cow, elephant, man) to perform unscheduled DNA synthesis (a measure of excision repair of DNA) after ultraviolet injury and found that the rate and extent of repair correlated with species life expectancy. Other studies have indicated increased bonding of repressor proteins to the DNA molecule with age, associated with disulfide bonding in the DNA-associated protein. Use of 2-mercaptoethanol, which breaks these bonds, has resulted in rejuvenation of immune responses in aged mice.

One of the most interesting areas of DNA influence on life span is the major histocompatability complex (MHC), which in humans corresponds to the HLA locus on chromosome 6. This cluster of genes not only determines immune response but also synthesis of enzymes that break down free radicals and synthesis of cyclic nucleotides that function as "second messengers" in hormone response. Studies of inbred mice, which differed only at this locus, showed marked differences in life span in these otherwise genetically identical animals. It would be extremely interesting to study the geometry of this locus.

Cytoplasm

In the cytoplasm proper the whole question of structured water in relation to cellular work needs to be looked at. It is possible that the enzyme functional alterations described above relate to disordered cytoplasmic structure resulting from ionic imbalances.

Free radical damage to proteins and lipids has been postulated as a mechanism for wear-and-tear aging. The golden-yellow pigment lipofuschin, which accumulates in certain aging cells, is a waste product of membrane lipid peroxidation by free radicals. Dr. Denham Harman has shown up to 50 percent increase in average life spans of some animals by supplementing their diets with free-radical scavengers such as BHT (bis-hydroxytoluene). Superoxide dismutase, one of the naturally occurring antioxidants, is among the products of the MHC locus.

Another area of interest is the cell membrane itself, where there is evidence that membrane receptors for various hormones decline with age. Conversely, there is evidence that mental stimulation actually increases the number of dendrites, and hence synaptic connections, per cell in the brain.

Tissue Level

The major theory at the tissue level is cogently stated in the following summary of an article entitled "The Role of Limited Cell Replicative Capacity in Pathological Age Change: A Review":

> Physiological functions are carried out by differentiated cells, with finite life spans, which age and need to be replaced. In young individuals, tissue functions are sustained at optimal levels because cellular dysfunction and cell loss are balanced by the emergence of newly differentiated cells as stem cells and their partially differentiated descendants replicate. However, with the passage of time the mitotic rates of these cells diminish. Eventually, replications occur too infrequently to offset the loss. It is at this point that the tissue begins to show structural changes and declining function which as they become pervasive, are identified as 'aging.'
>
> In this paper the theory is set forth that: (1) Diminishing mitotic activity in older tissues results from limited stem-cell replicative capacity. (2) All stem cells, regardless of tissue, exhibit similar replicative patterns over time, progressing from the actively proliferating to the nonproliferating state. However, stem cells in different kinds of tissue have different

rates of replicative decline, with the result that some tissues show age earlier than others. (3) The combination of two cellular properties—differentiated cell aging and limited cell replicative capacity—is sufficient to establish the framework in which other pathological changes characteristic of aged people and animals take place.

In the interstitium between cells there is increased cross-linking of collagen and decreased solubility of collagen with increasing age. This was the basis for one of the earliest aging theories, the cross-linking theory, which postulated declining function with the increase of extracellular material. While obviously trivial as an etiologic theory, the phenomenon has become widely utilized as a biomarker of the aging process.

Organ Level

Changes in organs generally correlate to what one might expect from the tissue changes cited above, that is, decrease in functionally active cells, accumulation of intracellular garbage such as lipofuschin, and increase in interstitial fibrous tissue and collagen. One organ that undergoes striking diminution with age is the thymus gland.

Systemic Level

Systemic changes in aging occur through mediation of the nervous, endocrine, and immune systems. Since certain cells (such as muscle and nerve cells) never divide after reaching the adult number of cells, and since many other cells never reach their potential replicative limit, some "clock" theorists have postulated that the "clock" is located in one of the above systems. One of these theories postulates that the pituitary gland secretes a so-called death hormone that causes a generalized blocking of cell receptivity to the action of thyroid hormone, with resulting decline in cellular energy metabolism. There is work under way to isolate this "death hormone," with an eye to producing an inhibitor.

Two manipulations consistently prolong total life span, as opposed to increasing average life expectancy, in all animal systems thus far tested. These are severe caloric undernutrition without malnutrition, and lowering core body temperature. The first is most effective in the first half of life and the second, which is only practical in cold-blooded species at present, in the second half of life. The accumulated evidence seems to indicate that caloric undernutrition would work in humans; however, in order to maintain the quality of the diet it would have to be supplemented, since normal food would not provide complete nutrient requirements within the caloric constraints.

Much more interesting are the implications of studies done on the function of certain systems, especially the immune system, in these animals. Both of these manipulations significantly modify age-associated changes in immune function, which account for many if not most of the changes considered to be characteristic of the aging process.

Immunologic changes in aging are manifest in two ways: One is a decreasing ability to respond to foreign antigens, including transformed (malignant) cells—which have become essentially *foreign* to the body in which they arise. The second is an increase in antibodies produced against the self (autoantibodies). Thus total antibody production is relatively unimpaired in older animals, but a significant portion of the antibodies produced are ineffective or harmful.

The following quote from an article on "Immunoregulatory Systems and Aging," by Walford (1983), summarizes the relevance of age-related immune decline:

> One possible experimental model for aging is the chronic graft-versus-host reaction (Walford 1962). When immunocompetent cells are introduced into a tolerant host, a graft-versus-host reaction ensues in which the introduced cells react against the recipient animal. This reaction, which is also obviously a model for a form of autoimmune state, is characterized by lymphoid depletion and hypoplasia, fibrosis, eosinophilic deposits, an increased number of plasma cells in lymphoid organs, hyaline changes in renal glomeruli, renal atrophy, immune complex formation, weight loss, arteriosclerosis, changes in skin and hair, thymic atrophy, amyloidosis, decreased responsiveness to isoantigenic stimuli, positive tests for autoantibodies, a decrease in the ratio of soluble to insoluble collagen (Liu and Walford 1970), disturbances in T and B cell collaboration, increased numbers of suppressor cells, and activation of latent viruses (Grebe and Streilein 1976). All these phenomena are also found in normal aging. The parallelism can hardly be regarded as other than striking.

The locus of these changes is primarily in the T-cell (thymus-dependent) system, which is responsible for cell-mediated immunity and also plays a key role in activating the B-cell system, which is responsible for antibody production. The loss of T-cell function follows involution of the thymus gland and can be reconstituted by administration of thymus hormones, such as thymosin.

The function of the immune system is also influenced by the endocrine and nervous systems. There is neuroanatomic and pharmacologic evidence of neural innervation of the thymus. The presence of cholinergic (neurotransmitter) receptors on the surface of thymosin-producing epithelial cells, as well as the presence of cholinergic and B-adrenergic receptors on T-lymphocytes, indicates these cells can be influenced by neurotransmitters. Profound alteration of thymic immunity can be produced by drugs that deplete synaptic catecholamines.

Thymosin a is able to accumulate in discrete subcortical

brain regions, and this may indicate the presence of receptors for this hormone on brain cells, as well as existence of a feedback mechanism. In addition, certain pituitary hormones, such as growth hormone, can apparently influence thymosin production. Pituitary hormone release is triggered by releasing factors secreted in the hypothalamus.

Another finding in calorically restricted mice is elevation of the naturally occurring hormone DHEA (dehydroepiandrosterone), which inhibits certain naturally occurring enzymes that activate carcinogens within the body. There is an inverse relationship between life expectancy and the ability to activate these enzymes across species. There is evidence that DHEA is important in maintaining the structural integrity of DNA. DHEA reaches peak concentrations a few years after puberty and declines to low levels with advancing age. It is possible that administration of DHEA would produce the effects of caloric restriction without the caloric restriction.

There is evidence that immune function can be stimulated by the administration of immunomodifiers, such as interleukin-2. Interleukin-2 is produced by white blood cells and influences T-cell function. In recent trials on cancer patients there was evidence of influence on certain aging parameters, and this will be actively studied in subsequent trials. A technology for producing human interleukin-2 from white cells collected from blood banks has already been patented.

In terms of central nervous system function, there is evidence that neurotransmitter secretion is not under closed-feedback loop control and that large doses of certain amino acids can modify brain function by altering neurotransmitter levels. There is also evidence that psychological states can alter immune responsiveness and other physiological parameters. It is possible to alter, or abolish, certain "physiological" responses, including immune responses, by hypnosis and other psychological manipulations. In this context, the relative retardation of aging in intellectually active people and the increased death rate among those who "retire" or cease to be involved in human activity, may have its physical basis in neuroendocrine changes relating to brain activity, or lack thereof.

Summary

A great deal of data exist that describe aging changes at the molecular, cellular, tissue, organ, organ system, and organismic level. The most coherent of the current theories indicate conformational changes in the cellular DNA and its associated proteins, affecting primarily the neuroendocrine and immune systems, which are responsible in one way or another for communication and learning within the organism. Disordered function of these systems then produces the spectrum of physical changes subsumed under the heading of aging. The immune system changes referenced above are among the more interesting from both a theoretical and a therapeutic standpoint. The antibody alterations described above might be profitably looked at as a loss of resolving power on the part of the immune system as the organism ages.

A number of modalities, especially thymic hormones and other modifiers of the immune system, have demonstrable effects on retarding the aging process and the potential to increase productive life span. Retarding the aging process per se would be the most effective attack on diseases of aging, most of which are a consequence of age-associated immune dysfunction. The central nervous system influence on immune and endocrine function is one area that has great promise in understanding life as a negatoentropic process, since mental capacity is capable of growth far beyond physical maturity as such, and is in fact the species-characteristic of man.

References

Cheney, K.E., et al. 1980. "Survival and Disease Patterns in C57BL/6J Mice Subjected to Undernutrition." *Exp. Geront.* **15:** 237-258.

Cherkin, A., et al., Eds. 1979. *Aging.* Vol. 8: *Physiology and Cell Biology of Aging* (New York: Raven Press).

Gershwin, M.E., et al. 1983. "Trace Metals, Aging and Immunity." *J. Am. Geriat. Soc.* **31(6):** 374-8 (June).

Goldstein, A., et al. 1981. *Current Status of Thymosin and Other Hormones of the Thymus Gland, Recent Progress in Hormone Research,* Vol. 37 (New York: Academic Press).

Hart, R.W., and R.B. Setlow. 1974. "Correlation Between Deoxyribonucleic Acid Excision Repair and Life Span in a Number of Mammalian Species." *Proc. Nat. Acad. Sci., USA* **71**(6): 2169-2173 (June).

Hayflick, L. 1977. "The Cellular Basis for Biological Aging." *Handbook of the Biology of Aging.* Ed. C.E. Finch and L. Hayflick (New York: Van Nostrand Reinhold), p. 159.

Holliday, R. 1981. "Cellular Aging: Further Evidence for the Commitment Theory." *Science* **213:** 1505-1508 (Sept.).

Holliday, R., et al. 1977. "Testing the Commitment Theory of Cellular Aging." *Science* **198:** 366-372 (Oct.).

Makinodan, T., and E. Yunis, Eds. 1977. *Comprehensive Immunology:* Vol 1, *Immunology and Aging* (New York: Plenum).

Robinson, A.B. 1979. "Molecular Clocks, Molecular Profiles, and Optimum Diets; Three Approaches to the Problem of Aging, Mechanisms of Aging and Development." **9**(1979): 225-236.

Rosenfeld, Albert. 1976. *Prolongevity* (New York: Knopf).

Walford, Roy L. 1983. *Maximum Life Span* (New York: Norton).

Walton, J. 1982. "The Role of Limited Cell Replicative Capacity in Pathological Age Change. A Review." *Mech. Aging and Devel.* **19**(1982): 217-244.

Weindruch, R., et al. 1983. "Influence of Dietary Restriction on Natural Killer Cell Activity in Mice." *J. Immunology* **130**(2): 993-6 (Feb. 1983).

Weksler, M. 1983. "Senescence of the Immune System." *Medical Clinics of North America* **67**(2) (March).

Environmental Effects on Flax Genetics Updated

by Ned Rosinsky, M.D.

Flax plants respond to certain environmental conditions with specific increases or decreases in plant size and weight that are then inheritable over many generations of offspring. This finding, stubbornly repeated over the past 25 years in a number of laboratories, flies in the face of the neo-Darwinian notion that variations are produced by random genetic changes. This work was recently updated using the tools of gene cloning to identify more precisely the genetic changes involved in the flax findings, at a conference on "Implications of Molecular Genetics in Plant Breeding" held at the University of Minnesota at St. Paul, June 4-6, 1984.* Although many genes are involved in the transformations of the plants, the major alterations involve repetitive sequences, genes that are present in multiple copies, and particularly the genes that code for ribosomal-RNA, the RNA that forms the ribosome organelles in the cell that are involved in the production of proteins.

The classic experiments in this field were first published in 1958 by Alan Durrant, working at the University College in Aberystwyth, Wales. He grew flax plants (Stormont Cirrus variety, *Linum usitatissimum*) under generally very favorable conditions for the first five weeks after being sown, which included a warm greenhouse with fertile soil and large (7-inch) pots. He found that the flax plants were responsive to certain other conditions that he added at the time of sowing and again at age five weeks when the plants were replanted in the field. The added conditions were various combinations of (1) a 1.5 percent solution of ammonium sulfate added to compost to saturation at the time of sowing, with subsequent watering and free drainage; (2) phosphate in the form of a 1.5 percent solution of triple superphosphate, which had been left for 24 hours and the sediment removed; (3) potassium as a 1.5 percent solution of potassium chloride; and (4) calcium as a 1 percent by weight addition of calcium hydrate to the soil.

Durrant labeled these four conditions *n*, *p*, *k*, and *g*, respectively, and tried every possible combination on the plants. He found that the largest plants were produced by adding *n*, *p*, *k*, and *g* (all four conditions); *p* and *k* (phosphate and potassium only); or *n* (ammonium sulfate only). The smallest ones were produced by adding *n* and *k* (ammonium sulfate and potassium) or *p* (phosphate), but in this case the phosphate had to be combined with acid soil. In all subsequent work he confined his conditions to either adding ammonium sulfate to get large plants, or phosphate with acid soil to get small plants. The scale of the changes was a twofold increase in weight in the large plants at maturity and a threefold decrease in weight in the small plants, creating overall a sixfold difference between the large and small plants.

Studies of the genetics of the large and small plants showed an increase in total DNA per cell in the large plants and a decrease in the small plants, with the total spread of values being 16 percent of the normal DNA content. One of the genes found to be affected codes for ribosomal-RNA, and it normally exists in multiple copies: there are approximately 2,500 copies of this one gene in a normal plant. The small plant has only 1,600 copies. However, the large plant has no increase in the number of copies, having the same 2,500 copies as the normal plant. Other differences that are inducible include height of the plant, enzymes that are involved in the production of plant growth hormones, and characteristics like hair growth on capsules. These changes in six major categories (weight, height, nuclear DNA content, r-DNA content, enzymes, and hair growth) do not always correlate: Depending on the inducing conditions, some of the heavy plants are tall, some intermediate in height; some of the small plants are hairy, some hairless, and so on.

Varying the conditions includes other interesting aspects. For example, (1) the small variety can be induced by growing the seeds in low temperatures for the first five weeks; (2) if the seeds are grown in 5-inch pots instead of 7-inch pots for the first five weeks before transplanting to the field (and the standard *n* or *p* is given to induce largeness or smallness), the nuclear DNA will gradually revert to the original amount within three generations, but the induced tallness or shortness will remain; and (3) after inducing smallness or largeness, if the subsequent generations are grown completely out of doors from the time of sowing (that is, the five-week greenhouse period is eliminated), then the size change will revert to the original size within three generations.

Some Hypotheses

In a recent review of the literature, C.A. Cullis at the John Innes Institute in Norwich, U.K. (1977), attempts to explain these results by postulating that in cell division in these plants certain genes are routinely excised from the major portion of the genome, replicate separately, and are then reintegrated into the genome. He also suggests that while these genes are excised and self-replicating, they can have that process increased or decreased by environmental conditions, resulting in a change in the number of copies of the gene being produced before it is reintegrated back into the rest of the genome.

Cullis is now investigating this hypothesis by attempting to clone the genes that are known to vary in these plants in order to more closely examine their properties. At the above-mentioned conference he reported that the genes for the 5S portion of the ribosome as well as several

*For information on the conference, contact R.L. Phillips, University of Minnesota at St. Paul.

other repetitive sequences have been cloned. Some of these sequences vary from one induced type to another, while others are invariant. In a parallel investigation, if the sequences are examined in the same plant in different growth phases—such as the adult plant, the plant tissue grown in culture plate conditions and the regenerated plant from such a culture—there are again variable and invariant repetitive sequences. Cullis found that the sequences that varied when the plant was transformed by environmental conditions were the same as those varying in the culture plate and regeneration conditions. He therefore postulated that the flax genome consists of two components, a variable portion and an invariant portion. Since the 15 pairs of flax chromosomes do not change visibly in size or shape with the 16 percent difference between the large and small induced plants, we can conclude that the changes must be spread widely through the genome on many of the chromosomes. Thus, the variable condition is a widespread aspect of chromosome organization in these plants.

Several other presentations at the conference related closely to the flax findings. Jack Van't Hof, at the Biology Department of Brookhaven National Laboratory in Upton, N.Y., described extrachromosomal DNA that contains ribosomal genes; this DNA is found in higher plants in root tip cells that are differentiating. Kenneth D. Tartof, at the Institute for Cancer Research in Philadelphia, has found that the r-DNA of fruit flies exists in multiple copies and that certain types of flies have a decreased or increased number of such copies. He has elaborated on several factors which seem to determine the number of copies present. Stephen M. Beverley, at the Department of Pharmacology at Harvard Medical School in Boston, has found repetitive DNA coding for drug resistance in the human parasite Leishmania. This gene exists as a closed loop outside the chromosome; with selection the number of copies can be increased, stabilized, and then incorporated within the chromosome. Numerous other papers demonstrated many new findings by plant breeders that are forcing the molecular biologists to radically rethink their notions of how the genome operates and changes with evolution.

References

Cullis, C.A. 1977. "Molecular Aspects of the Environmental Induction of Heritable Changes in Flax." *Heridity* **38:** 129-154.

————. 1973. "DNA Differences Between Flax Genotrophs." *Nature* **243:** 515-516.

Growth of Neurons in Adult Brains Of Birds Demonstrated

Studies on brains of canaries, performed by Dr. Fernando Nottebohm and collaborators at Rockefeller University, have upset the neurobiology dogma that no new neurons are formed after infancy. The experiments, performed on adult canaries, indicate that there is extensive birth and death of neurons in the forebrain area, which controls complex learned behavior. The findings arose in the course of studies on birdsong beginning approximately 15 years ago.

The neural pathways involved in birdsong are anatomically discrete, localized in an area in the bird forebrain called the nucleus hyperstriatum ventralis, par caudalis, or HVc, which responds to sound. Neurons from the HVc project to the robust nucleus of the archistriatum, or RA, which in turn projects to the hypoglossal motor nerves that activate the voice. At one month of age, when song learning begins, the HVc is only one-eighth of its adult volume, and song learning occurs with the growth of the system.

Song learning is hormonally controlled by testosterone levels, which are high in the spring when males sing vigorously and which decline in the fall when the birds are essentially mute. The volume of the HVc in the fall shrinks to half the springtime volume. When female canaries are given testosterone and induced to sing, both the HVc and the RA double in volume and the number of dendrites also doubles.

To test the possibility that new neurons might be formed when birds learn songs, Nottebohm treated female canaries with testosterone and then injected them with tritiated thymidine, which labels the nuclei of dividing cells. When the birds were killed and the brains examined, the label was found in the nuclei of cells that looked like neurons. Subsequent electrophysiolgical studies confirmed the cells to be neurons that fired in response to sound. These findings were present in females treated with testosterone as well as those treated with cholesterol, a hormonally neutral treatment.

The new neurons originate in an area of the forebrain adjacent to the lateral ventricle, known as the ventricular zone. From this area the new neurons migrate up to 1 mm over a period of two weeks to reach the HVc.

Subsequent studies indicate the formation of new neurons in other areas of the forebrain as well as the cerebellum, midbrain, and medulla. This occurs in the context of evidence that these cells replace old ones that die off. The implications of growth of new neurons in response to learning are to say the least startling and may have great relevance to the problems of brain injury and aging.

—John Grauerholz, M.D.

References

Paton, J., and F. Nottebohm. 1984. *Science* **225:** 1046.

Kolata, Gina. 1984. *Science* **224:** 1325.

Coherent Effects of DNA Explored

by Ned Rosinsky, M.D.

Most biologists think of DNA as a passive information tape that codes for protein structure and is based on the Watson-Crick double helix model, which is derived mainly from X-ray crystallography data. The dynamic, time-dependent aspect of DNA functioning is largely ignored, or at least assumed to follow a simple extrapolation of the dynamics of small molecules. However, such processes as the transcription of RNA from DNA imply that some kind of coherent process is involved in DNA functioning. Over the past decade a group of biophysicists and biochemists has been delving into the area of coherent effects in DNA using a variety of contexts; this group is putting together a picture that is in stark contrast to the passive information-tape idea.

Earl Prohofsky, a leader in the field working at Purdue University, points out that several aspects of DNA imply long-range interactions and coherence in the molecule. First, the speed of sound in parallel-oriented DNA films, in the direction of the longitudinal axis of the DNA, is from 1,800 to 3,000 m/sec, much faster than the speed of sound in the surrounding water and also much faster than the speed could be if the main interaction were covalent bonds in the phosphate-oxygen or oxygen-carbon areas of the chain backbones (Figure 1).

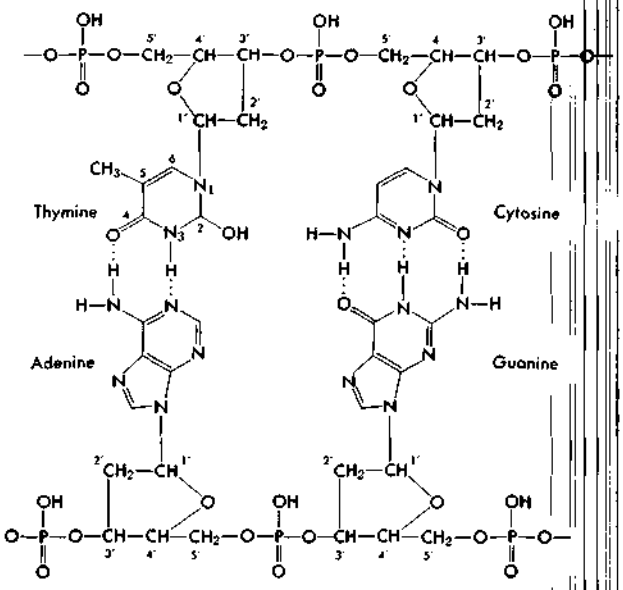

Figure 1. Detail of DNA Segment. In this diagrammatic representation of a segment of DNA, the backbone of each of the two strands can be seen to consist of phosphate groups alternating with sugar groups. Backbone sequence in detail consists of phosphorous joined to oxygen, joined to carbon in the sugar. Another carbon of the sugar then joins to an oxygen that joins to the next phosphorous, continuing the sequence. If we assume that this chain determines the transmission of acoustic mode waves, the main interaction would have to be in the oscillation of the highly polarized phosphorous-oxygen and the oxygen-carbon bonds. However, the strength of these bonds is far too small to support the stiffness needed to generate the known velocity of waves traveling along the DNA molecule.

This result indicates interactions among sequential base pairs in the core of the double helix as the determining action for acoustic mode transmission.

Furthermore, this sound speed is similar to that of crystallized methyl-thiamine, a substance similar to the thiamine base in the core of the DNA. Thus Prohofsky reasons that the stiffness responsible for the rapid speed of sound in DNA is predominantly the result of base pair-to-pair interaction; these are the bases usually represented as steps in a DNA ladder. Note here that Prohofsky is dealing with supercoiled or A-form DNA, which is the state of DNA generally when it is not transcribing RNA or replicating itself (Figure 2a). The form of DNA when transcribing or replicating, termed B-form, is shown in Figure 2b.

A second qualitative indication of the state of DNA is Brillouin scattering data, in which photons scattered from DNA pick up or release energy. The pattern of such scattering again suggests long-range coherence in DNA, in that an extended area of the molecule apparently absorbs many photons and then reemits energy of higher photon quantum size. However, the first datum needed here is the lower limit of size of DNA that can support such an effect, and that experiment has not been done yet.

However, Prohofsky's main work has been to go beyond these qualitative considerations and calculate in detail the predicted resonance frequencies for A and B DNA using the main oscillation modes expected of a double helix and assuming long-range phase coherence (Figure 3). He and his group have been extremely successful in these predictions, in the infrared region of the spectrum (1–5-μm wavelength area) where most resonances of this type would be expected to occur. Using his model he has predicted the major curve peaks and shapes for the more than 100 absorption peaks in the relevant frequency range, to within 10 to 15 percent accuracy for each peak.

Prohofsky has outlined the possible functional significance of these types of dynamics. He believes that these oscillation modes are involved in the major transformations of DNA, such as from A to B and to other forms as well; in the unwinding and separation of the DNA strands in transcription and replication; and in the DNA-enzyme interactions involved in other aspects of DNA function. This last category includes the presumed activity that regulates the timing for when a particular gene begins the process of transcription; this is usually termed turning on (or off) the genome. Prohofsky hypothesizes that DNA may be energized for such transformations by receiving energy of a particular frequency, possibly from

ATP via an enzyme; the quantum of energy moves along the DNA molecule until it reaches an area of specific resonance, and then it performs work in a directed geometrical fashion.

Prohofsky acknowledges that his model of DNA is oversimplified and he has begun enlarging it to include water hydration effects. He finds that the addition of water, as predicted, damps out certain modes and not others. Specifically, the water damps out the higher-frequency modes, and not the lower. The modes are divided into optic and acoustic, as in Figure 3, and it is the optic modes that are damped out by water.

Prohofsky hopes that the idea of coherent resonance and the geometrical character implied in that idea can be shown to underlie the activity of much more than DNA dynamics, extending more generally to enzyme activity and even to the structure of cell water, which at this point is a wide open question.

Coherent Action and Biological Work

The key idea in this work is that coherent action underlies the ability for qualitative transformations, or bio-

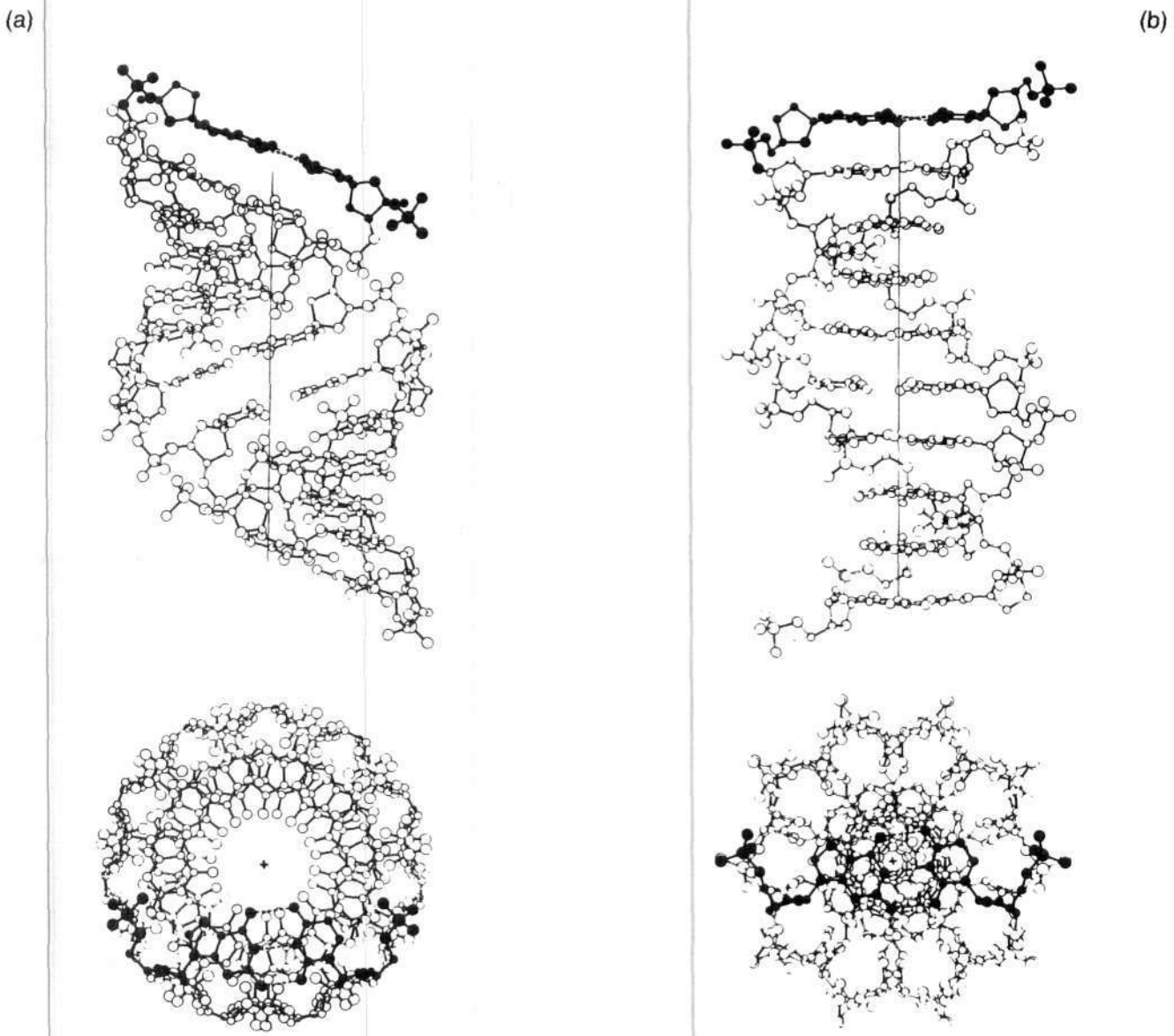

Figure 2. A-form and B-form DNA. Super-coiled or A-form DNA is shown in (a). This is the usual form of DNA when it is not transcribing RNA or replicating itself. When it is transcribing or replicating, it is generally in the more familiar B-form, shown in (b).
Source: E. Morton Bradbury, Norman Maclean, and Harry R. Matthews, *DNA, Chromatin and Chromosomes* (New York: John Wiley, 1981), pp. 6-7.

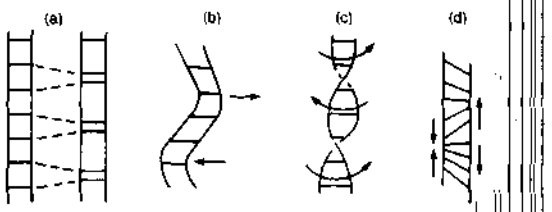

Figure 3. The oscillation modes of a double helix. The DNA double helix is treated as a flexible ladder or "slinky" with recurring distortions possible. Several modes are shown: a longitudinal mode (a), a transverse mode (b), a tortional mode (c), and an optical mode (d). The first three modes can become translations or rotations of the entire molecule if the wavelength is infinite; these modes are therefore termed "acoustic." Because it does not result in a simple translation or rotation even if the wavelength is infinite, (d) is termed an "optical" mode. This established terminology should not be taken to imply the involvement of a distinction between what is usually thought of as sound and light. All the modes are electromagnetic.

Source: E. Prohofsky, *Biopolymers*, Vol. 20 (New York: John Wiley, 1981), p. 833.

logical work. Prohofsky has uncovered an aspect of this by using models applying the lowest order of coherent effects, an extrapolation of a "slinky" model in which the range of interaction of any particular turn is extended to cover the 20 or so neighboring turns. It would be interesting to see Prohofsky push this idea forward by taking a more radical view of biological work as self-similar qualitative transformations, deriving the necessary invariants for such processes, and then mapping the DNA data to expand on the empirical aspects of such invariants.

For example, it may be helpful to consider the various oscillation modes exemplified by Figure 3 to be modes of action on an expanding logarithmic spiral, rather than on a cylindrical spiral of constant radius (Figure 4). The expanding shape of separating DNA is directly suggestive of this approach, in which a quantum of energy added to the DNA at a distant point travels unutilized until it reaches the expanding (separating) portion of the DNA. At this position, the resonating frequency of the DNA changes to the quantum in question, so that at that

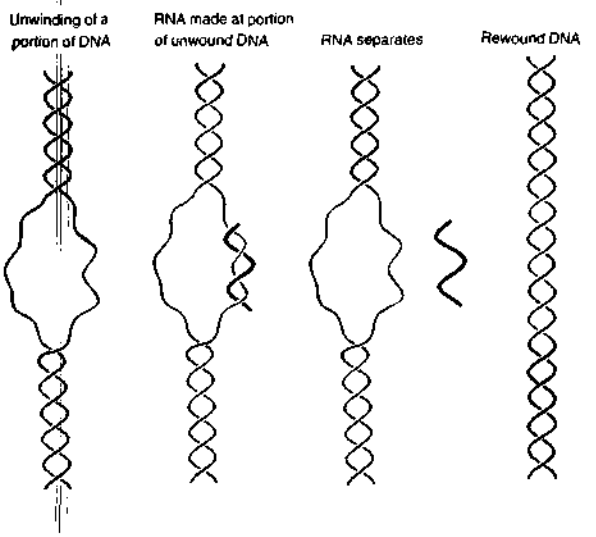

Figure 4. DNA transcribing RNA. In order to produce RNA, a portion of DNA unwinds, the RNA is formed, the RNA separates from the DNA, and the DNA rewinds, as shown here. A more detailed representation of the unwinding process suggests a gradual separation of the double helix, which can be pictured as a conical spiral. The resonant frequency in this conical spiral region should vary at different positions, so that an input of a photon of a specific frequency should be absorbed and act at only a particular location on the cone, possibly to further the unwinding process, RNA transcription, and so on.

point the quantum is used to further the transformation (the separation); that is, at that level of the expanding DNA cone, the size of the singularity relevant for forcing transformations is exactly equal to the quantum in question, so it is utilized. In general, however, we might expect there to be a more complex relationship than this between an underlying spiral work function and the overt appearance of the DNA.

References

Mei, W.N., M. Kohli, E.W. Prohofsky, and L.L. Van Zandt. 1981. "Acoustic Modes and Nonbonded Interactions of the Double Helix." *Biopolymers* **20:** 833-852.

Kohli, M., W.N. Mei, E.W. Prohofsky, and L.L. Van Zandt. 1981. "Calculated Microwave Absorption of Double-Helical B-Conformation Poly(dG)-Poly(dC)." *Biopolymers* **20:** 853-864.

Swicord, M.L., and C.C. Davis. 1982. "Microwave Absorption of DNA Between 8 and 12 GHz." *Biopolymers* **20:** 2453-2460.

Basic Electrodynamics: Riemann and His Italian School Versus Maxwell

by Giuseppe Filipponi

Editor's Note: *English translations of E. Betti's 1868 work "On Electrodynamics" and B. Riemann's 1858 paper "A Contribution to Electrodynamics" follow this report.*

Modern textbooks tell us that James Clerk Maxwell was the scientist in the last century who made the most fundamental discoveries about electromagnetic phenomena. Looking a bit more deeply into the scientific debate over the foundations of electrodynamics, however, this story turns out to be completely false. Not only did Bernhard Riemann and Wilhelm Weber in Göttingen, working in close collaboration with E. Betti and E. Beltrami in Pisa, develop a theory of electrodynamics based on the retarded potential that was much more advanced than that of Maxwell; but Betti and Beltrami conclusively showed that Maxwell's basic assumptions on electricity and magnetism were *wrong!*

Riemann, the most accomplished student of Gauss, Dirichlet, and Weber, spent the last years of his life in Italy in close scientific collaboration with Betti and his students, and Betti reports that Riemann proposed that his group make a concerted attack on the false assumptions underlying Maxwell's electrodynamics.

Maxwell, in turn, in his "Treatise on Electricity and Magnetism" sharply attacked Riemann and Betti's hypothesis on electromagnetic phenomena and said that they prejudiced researchers against his mechanical interpretation of electromagnetism.

Maxwell's approach to and interpretation of electromagnetic phenomena is the same as that of Descartes on the solar system. According to Maxwell, all space is filled with a very dense elastic substance he calls *ether*. In his view, electrical and magnetic phenomena are simply elastic perturbations of this medium; in other words, what we see as electromagnetic phenomena are simply the movements of ether. All of Maxwell's theory is based on this assumption.

Maxwell and the British empiricist school made this same assumption for sound waves, which they described as simple elastic movements of the air molecules.

Betti and Beltrami conclusively demolished this kind of mechanical interpretation. In Beltrami's paper "On the Mechanical Interpretation of Maxwell's Equations," he says:

> As a part of any preconception about a possible correlation between action at a distance and pressures and tensions generated inside an elastic medium by a small deformation of this medium, that is, a small displacement of some of its parts, it is obvious to ask whether deformations really exist that are able to create these tensions? . . . The conclusions I reach are completely negative. In an isotropic medium it is impossible to create deformations able to produce the pressure system defined by Maxwell's formulas.
>
> In order to be more precise, I can say that these kinds of deformations are possible only when the potential function has the simple form obtained when all the electric charges can be considered as collected in a given point; then this function is also linear in respect to the coordinates. But since it is obviously a very simple special case that we rarely find in nature, we can say that given a potential function generally it is not possible to produce a pressure system defined by Maxwell's formulas.

The hypotheses of Betti and Beltrami about electromagnetic phenomena are completely different from Maxwell's mechanical ideas. For them these actions as well as the acoustic waves are not to be simply considered and studied as a movement of air or ether parts. Their primary concern was the way in which this kind of energy is propagated and performs work. In the case of acoustic waves, this action moves the air, not vice versa. So also with electromagnetic phenomena, Betti and Beltrami saw the medium as only a medium of this action, nothing else.

Obviously the way in which they started to study these phenomena was by studying their geometrical and topological configurations. This work was done using the tools already developed by Riemann in his geometry and in the field of harmonic complex functions.

Betti's Hypothesis on Electrical Current

Betti took Riemann's work on electrodynamics and developed it, making a new hypothesis on the geometric behavior of electrical current. According to Betti's hypothesis, the constant current in a linear conductor is not a simple flow of charge but, rather, a periodic polarization of the line elements of the linear conductor. Practically speaking, the electrical current is a wave with a very small period that is always the same for each current and each conductor.

Starting from this hypothesis, Betti first developed all the laws of electrodynamics and electromagnetism and then, as had Riemann, all the electrostatic principles. For Betti and Riemann, fixed electric charges do not exist inside conductors or dielectrics. Conductors and dielectrics are considered as a system of electrical currents organized in a way that accounts for the composition of the internal and external magnetic effects.

Beltrami gave a general theory of the so-called neutral solenoid, a special configuration of solenoidal electrical current that has no magnetic or electric effect outside itself, but that can be at very high energy density.

Interestingly, Betti's model for a macroscopic electrical current is very similar to de Broglie's model of the elec-

tron, in which he incorporated the principles of quantization.

Beltrami's Filaments and Betti's Numbers

The geometrical and topological studies of Betti and Beltrami were so advanced that only in this century, with Winston Bostick's analysis of filament formation inside a plasma, do we have empirical proof of their work. These are the so-called Beltrami filaments. In "Hydrodynamic Considerations," Beltrami demonstrated that the conditions exist by which a new potential function is created inside a fluid moving in a constant flow pattern. This potential determines the formation of stable helical motion inside the fluid, in such a way that every flow line is at the same time the axis of local vortical motion.

Examples of this are in storms or cyclones of the Earth atmosphere as well as the filaments in a plasma. These plasma filaments are generated in pairs rotating in opposite directions, and locally they increase the energy density of the plasma thousands of times. In other words, the system evolves while increasing its local energy density.

Betti tried to confront the same problem from a more general standpoint. Since the harmonic complex functions used by Riemann, Betti, and Beltrami to represent the electromagnetic potential of a system of electrical current are related to the topological characteristics of the system, Betti developed the concept of the Riemannian manifold from a topological standpoint. He defined the various kinds of order and species of topological connections of the manifold according to its dimensions ("Betti's numbers").

For a system of electrical currents characterized by a simply connected topology, the potential function is single valued (*monodroma*), whereas for higher-ordered topologies, the potential function is multivalued (*polidroma*). This means that in the latter case the system formed by the electrical currents and their magnetic and electrical fields can change its organization in a nonlinear way. Betti's topological work aimed at developing a theory of these phenomena. This approach is ostensibly at odds with that of Maxwell, which, as Beltrami showed, works only in the simplest cases. Even if Betti's and Beltrami's work did not produce a comprehensive theory of electromagnetism, which we still lack today, they were headed in the right direction. The superiority of their method in respect to that of Maxwell is proved by the many successful technological applications developed with the help of their ideas.

The reaction of Maxwell to the hypotheses of Riemann and Betti was very polemical. In his "Treatise on Electricity and Magnetism," he says, "Betti and Riemann always speak about propagation of electromagnetic effects but never say anything about the medium in which this propagation occurs." Maxwell then says that in Riemann's work on electrodynamics and also in Betti's work on the same subject, Clausius found a lot of mathematical imperfections. Maxwell said he did not understand why Betti and Riemann refused his mechanical interpretation of electromagnetic phenomena, that the only explanation is that they have some prejudice against him.

Pacinotti's Ring and Ferraris's Electric Engine

The work of Betti and Beltrami had great impact on their successors. During 1850 the Count of Cavour, the founder of the Italian state, gave a speech saying that using electrical and magnetic phenomena the Italian economy would be able to use the weather power of the Alps mountains. In such a way, he said, we can have much more energy for the Italian industry than England has with the coal under its ground.

Pacinotti was a pupil of Betti who at the early age of 17 invented the first efficient electrical engine, based on the "Pacinotti ring." There is a famous anecdote, according to which in 1859 Pacinotti participated in the Battle of Goito, where the Piedmontese troops defeated the Austrian army. It was during the fight that Pacinotti had the idea to improve his engine through a device called a "collector."

A few years later, Galileo Ferraris, a contemporary of Tesla, made the most decisive breakthrough that allowed an electrical engine to operate using alternating currents. It worked by creating a rotating magnetic field by harmonically juxtaposing two alternating magnetic fields, generated by the alternating currents. The movement of the mechanical parts was reduced to a minimum and the engine was extremely efficient. It became known as our modern electric engine.

On Electrodynamics

by Enrico Betti

Editor's Note: This 1868 essay was translated from the Italian by Nora Hamerman. It was published in *Nuovo Cimento*, Serie I, Tomo XXVII, pp. 402-407, in 1868.

I

Gauss, in a letter to Weber published in the fifth volume of his *Collected Works*, wrote in 1845 that in order to deduce the forces to be added to the force which acts between the particles of electricity at rest, when they are in relative motion, it is necessary to assume that the magnetic action is not instantaneous, but that instead it propagates over time in a similar way to what has been discovered for light, and he added that he abandoned this type of research in 1836 without success, but with the hope of succeeding in it at a later date, and with the opinion that it was necessary to form a constructible representation of *how* this propagation occurred. In 1858, Riemann presented at the Academy of Science in Göttingen a paper published post mortem in number six of the *Annals* of Poggendorf of 1867, in which he deduced the potential of two closed constant currents upon each other, admitting that the action of electricity propagates in space with uniform velocity equal to the speed of light, and assuming that the current consists of the motion of the two electricities, positive and negative, that travel at the same time through the wire in opposite directions, and adding that the sums of the products of the positive and negative electricities multiplied by a function of the coordinates of the points in the wire are negligible with respect to the sums of only the positive electricities and only the negative ones multiplied by the same function. This completely ideal concept of electric current is scarcely coherent with what is known about it, and it seems that Riemann was not satisfied with it, since he withdrew the article from the Secretariat of the Academy and abstained from publishing it. Hence it seems to me that it is not without importance to demonstrate one can explain electrodynamic actions by means of their propagation over time, and maintaining that the action of dynamic electricity follows Newton's law as does static electricity, without basing oneself upon that concept, but instead assuming that the current consists in a periodic polarization of the elements in the wire, which is more consistent with all the known facts.

II

The potential of a constant closed current [acting] on another constant closed current, which has been verified by the most accurate experiments, is

$$P = \epsilon\epsilon' \int_s\int_{s'} \frac{\cos(ds, ds')}{r}\, ds\, ds',$$

where s, s' are the intensities of the two currents, r the distance of two elements ds and ds' of the closed curves traveled by the currents; (ds, ds') the angle between these; and the integrals must be extended to all the outlines of these curves.

Now, since (x, y, z) are the coordinates of a point of the curve s, and (x', y', z') those of a point of the curve s', it will be

$$r^2 = (x - x')^2 + (y - y')^2 + (z - z')^2.$$

where

$$\frac{1}{2}\frac{d^2(r^2)}{ds\, ds'} = -\frac{dx}{ds}\frac{dx'}{ds'} - \frac{dy}{ds}\frac{dy'}{ds'} - \frac{dz}{ds}\frac{dz'}{ds'} = -\cos(ds, ds'),$$

and hence

$$P = -\frac{\epsilon\epsilon'}{2}\int_s\int_{s'} \frac{d^2(r^2)}{ds\, ds'}\frac{ds\, ds'}{r}.$$

Integrating by parts first the ratio to s and later the ratio to s', and observing that the integrals of the differentials of continuous functions extended to an entire closed curve are zero, we have

$$P = -\frac{\epsilon\epsilon'}{2}\int_s\int_{s'} r^2 \frac{d^2(1/r)}{ds\, ds'}\, ds\, ds'. \qquad (1)$$

III

The elements of the two curves s and s' are polarized periodically; that is, they interact mutually as if they were magnetic elements with the axis in the direction of the tangents to the curves, and that they would have the respective moments m and m' variable in time, that is,

$$m = f(t)ds, \quad m' = (Ft)\, ds',$$

where $f(t)$ and $F(t)$ are functions that take up the same values at the tiniest intervals of time equal to p.

Assuming that the action is propagated in space with the velocity c, the potential of one line over the other in an entire period will be

$$W = \int_0^p dt \int_s\int_{s'} f(t)\, F\left(t - \frac{r}{c}\right)\frac{d^2(1/r)}{ds\, ds'}\, ds\, ds'. \qquad (2)$$

Assuming that the moments of the current not only have the same period but also vary with the same law, and differ only in phase. Then we will have

$$f(t) = e\phi(t),$$
$$F(t) = e'\phi(t + \sigma),$$

since $\sigma < p$.

Because of the smallness of σ and of r/c, we can write

$$F\left(t - \frac{r}{c}\right) = e'\phi\left(t + \sigma - \frac{r}{c}\right)$$
$$= e'\phi(t) + \left(\sigma - \frac{r}{c}\right)\phi'(t) + \left(\sigma - \frac{r}{c}\right)^2 \frac{\phi''(t)}{2}.$$

Substituting this value in formula (2), and observing that we have

$$\int_s\int_{s'} \frac{d^2(1/r)}{ds\, ds'}\, ds\, ds' = 0,$$

and that s, on account of the periodicity of $\phi(t)$, it is

$$\int_0^p \phi(t)\phi'(t)\, dt = 0,$$

one obtains

$$W = \frac{ee'}{2}\int_0^p \phi(t)\phi''(t)dt \int_s\int_{s'}\left(\sigma - \frac{r}{c}\right)^2 \frac{d^2(1/r)}{ds\, ds'}\, ds\, ds'.$$

Now let the duration p be of a very small period also with respect to the time in which the electrical action is propagated to the unit of distance, such that σ can be negligible with respect to r/c. Then we will have

$$W = \frac{ee'}{2}\int_0^p \frac{\phi(t)\phi''(t)}{c^2}\, dt \int_s\int_{s'} r^2 \frac{d^2(1/r)}{ds\, ds'}\, ds\, ds'.$$

Because of the periodicity of $\phi(t)$, integrating by parts; one obtains

$$\int_0^p \phi(t)\phi''(t)dt = -\int_0^p (\phi'(t))^2\, dt.$$

Hence, writing

$$\int_0^p (\phi'(t))^2\, dt = a^2, \quad ae/c = s, \quad ae'/c = s' \ (*).$$

we have

$$W = -\frac{\epsilon\epsilon'}{2}\int_s\int_{s'} r^2 \frac{d^2(1/r)}{ds\, ds'}\, ds\, ds'$$

which coincides with the potential given by formula (1) and as in it, s and s' are quantities proportional to the intensity of the two currents.

Hence the electrodynamic actions can be explained, granting that they are propagated in space with velocity equal to the speed of light, that they act according to Newton's law like electrostatic actions, that the currents consist of a kind of polarization of their elements, which is periodically variable, that the law of variation is equal in all currents, and that the duration of the period is small also with respect to the time the action takes to propagate itself to the unit of distance.

Pisa, May 25, 1868

*In the original memoir, the denominator c was left out.

A Contribution to Electrodynamics

by Bernhard Riemann

Editor's Note: *This 1858 paper, presented by Riemann to the Royal Society of Sciences at Göttingen, was translated from the German by Uwe Parpart Henke. It was published in Poggendorf's* Annalen der Physik und Chemie, *Bd. CXXXI, along with the footnote by Weber that appears at the end of this translation.*

I have taken the liberty of informing the Royal Society of an observation which brings the theory of electricity and of magnetism into close coherence with the theories of light and radiating heat. I have found that the electrodynamic effects of galvanic current can be explained if one assumes that the effect of an electric mass on other masses does not occur instantaneously, but is propagated with a constant velocity (equal to the velocity of light inside the boundaries of observational error). In this assumption, the differential equation for the propagation of electricity becomes the same as the equation for the propagation of light and radiating heat.

Let S and S′ be two conductors through which constant galvanic currents flow and which do not move in relation to each other. ε is a particle of electric mass inside conductor S which is located at point (x, y, z) at time t. ε′ is a particle of electric mass of S′ which is located at point (x', y', z') at time t'. In terms of the motion of the particles of electric mass, in which the positive and negative electric particles have opposite directions in every particle of the conductor, I will make the assumption that the particles of electric mass are distributed at every instant in such a way that the sums, $\Sigma\varepsilon f(x, y, z)$ and $\Sigma\varepsilon' f(x', y', z')$, which are extended over all the mass particles in the conductor, can be neglected in favor of those sums that are extended only over the positive or only over the negative particles of electric mass as long as function f and its differential equation are continuous.

This provision can be satisfied in many diverse ways. If one assumes, for example, that the conductor is crystalline in its smallest particles so that the same relative distribution of electricity is periodically repeated at distances which are definite and infinitely small compared to the conductor's dimensions, and if β designates the length of such a period, then these sums are infinitely small compared to the conductor's dimensions, and if β designates the length of such a period, then these sums are infinitely small like $c\beta^n$—if f and its derivatives are continuous up to the $(n - 1)$-th order—and are infinitely small like $e - (c/\beta)$—if they are all continuous.

The Empirical Law of Electrodynamic Effects

If the specific current intensities u, v, w are parallel respectively to the three axes (x, y, z), according to mechanical measurement at time t, and if the specific current intensities u', v', w' are parallel respectively to axes (x', y', z'), and if r describes the distance between both points, while c is the constant determined by Kohlrausch and Weber, then, according to experiments, the potential of the forces exerted by S and S′ is

$$-\frac{2}{cc}\int\int\frac{uu' + vv' + ww'}{r}\,dS\,dS',$$

and this integral extends over all the elements dS and dS' of conductors S and S′. If, instead of the specific current intensities, one introduces the product from the velocities into the specific densities, and then takes the masses contained in the specific densities as their product and introduces this into the element of volume, then this expression changes to

$$\sum\sum\frac{\epsilon\epsilon'}{cc}\,\frac{1}{r}\,\frac{dd'(r^2)}{dt\,dt},$$

if the change in r^2 during time dt which originates in the motion of ε is denoted by d, and the change which originates in the motion of ε′ is denoted by d'.

By disregarding

$$\frac{d\sum\sum(\epsilon\epsilon'/cc)(1/r)(d'(r^2)/dt)}{dt},$$

which disappears through summation for ε, this expression can be turned into

$$-\sum\sum\frac{\epsilon\epsilon'}{cc}\,\frac{d(1/r)}{dt}\,\frac{d'(r^2)}{dt}$$

and this, through the addition of

$$\frac{d'\sum\sum\frac{\epsilon\epsilon'}{cc}\,rr\,\frac{d(1/r)}{dt}}{dt},$$

which becomes zero through summation for ε′, changes into

$$\sum\sum_{\epsilon\epsilon'}\frac{rr}{cc}\,\frac{dd'(1/r)}{dt\,dt}.$$

The Derivation of This Law From the New Theory

According to the assumption up to now about electrostatic effects, the potential function U of arbitrarily distributed electrical masses is determined by the condition that

$$\frac{\partial^2 U}{\partial x^2} + \frac{\partial^2 U}{\partial y^2} + \frac{\partial^2 U}{\partial z^2} - 4\pi\rho = 0,$$

and by the condition that U is continuous and is constant at an infinite distance from the active masses if q denotes its density in points (x,y,z). A particular integral of equation

$$\frac{\partial^2 U}{\partial x^2} + \frac{\partial^2 U}{\partial y^2} + \frac{\partial^2 U}{\partial z^2} = 0,$$

which generally remains continuous outside of points (x',y',z'), is $f(t)/r$ and this function forms the potential function which is generated from point (x',y',z') if mass $-f(t)$ is in the same point at time t.

Instead of this, I will now assume that potential function U is determined by the condition

$$\frac{\partial^2 U}{\partial t^2} - \alpha\alpha\left(\frac{\partial^2 U}{\partial x^2} + \frac{\partial^2 U}{\partial y^2} + \frac{\partial^2 U}{\partial z^2}\right) + \alpha\alpha 4\pi\rho = 0$$

so that the potential function which is generated from point (x', y', z') equals $f[t - (r/\alpha)]/r$ if mass $-f(t)$ is in the same point at time t.

If one denotes the coordinates of mass ε at time t by x_t, y_t, z_t and the coordinates of mass ε' at time t' by $x_{t'}',y_{t'}',z_{t'}'$, and if one uses the abbreviation

$$\left((x_t - x'_{t'})^2 + (y_t - y'_{t'})^2 + (z_t - z'_{t'})^2\right)^{-1/2} = \frac{1}{r(t,t')} = F(t,t'),$$

then, according to this assumption, the potential of ε on ε' at time t equals

$$-\varepsilon\varepsilon' F\left(t - \frac{r}{\alpha}, t\right).$$

Therefore, the potential of the forces exerted by all of the ε mass of conductor S on the ε' mass of conductor S' from time 0 up to time t will be

$$P = -\int_0^t \sum\sum_{\varepsilon\varepsilon'} F\left(t - \frac{r}{\alpha}, \tau\right) d\tau,$$

with the sums extended over all the masses of both conductors.

Because the motion for opposite electric masses is an opposing motion in every particle of the conductor, function $F(t,t')$ has the property of being able to change its signs with ε through the derivation according to t, and with ε' through the derivation according to t'. Then, given the assumed distribution of electricity, if one denotes the derivations according to t by superscripts, and the derivations according to t' by subscripts, $\Sigma\Sigma\varepsilon\varepsilon' F^{(n)}(\tau,\tau)$, which is extended over all the electric masses, does not become infinitely small in comparison to the sum which only extends over one kind of electric mass if n and n' are both uneven.

We will now assume that, during the force's propagation period from one conductor to another, the electric masses cover only a very small path, and we will consider the effect during a time period in contrast to which the propagation period become insignificant. In the expression for P, one can first of all replace $F(\tau - r/\alpha, \tau)$ by

$$F\left(\tau - \frac{r}{\alpha}, \tau\right) - F(\tau, \tau) = -\int_0^{r/\alpha} F'(\tau - \sigma, \tau) d\sigma$$

because $\Sigma\Sigma\varepsilon\varepsilon' F(\tau,\tau)$ can be neglected. In this way, one obtains

$$P = \int_0^t d\tau \sum\sum_{\varepsilon\varepsilon'} \int_0^{r/\alpha} F'(\tau - \sigma, \tau) d\sigma$$

or, if one reverses the order of integration and replaces $\tau + \sigma$ by τ,

$$P = \sum\sum_{\varepsilon\varepsilon'} \int_0^{r/\alpha} d\sigma \int_{-\sigma}^{t-\sigma} dx\, F'(\tau, \tau + \sigma).$$

If one changes the limits of the inner integral in 0 and t, then what is added through this to the upper limits is the expression

$$H(t) = \sum\sum_{\varepsilon\varepsilon'} \int_0^{r/\alpha} d\sigma \int_{-\sigma}^{0} d\tau\, F'(t + \tau, t + \tau + \sigma)$$

and the value of this expression for $t = 0$ is subtracted at the lower limits. Thus, we have

$$P = \int_0^t d\tau \sum\sum_{\varepsilon\varepsilon'} \int_0^{r/\alpha} d\sigma\, F'(\tau, \tau + \sigma) - H(t) + H(0).$$

One can replace $F'(\tau, \tau + \sigma)$ by $F'(\tau, \tau + \sigma) - F'(\tau,\tau)$ in this expression because $\Sigma\Sigma\varepsilon\varepsilon'(r/\alpha)F'(\tau,\tau)$ can be neglected. Through this, one obtains an expression as a factor of $\varepsilon\varepsilon'$ which changes its signs with ε as well as with ε', so that its terms do not cancel each other out through summation, which also allows infinitely small fractions of individual terms to be neglected. Therefore, when one replaces $F'(\tau, \tau + \sigma) - F'(\tau,\tau)$ by $\sigma[d\sigma'(1/r)/d\tau\, d\tau]$ and carries out integration for σ up to a fraction that can be neglected, one gets

$$P = \int_0^t \sum\sum_{\epsilon\epsilon'} \frac{rr}{2\alpha\alpha} \frac{dd'(1/r)}{d\tau\, d\tau} d\tau - H(t) + H(0).$$

It is easy to see that $H(t)$ and $H(0)$ can be neglected, for

$$F(t+\tau,\ t+\tau+\sigma) = \frac{d(1/r)}{dt} + \frac{d^2(1/r)}{dt^2}\tau + \frac{dd'(1/r)}{dt\, dt}(\tau+\sigma) + \cdots,$$

and, consequently,

$$H(t) = \sum\sum_{\epsilon\epsilon'} \left(\frac{rr}{2\alpha\alpha} \frac{d(1/r)}{dt} - \frac{r^3}{6\alpha^3} \frac{d^2(1/r)}{dt^2} + \frac{r^3}{6\alpha^3} \frac{dd'(1/r)}{dt\, dt} + \cdots \right).$$

But, this is only the first term of the factor $\epsilon\epsilon'$ with the factor in the first component of P having the same order, and, because of summation for ϵ', this supplies only a fraction, which can be neglected, of the same term.

The value for P, which results from our theory, agrees with the empirical

$$P = \int_0^t \sum\sum_{\epsilon\epsilon'} \frac{rr}{cc} \frac{dd'(1/r)}{d\tau d\tau'} d\tau$$

if we assume that $\alpha\alpha = \frac{1}{2}cc$.

According to Weber and Kohlrausch's definition, $c = 439{,}450 \times 10^6$ mm/sec, which results in α being 41,949 geographical miles/sec, while Busch found the speed of light to be 41,994 miles/sec from Bradley's aberration observations, and Fizeau found it to be 41,882 miles/sec by direct measurement.

Note by the German Editor

This paper was presented by Riemann to the Royal Society of Sciences at Göttingen on February 10, 1858, according to a note added to the title of the manuscript by the Secretary of the Society at that time, but it was later retracted. After the paper had been published after Riemann's death, it was subjected to criticism by Clausius (Poggendorff's Annalen Bd. CXXXV, p. 606), whose essential objection consists of the following.

According to the provisions, sum

$$P = -\int_0^t \sum\sum_{\epsilon\epsilon'} F\left(\tau - \frac{r}{\alpha},\ \tau\right) d\tau$$

has an infinitesimally small value. Therefore, by virtue of a noninfinitesimally small value that will be found later for it, the operation must contain a mistake, for Clausius found an unjustified reversal of the sequence of integration in the exposition.

The objection appears to me to be well-founded, and I am of Clausius's opinion that Riemann himself discovered the same and retracted the work before publication because of this.

Although the most essential content of Riemann's deduction collapses as a result of this, I have decided to include this treatise in the present collection because I did not want to presume to decide whether it nevertheless did not still contain some kernels of further fruitful thought on this highly interesting question.

Weber

IJFE Seminar Report

A Modern Approach to Astronomy From the Point of View of Kepler

by Carol White

Almost 400 years ago, astronomer Johannes Kepler laid the basis for modern astronomy. While he is best known for his three laws of planetary motion, his primary interest was to develop a theory to account for the creation of the planets. His work has not yet been qualitatively superseded: Unfortunately, since the death of Bernhard Riemann in 1866, scientists have increasingly been diverted from the path of Kepler into the sterile direction of Newtonian physics.

Recently the editors of the IJFE held a three-day science seminar in Virginia at the home of FEF board member Lyndon H. LaRouche, Jr. The topic was a modern approach to astronomy from the point of view of Kepler, and the participants included, in addition to the IJFE editors and other FEF staff members, the well-known Mexican astronomer Dr. Luis Carrasco.

For almost two decades, Carrasco has been studying the process of structure formation in the universe. The most exciting feature of his work is his acknowledged debt to Johannes Kepler (1571-1630). Only recently has mainstream astronomy recognized just how correct Kepler was in identifying the crucial role of the magnetic field in the process of planet and star formation as well as in governing planetary orbits. (Kepler based his version of the magnetic fields on the surprisingly modern work of the British physicist William Gilbert, as can be seen from Kepler's *Epitome of Copernican Astronomy* and Gilbert's *De Magnete*.)

Carrasco has generalized this method to apply to the formation of galaxies and clusters of galaxies as well. Kepler's Third Law, which relates the period of revolution of the planets to their distance from the Sun, has been generalized by astronomers to estimate the relative mass of the Sun and Earth. The comparison is made between the orbit of the Moon around the Earth at a given distance, and the predicted period of a body around the Sun at the same distance.

$$R^3/T^2 = KM,$$

where R is the mean radius of the orbit, T is the time of revolution, and M is the mass.

Carrasco has generalized this as a relationship between what he calls specific angular momentum and the mass of the structure in question. The correlation he finds can be expressed as:

$$\omega^2 R \text{ is correlated to } M^3,$$

where ω is the orbital angular velocity.

The Carrasco law implies a lawful relationship between the radius of a planet and its mass. Such indeed was also asserted by Kepler. Empirically, he has found that the specific angular momentum does correlate with a value of mass—which implies the relationship between mass and radius implied above.

Carrasco's Theory

Carrasco discovered this relationship as a by-product of his study over the past 17 years of the connection between the reduction of angular momentum and the formation of planets, stars, galaxies, and clusters of galaxies. He began this work by studying the activity of sunspots, which provide a means of measuring the spin angular momentum of stars.

He contends that these sunspots are intimately connected to the generation of solar flares. Synchrotron radiation from solar flares provides a means of detecting them. These solar flares are the vehicle, according to Carrasco, through which the Sun sheds angular momentum, partly by losing mass, but mainly by the interaction of the magnetic field carried out of the star and the plasma gas disk surrounding the star. This magnetic field of the flare remains connected to the star, and therefore it transfers angular momentum to the plasma gas disk as it is dragged through this disk by the rotation of the star.

As is well known, the angular momentum of a rotating body determines its stability. Therefore, for a star to form, there is a maximum angular momentum that it will tolerate. If the angular momentum of the gas from which the star is to be formed is too great, then centrifugal force will prevent its formation. Carrasco has determined that the angular momentum does not operate as a maximum, allowing star formation to occur at any point below that maximum. On the contrary, star formation seems to occur only at preferred bands of angular momentum—such that there is also a minimum angular momentum necessary to allow for star formation.

This result is not predicted by mechanical theory. This being the case, Carrasco has looked for a process by which angular momentum is shed that will then correlate to a rate of star formation. This implies, for stars like the Sun, a time in which they had a far greater angular momentum than at present. In the early period of the Sun's life, it would have been rotating at a far greater speed than currently and would have been experiencing a great deal more flaring. This process appears to be important to understanding the morphology of all stars. Carrasco predicted that high levels of solar flaring should be seen in the case of young stars. This was corroborated within the past few years when the Einstein X-ray detecting satellite observed such high levels of solar flaring in young stars.

In 1958, Winston Bostick predicted that the plasma effects that he was observing in a laboratory situation, with his plasma-focus experiment would be discovered in the activity of stars and galaxies. In particular he singled out the development of vortex filamentary structure.

Recent observations seem to corroborate his hypothesis (Maitra 1984). Bostick argues that phenomena such as sunspots are like the plasmoids that he has observed in the laboratory. He hypothesizes that flaring on a large scale occurs when two such vortices come together so that their magnetic field lines coalesce and are transformed into flares. The shock wave created by this flaring in turn detonates smaller flaring over the surface of the star.

Carrasco has observed a correlation between the mass of stars and the degree of angular momentum. He finds a linear relationship between, on the one hand, the logarithm of the ratio between angular momentum per unit mass and, on the other, the logarithm of mass per se. In other words, both *exponential* functions—of the angular momentum and the mass—are correlated. He has also found that this correlation differentiates stars according to their age. That is, for the older stars with the same mass, their trend line will occur at an overall reduced angular momentum. The significance of this is that stars, regardless of their age, will tend to shed mass in a uniform manner over time.

The most massive stars have the largest angular momentum because they are not convective. Large stars have large stellar winds, but they are not magnetized, and therefore do not shed angular momentum to the same degree. Small stars shed angular momentum with great efficiency without the same degree of loss of mass. With this model, it is possible to predict the age of stars by criteria other than those currently used. This analysis has been extended to binary stars, which also store angular momentum. Most stars are part of binary systems, even if one of the pair is no longer observable.

A step-function graph of these logarithmic categories extends from the formation of planets and asteroids—at the lowest, left-hand corner of the graph—to the formation of clusters of galaxies at the top right. For each category of cosmic mass, there is a rising step, or line, crossing a diagonal linear trend line. The step indicates the relationship within a given category, while the trend line shows the interrelationship between categories. These steps are discrete quantizations. He has found a higher continuous function that makes the function continuous by introducing the mean density of cosmic mass into his equation.

Kepler's Law Extended

Except in the case of spiral galaxies, which vary by a different law (the three-fourths power of mass), these cosmic structures vary according to the two-thirds power of the mass—which is a direct extension of the method of Kepler. Carrasco has accounted for the dissimilarity of spiral galaxies by a corrective factor. In general, spiral galaxies are less dense than elliptical galaxies. Star formation seems to occur in their arms, where a mean magnetic field has been located running through them. While it is clear that there is rotational action in the spiral arms, it has not yet been possible to locate vortex filaments along the lines discovered by Bostick, although Carrasco thought that these would most likely be present. In fact, the shapes of the galaxies that he describes are similar to "barred" spiral formations seen by Bostick in his experiments.

Galaxies, as such, are divided into two main categories—spiral galaxies such as our own—and elliptical galaxies. The elliptical galaxies—ellipsoids with three different axes—are far more dense than spiral galaxies, yet they have less angular momentum than spiral galaxies by a factor of 20. Carrasco presumes that they have down-shifted by some law that is independent of their mass, in which the change of angular momentum per unit of angular momentum is a constant fraction related to time.

In a sense, stars keep a "memory" of the condition of their formation, maintaining themselves in relation to each other in galaxies. Elliptical galaxies have stopped the process of star formation. They have very little surrounding gas left, and this is ionized and therefore too "hot" to support continued star formation. Their lower angular momentum means that they accomplished their star formation at an earlier period. This is not the case with spiral galaxies, which are still forming new stars. This offers another possible approach to the question of the red-shift. Rather than the usual interpretation that the observed red-shift represents an expansionary process in the universe, it may be due to a down-shift of frequency directly related to the work of star formation.

Carrasco has discovered another Keplerian relationship. Within galaxies there are peaks and valleys of angular momentum that occur at discrete intervals along radial distances from the center of the galaxy. Sharp peaks of star formation correlate with these valleys. In spiral galaxies these discrete nodes of star formation occur within the spiral arms. The radial patterning suggests that the universe is structured in magnetic "sheets." This may indicate a global filamentary structure of the universe rotating as a whole.

In the discussion that followed Carrasco's presentation, Lyndon LaRouche emphasized the necessity of throwing out the so-called laws of physics and approaching the subject afresh from the point of view of Kepler. But for Kepler's method to be understandable to a modern audience, it is necessary to rework Kepler from the standpoint of Gauss's conical work functions.

LaRouche emphasized the falseness of Newton's notion of gravitational force. Gravity is merely the measure of the work done by an object when it moves out of a Keplerian, force-free orbit. In this sense it registers work done upon the universe. Newton's treatment of gravity as the pairwise interaction between masses was a deliberate attempt to stifle the advance of science. The practically useful calibration of the inverse square law was in any case first introduced by Kepler, himself, with regard to optics and was later applied by the secretary of the Royal Society, Robert Hooke, to transform Kepler's

laws into the form of "Newton's" so-called law.

The approach by Carrasco is not only a fruitful application of Kepler's method, but very useful pedagogically. Therefore, LaRouche suggested that it would be useful to present a morphology of cosmic species to help the student. He urged that such a classification of these different "animal" species be made available to as broad an audience as possible as quickly as possible.

The LaRouche Hypothesis

LaRouche suggested his hypothesis that nuclear fusion can only occur as a polarized process for Carrasco's consideration. This would imply that the present assumption by astrophysicists that fusion in the Sun could not produce the heavy elements found on Earth, *sui generis*, is incorrect, since a polarized plasma would raise the efficiency of the fusion process by as much as one order of magnitude.

LaRouche also suggested that the gaseous disk surrounding the Sun was polarized and that the creation of heavy elements occurred there. This would have been part of the process of planet formation. Carrasco noted that there are very short-lived isotopes formed on the surface of stars, elements like technetium, which could not have been formed at their center and traveled to the surface, because they are too short-lived.

While this is suggestive of corroboration of the LaRouche hypothesis, the isotopes are also too short-lived to have been cannibalized in the process of planet formation. Carrasco also noted that certain stars have a high metallic content and very high magnetic fields. In the same connection, he remarked that the spiral arms of galaxies emit polarized radiation that is diffracted through dust that has been aligned by the magnetic fields within the arms of the spiral.

Reference

Maitra, R. 1984. "New Radio Telescope Images Show Galaxy in Creation." *New Solidarity* (July 20), p. 8.

Abstracts

Fusion

Abstracted by
Charles B. Stevens

Advanced Fusion Burning Core Experiment
by Bruno Coppi
Massachusetts Institute of Technology, Cambridge, Mass.
Report PTP-84/8, (March 1984)

The purpose of this experimental machine is to achieve thermonuclear-ignited plasmas at a cost of about one-tenth that projected for burning core experiments based on more conventional types of tokamak designs. The idea is to use high magnetic fields in order to produce stable tokamak plasmas that are capable of sustaining high plasma electric current densities such that ignition conditions can be attained or at least approached with only ohmic heating from the plasma current. This paper explores the physics of fusion burning plasmas for which very high plasma currents are needed. Specifically, it refers to currents up to 10–12.5 MA and to a design concept called the burning core experiment or BCX that employs the high-field technologies and solutions developed for the Alcator tokamak program and for the subsequent designs of the Frascati (Italy) Torus and the Ignitor device. The latest motivations to undertake this study came from:

(1) The excellent results concerning the confinement of ohmically heated plasmas obtained with currents of about 1 MA or higher in such diverse tokamaks as Alcator C, TFTR, and JET.

(2) The recognized validity of the structural analysis for the Ignitor that can be adopted for machines capable of producing much higher currents.

(3) The successful demonstration of the JET design of a low-aspect-ratio, compact structure in which the toroidal magnet is mechanically coupled to the transformer.

(4) The evidence that performance in ohmic heating experiments is determined by the maximum value of the poloidal magnetic field that is generated by the plasma current. On this basis it appears that the ignition conditions of deuterium-tritium plasmas can be approached by ohmic heating alone, given poloidal magnetic fields in the range of 40 to 50 kG over the plasma column and peak current density of about 2.5 kA/cm^2.

(5) Advances in radiofrequency heating (RF) involving high-density plasmas. Thus ohmic heating can be backed up with 8 MW of RF (at either the ion cyclotron or lower hybrid frequency) in case confinement may degrade as plasma regimes significantly different from those achieved so far are reached.

(6) The widespread interest in determining if tokamaks can be scaled to conditions needed for burning advanced fusion fuels such as deuterium–helium-3 (D–^{3}He). For achieving ignition with this reaction the 14.7-MeV product protons would have to be confined. This requires plasma currents in the range of 6 MA, well within the BCX design range. Therefore, one of the goals of the BCX is to study substantial burning of D–^{3}He. Coppi also notes that the so-called D–D-catalyzed reaction chain can be studied once the confinement of the produced 14.7 protons is assured.

"Laser Fusion in New Types of Targets"
by Chiyoe Yamanaka
Invited Paper, June 19, 1984
Thirteenth International Quantum Electronics Conference
Anaheim, Calif.

In laser fusion two general types of targets have been experimentally and theoretically explored: (1) direct drive targets in which the incident laser beam ablatively drives the implosion of the fuel pellet; and (2) indirect drive targets in which the incident laser beam is used to generate a second type of energy that, in turn, drives the implosion of the fuel pellet.

This paper by the head of the laser fusion program at the Institute of Laser Engineering at Osaka University in Japan reviews recent work at Osaka on the second type of laser fusion target.

A new, indirect drive target consists of two spherical shells that form a cavity into which the laser beams are injected. The original concept of this target was that the outer shell constituted a tamper that traps the laser beam energy within the cavity. In this way the efficiency at which the incident laser energy is converted into hydrodynamic compression is greatly increased over that of simple direct drive ablative implosion (Azechi et al. 1981). This scheme has been tested with a double-foil target (Yamada et al. 1982). Efficient spherical compression of this target was recently demonstrated, and it showed good implosion uniformity (Miyanaga et al. 1983). This target has also been explored using numerical sim-

ulations (Nishihara et al. 1980, 1982). High laser absorption efficiency, high hydrodynamic efficiency, and good uniformity of irradiation of the internal fuel shell have been shown in these calculations.

It has been found that the smaller size of the cavity between the inner and outer shell is desirable for obtaining higher hydrodynamic efficiency through the effect of the tamper. But it also has been recently proposed that using a larger-cavity target of which the outer shell consists of high-Z material such as gold leads to the generation of X-rays. This occurs when the laser beams are incident upon the inner surface of this gold outer shell. Calculations (Noaki and Nishihara 1980, Nishihara 1982, Yabe et al. 1983) and experiments (Mochizuki et al. 1983) have shown that X-ray-driven ablation of an inner shell also leads to high hydrodynamic efficiency.

Thus, the new indirect drive target can be classified into two types according to the cavity size. The compression mechanisms of these two types are quite different. In the case of small cavity size, it is the high plasma pressure between the shells that drives the implosion of the inner shell, whereas X-ray radiation from the outer shell drives an ablative type of implosion in the large-cavity target. In this second case the conversion efficiency from laser energy to X-ray energy is about 50 percent for short-wavelength lasers (Mead et al. 1981, Nishimura et al. 1983). And while the emitted X-ray spectrum is not a perfect Planckian (Okada and Mochizuki 1983), it closes to blackbody radiation of the order of 100 eV (Mead et al. 1981, Nishimura et al. 1983, Mizui et al. 1981).

References

Azechi, H., et al. 1981. *Japan. J. Appl. Phys.* **20:** L477.

Mead, W.C., et al. 1981. *Phys. Rev. Lett.* **47:** 1289.

Miyanaga, N., et al. 1983. *Japan. J. Appl. Phys.* **22:** L551.

Mizui, J., et al. 1981. *Phys. Rev. Lett.* **47:** 1000.

Mochizuki, T., et al. 1983. *Japan. J. Appl. Phys.* **22:** L133.

Nishihara, K. 1982. *Japan. J. Appl. Phys.* **21:** L571.

Nishihara, K., and T. Yuchi. 1983. ILE Quart. Prog. Rep. on Inertial Fusion Program, Osaka U., *ILE-QPR-83-5*, 25.

Nishihara, K., et al. 1980. Report on IAEA Technical Meeting on Advances in Inertial Confinement Systems, Takarazuka, Japan, 1979, 1979; *Rev. Laser Eng.* **8:** 70.

Nishihara, K., et al. 1982. Proc. Japan-U.S. Seminar on Theory and Application on Multiply-Ionized Plasma Produced by Laser and Particle Beams, Nara, Japan, May 1982; *Rev. Laser Eng.* **10:** 183.

Nishimura, H., et al. 1983. *Phys. Fluids* **26:** 1638.

Nozaki, K., and K. Nishihara. 1980. *J. Phys. Soc. Japan* **48:** 993.

Okada, K. and T. Mochizuki, 1983. ILE Quart. Prog. Rep. on Inertial Fusion Program, Osaka U., ILE-QPR-83-6, 26.

Yabe, T., et al. 1983. *Japan. J. Appl. Phys.* **22:** L88.

Yamada, K., et al. 1982. *J. Phys. Soc. Japan* 51: 280.

"Ion Beam Pulse Compression by Its Conversion into Soft X-Rays"

by Takashi Yabe
Institute of Laser Engineering, Osaka University

Japan. J. Appl. Phys., Vol. 23, No. 1 (Jan. 1984), pp. L57-58

This paper proposes a new method of achieving the conversion of beam driver energy into blackbody radiation (soft X-rays) for use in inertial confinement fusion indirect-type targets. In the process of the transformation of the beam energy into blackbody radiation, the effective power density of the beam energy is increased by a factor of 10. In the particular case of ion beams it is proposed that an ion beam of 10^{13} W/cm^2 at 100-nsec pulse lengths can be converted into a focusable X-ray pulse of 10^{14} W/cm^2 with a 10-nsec pulse length. This general method could also be used for energy focusing into small volumes by both light and heavy ion beams and even with krypton fluoride laser pulses.

Figure 1 illustrates the basic idea. The energy converter consists of low-density and high-density layers both made up of high-Z materials—gold foam and solid gold, respectively. The ion beam is incident on the high-density layer. Using the characteristics of the ion beam stopping power, the thickness of the outer layer is chosen so that the ion beam is passed through the solid gold layer and is mainly absorbed in the low-density layer, resulting in the generation of X-rays. Since the mean free path of X-rays is shorter for a higher-density layer, most of the energy is transported toward the low-density side. The resulting X-ray pulse can be compressed by as much as a factor of 10.

This method has many advantages: (1) The radiation energy mainly

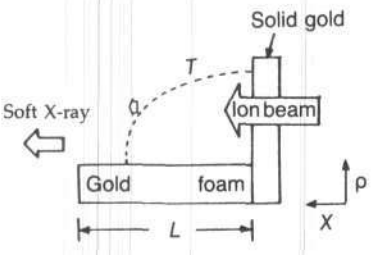

Figure 1. Schematic of Ion Beam Pulse Compression.

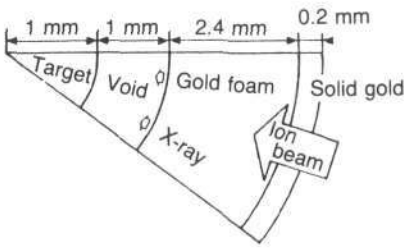

Figure 2. Schematic of inertial confinement configuration that uses the ion beam compression proposed. The outer two layers act as energy converter from ion beam to X-ray. Even if the ion beam focusing is poor, the converted X-ray is emitted at a surface close to a target placed inside. The vacuum spacing between the target and emitter can be changed to adjust the target size to the ion beam focusing size.

goes toward the low-density side when the energy is absorbed between the high and low-density layers as shown by our previous simulations. Hence the system illustrated in Figure 2 could be used for efficient compression. (2) Even if the ion beam focusing is poor, the compressed X-ray pulse can be emitted from a surface close to a target as shown in Figure 2. (3) X-ray pulse shaping is possible if various materials or multishells are placed at the inner surface of the emitter. (4) The vacuum spacing between the target and the emitter can be arbitrarily changed to adjust the target size to the focusing size of the ion beam. (5) The method could be used for other drivers like the KrF laser that have long pulse shapes.

"New Scheme of Cannonball Target Driven by Ion Beam"

by Kazuo Imasaki, Shuji Miyamoto, Satoshi Higaki, Tetsu Ozaki, Sadao Nakai, and Chiyoe Yamanaka
Institute of Laser Engineering, Osaka University
Japan. J. Appl. Phys., Vol. 23, No. 2 (Feb. 1984), pp. L83-L84

A new concept of ion beam targets is proposed. Ion beam energy was injected inside a solid gold shell. Energy of the radiation converted from the beam was confined and transported inside. This effect was called the Mahobin effect. If the Mahobin target is compared with a direct drive target, several advantages such as power amplification, brightness reduction, and higher gain can be expected. Total implosion efficiency was estimated to be more than 10 percent.

"ICF With Momentum-Rich Beams and Overview of Momentum-Rich Ion Beam Fusion"

by A.W. Maschke
Accelerator Department
Brookhaven National Laboratory
INS International Symposium on Heavy Ion Accelerators and Their Applications to Inertial Fusion, Tokyo, Japan
Jan. 23-27, 1984

The momentum-rich beam (MRB) fusion concept is a new method of achieving thermonuclear ignition in a single-shell D-T target. The advantage of the system is that 1.25 to 1.50 MJ is needed for ignition, and the acceleration system for producing the beams may be 80 percent efficient or better. This combination of circumstances means that the driver costs for a full-scale ignition system are an order of magnitude less expensive than a comparable laser or heavy ion driver.

Using state-of-the-art ion source brightness parameters, and high gradient acceleration columns, it is possible to focus large-current (tens of kilojoules) heavy ion beams to a few millimeters spot size, using a 1-m radius spherical ion source. Heavy ion energies of 500 to 1,000 keV have the velocity required for volume ignition of D-T. The beam "mass" is typically 10 times greater than that of the D-T that is to be burned. A spherical array of ion sources is envisioned, using time-of-flight bunching to achieve the required power density at the central focus. Beam space-charge neutralization is assumed to take place in a background plasma. The D-T, originally a gas ball a few millimeters in diameter, is compressed and heated by the direct transfer of the beam energy to the fuel. The necessary inward momentum is produced directly by the accelerator, not by ablation.

The MRB program at Brookhaven National Laboratory is divided into two parts. One part is a program to investigate the physics of interaction between the MRBs and the pellet. This is done with the LASNEX hydro code at Lawrence Livermore National Laboratory. The second part is a program to develop the required accelerator technology. A test of a full-current Cs beam accelerated up to 500 keV is under construction. This is designed to demonstrate that the required beam brightness can be obtained. The next step in the program would be to design a $1 \times 1\text{-m}^2$ module. An array of nine of these would provide about 5 kJ of Cs beam focused to a few millimeters. This should be adequate to verify most of the physics associated with the beam-beam and beam-pellet interactions. A next step after this would be construction of the full 10-m radius system, but using 20 of the 5-kJ modules. If the beam pellet physics works out all right at this scale, one can have reasonable confidence in the results after upgrading the system to the full 500 kJ.

For power reactors, pellet costs must be kept low in order that inertial confinement fusion be economically feasible. This is especially true for MRB fusion since the pellet yields are small and the repetition rate high. With a pellet gain of 20 and a driver input of 500 kJ, each pellet will produce about 20 cents worth of electricity, assuming a busbar price of 60 mils/kW-hr. It is difficult to prove that the pellet factory can operate at the required efficiency until one has actually built a pellet factory. However, the author notes, it is comforting to know that small steel spheres, with the precision needed for MRB pellets, can be obtained for less than ½ cent each.

"Accelerated Decay of a Nuclear Excitation in a Crystal During Resonant Gamma Scattering"

by G.V. Smirnov, Yu. V. Shvyd'ko, and E. Realo
I.V. Kurchatov Institute of Atomic Energy, Moscow
JETP Letters, Vol. 39, No. 1 (Jan. 10, 1984), pp. 41-45

Progress toward achieving coherent sources of radiation in the gamma-ray range can greatly benefit from advances in using macroscopic effects to enhance "natural" rates of radioactive decay. This paper reports an experiment that demonstrates that this is possible. In particular, the time dependence of the coherent scattering of resonant gamma-rays by nuclei in a crystal has been measured. For the first time, it has been found possible to observe an acceleration of the decay of an excited nuclear state along the direction of the Bragg angle.

The duration of the resonant interaction of a gamma-ray with a nucleus is determined by the lifetime of the excited state that is formed after the capture of the gamma-ray. This time is very long for the low-lying isomer states that are characteristic of Mossbauer transitions. For the interaction of a gamma-ray with a system of resonant nuclei forming a crystal, it seems natural to assume that the decay of each individual excited nucleus occurs independently, especially since the nuclei essentially do not interact with each other.

As far back as the early 1960s it was suggested that under certain conditions there might be a mutual effect of nuclear oscillators in an emission process, resulting in changes in the decay characteristics of the excited state.

The experiments described used a method involving the rapid opening of a shutter blocking the beam of Mossbauer gamma-rays, so that the time could be determined at which resonant radiation arrives at the system of scattering nuclei. A given intensity level is reached approximately twice as fast under coherent-scattering conditions as under incoherent-scattering conditions. This result provides direct evidence of an acceleration of the decay of a collective excitation of nuclei in a crystal during coherent resonant scattering of gamma-rays. The time evolution of the two processes is substantially different even if the incident beam is poorly collimated (with a divergence of about 1 degree in the present experiments). The difference should be much more apparent in the case of a hard collimation near the Bragg angle.

"Coherent Excitation of Mossbauer Nuclei by Synchrotron Radiation"

by A.I. Chechin, N.V. Andronova, M.V. Zelepukhin, A.N. Artem'ev, and E.P. Stepanov
I.V. Kurchatov Institute of Atomic Energy, Moscow
JETP Letters, Vol. 37, No. 11, June 5, 1983, pp. 633-636

Diffraction of synchrotron radiation by Mossbauer nuclei has been observed for the first time. The measured temporal distribution of the resonantly scattered gamma-rays is radically different from that of the decay of isolated nuclei. The decay of excited nuclei in a crystal is directional in nature and occurs much more rapidly.

"Multistep Pumping Schemes for Short-Wavelength Lasers"

by George Baldwin
Physics Division, Los Alamos National Laboratory
Laser Interaction and Related Plasma Phenomena, Vol. 6
Eds. Heinrich Hora and George Miley (New York: Plenum, 1984)

Studies of the feasibility of gamma-ray lasers (grasers) have been under way at Los Alamos National Laboratory for several years, and a new approach to making an X-ray laser has been recently conceived. This article reports on attempts to reduce the pumping power requirements.

The major obstacle to development of short-wavelength lasers, whether they use atomic or nuclear transitions, is that of pumping the desired transitions without simultaneously creating conditions that hinder lasing. It is almost certain that the approaches to overcoming this obstacle will involve other disciplines, such as solid-state or plasma physics. Suggested here are several approaches whose merit can be established only after further theoretical and experimental investigations.

A novel approach to the pumping of atomic states for an X-ray laser, recently conceived by Nicholas DiGiacomo, features high pumping efficiency, tunability, wide choice of transition type, and freedom from the multitude of parasitic processes that plasmas present. Essentially the idea is to subdivide the pumping process into three steps:

(1) Atoms of a selected species are multiply ionized (for example, atoms of potassium are stripped down to sodiumlike K^{+8} ions).

(2) The ions are accelerated to relativistic energies and accumulated as dense bunches by repeated injection into a storage ring.

(3) In a straight section of the storage ring, the ions are pumped to a selected excited state by a beam of optical laser radiation that intersects

the ion trajectory at an angle appropriate to match, through Doppler effect, the transition energy of the ion.

The article also discusses various ways to reduce excitation requirements for grasers:

(1) Eliminating resonant absorption by the lower states of the transition.

(2) Reducing the internal conversion coefficient by exciting atomic electrons from highly converted low-angular-momentum substates to other states having smaller electron density at the nucleus.

(3) Reducing the inhomogeneous broadening.

(4) Alternatively, the pumping and lasing steps could be separated.

(5) Another possibility is two-step pumping, in which most of the excitation is provided by a slow process that creates a long-lived isomer, provided that isomer can subsequently be rapidly converted into a short-lived species capable of lasing on a recoilless line. A primary pump (neutrons) generates gamma radiation that, in turn, pumps the graser by resonant recoilless absorption.

(6) Some researchers have suggested that it may be possible to induce nuclear anti-Stokes or two-photon transitions with optical radiation.

(7) Selective photoionization has been proposed as a way to isolate isomeric nuclei and achieve a high inversion density.

(8) Elimination of terminal-state resonance absorption is possible in principle by polarizing the nuclei into magnetic substates. If the magnetic quantum numbers of nuclei in the upper and lower states differ by more than the difference of their spins, resonance absorption of the emitted radiation is forbidden. A population inversion would not then be required for lasing. This would reduce excitation requirements by several orders of magnitude.

The author discusses two experiments—solid phase and gas phase—in the laser-induced change of decay rate of uranium-235m. It has long been recognized that the internal conversion coefficient of a nuclear transition can, in principle, be modified by perturbing the electronic structure of the radioactive atom. Also proposed is the first laser-based separation of nuclear isomers, which is expected to be achieved within a year.

"Chemically Ignited Thermonuclear Reactions—A Near-Term Means for a High Specific Impulse-High Thrust Propulsion System"

by F. Winterberg
Desert Research Institute,
University of Nevada System
Acta Astronautica, Vol. 10,
No. 5-6 (1983), pp. 443-452

Ordinary chemical rockets are limited to specific impulses of less than 450 sec, while fission-reactor-powered rockets can attain specific impulses up to 1,000 sec. This paper proposes to use small fusion-powered explosions to attain specific impulses on the order of 3,000 sec. Such a propulsion system would be ideally suited for fast, economical transport of large spacecraft within the solar system. Small, clean fusion-powered explosions can be achieved by the combination of metallic shells imploded with chemical explosives and the recently proposed use of the magnetic booster target inertial fusion concept. In this way high-gain inertial fusion could be achieved without the use of fission explosives in the near-term.

In the magnetic booster concept a dense, magnetically confined thermonuclear plasma of low gain is compressed to generate sufficient energy densities to compress solid fusion fuel to superdensities at which high-gain inertial confinement is achieved. For the most easily ignitable fusion reaction, that of D-T, the total yield could be reduced to the range of 100 tons of TNT, on the order of 10 MJ, while still maintaining a significant energy gain. This has major engineering and technical advantages over necessarily large fission-only and fission-ignited fusion explosions, which have been previously proposed for intrasolar propulsion. Typically, the new proposed propulsion concept should give specific impulses on the order of 3,000 sec, corresponding to an exhaust velocity of about 30 km/sec, based on one fusion explosion per second. The average thrust is on the order of 1,000 tons.

"Relativistic Collective-Effect Accelerator for the Attainment of Ultrahigh Energies"

by F. Winterberg
Desert Research Institute,
University of Nevada System
Particle Accelerators, Vol. 14 (1983),
pp. 1-14

A new kind of collective circular particle accelerator with a circumference of 10 km could achieve particle energies up to 1,000 TeV with luminosities (current densities) up to $10^{33}/cm^2/sec$. To attain these ultrahigh particle energies and luminosities, the author proposes that an electron cloud be produced with a large toroidal magnetic solenoid. This can be done by inductive charge injection through the action of a traveling magnetic wave running around the torus. At the same time, the traveling magnetic wave accelerates the electron cloud to relativistic energies. By continuous inductive charge injection in the front of the wave, the cloud can then be relativistically densified. This densified cloud can then become the source of ultrastrong electric and magnetic fields, which can be many times larger than is possible using only externally generated fields. Ions being held by these large fields in a circular orbit can be accelerated to ultrahigh energies.

Astrophysics

Abstracted by
Robert Gallagher

"On the Initial Distribution and Evolution of Angular Momentum for Main Sequence Stars,"

L. Carrasco, J. Franco and M. Roth
Astron. Astrophys. Vol. 86 (1980) pp. 217-220

This paper elaborates a mechanism by which stars transfer angular momentum to convective envelopes surrounding them.

From published photometric periods of rotation for BY Dra type stars (that is, data based on periodic variations in their light curves), the authors have computed the angular momentum per unit mass (J/M). They present a model for stellar loss of angular momentum with time as a function of the rate of steller mass loss.

The model is based in part on the assumption that stellar loss of angular momentum occurs through the development of drag as a result of the interaction of solar flares and other solar activity with magnetized convective envelopes of plasma surrounding the rotating star. E. Schatzman first proposed this stellar braking mechanism.

The authors state: "For fast convective rotators it is plausible to think of dynamo-generated magnetic fields and the associated mass loss connected with stellar activity, which implies a loss of angular momentum. . . . The torques responsible for changing the stellar angular momentum are those due to the interaction between the mass lost by stellar flaring and stellar winds with the magnetic field associated to active stellar areas and the general magnetic field of the star respectively."

They conclude: "The model fits satisfactorily the J/M values of the upper and intermediate main sequence stars, for both, the nonemission field stars and the younger clusters if one allows the model to simulate the evolution up to the commonly accepted ages of 10^7, 2×10^8 and 5×10^9 yr for the Pleiades cluster, the Hyades cluster, and the nonemission field stars respectively. Perhaps of more interest is the behavior of the model for types later than G2. . . . The J/M distribution goes through a minimum and turns up toward larger values approaching asymptotically the initial ZAMS distribution." The Sun is at the minimum of the distribution curve.

"Density Scaling of the Angular Momentum Versus Mass Universal Relationship"

L. Carrasco, M. Roth, and A. Serrano
Astron. Astrophys. Vol. 106 (1982), pp. 89-93

The authors argue that loss of angular momentum is a requirement for formation of a galaxy. In a later paper published, the authors correlate loss of angular momentum in interstellar gas with star formation. Together, these suggest that galaxy-formation is dependent on star formation and, in general, that the formation of "structure" at one scale is dependent on differentiation at lower levels.
show that the law is scaled by the specific density of all objects so that $J\ \rho^{1/6}$ is proportional to $M^{**0.66;0.75}$

They write: "This law appears as a physically natural consequence if the amount of angular momentum present in the 'cloud' [material] from which all objects are formed is different from zero. As a Jean's unstable system undergoes gravitational contraction, the rotational energy increases faster than the binding [gravitational] energy. . . . To proceed further with the contraction of the system, a mechanism for removal of angular momentum must be present. Only after the system has been able to dispose of angular momentum up to an amount consistent with mechanical equilibrium, can the identity of the new system be granted. This statement is implicit in the long known angular momentum problem in star formation. . . ."

"The trend between log Q and log M . . . simply states that at the time of formation, astronomical objects have complied with a balance between their rotational and gravitational energies. A remarkable fact is the extent to which these objects retain memory of their initial distribution of angular momentum." In reference to the latter, the authors show that the loss of angular momentum is self-similar, that is, logarithmic.

The authors argue that loss of angular momentum is a requirement for formation of a galaxy. In a later paper published, the authors correlate loss of angular momentum in interstellar gas with star formation. Together, these suggest that galaxy-formation is dependent on star formation and, in general, that the formation of "structure" at one scale is dependent on differentiation at lower levels.

International Journal of Fusion Energy

Information for Contributors

Manuscripts should be sent to David Cherry at the Fusion Energy Foundation, Box 1438, Radio City Station, New York, N.Y. 10101.

Manuscripts should be submitted in triplicate (with three sets of illustrations, of which one is an original.) They should be typewritten on one side of letter (quarto) paper and double spaced with at least 25mm (1 inch) margins. All pages must be numbered in sequence beginning with the title page.

TITLE PAGE of the manuscript should contain the complete article title; names and affiliations of all authors; name, address, telephone number, and cable or Telex number for all correspondence.

ABSTRACT of no more than 200 words should summarize the work and major conclusions.

TEXT should define all abbreviations at first mention. American measuring units should be accompanied by metric translation. In general, the meter/kilogram/second/ampere system of units should be used. Letters of permission should be submitted with any material that has been previously published.

FOOTNOTES should appear at the bottom of the respective page and must be numbered consecutively.

REFERENCES must be numbered consecutively in the text and listed on a separate page. The references should include for articles: author, title, periodical name, volume no., pages, and year of publication; for books: author, title, place of publication, publisher's name, and year of publication.

TABLES, FIGURES, and ILLUSTRATIONS must be prepared each on a separate page, numbered in order of appearance, and have a title and descriptive legend. Photographs should be glossy black and white prints.

ACKNOWLEDGMENTS. Illustrations from other publications must be acknowledged. Include the following when applicable: author(s), title of journal or book, publisher and place of publication (if book), volume number, page(s), month and year of publication. The author is responsible for obtaining the publisher's permission to reprint.

REPRINT order forms will be sent to the author with proofs of the article.